Molecular Modulation of the WRKY53, WRKY18, and WRKY25 Regulatory Subnetwork of Leaf Senescence

Dissertation

der Mathematisch-Naturwissenschaftlichen Fakultät

der Eberhard Karls Universität Tübingen

zur Erlangung des Grades eines

Doktors der Naturwissenschaften

(Dr. rer. nat.)

vorgelegt von

Ana Gabriela Andrade Galán

aus Quito/Ecuador

Tübingen

2025

Gedruckt mit Genehmigung der Mathematisch-Naturwissenschaftlichen Fakultät der Eberhard Karls Universität Tübingen.

Tag der mündlichen Qualifikation:	08.12.2025
Dekan:	Prof. Dr. Thilo Stehle
1. Berichterstatter/-in:	apl. Prof. Dr. Ulrike Zentgraf
2. Berichterstatter/-in:	Prof. Dr. Thomas Lahaye

Contents

1. Abbreviations

ABA	Abscisic Acid
AD-protein	Activation Domain Protein
ANAC	Arabidopsis NAC
APX	Ascorbate Peroxidase
AtNAP	Arabidopsis NAC-LIKE Activated by AP3/PI
bHLH	basic Helix-Loop-Helix
bZIP	Basic Leucine Zipper
BRs	Brassinosteroids
CAT	Catalase
C2C2-GATA	Zinc finger domain type
COI1	Coronatine-Insensitive 1
DBD	DNA Binding Domain
EAR	ERF-associated amphiphilic repression motif
ESR/ESP	Epithiospecifying Senescence Regulator / Epithiospecifying Protein
GBF1	G-Box Binding Factor 1
H_2O_2	Peróxido de hidrógeno
HO·	Hidroxilo radical
JA	Jasmonic Acid
JA-Ile	Jasmonoyl-L-isoleucine
JA-Ile	Jasmonate isoleucine conjugate
JAs	Jasmonates
JAZ	Jasmonate ZIM Domain proteins
KIX8/KIX9	Kinase Inducible Domain Interacting 8 / 9
LOX3	Lipoxygenase 3
MeJA	Methyl Jasmonate
MEKK1	Mitogen-Activated Protein Kinase Kinase Kinase 1
MYC2	MYC2 transcription factor

NAC	NAM, ATAF1/2, CUC2
NINJA	Novel Interactor of JAZ
OPR3	12-Oxophytodienoate Reductase 3
ORE1	ORESARA1
ORS1	ORESARA1 SISTER1
PPD1/PPD2	PEAPOD1 / PEAPOD2
REV	REVOLUTA
ROS	Reactive Oxygen Species
SAGs	Senescence-Associated Genes
SA	Salicylic Acid
SOD	Superoxide Dismutase
START	Steroidogenic Acute Regulatory protein-related lipid Transfer
TIFY	Nombre de la familia TIFY
TPL	TOPLESS
TRD	Transcriptional Regulatory Domain
VNI2	VND-INTERACTING2
W-box	WRKY binding motif
WRKY	Nombre de la familia WRKY
$^1O_2$	Singlet Oxygen
$O_2^{\cdot -}$	Superóxido

2. Summary

Senescence represents the final stage of plant development and strongly impacts yield quantity and quality. This regulated process involves epigenetic, transcriptional, and biochemical mechanisms and is influenced by phytohormones, biotic and abiotic stresses, signaling molecules such as Ca^{2+} and H_2O_2, and intrinsic factors like developmental stage and nutrient status.

In this doctoral research, I investigated the regulatory network governing senescence, focusing on transcription factors of the WRKY family. Among them, WRKY53 is a central regulator that activates senescence-associated genes (SAGs) and integrates environmental signals, particularly through H_2O_2-dependent activation. WRKY transcription factors form a network, since their promoters often contain WRKY binding motifs. Within this network, WRKY25 activates and WRKY18 represses *WRKY53*, yet mutants of either gene show accelerated senescence, indicating complex regulation. This work examined the WRKY25–WRKY18–WRKY53 subnetwork in detail, revealing that WRKY25 functions as a dual regulator, sensing reactive oxygen species (ROS) and balancing the network under oxidative stress. Domain-specific analyses highlighted distinct roles for the N- and C-terminal regions of WRKY25. Based on these findings, WRKY25 is proposed to act as a redox switch modulating *WRKY53* expression through other network components.

A novel feedback mechanism was also identified between H_2O_2, catalases, and WRKY53. WRKY53 is transcriptionally induced by H_2O_2, while catalases interact directly with WRKY53 at the protein level, resulting in mutual inactivation. This illustrates a fine-tuned redox-dependent loop.

Beyond WRKYs, WRKY53 is controlled by other transcription factor families. Among them, the HD-ZIPIII factor REVOLUTA (REV) was characterized as a positive regulator of *WRKY53* and its H_2O_2 response. Regulation of REV activity by TIFY proteins was studied in depth, suggesting two mechanisms: a jasmonate (JA)-independent pathway through TIFY8 controlling REV in senescence, and a JA-dependent pathway involving PEAPODs and several JAZ proteins.

Altogether, this study uncovers new mechanistic insights into transcriptional and post-transcriptional regulation of plant senescence. It highlights the ability of transcription factors to perceive environmental signals and integrate them into developmental programs. These findings deepen our understanding of senescence and open promising avenues for crop improvement by manipulating senescence pathways to optimize yield and quality.

3. Zusammenfassung

Die Seneszenz stellt die Endphase der Pflanzenentwicklung dar und beeinflusst die Quantität und Qualität des Ertrags erheblich. Dieser streng regulierte Prozess umfasst epigenetische, transkriptionelle und biochemische Mechanismen und wird durch Phytohormone, biotische und abiotische Stressfaktoren, Signalmoleküle wie Ca^{2+} und H_2O_2 sowie intrinsische Faktoren wie Entwicklungsstadium und Nährstoffstatus gesteuert.

In dieser Doktorarbeit wurde das regulatorische Netzwerk untersucht, das die Seneszenz steuert, mit Schwerpunkt auf Transkriptionsfaktoren der WRKY-Familie. WRKY53 fungiert als zentraler Regulator, aktiviert seneszenzassoziierte Gene (SAGs) und integriert Umweltsignale, insbesondere über H_2O_2-abhängige Aktivierung. WRKY-Faktoren bilden ein Netzwerk, da ihre Promotoren häufig WRKY-Bindungsmotive enthalten. Innerhalb dieses Netzwerks aktiviert WRKY25 *WRKY53*, während WRKY18 es hemmt; Mutanten eines der beiden Gene zeigen jedoch beschleunigte Seneszenz, was auf komplexe Regulation hinweist. Untersuchungen des WRKY25–WRKY18–WRKY53-Subnetzwerks zeigten, dass WRKY25 als dualer Regulator wirkt, ROS wahrnimmt und das Netzwerk unter oxidativem Stress ausbalanciert. Domänenspezifische Analysen zeigten unterschiedliche Rollen der N- und C-terminalen Regionen von WRKY25. WRKY25 wird als Redox-Schalter vorgeschlagen, der *WRKY53* über andere Netzwerkkomponenten moduliert.

Ein neuartiger Feedback-Mechanismus zwischen H_2O_2, Katalasen und WRKY53 wurde identifiziert. WRKY53 wird durch H_2O_2 transkriptionell aktiviert, während Katalasen direkt mit WRKY53 interagieren, was zu gegenseitiger Inaktivierung führt. Dies zeigt eine fein abgestimmte redoxabhängige Regelungsschleife.

Darüber hinaus wird WRKY53 von Transkriptionsfaktoren anderer Familien kontrolliert. Der HD-ZIPIII-Faktor REVOLUTA (REV) wirkt als positiver Regulator von WRKY53 und seiner H_2O_2-Antwort. Die Regulation von REV durch TIFY-Proteine erfolgt über zwei Wege: einen JA-unabhängigen über TIFY8 und einen JA-abhängigen über PEAPODs und mehrere JAZ-Proteine.

Diese Arbeit liefert neue mechanistische Einblicke in die transkriptionelle und posttranskriptionelle Regulation der Pflanzen-Seneszenz. Sie zeigt, wie Transkriptionsfaktoren Umweltsignale direkt wahrnehmen und in Entwicklungsprogramme integrieren. Die Ergebnisse erweitern das Verständnis der Seneszenz und eröffnen vielversprechende Möglichkeiten zur Optimierung von Ertrag und Qualität durch gezielte Manipulation der Seneszenzprozesse.

4. List of publications/manuscripts of the dissertation

1. The transcription factor WRKY25 can act as redox switch to drive the expression of WRKY53 during leaf senescence in Arabidopsis, Ana Gabriela Andrade Galan, Jasmin Doll, Edda von Roepenack-Lahaye, Natalie Faiss, and Ulrike Zentgraf, Scientific Reports, 2025

2. The Non-JAZ TIFY Protein TIFY8 of Arabidopsis thaliana Interacts with the HD-ZIP III Transcription Factor REVOLUTA and Regulates Leaf Senescence, Ana Gabriela Andrade Galan, Jasmin Doll, Svenja Corina Saile, Marieluise Wünsch, Edda von Roepenack-Lahaye, Laurens Pauwels, Alain Goossens, Justine Bresson and Ulrike Zentgraf, International Journal of Molecular Science, 2023

3. Complex Formation between the Transcription Factor WRKY53 and Antioxidative Enzymes Leads to Reciprocal Inhibition, Ana Gabriela Andrade Galan, Jasmin Doll, Natalie Faiss, Patricia Weber, and Ulrike Zentgraf, Antioxidants, 2024

Nr.	**Accepted manuscript (peer-reviewed) yes/no**	**№ of authors**	**Position of candidate in list of authors**	**Scientific ideas by the candidate (%)**	**Data generation or/and programming by the candidate (if applicable) (%)**	**Analysis/ interpretation/ technical work by the candidate (if applicable) (%)**	**Paper writing done by the candidate (%)**
1	yes	5	1	70	90	95	90
2	yes	9	1	25	50	50	10
3	yes	5	1	10	30	35	10

5. Additional publications not discussed in this thesis

1. Specificity of H_2O_2 signaling in leaf senescence: is the ratio of H_2O_2 contents in different cellular compartments sensed in Arabidopsis plants?, Ulrike Zentgraf, Ana Gabriela Andrade Galan, Stefan Bieker, Cellular and Molecular Biology Letter, 2022
2. Editorial for Special Issue “Leaf Senescence” in Plants, Ulrike Zentgraf, Ana G. Andrade, Jasmin Doll, Plants, 2021

In this case, my contribution consisted of assisting in writing, reviewing, and editing the two reviews mentioned above, which are included in the Appendix section.

6. Introduction

6.1 Senescence and its agricultural importance

Crop plants play an undeniably crucial role in producing food, fiber, and even fuel for humanity. The successful cultivation of these plants depends on their fitness, which in turn requires the proper initiation and progression of senescence [1,2].

Senescence is an age-dependent, programmed phase that occurs throughout a plant's development. It manifests at various levels. At the whole-plant level, senescence results in the death of the entire plant, as observed in crops like rice, corn, and soybean. The most impressive example at the organ level is the color changes and eventual death of leaves during autumn in perennial trees [3–6]. All these changes involve highly regulated processes, such as the transport and remobilization of minerals and nutrients, alongside a decline in photosynthetic capacity.

The aim of senescence is the remobilization of nutrients from leaves to developing organs or storage tissues to ensure the viability of the next generation or growing season. This nutrient redistribution is vital for maintaining the quality of agricultural products [1–3,6,7].

Additionally, senescence plays a significant role in determining the shelf-life of fresh vegetables, fruits, and flowers. Stress conditions during harvest, storage, and transportation can accelerate the onset and progression of post-harvest senescence, severely affecting shelf-life performance. Post-harvest senescence can also alter nutrient content and the profile of volatile organic compounds, which, for example, may impact the aroma of vegetables and salads [8,9].

Given these factors, senescence is closely associated with crop yield especially in terms of both quantity and quality [1,3]. However, the relationship between senescence and plant productivity is complex. A key challenge is finding the right balance between maximizing yield by full photosynthetic capacity or by promoting senescence to reallocate nutrients and minerals in crops where non-leaf biomass is harvested [3]. In this context, understanding the processes and regulatory mechanisms of senescence is fundamental in plant research. Such insights provide essential knowledge and tools to manipulate this trait, improving both the productivity and quality of valuable crops.

6.1.2 Leaf senescence

Leaves are a defining feature of plants as autotrophs, enabling them to produce their own nutrients through photosynthesis. During their development, leaves become photosynthetically

active and serve as reservoirs for accumulated nutrients [6,10]. During senescence, plants strategically sacrifice older leaves for their overall benefit. The primary purpose of leaf senescence is to remobilize nitrogen, carbon, and mineral resources from senescing tissues to developing parts of the plant before the leaves ultimately die. This process enhances the plant's fitness, ensures optimal production of offspring, and supports plant survival [2,3,6,8].

Leaf senescence can be categorized into two types: **sequential and monocarpic leaf senescence. Sequential leaf senescence** occurs before anthesis, allowing nutrients to be reallocated from older leaves to newly developing, non-reproductive organs [8]. On the other hand, **Monocarpic Leaf Senescence** occurs after anthesis and governs the redistribution of nutrients to the now developing reproductive organs (Figure 1). In monocarpic plants, all leaves may undergo senescence, eventually leading to the death of the entire plant [8].

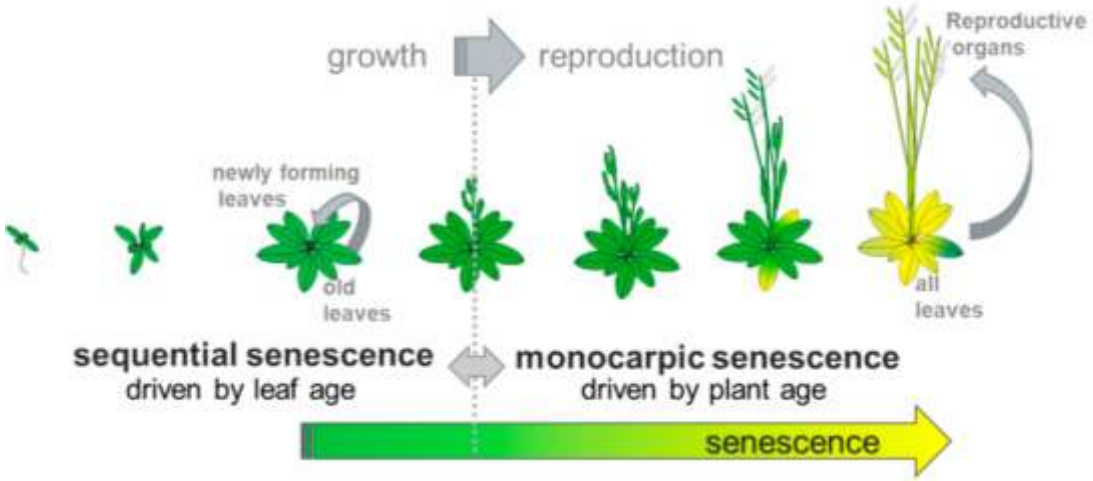

Figure 1: In the model plant *Arabidopsis thaliana*, leaf senescence occurs throughout plant development. During the transition from the vegetative growth phase to the reproductive phase, the pattern of senescence changes: it shifts from sequential senescence, where leaves age progressively over time, to monocarpic senescence, where the entire plant undergoes a coordinated senescence program associated with reproduction (taken from [11])

The primary driving force behind leaf senescence is the plant's developmental age. However, this process is far from being a passive journey toward the plant's demise. On the contrary, it is a highly active and coordinated process. Leaf senescence is not only developmentally programmed but also involves complex interactions with various environmental or external signals. These cues must be integrated with age-related information to fine-tune the onset, progression, and completion of senescence [1,3,5,12].

Consequently, senescence regulation involves multiple layers of control, including transcriptional and post-transcriptional mechanisms, protein modifications, and signaling pathways mediated by hormones and other small molecules like reactive oxygen species (ROS) [4,5,10,12,13].

6.2 Signaling molecules in senescence

Senescence‘s timing and progression requires a high degree of flexibility. Plant cells must perceive various cues or signals that trigger senescence[3,12]. These include not only developmental signals but also environmental factors that induce senescence in response to changing conditions. This process involves complex signal transduction events, which engage multiple signaling components at different regulatory levels and interact with one another [14,15].

To date, almost all major phytohormones have been reported to play a role in senescence signaling pathways. Additionally, over the last two decades, H_2O_2 and other ROS have been identified as signaling molecules in the regulation of senescence.

6.2.1 Phytohormones

Developmental- or-stress induced-leaf senescence is regulated by antagonistic and synergistic actions of various hormones. However, it has been suggested that phytohormones like auxin and brassinosteroids (BRs) may affect senescence by modulating plant development. On the other hand, ethylene, jasmonates (JAs), salicylic acid (SA) and abscisic acid (ABA) appear to modulate senescence primarily by responding to environmental cues and stress [14]. So far, the early signaling events after hormone perception have been identified but less is known about the molecular mechanisms that trigger the changes leading developmental senescence. In this context, this thesis is focused on getting more insights on the action of jasmonates (JAs) including jasmonic acid (JA), jasmonate isoleucine conjugate (JA-Ile), and methyl jasmonate (MeJA).

6.2.1.1 Jasmonates (JAs)

During plant growth JAs regulate a wide range developmental processes such as seed germination, root growth, fertility, senescence and plant defense against biotic and abiotic stresses [16]. JAs were first linked to senescence through an experiment demonstrating that exogenously applied methyl jasmonate accelerated leaf senescence [17]. Later, it was shown in Arabidopsis that JAs activate senescence-associated promoters in 14 out of 125 senescence-enhancer trap lines [18]. In addition, the application of methyl jasmonate increments the

transcript abundance of the genes associated with age-dependent senescence like SEN4, ERD1, and SAG2 [19,20].

Genes involved with JA synthesis (e.g. LOX3, AOC1, AOC4, and OPR3) and signaling (e.g. MYC2, JAZ1, JAZ6, and JAZ8) display an increased expression which occurs before chlorophyll loss from the tissue during developmental leaf senescence [21]. Additionally, it has been observed that endogenous JA content increases in senescence leaves compared to non-senescing ones [21,22]. Even though there is large research on JA and senescence as well as the role of JAs in the initiation of senescence, the mechanism by which they behave as signals is still not clear.

6.2.2 Reactive oxygen species (ROS): H_20_2

ROS are oxygen-containing molecules with a chemical reactivity higher than molecular oxygen (O_2) [23]. In all organisms, aerobic cellular processes are characterized by high rates of electron or energy transfer. This aerobic metabolism inevitably generates ROS through energy transfer to, or partial reduction of, O_2 [23–25]. ROS can also be produced by multiple enzymatic reactions, either as primary products or by-products [26]. The major forms of ROS in plants are singlet oxygen ($^1O_2$), superoxide ($O_2^{\cdot-}$), hydrogen peroxide (H_2O_2), and hydroxyl radical ($HO^{\cdot}$) [23–26]. Almost all ROS have very short half-lives and relatively high oxidation potentials. Whereas the estimated lifetime of $HO^{\cdot}$ is on the order of nanoseconds, that of $^1O_2$ is on the order of microseconds. H_2O_2, and $O_2^{\cdot-}$ have considerably longer lifetimes, ranging from milliseconds to seconds. Additionally, $O_2^{\cdot-}$, H_2O_2, and $HO^{\cdot}$ are produced in almost every cellular compartment [23,27].

It is widely known that the high production of these molecules leads to toxicity and cellular damage. To counteract this, plants have developed and expanded a range of enzymatic and non-enzymatic ROS scavengers [23,25–27]. Each production site is endowed with antioxidant systems to buffer the local redox environment. Interestingly, fluctuations in environmental conditions lead to changes in compartmental redox balance and ROS homeostasis [23,24].

Over the past few decades, the concept of ROS as harmful oxidative molecules has been extended and their role as signaling molecules in processes like pathogen infection or wounding has been included [23,25,26,28–30]. In this context, ROS production and scavenging require a delicate balance that must be maintained in all cellular compartments. Various compartment-specific systems can sense and regulate processes such as gene expression [23–27].

During the past two decades, the role of ROS, especially H_2O_2, as signaling molecules during both developmental and stress-induced senescence has been identified [24,31]. ROS can influence a variety of physiological changes by oxidizing almost all types of macromolecules [23,24,26]. Alternatively, ROS can modulate regulatory processes by directly impacting gene expression through changes in the expression and activity of transcription factors [23,24].

ROS levels are controlled by both production and scavenging. Studies have identified a network of at least 152 genes involved in managing ROS levels in Arabidopsis [24,25]. Moreover, in Arabidopsis and oil-seed rape, a senescence-related H_2O_2 elevation lasts for more than a week during the induction of monocarpic senescence. This contrasts with the oxidative burst signal observed after pathogen infection or wounding, which lasts for minutes to hours [24,31]. This long-term intracellular increase in H_2O_2 at the onset of monocarpic senescence is mainly due to sophisticated regulation of the H_2O_2 scavenging activities of catalases (CAT) and ascorbate peroxidases (APX), at least in Arabidopsis and oil-seed rape [24,31].

6.3 Molecular Regulation of Senescence

6.3.1 Antioxidative enzymes

As previously mentioned, H_2O_2 acts as a signaling molecule during senescence, along with other ROS, however, excessive accumulation can be harmful to cells. Thus, maintaining a balance between ROS production and scavenging is essential. Both non-enzymatic ROS scavenging molecules and antioxidative enzymes contribute to stabilizing ROS levels. Catalases (CAT), ascorbate peroxidases (APX), and superoxide dismutase (SOD) are present in various cellular compartments in multiple isoforms to fulfill this role [32,33].

The long-term intracellular increase of H_2O_2 at the onset of monocarpic senescence in *Arabidopsis* and oilseed rape is primarily achieved through tight regulation of CAT and APX activities [24,31]. During bolting, *CAT2* expression declines due to the bZIP transcription factor G-Box binding factor 1 (GBF1), which inhibits *CAT2* transcription [24,33,34]. This suppression reduces catalase activity, leading to an increase in intracellular H_2O_2, as CAT2 accounts for approximately 80% of total CAT activity in leaves and has a high turnover rate [35]. Interestingly, APX1 activity decreases simultaneously during bolting and flowering, even though its gene expression remains unchanged. This reduction appears to occur post-transcriptionally, as H_2O_2 can damage the component 1 of APX1, resulting in its inactivation. Thus, APX activity can be inhibited by its own substrate, H_2O_2; however, this inhibition occurs only during bolting and flowering [36,37]. Exogenous H_2O_2 application is effective only during

these stages, suggesting that APX1 becomes sensitive to H_2O_2 through a yet unknown mechanism. Consequently, H_2O_2 concentration increases further during this period, creating a positive feedback loop. As the plant continues to develop, APX1 inhibition ceases, while *CAT3* expression and activity rise, partially restoring antioxidative capacity [33,34,36,37].

In fact, this model is supported by *gbf1* mutants, in which *CAT2* downregulation is abolished, eliminating the H_2O_2 increase and making it impossible to initiate a positive feedback loop via APX1 inhibition. As a result, these mutants exhibit delayed senescence due to the absence of long-term H_2O_2 accumulation [34].

Interestingly, all three catalase genes have been identified as direct target genes of *WRKY53*[38]. Additionally, an increase in *WRKY53* expression has been observed, corresponding to the long-term intracellular accumulation of H_2O_2. This is particularly noteworthy, as WRKY53 expression has also been shown to be induced by H_2O_2 [24,33].

6.3.2 Transcriptional Regulators of Senescence

The regulation of the onset, progression, and completion of leaf senescence is highly coordinated and requires a massive reprogramming of gene expression. Temporal profiling of the transcriptome during Arabidopsis leaf senescence has revealed that several thousand genes (approximately 12-16%) are upregulated and downregulated during the onset and progression of senescence in *Arabidopsis thaliana* [3,21,39–42]. For example, genes related to photosynthesis are downregulated, and others related to the breakdown of cellular components and mobilization of nutrients and minerals are upregulated. In fact, 827 genes whose transcript levels were increased at least 3-fold during leaf senescence were identified in a global study of gene expression in *Arabidopsis* leaves [40] including many known senescence-associated genes (SAGs). It has been reported that the key mechanisms that control the expression of these SAGs are the dynamic activation of transcription factors [43]. Two transcription factor families, namely WRKY and NAC factors, are notably overrepresented in the transcriptome of Arabidopsis during senescence [41,42,44,45].

NAC transcription factors typically possess a highly conserved N-terminal NAC domain responsible for DNA binding and dimerization, while the diverse C-terminal domains function as transcriptional regulatory domains (TRD)[46]. Similar to the WRKY factors, these transcription factors form complex regulatory networks that act as control systems for leaf senescence [46]. In *Arabidopsis*, over 30 NACs show enhanced expression during normal leaf senescence. As examples, ANAC092/ORESARA1 (ORE1), ANAC029/*Arabidopsis* NAC-

LIKE Activated by AP3/PI (AtNAP), ANAC059/ORESARA1 SISTER1 (ORS1), and ANAC016 have been identified as positive regulators, while ANAC042/JUNGBRUNNEN1 (JUB1) and ANAC083/VND-INTERACTING2 (VNI2) function as negative regulators of leaf senescence [47–50].

6.3.2.1 WRKYs transcription factors

WRKYs are one of the intensively studied families of transcription factors in senescence, with their regulatory role already characterized across various plant families [10,45,51]. The WRKY transcription factor family is defined by a highly conserved **WRKYGQK** amino acid sequence in their DNA-binding domain (DBD), which gives the family its name [52,53]. This DBD, known as the WRKY domain, is approximately 60 amino acid residues long and is typically located at the N-terminus. Additionally, WRKY DNA binding domains (DBDs) possess a characteristic zinc finger structure at their C-terminal end [51–55].These features allow WRKY transcription factors to be classified into three groups based on the number of WRKY domains and the type of zinc finger they possess. Group I is unique in having two WRKY domains, whereas groups II and III have only one. Furthermore, group II contains a C-X_{4-5}-C-X_{22-23}-H-X-H (C2H2) zinc finger, while group III features a C-X_7-C-X_{23}-H-X-C (C2HxC) zinc finger. The WRKY domain binds to a consensus motif (C/TTGACC/T), referred to as the W-box, which is present in the promoters of their target genes [44,52–55].

One particularly intriguing feature of WRKY transcription factors is that their own promoters can harbor one or more W-boxes (Figure 2) [53,54]. The ability to regulate themselves and each other suggests the formation of a sophisticated WRKY-driven transcriptional network. In addition, WRKY proteins can physically interact with each other and with other associated proteins, forming homo- and/or heterodimers, or even higher-order complexes with diverse functional properties (Figure 2). These interactions also highlight their role in regulatory processes that require fine-tuned control [10,51,52].

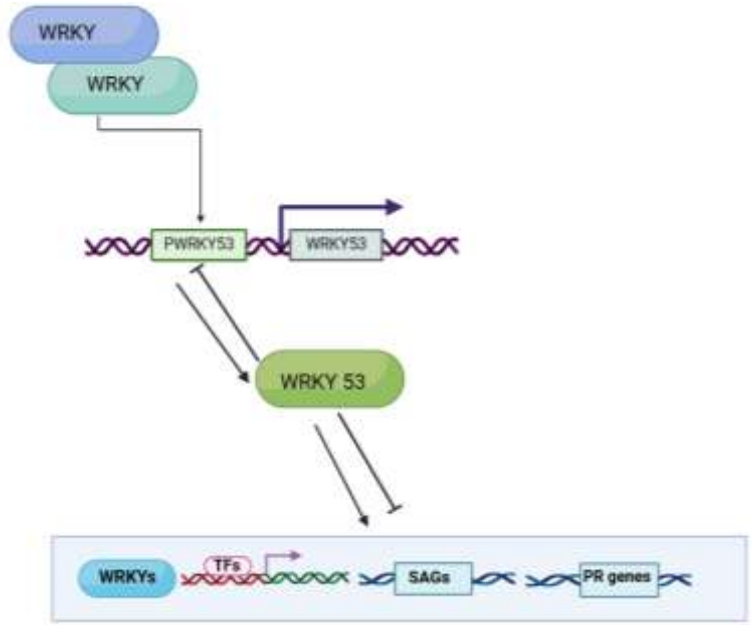

Figure 2: WRKY transcription factors contain one or more W-box elements within their own promoters. This arrangement establishes a complex regulatory network, allowing WRKY proteins to regulate not only other WRKY genes but also themselves in positive or negative feedback loops, as observed for WRKY53.

Several WRKY factors have been identified as regulators of leaf senescence in *Arabidopsis*. These include WRKY6 [56], WRKY22 [57], WRKY26 [58], WRKY42 [59], WRKY45 [60], WRKY53 [38,61], WRKY54 [62], WRKY55 [63], WRKY70 [62], WRKY71 [64], and WRKY75 [65]. Among these, WRKY53 has been extensively studied and is recognized as a key component of the complex regulatory network governing senescence. This recognition stems from its tightly regulated expression and activity and its significant biological relevance during the senescence process. WRKY53 functions as a positive regulator of developmental senescence, exhibiting interesting sequential and monocarpic senescence-associated expression patterns [38,61].

WRKY53 is tightly regulated by multilayered mechanisms that control its expression, activity, and protein stability. At the onset of senescence, epigenetic regulation and activation of the WRKY53 locus are observed, marked by changes in histone modifications such as H3K4me2 and H3K4me3 [66,67]. In contrast, DNA methylation remains low and unchanged during this process [68].

WRKY53 activity is regulated by proteins such as mitogen-activated protein kinase kinase (MEKK1) and the epithiospecifying senescence regulator (ESR/ESP). MEKK1 binds directly

to the promoter of the *WRKY53* gene, facilitating the switch from leaf age-dependent to plant age-dependent expression. Additionally, MEKK1 can phosphorylate the WRKY53 protein, enhancing its DNA-binding activity [68,69]. On the other hand, WRKY53 interacts with ESR/ESP at the protein level, and ESR/ESP inhibits its DNA-binding activity. The expression of ESR/ESP and WRKY53 is antagonistically regulated in response to jasmonic acid (JA) and salicylic acid (SA), with each protein capable of negatively affecting the expression of the other. Besides that, ESP/ESR is involved in defense response, therefore this interaction creates a crosstalk between senescence and pathogen response [70].

WRKY53 expression is also regulated by other transcription factors, such as activation domain protein (AD-protein) and GATA4. The AD-protein, through autophosphorylation, increases its DNA-binding activity at the *WRKY53* promoter region, leading to changes in *WRKY53* transcription levels and positioning it as a positive regulator of *WRKY53* expression [68,71]. Similarly, GATA4 is a positive regulator of *WRKY53* expression, with its levels varying in leaves according to the plant's age [68].

In this context, it became evident that WRKY53 is influenced, regulated by, and capable of interacting with multiple proteins. Notably, at least 12 proteins - or possibly more - have been reported to bind to the promoter of WRKY53[68]. Moreover, WRKY53 can interact with itself as well as with other WRKY proteins, such as WRKY30, as reported [62].

Interestingly, WRKY18 and WRKY25 have been identified as effective regulators of *WRKY53* expression. WRKY18 serves as a negative upstream regulator, a downstream target, and a protein interaction partner of WRKY53 [72]. In contrast, WRKY25 acts as a positive upstream regulator, also functioning as a downstream target and protein interaction partner [73]. Moreover, these two WRKYs exhibit altered senescence-associated phenotypes. For example, *wrky18* mutant plants show an accelerated senescence phenotype, consistent with its role as a repressor of *WRKY53* [73]. Interestingly, *wrky25* mutants also show accelerated senescence, which is inconsistent with its role as an activator of *WRKY53* expression [72]. This suggests that WRKY18, WRKY25, and WRKY53 interact and regulate each other in a more complex manner, indicating another unknown level of regulation among them. They may form a subnetwork that influences senescence through WRKY53.

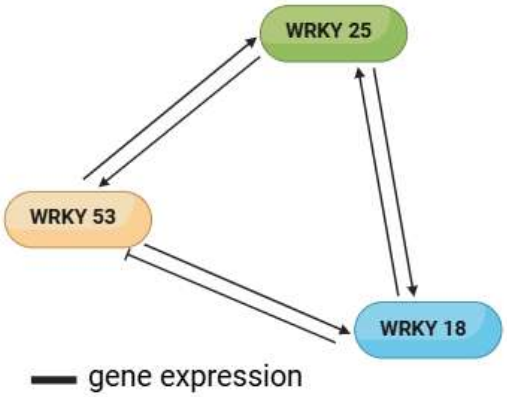

Figure 3: The small regulatory subnetwork involving WRKY18, WRKY25, and WRKY53. In this network, WRKY18 functions as a negative upstream regulator and is also a downstream target of WRKY53, whereas WRKY25 acts as a positive upstream regulator and simultaneously serves as a downstream target. Moreover, WRKY25 can activate *WRKY18* expression and *vice versa*

6.3.2.2 Other transcription Factors

In addition to the small WRKY subnetwork mentioned above, another transcription factor, namely REVOLUTA (REV), can interact with the *WRKY53* promoter [74,75]. REV is a member of the class III homeodomain leucine zipper (HD-ZIPIII) transcription factor family, known for its involvement in several developmental processes during early plant development [76,77]. This family plays crucial roles in embryo patterning, meristem initiation and homeostasis, lateral organ polarity, inflorescence architecture, ovule development, and vascular development in Arabidopsis. More specifically, REV specifies the domain that later develops into the upper side of the leaf, establishing the dorsoventral axis of leaves. Additionally, REV plays multiple roles in meristem organization, leaf polarity setup, and vascular development [76–79].

REV possesses four characteristic functional domains from N-terminus to C-terminus: the homeodomain responsible for DNA binding; the basic leucine zipper domain (b-ZIP) responsible for DNA-binding and dimerization; a highly conserved lipid or steroid-binding START (Steroidogenic acute regulatory protein-related lipid transfer) domain; and the C-terminal MEKHLA domain [76–80].

CHiP-Seq analysis identified two REV-binding sites in the *WRKY53* promoter [74,81]. In fact, *WRKY53* expression can be promoted by REV, as demonstrated by the *rev5* mutant, which shows a lower *WRKY53* expression and a strong delayed senescence phenotype. This indicates that REV is involved in later stages of development and serves as an important driver of age-

induced senescence by controlling the expression of *WRKY53* and other SAGs [74]. Notably, the interaction between REV and the *WRKY53* promoter depends on the developmental stage [74]. During senescence progression, REV changes its binding preferences to different sites in the *WRKY53* promoter. Additionally, the activation of *WRKY53* expression by REV appears more effective at the onset of monocarpic senescence, suggesting that REV can adapt its properties according to developmental stages. These findings also imply that REV requires specific modifications or interaction partners to activate *WRKY53* expression during senescence [74].

In addition, it has been observed that several proteins can interact with both the native REV and a truncated version lacking the MEKHLA domain. Among these proteins, a non-canonical member of the TIFY family, TIFY8, has been identified [82]. This large, plant-specific transcription factor family is characterized by the highly conserved TIFY domain. The TIFY domain, from which the family derives its name, is highly conserved, consisting of approximately 28 amino acids and a core TIF[F/Y]XG motif within a zinc-finger [83].

The 18 members of the TIFY family in Arabidopsis can be categorized into two classes based on the presence of a C2C2-GATA domain. Class I, which consists of three members, is characterized by the presence of this domain, whereas the remaining 15 members belong to Class II and lack it. Class II includes the 12 Jasmonate ZIM domain (JAZ) proteins [83,84].

The 12 JAZ proteins are distinguished from the other TIFY proteins by the presence of a C-terminal region known as the Jas domain, which facilitates interactions with several transcription factors (e.g., bHLH- and R2R3-MYB-type factors) that regulate various JA-dependent responses [85]. Additionally, the Jas domain mediates interaction with CORONATINE-INSENSITIVE1 (COI1), the F-box subunit of the E3-ubiquitin ligase complex SCF^{COI1}. Jasmonoyl-L-isoleucine (JA-Ile) can bind to the Jas domain, acting as a "molecular glue" between the JAZ proteins and COI1. Consequently, in the presence of JA-Ile, this interaction directs JAZ proteins to 26S-mediated proteasomal degradation [20,85] .

Furthermore, the ZIM domain mediates both homo- and heterodimerization among JAZ proteins. This domain also enables the recruitment of the co-repressor TOPLESS (TPL) through interaction with the NOVEL INTERACTOR OF JAZ (NINJA) protein [84,86]. NINJA interacts with TPL via its ETHYLENE RESPONSE FACTOR (ERF)-associated amphiphilic repression (EAR) motif. In this complex, the presence of TOPLESS inactivates JAZ-bound

transcription factors. However, in response to JA-Ile, these transcription factors can be rapidly released and activated [86].

Unlike JAZ proteins, PEAPOD1 (PPD1) and PEAPOD2 (PPD2), the other two members of Class II, contain an additional N-terminal PPD-domain and a divergent C-terminal Jas domain (Figure 4) [85]. These PEAPOD proteins are known to be negative regulators of meristematic proliferation, playing a role in organ size regulation. They are also involved in controlling curvature and lamina size in Arabidopsis. Unlike JAZ proteins, which recruit TOPLESS via NINJA, PEAPOD proteins recruit TOPLESS via KIX8 (KINASE INDUCIBLE DOMAIN INTERACTING8) or KIX9 [87].

Interestingly, the last member of Class II, TIFY8, is even more divergent, as it lacks any specific protein domains beyond the ZIM domain. Despite having a functional ZIM domain, no interactions with JAZ proteins have been observed (Figure 4) [85]. As TIFY8 lacks the Jas domain, its stability is not affected by JA treatment. Additionally, no direct DNA-binding activity has been reported. Nevertheless, TIFY8 can interact with the PEAPOD proteins PPD1 and PPD2, as well as with NINJA in Arabidopsis. Moreover, KIX8 and KIX9 have been identified in TIFY8 protein complexes in Arabidopsis [85]. However, the interaction with REV implies a new possible function of TIFY8, either in early leaf development or senescence or both.

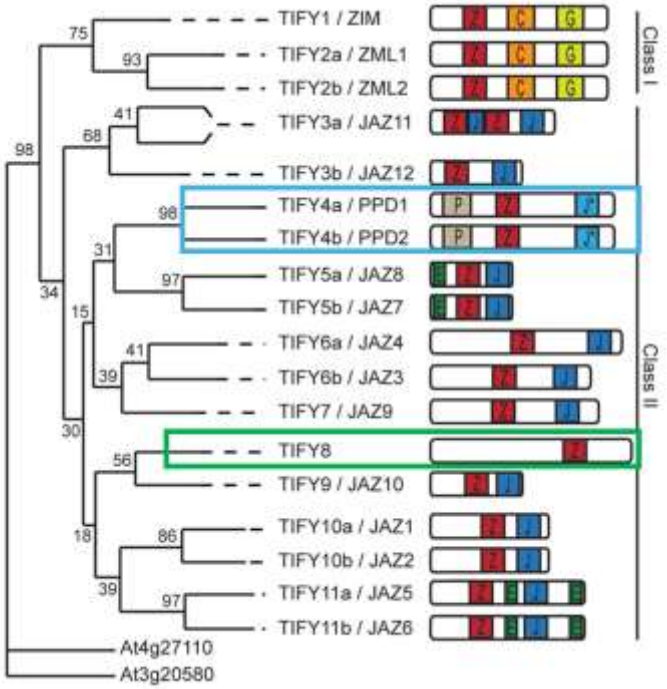

Figure 4: The TIFY protein family in *Arabidopsis thaliana*. A phylogenetic tree of Arabidopsis TIFY family members constructed based on the protein sequences of the ZIM (**Z**inc finger protein expressed in **I**nflorescence **M**eristem domain (Z). Additional protein domains are indicated as follows: C (**C**ONSTANS, **C**O-like, and **T**OC1 (CCT) domain); G (C2C2-GATA zinc-finger); P (**P**EA**P**OD (PPD) domain); J (Jas domain); J* (Jas-like domain); E (EAR domain). (Figure taken from [85]*).*

7. Objectives

Leaf senescence is primarily governed by developmental age. It is an active, complex, and highly regulated process in which leaf cells undergo tightly controlled changes in cell structure, metabolism, and gene expression. In addition to age, senescence is influenced by internal and environmental signals. The onset and progression of senescence represent an integrated response of leaves to these factors, yet one key question remains: how does a plant sense and integrate these parameters into the senescence program? Over the past decades, research has sought to answer this question. It is well known that nearly all plant hormones influence the senescence program in either antagonistic or synergistic ways. Also, a role as signaling components for small molecules such Ca^{2+} and more recently the reactive oxygen species, especially H_2O_2 has been established.

WRKY53 is a positive regulator of senescence, while WRKY18 acts as a strong negative regulator, and WRKY25 serves as a positive regulator of *WRKY53* expression during senescence. Both are also downstream targets and protein interaction partners. This suggests that the regulatory relationship among these three WRKY factors is more complex than previously assumed and is likely organized through a small yet intricate subnetwork. However, the molecular mechanisms governing interactions within WRKY18/WRKY25/WRKY53 subnetwork and their correlation with leaf senescence remained elusive. The first aim of this study was to investigate this subnetwork in more detail, focusing on characterizing the interactions, specificity, and selectivity of WRKY18, WRKY25, and WRKY53. By dissecting their protein structures, further insight into the functional impact of the different domains on transcriptional regulation and on senescence should be gained. Moreover, the potential role of H_2O_2 as a signaling molecule that directly influences this subnetwork through the redox-sensitive WRKY25, possibly via a specific structural feature, should be analyzed.

As a second goal, this study explores additional regulatory levels of WRKY53. Previous studies have shown that *WRKY53* expression is regulated by transcription factors beyond WRKYs. One such factor is REV, which can interact with TIFY8. Therefore, I analyzed the interaction interface between REV and TIFY8 in more detail and investigated its biological function in senescence. Additionally, I aimed to determine whether JAs plays a role in TIFY8-REV regulation.

Furthermore, *WRKY53* expression can be induced by H_2O_2, while at the same time all three catalase genes are direct target genes of WRKY53 creating a feedback loop. On top of that, *in*

vivo pull-down experiments hinted at a direct interaction between antioxidative enzymes and the WRKY53 protein. Therefore, the third objective of this study was to verify these interactions, to analyze its impact on protein function, and to characterize this newly identified feedback loop involving WRKY53 and the antioxidative enzymes in more detail.

By integrating these approaches, this study enhances our understanding of plant senescence regulation because it constitutes a step forward in elucidating the molecular mechanisms underlying leaf senescence. Moreover, this study highlights the significant role of redox conditions in senescence but also in other plant regulatory processes.

8. Results, Discussion and Conclusions

Senescence is the final developmental stage of plant cells, tissues, organs, and ultimately, the entire plant. Consequently, it has a major impact on agronomically important traits such as crop yield quantity and quality like, e.g., grain protein content, fertilizer use efficiency, and even the shelf-life of fresh vegetables, fruits, and flowers [1–3,5]. This process aims to optimize nutrient remobilization from senescing parts -primarily leaves- towards young organs, seeds, or storage tissues.

Therefore, it involves dramatic changes in molecular programming and physiological processes in a highly coordinated and systematic manner. All these changes are required to be genetically controlled and tightly regulated, modulated in an age-dependent way. The initiation, progression, and termination of senescence are governed through multiple, intricate layers of control, including transcriptional and post-transcriptional regulation, protein modifications, and hormone signaling [6,10,88]. These regulatory networks must integrate, via the perception and transduction of a diverse array of signals, cues from the leaf's previous developmental stages, along with various endogenous and environmental factors such as age, sugar status, abiotic and biotic stresses, polyamines (PAs), phytohormones, and small molecules such as intracellular calcium and ROS [4,10,13].

Despite the importance of understanding senescence regulation as an integrated process, many aspects remain unclear. One of the most critical knowledge gaps lies in deciphering how plants perceive and integrate these diverse signals to activate the senescence program. While a precise initial signal(s) that triggers leaf senescence remains unidentified, significant progress has been made in elucidating key upstream components of the regulatory cascade. Specific transcription factors (TFs) have been shown to activate senescence-associated genes (SAGs) with diverse expression patterns. Here, the WRKY TF family has emerged as a well-established and central regulator of leaf senescence [52,55].

WRKY TFs are not only central regulators of senescence but also play essential roles in plant responses to pathogens and abiotic stresses such as drought and cold, underscoring the functional versatility of this TF family [89,90]. A defining feature of WRKYs is their ability to bind W-box elements -the minimal consensus sequences required for DNA-binding- present in their own promoters. This property enables both self-regulation and cross-regulation among WRKY family members. The capacity of WRKYs to bind their own or other WRKY gene promoters establishes feedback loops, both positive and negative, that finely tune gene

expression, facilitate the formation of dynamic transcriptional complexes, and coordinate the integration of multiple signaling pathways [52,54,89,91]. For example, several WRKYs are known to form regulatory subnetworks; in *Arabidopsis thaliana*, WRKY18, WRKY40, and WRKY60 constitute a well-established regulatory module in the basal immune response [92,93]. The formation of homo- and heterodimers is a common feature of WRKY protein interactions, promoting the assembly of transcriptional complexes with combinatorial functions. Mechanistically, the WRKY18–WRKY40–WRKY60 complex can act redundantly, synergistically, or antagonistically on defense-related genes such as *PR1* and *PDF1.2*, depending on the physiological context and the specific WRKY combinations involved [92]. This functional diversity is largely dictated by pathogen-induced co-expression and the presence of W-box elements in their promoters, supporting mechanisms of autoregulation and cross-regulation. Moreover, under different scenarios, the interactions among these TFs and their transcriptional regulation can follow distinct regulatory logics. For instance, these three WRKYs participate in ABA signaling, where WRKY18 and WRKY40 cooperate to activate the transcription of *WRKY60* in response to ABA [92,93].

In the context of senescence, WRKY54 and WRKY70 function cooperatively as negative regulators by modulating senescence-associated genes (SAGs) such as *SAG12* and *ORE1* [62]. Their direct protein-protein interaction enables coordinated transcriptional control. These two negative regulators, together with the positive regulator WRKY53, have also been shown to interact independently with WRKY30 in the regulation of senescence, with hormonal signals such as salicylic acid and ethylene modulating their activities [62,94].

WRKY53, WRKY54, and WRKY70 exemplify how a regulatory network can integrate both internal and environmental cues to control the onset and progression of leaf senescence, potentially through interactions with WRKY30, although this remains unclear [62]. Despite clear evidence supporting the formation of WRKY regulatory subnetworks, the mechanisms that confer specificity within these networks remain poorly understood. One proposed explanation is the influence of dimerization partners, which can shape both transcriptional regulation and biological function. Understanding this requires a detailed characterization of the structural properties of WRKY transcription factors.

Several studies have investigated the specific WRKY transcription factor's binding preference for specific promoter configurations and W-box motifs. Emerging evidence suggests that not only the W-box core sequence and its flanking nucleotides, but also the length and sequence of

spacers between W-boxes -and even their orientation (forward or reverse)- play critical roles in recognition specificity [90,95,96]. These studies have examined the molecular properties of WRKY DNA-binding domains (WRKY-DBDs), primarily using structural data from Group I and Group III members. For instance, WRKY1 (a Group I member) possesses two WRKY domains, with the N-terminal domain binding W-boxes more effectively and with a distinct binding mode compared to the C-terminal domain [97,98]. However, it remains unclear whether WRKY structure exerts a definitive influence on the specificity and diverse regulatory roles that WRKYs may adopt within their subnetworks. This complexity becomes even greater when integrating such analyses into the context of senescence.

This leads to one of the central questions addressed in our research: what determines the specificity of the interactions and the function as repressor or activator? In our study, we focused on WRKY53, a positive regulator of senescence and a central hub in the senescence regulatory network that is tightly controlled through multiple layers. In recent years, two additional WRKY transcription factors, both expressed at the onset of senescence, have been identified as regulators of *WRKY53* expression: WRKY18, which acts as a repressor, and WRKY25, which functions as an activator [72,73]. This finding is intriguing because, although *wrky18* mutant plants exhibit an accelerated senescence phenotype consistent with its role as a repressor of WRKY53, *wrky25* mutant plants also display accelerated senescence, seemingly inconsistent with WRKY25's proposed role as an activator [72,73]. Based on this observation, we propose that WRKY18, WRKY25, and WRKY53 may form a small regulatory subnetwork, in which they interact and regulate one another in a more complex manner than initially assumed. A key question, therefore, is how these interactions and regulatory mechanisms are coordinated within the subnetwork.

Notably, WRKY25 is the only member of this subnetwork belonging to Group I WRKYs, characterized by two WRKY domains located at the N- and C-terminal, whereas WRKY18 contains only a single WRKY domain. This raises the possibility that the number or arrangement of WRKY domains may be associated with their functional roles as activators or repressors. Importantly, WRKY25 has also been identified as a redox-sensitive transcription factor, prompting questions about the influence of ROS on subnetwork regulation, particularly in cooperation with WRKY18.

Our main hypothesis integrates two aspects: (i) WRKY25's domains may be directly involved in its regulatory and activating functions, and (ii) its redox sensitivity could enable it to

integrate environmental cues, specifically oxidative signals such as H_2O_2 content into the regulatory subnetwork. Such a mechanism would represent a pathway in which an environmental signal is directly sensed by a transcription factor through a structural feature, thereby advancing our understanding of plant senescence regulatory networks. However, our research did not address the broader physiological context in which oxidative signals change, beyond what has been described in the senescence framework.

Potschin et al. [72] screened the W-boxes of the *WRKY53* promoter for DNA–protein interactions with other leaf senescence-associated WRKY proteins. Out of the 15 WRKYs analyzed using ELISA-based DNA–protein interaction assays and reporter gene expression assays, WRKY18 and WRKY25 emerged as the strongest positive and negative regulators of the *WRKY53* promoter.

Among the 15 WRKYs expressed at the onset of senescence, it cannot be completely ruled out that, besides WRKY18 and WRKY25, which act as a repressor and an activator, respectively, other members may also influence *WRKY53* and, consequently, the small regulatory subnetwork that is the focus of this study. For example, WRKY6 and WRKY70 have been identified as a repressor and an activator, respectively, of *WRKY53* expression. These two WRKYs are also recognized as key nodes in the regulation of senescence [52,54,56]. However, I focused on the two strongest *WRKY53* regulators to identify possible mechanisms used within the WRKY networks

Unlike WRKY53, which is involved in the onset of senescence, WRKY6 coordinates senescence progression and stress-response signaling networks. It functions as a transcriptional activator during leaf senescence in *Arabidopsis*, activating different senescence-associated genes (SAGs). Its activity is finely regulated through crosstalk with hormonal signaling pathways, notably the salicylic acid (SA)-mediated NPR1–WRKY46–WRKY6 cascade and is further modulated by physical interaction with DELLA proteins, which repress *WRKY6* transcriptional activation under dark-induced senescence conditions [56,99]. In contrast, WRKY70 acts as a negative transcriptional regulator of leaf senescence in *Arabidopsis*, repressing SAGs and acting redundantly with WRKY54 to fine-tune senescence progression. It integrates SA and jasmonic acid (JA) signaling pathways to balance defense responses and the onset of senescence. Loss-of-function mutants of WRKY70 exhibit accelerated senescence, highlighting its critical role in senescence repression [62,94].

Although there is evidence for the role of WRKY6 and WRKY70 in senescence, there is no evidence that this regulation occurs together with, or through, WRKY53 [54,56,62,99]. Nonetheless, this does not rule out that WRKY53, as observed with WRKY18 and WRKY25, may potentially form subnetworks or integrate additional transcription factors depending on the biological context. Importantly, based on our evidence, WRKY25 and WRKY18 are the strongest activator and repressor, respectively, of *WRKY53* expression, and these characteristics are likely to define the functional dynamics of the proposed subnetwork.

Another interesting finding in our study is that WRKY25 and WRKY53 can repress their own expression while activating each other. This is not the case for WRKY18, which transcriptionally represses *WRKY53* and itself, adding further complexity to the analysis of this subnetwork.

The fact that WRKY25 belongs to Group I of the WRKY family, containing two WRKY domains and is a redox-sensitive protein, suggested that it might possess a unique functional feature within the subnetwork. Based on this, along with additional experimental evidence, we proposed WRKY25 as the primary modulator of this subnetwork. To investigate this, our efforts focused on determining the specific roles of its different domains in regulatory functions. Several studies on Group I WRKYs have primarily focused on the distinct roles of their two WRKY domains in DNA-binding and transcriptional activation. Initially, W-box binding was thought to be mediated solely by the C-terminal WRKY domain, as observed in studies of WRKY1 and WRKY4. In some cases, the N-terminal domain displayed weaker binding [100,101]. Maeo et al. [98] examined the DNA-binding mechanisms of tobacco WRKY transcription factors, highlighting conserved residues within the WRKY domains. Their study demonstrated that the C-terminal WRKY domain exhibits stronger binding affinity to the W-box (TTGACC) compared to the N-terminal domain. A similar pattern was observed in WRKY33, where the C-terminal DNA-binding domain (DBD) showed higher affinity and specificity for W-box sequences (TTGACC/T) than the N-terminal DBD. The N-terminal DBD binds W-boxes with lower affinity, suggesting a modulatory or stabilizing role in target gene recognition [97,100,102–104] . Notably, WRKY33 possesses a structural extension in its C-terminal domain (CTD) that is absent in WRKY25 [102].

In this thesis, I used and generated various deletion constructs and domain-swapping chimeras between WRKY18 and WRKY25 to determine the role of each domain. One chimera contained the N-terminal region of WRKY25, including its WRKY DBD1 (W25N–W18C), while another

contained the C-terminal region of WRKY25, including its WRKY DBD2 (W18N–W25C). Transactivation assays with these constructs demonstrated that both DNA-binding domains are required for a fully functional WRKY25 protein. Analysis of the chimeras revealed that the N-terminal domain of WRKY25 is essential for activating *WRKY53* expression. Specifically, the chimera containing the N-terminal domain of WRKY25 retained the ability to activate *WRKY53*, like the native WRKY25, whereas the chimera containing only the C-terminal DBD lost this capacity.

These results are consistent with studies on WRKY1, which showed that the N-terminal domains of Group I WRKYs can bind W-box DNA as effectively as, or even better than, the C-terminal domains, albeit through distinct binding modes [97]. This highlights the critical role of the N-terminal domain of WRKY25 in activating *WRKY53* and suggests that it is a key determinant of WRKY25's modulatory function within the subnetwork.

A notable peculiarity of WRKY25 is its inability to homodimerize, in contrast to WRKY18 and WRKY53, which do form homodimers. This feature highlights WRKY25 as a central modulator within the subnetwork, particularly because it can form heterodimers, especially with WRKY18, suggesting that the presence of a protein partner is necessary to modulate the regulatory dynamics of the subnetwork. In this thesis, the analysis demonstrated that both chimeras were able to interact with native WRKY18, with interactions involving the N-terminus of WRKY25 producing a stronger signal. In contrast, only the W25N–W18C chimera could form a dimer with WRKY25 itself. These results indicate a predominant role of the WRKY25 N-terminus in mediating protein–protein interactions, while the C-terminus appears to inhibit self-interaction. This observation aligns with previous findings emphasizing the importance of N-terminal leucine zipper sequences in mediating WRKY–WRKY interactions [105,106].

The WRKY18/WRKY25 heterodimer functions as an activator of *WRKY53* expression, despite WRKY18 alone, or as a homodimer acting as a strong repressor of both *WRKY53* and its own expression. Dimerization among WRKYs is widely documented, and it is particularly interesting that their DNA-binding activities and regulatory effects vary depending on the context. For instance, overexpression of *WRKY18* enhances resistance to *Pseudomonas syringae*, whereas co-expression with *WRKY40* or *WRKY60* renders plants susceptible to the pathogen. Similarly, the WRKY60–WRKY18 interaction increases *WRKY18*'s DNA-binding ability, while the WRKY60–WRKY40 interaction decreases *WRKY40*'s binding [93,107].

In this study, I speculated that WRKY25, in response to specific signals, shifts the balance between positive and negative effects on *WRKY53* expression within the subnetwork by sequestering WRKY18 into heterodimers. This reduces WRKY18's repressor activity and thereby enhances *WRKY53* expression. Complementation lines of *wrky25* mutant plants, generated using native *WRKY25*, deletion constructs, and chimeras between *WRKY25* and *WRKY18* cDNAs, further supported this modulatory role. Notably, the senescence phenotype of *wrky25* mutants appears to conflict with its direct activation of *WRKY53* expression, indicating that WRKY25 operates within a complex regulatory network, in which the loss of functional WRKY25 protein disrupts network balance and produces seemingly contradictory phenotypes.

A key observation from these lines is that the two WRKY25 domains appear to have opposing roles within the subnetwork: the N-terminal region promotes *WRKY53* expression, while the C-terminal region limits excessive *WRKY53* activation, fine-tuning senescence progression. This is evident in 7-week-old plants, where transformations with the two chimeras produced distinct outcomes: the presence of the WRKY25 N-terminus accentuated accelerated senescence, whereas the C-terminus partially delayed senescence relative to both *wrky25* and Col-0 plants. Corresponding changes in *WRKY53* expression levels further reflect the distinct contributions of each domain to subnetwork regulation.

Finally, transactivation assays in Arabidopsis protoplasts revealed that the chimera containing the N-terminus of WRKY25 switched from an activator to a repressor of *WRKY53* expression under oxidative conditions. This finding aligns with the observed downregulation of *WRKY53* under oxidative stress in these lines and suggests that both N- and C-terminal domains of WRKY25 are involved in transducing H_2O_2 signals, integrating environmental cues into the regulatory subnetwork.

Today, research, mainly in *Arabidopsis*, is uncovering key aspects of the ROS signaling pathway in plants, reinforcing the idea that ROS sensing mechanisms require specialized sensors capable of detecting ROS molecules such as H_2O_2. At the molecular level, initial ROS-sensing events include oxidative post-translational modifications (PTMs) of sensory proteins and the oxidation of metabolites [23] . There are at least three known mechanisms by which plant cells can sense ROS: first, through receptor proteins; for example, HPCA1, a plasma membrane–localized leucine-rich repeat receptor kinase, senses extracellular H_2O_2 via oxidation of two pairs of extracellular cysteine residues, triggering autophosphorylation and

activation of Ca^{2+} channels in guard cells [26,108]. Second, through redox-sensitive transcription factors, whose expression is modulated by ROS, including members of the WRKY, Zat, RAV, GRAS, and MYB families. Third, ROS can directly inhibit phosphatases; for instance, OXI1, a serine/threonine protein kinase, participates in ROS sensing and activates mitogen-activated protein kinases (MAPK3 and MAPK6), which function downstream of OXI1 to regulate defense mechanisms in response to ROS stress [26].

In this study, we propose WRKY25 as a direct ROS-sensing transcription factor and hypothesize that its capacity to sense H_2O_2 influences the dynamics of the WRKY18/WRKY25/WRKY53 subnetwork. Existing evidence indicated that the activity of the WRKY25 protein is redox-sensitive; however, the molecular basis of this sensitivity, whether direct or indirect, remained unclear.

Protein post-translational modifications can alter protein function or stability by covalently attaching functional groups or through other chemical alterations, and cysteine residues can form disulfide bonds that are essential for maintaining structure and stability [23,26]. Interestingly, these cysteine bonds can also act as redox switches regulating protein activity. To explore how WRKY25 senses H_2O_2, I first focused on cysteine 17, the only cysteine in the WRKY25 protein outside of the essential zinc finger for the DNA-binding domain. Transactivation assays with a WRKY25 C17 mutant under oxidative stress showed no significant changes in redox response, suggesting that this residue is not involved in ROS sensing. WRKY25 contains four additional cysteines that participate in the DNA-binding zinc finger structure, which were not mutated to preserve protein integrity, leaving open the possibility that one or more of these residues mediate redox sensitivity, and further research is needed to investigate this hypothesis.

Beyond disulfide bridges, regulatory switches involving covalent crosslinks such as NOS and SONOS bridges, covalent links between cysteine and one or two lysine residues, have recently been described as allosteric redox switches. These covalent lysine-cysteine redox switches are widespread, including DNA-binding proteins, where NOS formation often interferes with DNA–protein interactions [109,110]. Based on this, I investigated whether WRKY25 might contain such redox switches. AlphaFold modeling predicted two potential redox switches within the N-terminal and C-terminal DNA-binding domains of WRKY25. In contrast, WRKY18, known to be redox-insensitive, lacks these predicted switches; notably, the lysine residue occupying the equivalent position in WRKY25's WRKY domain is absent in

WRKY18. Chimeric constructs containing the N-terminal or C-terminal domains of WRKY25 retained the respective predicted redox switch, consistent with oxidative signal sensitivity observed in transactivation assays and in planta complementation lines.

To investigate this further, I first applied oxidative conditions directly *in planta* by treating plants with H_2O_2 or 3-amino-1,2,4-triazole (3AT). Arabidopsis seedlings of overexpressor and mutant lines exhibited significant changes in gene expression based on qPCR results that aligned with our hypothesis. I also attempted a similar approach in tobacco leaves, combining oxidative treatments with BiFC interaction assay, but obtaining conclusive results in this system proved challenging. Next, I investigated whether protein structural changes occur under ROS conditions with the help of Edda von Roepenack-Lahaye of our analytic department. The purified recombinant WRKY25 proteins were digested, and the resulting peptides were analyzed using LC–MS. Interestingly, we detected evidence supporting the presence of putative redox switches, as NOS-linked peptides were detectable. However, without isotopically labeled synthetic standard peptides, no quantitative conclusions can be drawn about the relative abundance of these modified peptides in the digested protein, since different peptides may have variable response factors. Nonetheless, the detection of mass/charge signals -each confirmed by five to nine transitions representing distinct peptide/fragment ion pairs- strongly suggests the presence of NOS bridges in WRKY25. However, direct evidence that changes in redox conditions lead to reversible NOS bridge formation is still pending.

It has been demonstrated that Limited Proteolysis coupled to Mass Spectrometry (LiP-MS) is a powerful tool for detecting protein structural changes. This method uses a broad-spectrum protease to digest only exposed or unfolded regions of the protein, followed by complete digestion and LC–MS analysis. That study successfully detected conformational changes induced by pH, temperature, metabolite–protein interactions, and drug–target interactions. Inspired by this, we attempted to introduce oxidative conditions to the protein before or during the LC–MS workflow [111]. Applying oxidative conditions directly *in planta* could provide more physiologically relevant information but is technically challenging due to ROS toxicity and the low biological concentrations that plants naturally manage. Alternatively, total plant extracts or specific tissues such as leaves could be used to study either the native protein or a tagged version expressed in planta, allowing us to better evaluate structural changes in a more natural context. However, the complexity of plant extracts makes peptide identification much more difficult, and the low abundance of native WRKY25 often necessitates transgenic overexpression with a tag [112]. Additionally, the rapid chemical reactions triggered by ROS

during *in vitro* applications, combined with the difficulty of precisely controlling oxidative conditions, further complicate experimental reproducibility. Overall, the application of oxidative conditions *in vitro, in vivo*, or *in planta* remains a significant challenge compared with other perturbations such as temperature, pH, or ligand binding [113,114]. At the same time, these limitations highlight important opportunities for deeper investigation into protein redox dynamics and the molecular mechanisms underlying ROS signaling

Taken together, our data support a model in which WRKY25 senses oxidative stress and regulates *WRKY53* expression. Under oxidative stress, WRKY25 expression increases, although its ability to activate WRKY53 is reduced. As WRKY25 accumulates, it forms heterodimers with WRKY18, relieving WRKY18-mediated repression and promoting WRKY53 activation. Concurrently, both WRKY25 and WRKY18 downregulate their own transcription, preventing overactivation. This regulatory balance allows WRKY25 to fine-tune the WRKY18/WRKY25/WRKY53 subnetwork, ensuring gradual and sustained progression of senescence.

In addition, other questions regarding the levels of regulation of WRKY53 have been explored in this thesis. It has been demonstrated that REVOLUTA (REV), an important HD-ZIP III transcription factor involved in development and physiological processes in *Arabidopsis thaliana*, mediates the transduction of H_2O_2 signals to regulate the expression of *WRKY53*. The accumulation of H_2O_2 during senescence induces *WRKY53* expression, and it seems that REV acts as a transcriptional intermediary, fine-tuning *WRKY53* activation according to the oxidative state of the cell [24,74,115].

Interestingly, in this study, as well as in others it was found that REV drives *WRKY53* expression, a WRKY for which a function in early development has not yet been described [24,75]. The interaction between REV and the *WRKY53* promoter appears to be developmentally regulated, and REV's preferential binding to distinct *cis-elements* within the *WRKY53* promoter [74] suggests the involvement of an additional factor that directs this specificity. The data showed that TIFY8, a non-JAZ member of the TIFY family in *Arabidopsis thaliana*, interacts with REV. TIFY8 is a negative regulator of leaf senescence, and together with REV, it negatively modulates the expression of *WRKY53*.

It has been proposed that TIFY8 acts as a transcriptional repressor, likely through its interaction with NINJA and/or KIX8/9, which serve as adaptors for TOPLESS, a mediator of transcriptional repression [86,87]. In this research, evidence was provided that the loss of

TIFY8 function leads to premature senescence and overexpression of *WRKY53*, whereas its overexpression delays senescence and represses these genes. Moreover, TIFY8 is predominantly expressed in leaves during early development, prior to senescence, a stage when REV-mediated activation of *WRKY53* is likely suppressed. Conversely, during the onset of senescence, REV and *WRKY53* mRNA levels increase, while TIFY8 expression decreases.

Altogether, this evidence allows me to conclude that TIFY8 functions as a negative regulator of senescence, most likely by inhibiting REV, which directly activates senescence-associated genes such as *WRKY53*. This conclusion agrees with the previously described role of TIFY8 as a transcriptional repressor.

Regulation of WRKY53 by the TIFY8–REV complex also provides a point of convergence for hormonal and environmental signals, as *WRKY53* integrates JA, SA, and ROS cues. It was identified that the effect of JA on REV, TIFY8, and *WRKY53* expression is development-dependent and varies with short- and long-term exposure. JA strongly induces REV in 5-week-old plants, potentially contributing to its increased expression during early senescence, while *tify8* and *rev* mutants show altered but relatively mild effects on each other's expression. JA levels remain largely unchanged, indicating that TIFY8 and REV do not affect JA biosynthesis, although JA can modulate REV activity, likely through PEAPOD or JAZ interactions.

Overall, these findings suggest that REV has a dual function that can be modulated by cofactors, with TIFY8 acting as a key transcriptional modulator that attenuates the activation of leaf senescence. REV appears to be regulated both JA-independently, through TIFY8, and JA-dependently, via PEAPOD and JAZ proteins, potentially acting at different developmental stages. Interestingly, TIFY8's ability to limit *WRKY53* activation independently of JA may enable the plant to finely tune senescence, balancing internal developmental signals with external conditions. It remains to be investigated whether additional signaling pathways converge on the TIFY8–REV–WRKY53 module to integrate diverse environmental and developmental cues.

While the physical interaction between TIFY8 and REV and its effect on *WRKY53* have been demonstrated, the precise molecular mechanisms remain to be elucidated. Another aspect that requires further study is how this interaction occurs mechanistically. It has been shown that the TIFY/ZIM domain of TIFY8 is involved in its interaction with REV; however, *in planta* this domain alone is not sufficient. Additional regions within the C-terminal part of the protein are also required for the interaction. REV also associates selectively with PEAPOD and certain

JAZ proteins, and these interactions may explain the enhanced REV-dependent activation of *WRKY53* after JA treatment, following JAZ degradation.

Functional differences between TIFY8, PEAPODs, and JAZs suggest that PEAPODs act mainly in early leaf development [116], whereas TIFY8 regulates senescence. This highlights the need to further investigate their contributions to REV function at different stages of plant development. Future studies should also explore whether TIFY8 recruits co-repressors, alters chromatin structure, or modulates REV's DNA-binding activity. Additionally, potential functional redundancy with other non-JAZ TIFY family members, as well as their involvement in other developmental or stress-related pathways, represent an important area for further investigation.

It has already been discussed that WRKY53 and WRKY25 mutually activate each other, forming a positive feedback loop, while WRKY25 also reduces intracellular H_2O_2 levels, indirectly lowering *WRKY53* expression. *WRKY25* expression is induced by H_2O_2 with the involvement of WRKY53, yet WRKY25 negatively regulates its own expression to prevent excessive responses [73,117]. It is important to consider that, beyond the small subnetwork already described and well characterized in this thesis, these transcription factors are part of a broader regulatory network that likely contains additional layers of control, including interactions with other transcription factors and antioxidative enzymes. In this thesis, the capacity of WRKY53 to directly regulate antioxidant enzyme activities was further explored. Therefore, it was possible to identify another feedback mechanism within the circuit formed by WRKYs, H_2O_2, and antioxidative enzymes.

The findings of this study reveal that the WRKY53 protein forms physical complexes with antioxidant enzymes, including catalases (CAT2, CAT3), superoxide dismutases (Cu/ZnSOD1, FeSOD1), and ascorbate peroxidase (APX1). These interactions result in reciprocal inhibition, in which WRKY53 reduces enzymatic activity while its own transcriptional function is simultaneously attenuated. Moreover, this study showed that WRKY53 specifically interacts with these antioxidant enzymes, rather than with other WRKY family members, and that the inhibition of antioxidative enzymes appears to be selective for specific isoforms. Interestingly, WRKY53 was also shown to inhibit CAT and APX activities across multiple developmental stages, with distinct activity profiles observed between Col-0 and *wrky53* mutants. Although previous studies have shown that APX activity during bolting is regulated post-transcriptionally [33,118] and still occurs in *wrky53* mutants—suggesting that WRKY53

inhibition is not the primary mechanism, and —the prolonged inhibition of APX1 activity in these mutants indicates a link to delayed senescence.

In addition, the interaction established here between WRKY53 and CAT2/CAT3 can direct the resulting complexes to peroxisomes and promote CAT translocation to the nucleus. This interaction inhibits catalase activity, although it remains unclear whether CAT is later released from WRKY53 once in the nucleus. This research opens several important questions. For example, does reciprocal inhibition require stable or dynamic complexes? What are the molecular mechanisms by which WRKY53 modulates enzymatic activity? Further clarification is also needed regarding possible conformational changes or effects on enzyme stability.

Future studies should address the functional relevance of this mechanism. This work proposes a new level of transcriptional and enzymatic regulation, in which WRKY53–antioxidant enzyme complexes allow the plant to integrate oxidative stress signals and precisely control leaf senescence.

Overall, these findings outline a novel regulatory mechanism that integrates developmental, oxidative, and hormonal signals to control senescence. Moreover, they expand our mechanistic understanding of senescence regulation and highlight the presence of a potential redox switch in plant regulatory proteins, offering new avenues for investigating redox-sensitive transcriptional regulation *in vivo.*

9. References

1. Zhou, M. & Yang, J. Delaying or promoting? Manipulation of leaf senescence to improve crop yield and quality. *Planta* **258,** 48 (2023).

2. Gregersen, P. L., Culetic, A., Boschian, L. & Krupinska, K. Plant senescence and crop productivity. *Plant Mol Biol* **82,** 603–622 (2013).

3. Guo, Y. *et al.* Leaf senescence: progression, regulation, and application. *Molecular Horticulture* **1,** (2021).

4. Fischer, A. M. The Complex Regulation of Senescence. *CRC Crit Rev Plant Sci* **31,** 124–147 (2012).

5. Thomas, H. Senescence, ageing and death of the whole plant. *New Phytologist* **197,** 696–711 (2013).

6. Pyung, O. L., Hyo, J. K. & Hong, G. N. Leaf senescence. *Annu Rev Plant Biol* **58,** 115–136 (2007).

7. Havé, M., Marmagne, A., Chardon, F. & Masclaux-Daubresse, C. Nitrogen remobilization during leaf senescence: Lessons from Arabidopsis to crops. *J Exp Bot* **68,** 2513–2529 (2017).

8. Zentgraf, U., Andrade, A. G. & Doll, J. Editorial for special issue "leaf senescence" in plants. *Plants* **10,** (2021).

9. Spadafora, N. D. *et al.* Short-term post-harvest stress that affects profiles of volatile organic compounds and gene expression in rocket salad during early post-harvest senescence. *Plants* **9,** (2020).

10. Woo, H. R., Kim, H. J., Nam, H. G. & Lim, P. O. Plant leaf senescence and death - regulation by multiple layers of control and implications for aging in general. *J Cell Sci* **126,** 4823–4833 (2013).

11. Zentgraf, U., Andrade, A. G. & Doll, J. Editorial for special issue "leaf senescence" in plants ulrike zentgraf *, ana g. Andrade and jasmin doll. *Plants* **10,** Preprint at https://doi.org/10.3390/plants10081490 (2021)

12. Guo, Y. Towards systems biological understanding of leaf senescence. *Plant Mol Biol* **82,** 519–528 (2013).

13. Yolcu, S., Li, X., Li, S. & Kim, Y. J. Beyond the genetic code in leaf senescence. *J Exp Bot* **69,** 801–810 (2018).

14. Jibran, R., Hunter, D. A. & Dijkwel, P. P. Hormonal regulation of leaf senescence through integration of developmental and stress signals. *Plant Mol Biol* **82,** 547–561 (2013).

15. Guo, Y. *Initiation, Progression, and Genetic Manipulation of Leaf Senescence in Plant Senescence: Methods and Protocols, Methods in Molecular Biology*. **1744,** (Springer Science+Business Media, 2018).

16. Wasternack, C. Jasmonates: An update on biosynthesis, signal transduction and action in plant stress response, growth and development. *Ann Bot* **100,** 681–697 (2007).

17. Ueda, J. & Kato, J. Promotive Effect of Methyl Jasmonate on Oat Leaf Senescence in the Light. *Z. Pflanzenphysiol.* **103,** 357–359 (1981).

18. He, Y. *et al.* Networking Senescence-Regulating Pathways by Using Arabidopsis Enhancer Trap Lines 1. *Plant Physiol* **126,** 707–16 (2001).

19. Jung, C. *et al.* Microarray-based screening of jasmonate-responsive genes in Arabidopsis thaliana. *Plant Cell Rep* **26,** 1053–1063 (2007).

20. Xiao, S. *et al.* COS1: An arabidopsis coronatine insensitive1 suppressor essential for regulation of jasmonate-mediated plant defense and senescence. *Plant Cell* **16,** 1132–1142 (2004).

21. Breeze, E. *et al.* High-resolution temporal profiling of transcripts during Arabidopsis leaf senescence reveals a distinct chronology of processes and regulation. *Plant Cell* **23,** 873–894 (2011).

22. Seltmann, M. A. *et al.* Differential impact of lipoxygenase 2 and jasmonates on natural and stress-induced senescence in arabidopsis. *Plant Physiol* **152,** 1940–1950 (2010).

23. Waszczak, C., Carmody, M. & Kangasjärvi, J. Reactive Oxygen Species in Plant Signaling. *Annual Review of Plant Biology Downloaded from www.annualreviews.org. Guest* **11,** 30 (2025).

24. Zentgraf, U., Andrade-Galan, A. G. & Bieker, S. Specificity of H2O2 signaling in leaf senescence: is the ratio of H2O2 contents in different cellular compartments sensed in Arabidopsis plants? *Cell Mol Biol Lett* **27,** (2022).

25. D'Autréaux, B. & Toledano, M. B. ROS as signalling molecules: Mechanisms that generate specificity in ROS homeostasis. *Nat Rev Mol Cell Biol* **8,** 813–824 (2007).

26. Mittler, R., Vanderauwera, S., Gollery, M. & Van Breusegem, F. Reactive oxygen gene network of plants. *Trends Plant Sci* **9,** 490–498 (2004).

27. Foyer, C. H. & Noctor, G. Stress-triggered redox signalling: What's in pROSpect? *Plant Cell Environ* **39,** 951–964 (2016).

28. Li, Y., Liu, W., Zhong, H., Zhang, H. L. & Xia, Y. Redox-sensitive bZIP68 plays a role in balancing stress tolerance with growth in Arabidopsis. *Plant Journal* **100,** 768–783 (2019).

29. Zandalinas, S. I. & Mittler, R. Vascular and nonvascular transmission of systemic reactive oxygen signals during wounding and heat stress. *Plant Physiol* **186,** 1721–1733 (2021).

30. Foyer, C. H. & Noctor, G. Oxidant and antioxidant signalling in plants: A re-evaluation of the concept of oxidative stress in a physiological context. *Plant Cell Environ* **28,** 1056–1071 (2005).

31. Bieker, S., Riester, L., Stahl, M., Franzaring, J. & Zentgraf, U. Senescence-specific Alteration of Hydrogen Peroxide Levels in Arabidopsis thaliana and Oilseed Rape Spring Variety Brassica napus L. cv. Mozart. *J Integr Plant Biol* **54,** 540–554 (2012).

32. Giri, M. K. *et al.* GBF1 differentially regulates CAT2 and PAD4 transcription to promote pathogen defense in Arabidopsis thaliana. *Plant Journal* **91,** 802–815 (2017).

33. Zimmermann, P., Heinlein, C., Orendi, G. & Zentgraf, U. Senescence-specific regulation of catalases in Arabidopsis thaliana (L.) Heynh. *Plant Cell Environ* **29,** 1049–1060 (2006).

34. Smykowski, A., Zimmermann, P. & Zentgraf, U. G-Box Binding Factor1 reduces CATALASE2 expression and regulates the onset of leaf senescence in Arabidopsis. *Plant Physiol* **153,** 1321–1331 (2010).

35. Feierabend, J., Schaan, C. & Hertwig, B. *Photoinactivation of Catalase Occurs under Both High-and Low-Temperature Stress Conditions and Accompanies Photoinhibition of Photosystem 11I. Plant Physiol* **100,** (1992).

36. Ye, Z. *et al. The developmental transition to flowering represses ascorbate peroxidase activity and induces enzymatic lipid peroxidation in leaf tissue in Arabidopsis thaliana*. *Plant Science* **158,** (2000).

37. Shirzadian-Khorramabad, R. *et al.* A mutation in Arabidopsis SAL1 alters its in vitro activity against IP3 and delays developmental leaf senescence in association with lower ROS levels. *Plant Mol Biol* **108,** 549–563 (2022).

38. Miao, Y., Laun, T., Zimmermann, P. & Zentgraf, U. Targets of the WRKY53 transcription factor and its role during leaf senescence in Arabidopsis. *Plant Mol Biol* **55,** 853–867 (2004).

39. Gepstein, S. *et al.* Large-scale identification of leaf senescence-associated genes. *Plant Journal* **36,** 629–642 (2003).

40. Buchanan-Wollaston, V. *et al.* Comparative transcriptome analysis reveals significant differences in gene expression and signalling pathways between developmental and dark/starvation-induced senescence in Arabidopsis. *Plant Journal* **42,** 567–585 (2005).

41. Zentgraf, U. Identification of a transcription factor specifically expressed at the onset of leaf senescence. *Planta* **213,** 469–473 (2001).

42. Guo, Y., Cai, Z. & Gan, S. Transcriptome of Arabidopsis leaf senescence. *Plant Cell Environ* **27,** 521–549 (2004).

43. Zentgraf, U., Jobst, J., Kolb, D. & Rentsch, D. Senescence-related gene expression profiles of rosette leaves of Arabidopsis thaliana: Leaf age versus plant age. *Plant Biol* **6,** 178–183 (2004).

44. Cao, J., Liu, H., Tan, S. & Li, Z. Transcription Factors-Regulated Leaf Senescence: Current Knowledge, Challenges and Approaches. *Int J Mol Sci* **24,** (2023).

45. Balazadeh, S., Riaño-Pachón, D. M. & Mueller-Roeber, B. Transcription factors regulating leaf senescence in Arabidopsis thaliana. *Plant Biol* **10,** 63–75 (2008).

46. Kim, H. J., Nam, H. G. & Lim, P. O. Regulatory network of NAC transcription factors in leaf senescence. *Curr Opin Plant Biol* **33,** 48–56 (2016).

47. Yang, S. D., Seo, P. J., Yoon, H. K. & Park, C. M. The arabidopsis NAC transcription factor VNI2 integrates abscisic acid signals into leaf senescence via the COR/RD genes. *Plant Cell* **23,** 2155–2168 (2011).

48. Kim, Y. S., Sakuraba, Y., Han, S. H., Yoo, S. C. & Paek, N. C. Mutation of the arabidopsis NAC016 transcription factor delays leaf senescence. *Plant Cell Physiol* **54,** 1660–1672 (2013).

49. Wu, A. *et al.* JUNGBRUNNEN1, a reactive oxygen species-responsive NAC transcription factor, regulates longevity in Arabidopsis. *Plant Cell* **24,** 482–506 (2012).

50. Balazadeh, S. *et al.* ORS1, an H2O2-responsive NAC transcription factor, controls senescence in arabidopsis thaliana. *Mol Plant* **4,** 346–360 (2011).

51. Cao, J., Liu, H., Tan, S. & Li, Z. Transcription Factors-Regulated Leaf Senescence: Current Knowledge, Challenges and Approaches. *Int J Mol Sci* **24,** (2023).

52. Goyal, P. *et al.* WRKY transcription factors: evolution, regulation, and functional diversity in plants. *Protoplasma* **260,** 331–348 (2023).

53. Song, H., Cao, Y., Zhao, L., Zhang, J. & Li, S. Review: WRKY transcription factors: Understanding the functional divergence. *Plant Science* **334,** (2023).

54. Rushton, P. J., Somssich, I. E., Ringler, P. & Shen, Q. J. WRKY transcription factors. *Trends Plant Sci* **15,** 247–258 (2010).

55. Chen, X., Li, C., Wang, H. & Guo, Z. WRKY transcription factors: evolution, binding, and action. *Phytopathology Research* **1,** (2019).

56. Robatzek, S. & Somssich, I. E. Targets of AtWRKY6 regulation during plant senescence and pathogen defense. *Genes Dev* **16,** 1139–1149 (2002).

57. Zhou, X., Jiang, Y. & Yu, D. WRKY22 transcription factor mediates dark-induced leaf senescence in Arabidopsis. *Mol Cells* **31,** 303–313 (2011).

58. Cao, J. *et al.* LSD 4.0: an improved database for comparative studies of leaf senescence. *Molecular Horticulture* **2,** (2022).

59. Niu, F. *et al.* WRKY42 transcription factor positively regulates leaf senescence through modulating SA and ROS synthesis in Arabidopsis thaliana. *Plant Journal* **104,** 171–184 (2020).

60. Chen, L., Xiang, S., Chen, Y., Li, D. & Yu, D. Arabidopsis WRKY45 Interacts with the DELLA Protein RGL1 to Positively Regulate Age-Triggered Leaf Senescence. *Mol Plant* **10,** 1174–1189 (2017).

61. Zentgraf, U. Identification of a transcription factor specifically expressed at the onset of leaf senescence. *Planta* **213,** 469–473 (2001).

62. Besseau, S., Li, J. & Palva, E. T. WRKY54 and WRKY70 co-operate as negative regulators of leaf senescence in Arabidopsis thaliana. *J Exp Bot* **63,** 2667–2679 (2012).

63. Wang, Y. *et al.* WRKY55 transcription factor positively regulates leaf senescence and the defense response by modulating the transcription of genes implicated in the biosynthesis of reactive oxygen species and salicylic acid in Arabidopsis. *Development* **147,** (2020).

64. Yu, Y. *et al.* Arabidopsis WRKY71 regulates ethylene-mediated leaf senescence by directly activating EIN2, ORE1 and ACS2 genes. *Plant Journal* **107,** 1819–1836 (2021).

65. Guo, P. *et al.* A tripartite amplification loop involving the transcription factor WRKY75, salicylic acid, and reactive oxygen species accelerates leaf senescence. *Plant Cell* **29,** 2854–2870 (2017).

66. Ay, N. *et al.* Epigenetic programming via histone methylation at WRKY53 controls leaf senescence in Arabidopsis thaliana. *The Plant Journal* **58,** 333–346 (2009).

67. Brusslan, J. A. *et al.* Genome-wide evaluation of histone methylation changes associated with leaf senescence in Arabidopsis. *PLoS One* **7,** (2012).

68. Zentgraf, U., Laun, T. & Miao, Y. The complex regulation of WRKY53 during leaf senescence of Arabidopsis thaliana. *Eur J Cell Biol* **89,** 133–137 (2010).

69. Miao, Y., Laun, T. M., Smykowski, A. & Zentgraf, U. Arabidopsis MEKK1 can take a short cut: It can directly interact with senescence-related WRKY53 transcription factor on the protein level and can bind to its promoter. *Plant Mol Biol* **65,** 63–76 (2007).

70. Miao, Y. & Zentgraf, U. The antagonist function of Arabidopsis WRKY53 and ESR/ESP in leaf senescence is modulated by the jasmonic and salicylic acid equilibrium. *Plant Cell* **19,** 819–830 (2007).

71. Miao, Y., Smykowski, A. & Zentgraf, U. A novel upstream regulator of WRKY53 transcription during leaf senescence in Arabidopsis thaliana. *Plant Biol* **10,** 110–120 (2008).

72. Potschin, M., Schlienger, S., Bieker, S. & Zentgraf, U. Senescence Networking: WRKY18 is an Upstream Regulator, a Downstream Target Gene, and a Protein Interaction Partner of WRKY53. *J Plant Growth Regul* **33,** 106–118 (2014).

73. Doll, J. *et al.* Arabidopsis thaliana WRKY25 Transcription Factor Mediates Oxidative Stress Tolerance and Regulates Senescence in a Redox-Dependent Manner. *Front Plant Sci* **10,** (2020).

74. Xie, Y. *et al.* Revoluta and wrky53 connect early and late leaf development in arabidopsis. *Development (Cambridge)* **141,** 4772–4783 (2014).

75. Bresson, J. *et al.* The genetic interaction of REVOLUTA and WRKY53 links plant development, senescence, and immune responses. *PLoS One* **17,** (2022).

76. Byrne, M. The REVOLUTA gene is necessary for apical meristem development and for limiting cell divisions in the leaves and tems of Arabidopsis. *PLoS Genet* **2,** 785–790 (2006).

77. Roodbarkelari, F. & Groot, E. P. Regulatory function of homeodomain-leucine zipper (HD-ZIP) family proteins during embryogenesis. *New Phytologist* **213,** 95–104 (2017).

78. Du, Q. & Wang, H. The role of HD-ZIP III transcription factors and miR165/166 in vascular development and secondary cell wall formation. *Plant Signal Behav* **10,** (2015).

79. Ramachandran, P., Carlsbecker, A., Etchells, J. P. & Turner, S. Class III HD-ZIPs govern vascular cell fate: An HD view on patterning and differentiation. *J Exp Bot* **68,** 55–69 (2017).

80. Byrne, M. E. Shoot meristem function and leaf polarity: The role of class III HD-ZIP genes. *PLoS Genet* **2,** 0785–0790 (2006).

81. Hong, S. Y. *et al.* Multi-level analysis of the interactions between REVOLUTA and MORE AXILLARY BRANCHES 2 in controlling plant development reveals parallel, independent and antagonistic functions. *Development (Cambridge)* **147,** (2020).

82. Reinhart, B. J. *et al.* Establishing a framework for the ad/abaxial regulatory network of Arabidopsis: Ascertaining targets of class III HOMEODOMAIN LEUCINE ZIPPER and KANADI regulation. *Plant Cell* **25,** 3228–3249 (2013).

83. Bai, Y., Meng, Y., Huang, D., Qi, Y. & Chen, M. Origin and evolutionary analysis of the plant-specific TIFY transcription factor family. *Genomics* **98,** 128–136 (2011).

84. Shyu, C. *et al.* JAZ8 lacks a canonical degron and has an EAR motif that mediates transcriptional repression of jasmonate responses in Arabidopsis. *Plant Cell* **24,** 536–550 (2012).

85. Cuéllar Pérez, A. *et al.* The non-JAZ TIFY protein TIFY8 from Arabidopsis thaliana is a transcriptional repressor. *PLoS One* **9,** (2014).

86. Pauwels, L. *et al.* NINJA connects the co-repressor TOPLESS to jasmonate signalling. *Nature* **464,** 788–791 (2010).

87. Gonzalez, N. *et al.* A repressor protein complex regulates leaf growth in arabidopsis. *Plant Cell* **27,** 2273–2287 (2015).

88. Schippers, J. H. M., Schmidt, R., Wagstaff, C. & Jing, H. C. Living to die and dying to live: The survival strategy behind leaf senescence. *Plant Physiol* **169,** 914–930 (2015).

89. Phukan, U. J., Jeena, G. S. & Shukla, R. K. WRKY transcription factors: Molecular regulation and stress responses in plants. *Front Plant Sci* **7,** (2016).

90. Ülker, B. & Somssich, I. E. WRKY transcription factors: From DNA binding towards biological function. *Curr Opin Plant Biol* **7,** 491–498 (2004).

91. Eulgem, T., Rushton, P. J., Robatzek, S. & Somssich, I. E. *The WRKY superfamily of plant transcription factors*. **5,** (2000).

92. Chen, H. *et al.* Roles of arabidopsis WRKY18, WRKY40 and WRKY60 transcription factors in plant responses to abscisic acid and abiotic stress. *BMC Plant Biol* **10,** 281 (2010).

93. Xu, X., Chen, C., Fan, B. & Chen, Z. Physical and functional interactions between pathogen-induced Arabidopsis WRKY18, WRKY40, and WRKY60 transcription factors. *Plant Cell* **18,** 1310–1326 (2006).

94. Li, J., Brader, G. & Palva, E. T. The WRKY70 Transcription Factor: A Node of Convergence for Jasmonate-Mediated and Salicylate-Mediated Signals in Plant Defense. *Plant Cell* **16,** 319–331 (2004).

95. Ciolkowski, I., Wanke, D., Birkenbihl, R. P. & Somssich, I. E. Studies on DNA-binding selectivity of WRKY transcription factors lend structural clues into WRKY-domain function. *Plant Mol Biol* **68,** 81–92 (2008).

96. Grzechowiak, M. *et al.* New aspects of DNA recognition by group II WRKY transcription factor revealed by structural and functional study of AtWRKY18 DNA binding domain. *Int J Biol Macromol* **213,** 589–601 (2022).

97. Xu, Y. ping, Xu, H., Wang, B. & Su, X. D. Crystal structures of N-terminal WRKY transcription factors and DNA complexes. *Protein Cell* **11,** 208–213 (2020).

98. Maeo, K., Hayashi, S., Kojima-Suzuki, H., Morikami, A. & Nakamura, K. Role of Conserved Residues of the WRKY Domain in the DNA-binding of Tobacco WRKY Family Proteins. *Biosc. Biotecnol. Biochem.* **11,** 2428–2436 (2001).

99. Zhang, D. *et al.* The NPR1-WRKY46-WRKY6 signaling cascade mediates probenazole/salicylic acid-elicited leaf senescence in Arabidopsis thaliana. *J Integr Plant Biol* **63,** 924–936 (2021).

100. Brand, L. H., Fischer, N. M., Harter, K., Kohlbacher, O. & Wanke, D. Elucidating the evolutionary conserved DNA-binding specificities of WRKY transcription factors by molecular dynamics and in vitro binding assays. *Nucleic Acids Res* **41,** 9764–9778 (2013).

101. Eulgem, T., Rushton, P. J., Schmelzer, E., Hahlbrock, K. & Somssich, I. E. Early nuclear events in plant defence signalling: rapid gene activation by WRKY transcription factors. *EMBO J* **18,** 4689–4699 (1999).

102. Zhou, J. *et al.* Characterization of the promoter and extended C-terminal domain of Arabidopsis WRKY33 and functional analysis of tomato WRKY33 homologues in plant stress responses. *J Exp Bot* **66,** 4567–4583 (2015).

103. Dong, X. *et al.* Structural basis for the regulation of plant transcription factor WRKY33 by the VQ protein SIB1. *Commun Biol* **7,** (2024).

104. Durgud, M. *et al.* Molecular mechanisms preventing senescence in response to prolonged darkness in a desiccation-tolerant plant. *Plant Physiol* **177,** 1319–1338 (2018).

105. Chi, Y. *et al.* Protein-protein interactions in the regulation of WRKY transcription factors. *Mol Plant* **6,** 287–300 (2013).

106. Cheng, X. *et al.* Structural basis of dimerization and dual W-box DNA recognition by rice WRKY domain. *Nucleic Acids Res* **47,** 4308–4318 (2019).

107. Chen, H. *et al.* Roles of arabidopsis WRKY18, WRKY40 and WRKY60 transcription factors in plant responses to abscisic acid and abiotic stress. *BMC Plant Biol* **10,** (2010).

108. Wu, F. *et al.* Hydrogen peroxide sensor HPCA1 is an LRR receptor kinase in Arabidopsis. *Nature* **578,** 577–581 (2020).

109. Rabe von Pappenheim, F. *et al.* Widespread occurrence of covalent lysine–cysteine redox switches in proteins. *Nat Chem Biol* **18,** 368–375 (2022).

110. Wensien, M. *et al.* A lysine–cysteine redox switch with an NOS bridge regulates enzyme function. *Nature* **593,** 460–464 (2021).

111. Feng, Y. *et al.* Global analysis of protein structural changes in complex proteomes. *Nat Biotechnol* **32,** 1036–1044 (2014).

112. Chen, Q. *et al.* Quantitative proteomics reveals redox-based functional regulation of photosynthesis under fluctuating light in plants. *J Integr Plant Biol* **64,** 2168–2186 (2022).

113. Malinovska, L. *et al.* Proteome-wide structural changes measured with limited proteolysis-mass spectrometry: an advanced protocol for high-throughput applications. . *Nat Protoc* **18,** 659–682 (2023).

114. Schopper, S. *et al.* Measuring protein structural changes on a proteome-wide scale using limited proteolysis-coupled mass spectrometry. *Nat Protoc* **12,** 2391–2410 (2017).

115. Zentgraf, U. & Doll, J. Arabidopsis wrky53, a node of multi-layer regulation in the network of senescence. *Plants* **8,** (2019).

116. Baekelandt, A. *et al.* Arabidopsis leaf flatness is regulated by PPD2 and NINJA through repression of CYCLIN D3 genes. *Plant Physiol* **178,** 217–232 (2018).

117. Andrade Galan, A. G., Doll, J., von Roepenack-Lahaye, E., Faiss, N. & Zentgraf, U. The transcription factor WRKY25 can act as redox switch to drive the expression of WRKY53 during leaf senescence in arabidopsis. *Sci Rep* **15,** (2025).

118. Miyake, C. & Asada, K. *Inactivation Mechanism of Ascorbate Peroxidase at Low Concentrations of Ascorbate; Hydrogen Peroxide Decomposes Compound I of Ascorbate Peroxidase*. *Plant CellPhysiol* **37,** (1996).

Appendix:

Publish manuscript 1: The transcription factor WRKY25 can act as redox switch to drive the expression of *WRKY53* during leaf senescence in Arabidopsis

Andrade Galan, A.G., Doll, J., von Roepenack-Lahaye, E., Faiss, N. and Zentgraf, U. The transcription factor WRKY25 can act as redox switch to drive the expression of *WRKY53* during leaf senescence in Arabidopsis. *Sci Rep* **15**, 27623 (2025). https://doi.org/10.1038/s41598-025-13023-1

scientific reports

OPEN

The transcription factor WRKY25 can act as redox switch to drive the expression of *WRKY53* during leaf senescence in arabidopsis

Ana Gabriela Andrade Galan, Jasmin Doll, Edda von Roepenack-Lahaye, Natalie Faiss & Ulrike Zentgraf✉

Senescence requires high plasticity and, therefore, must be coordinated by a complex regulatory network. Notably, WRKY transcription factors highly impact senescence regulation. WRKYs can form homo- and heterodimers and contain the binding motifs of WRKY factors in their promoters already forming a complex regulatory network between themselves. For the Arabidopsis hub gene *WRKY53*, WRKY18 acts as a strong negative while WRKY25 serves as strong positive regulator, creating a smaller subnetwork with high complexity, which we analyzed in detail. Activation of *WRKY53* expression by WRKY25 is redox sensitive while repression by WRKY18 was not. Deletions and domain-swapping between WRKY18 and WRKY25 revealed that the N-terminal domain of WRKY25 is crucial for its activator effect on *WRKY53* expression. Moreover, WRKY25 does not form homodimers but is able to heterodimerize with WRKY18 also requiring its N-terminal domain. The impact on senescence regulation and on *WRKY53* expression was validated *in planta* using transgenic complementation lines of the *wrky25* mutant. Modeling WRKY25 *in silico* indicated a putative covalent lysine-cysteine NOS redox switch. LC–MS analyses suggest that the NOS bridges really exist. We propose that WRKY25 acts as a redox sensor, balancing the expression and interactions of the WRKY53/WRKY25/WRKY18 network to ensure progressive senescence induction.

Keywords *Arabidopsis thaliana*, Senescence regulation, WRKY transcription factors, WRKY homo- and heterodimerization, Redox regulation, NOS bridge

In agricultural production, well-timed leaf senescence plays an important role not only for the fitness of the whole plant but also influences crop yield quantity and quality[1–3]. Senescence is the tightly regulated and programmed final stage of plant development. The aim of senescence is to maximize the relocation of vital nutrients such as carbon, nitrogen, and mineral resources out of senescing tissues to developing parts of the plants[4,5]. The age of individual leaves and the age of the whole plant are the main factors driving developmental senescence under normal non-stress conditions. The plant senses these parameters through a multitude of well-coordinated signals that initiate and modulate senescence. It has been widely described that nearly all plant hormones can influence the senescence program, as well as small signaling molecules such as peptides, calcium, and reactive oxygen species (ROS)[6–14].

At the transcriptional level, several thousand genes are upregulated and downregulated during the onset and progression of senescence in *Arabidopsis thaliana*, leading to extensive reprogramming of the transcriptome and highlighting the crucial role of transcription factors[15–22]. Among these genes, two transcription factor families namely WRKY and NAC factors, are notably overrepresented in the transcriptome of Arabidopsis during senescence[16]. For many factors belonging to these families, a regulatory role has already been characterized across various plant families[21,23,24]. A notable feature of the WRKY family members is the presence of the W-box (TTGAC(C/T)) DNA-binding motif in their own promoters. This motif allows WRKY transcription factors to regulate each other, forming a complex WRKY-driven transcriptional network[23].

In *Arabidopsis thaliana*, WRKY53 has been characterized as a positive regulator of developmental senescence and functions as one of the key regulatory hubs involved in several senescence-associated processes such as remobilization, nutrient transport, ROS signaling, and the degradation of ROS molecules[6,10,11,26–28]. Expression

Center for Plant Molecular Biology (ZMBP), University of Tübingen, Auf der Morgenstelle 32, 72076 Tübingen, Germany. ✉email: ulrike.zentgraf@zmbp.uni-tuebingen.de

and activity as well as degradation of WRKY53 are tightly regulated involving many feedback controls including even several double bottoms. In addition, WRKY53 is involved in epigenetic control of other senescence regulators (for review see[28]).

Among the WRKYs expressed in mature green leaf tissue, WRKY18 and WRKY25 have been identified as most effective repressors and activators of *WRKY53* expression, respectively. WRKY18 serves as a negative upstream regulator, a downstream target, and a protein interaction partner of WRKY53[29]. In contrast, WRKY25 acts as a positive upstream regulator, but also as downstream target and protein interaction partner of WRKY53[13]. Moreover, plant lines with altered expression of these two WRKYs exhibit altered senescence-associated phenotypes. Plants lacking *WRKY18* expression show accelerated senescence, consistent with its role as a repressor of *WRKY53*[29]. Contradictory with its role as an activator of *WRKY53* expression, *wrky25* mutants also show accelerated senescence[13]. Therefore, regulation appears to be more complex and is most likely organized through a small, yet intricate, subnetwork, in which the loss of WRKY25 creates an imbalance leading to this contradictory phenotype. The molecular mechanisms governing interactions within the WRKY18/WRKY25/WRKY53 network and their correlation with leaf senescence remain elusive. Furthermore, a signaling molecule modulating this subnetwork has not yet been characterized in detail. Interestingly, the WRKY25 DNA-binding activity depends on the redox conditions[13].

Here, we could show that WRKY25 can act as a redox switch, balancing the expression and interactions of the WRKY18/WRKY25/WRKY53 subnetwork to ensure the progressive induction of senescence in *Arabidopsis thaliana*. In addition, the heterodimer of WRKY18 and WRKY25 was identified as an activator of *WRKY53* expression. Dissecting the protein structures by means of deletion constructs and domain-swapping between WRKY18 and WRKY25 revealed that the N-terminus of WRKY25 is crucial for its activator effect on *WRKY53* expression and its ability to heterodimerize. Redox conditions were identified to be critical for regulatory effects and a putative redox switch was discovered in the WRKY25 protein. This study enhances our understanding of plant senescence regulation and highlights the significant role of redox conditions in plant regulatory processes.

Results

Transactivation potential with the WRKY53/WRKY25/WRKY18 subnetwork

To gain further insight into the potential regulatory subnetwork formed by WRKY18, WRKY25, and WRKY53, we studied the interactions among these three WRKYs and their effects on each other's expression in more detail. Therefore, *Arabidopsis thaliana* protoplasts were transiently co-transformed and utilized as an *in vivo* transactivation system using reporter gene expression. In this system, reporter constructs containing approx. 3000 bp promoter fragments of *WRKY18*, *WRKY25*, and *WRKY53* in front of the glucuronidase (*GUS*) reporter gene, respectively, were co-transformed with different effector constructs (WRKY18, WRKY25, or WRKY53 under the control of a CaMV 35S promoter, respectively). Based on the measured activity of the GUS enzyme in relation to a co-transformed luciferase control, we confirmed that WRKY18, WRKY25, WRKY53 downregulated the reporter gene expression driven by their own promoters (Fig. 1A). As expected, the *WRKY53* expression was upregulated by the WRKY25 effector protein and downregulated by WRKY18 as effector protein (Fig. 1A). In the same context, *WRKY18* expression could be slightly increased by WRKY25 and WRKY53 effectors while *WRKY25* expression could slightly be activated by WRKY18 and WRKY53 effector proteins (Fig. 1A). This indicates that WRKYs can function as activators and repressors depending on the promoter they are interacting with and that WRKY18 had the strongest repressing effect while WRKY25 had the strongest activating effect.

Given that WRKYs have been previously observed to form dimers, protein–protein interactions were evaluated to identify homodimerization within this subnetwork. To detect these interactions, Bimolecular Fluorescence Complementation (BiFC) assays were performed in Arabidopsis protoplasts combined with cell sorting or in *Nicotiana benthamiana* leaves combined with laser scanning microscopy. To achieve fluorescence by protein–protein interaction, they were transiently transformed with constructs containing either WRKY18, WRKY25, or WRKY53 fused to one half of the yellow fluorescent protein (YFP), paired with the same respective WRKY fused to the other half of the YFP. If homodimers can be formed, both halves of YFP are brought in close proximity and can emit fluorescence. A sequence encoding a red fluorescence protein (RFP) is present in the same vector backbone as transformation and expression control. In both transformation systems, homodimerization of WRKY18 and WRKY53 was observed. In *N. benthamiana* leaves, this was evidenced by the fluorescence intensity ratio (YFP/RFP) calculated from microscopy image measurements. In contrast, WRKY25 did not exhibit homodimerization in either system. (Fig. 1B and S1).

The heterodimer WRKY18-WRKY25 is an activator of WRKY53 expression

To address the question whether these WRKYs could also form heterodimers and what impact this would have on the subnetwork, we examined the potential heterodimerization, as heterodimer formation within the WRKY family has been widely documented[30–32]. Using the BiFC system in *N. benthamiana* leaves, it was possible to identify interactions among all three WRKYs, however the WRKY18/WRKY25 heterodimer stood out above the others based on a stronger YFP signal under the confocal microscope and a higher intensity calculated from the YFP/RFP ratio (Fig. 2A and S2). Therefore, we were curious what would be the consequences of the WRKY18/WRKY25 heterodimer formation within the subnetwork. Testing WRKY18/WRKY25 heterodimer in our in vivo transactivation system on the different promoters revealed that only the expression of the reporter gene driven by the *WRKY53* promoter was strongly upregulated by the heterodimer (Fig. 2B) indicating that the heterodimer behaves more similar to WRKY25. Consistently, the heterodimer downregulated the *GUS* expression driven by the promoter of *WRKY25* (Fig. 2B) whereas the heterodimer was less efficient in inhibiting the reporter gene expression by the *WRKY18* promoter also suggesting that the heterodimer acts more like WRKY25 alone (Fig. 2B). These results demonstrate that WRKY25 and WRKY18 can heterodimerize and that this heterodimer significantly influences the subnetwork's activity.

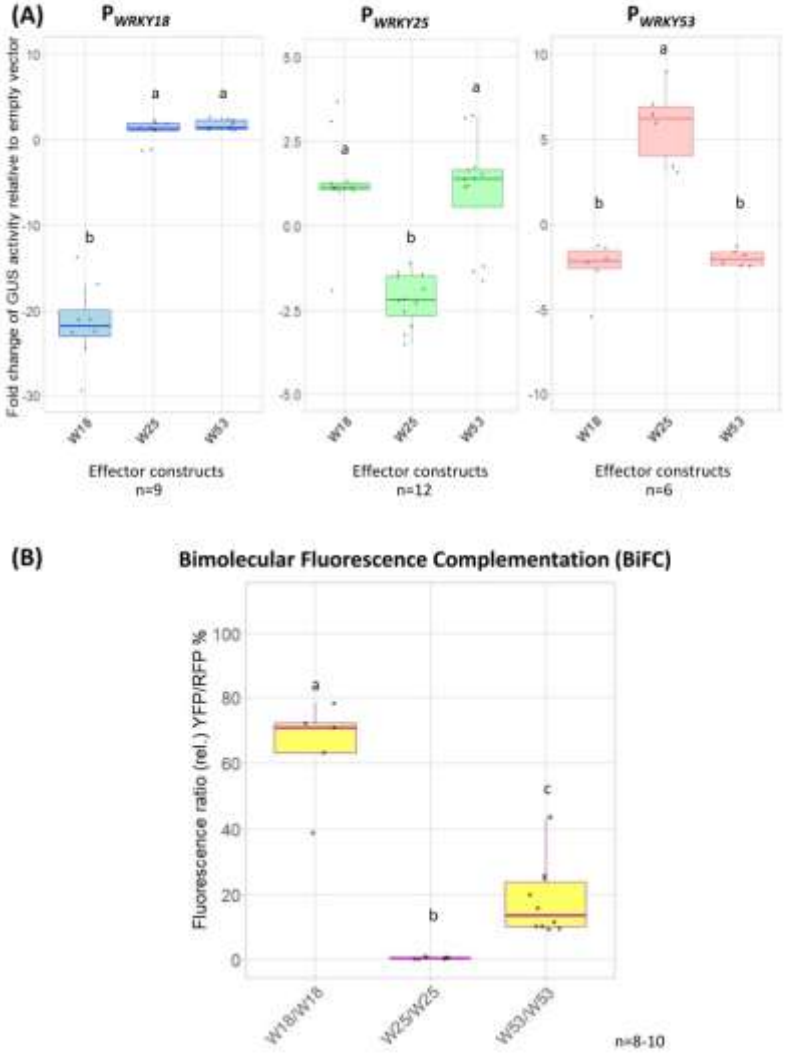

Fig. 1. Transactivation assays in Arabidopsis protoplasts for P_{WRKY18}, P_{WRKY25}, P_{WRKY53}, and *in planta* homodimerization of WRKY18, WRKY25, and WRKY53 in *Nicotiana benthamiana*. (**A**) Arabidopsis root protoplasts were transiently transformed with fragments of the promoters of *WRKY18* (3000 bp), *WRKY25* (3000 bp), *and WRKY53* (2759 bp), each fused to the *GUS* reporter gene, along with 35S:*WRKY18* (W18), 35S:*WRKY25* (W25), or 35S:*WRKY53* (W53) as effector constructs. Relative GUS activity (normalized to values of the empty vector) is shown as boxplots. Sample sizes (n) are indicated for each group within the figure and represent independent biological replicates (**B**) Leaves of *N. benthamiana* were transformed with pBiFCt2in1-NN constructs containing the possible combinations for the homodimerization of the three WRKYs of the subnetwork. These transformed leaves were analyzed under a confocal laser scanning microscope: yellow fluorescence (YFP) indicates interaction (BiFC), red fluorescence (RFP) serves as a transformation control. Boxplots representing the relative fluorescence ratio (%YFP/RFP) are presented. Sample size (n) is indicated in the figure and represents independent biological replicates. In both (**A**) and (**B**) one-way ANOVA followed by Tukey's HSD post-hoc test was performed to determine statistically significant differences among effectors. Different lowercase letters indicate statistically distinct groups ($p \leq 0.05$).

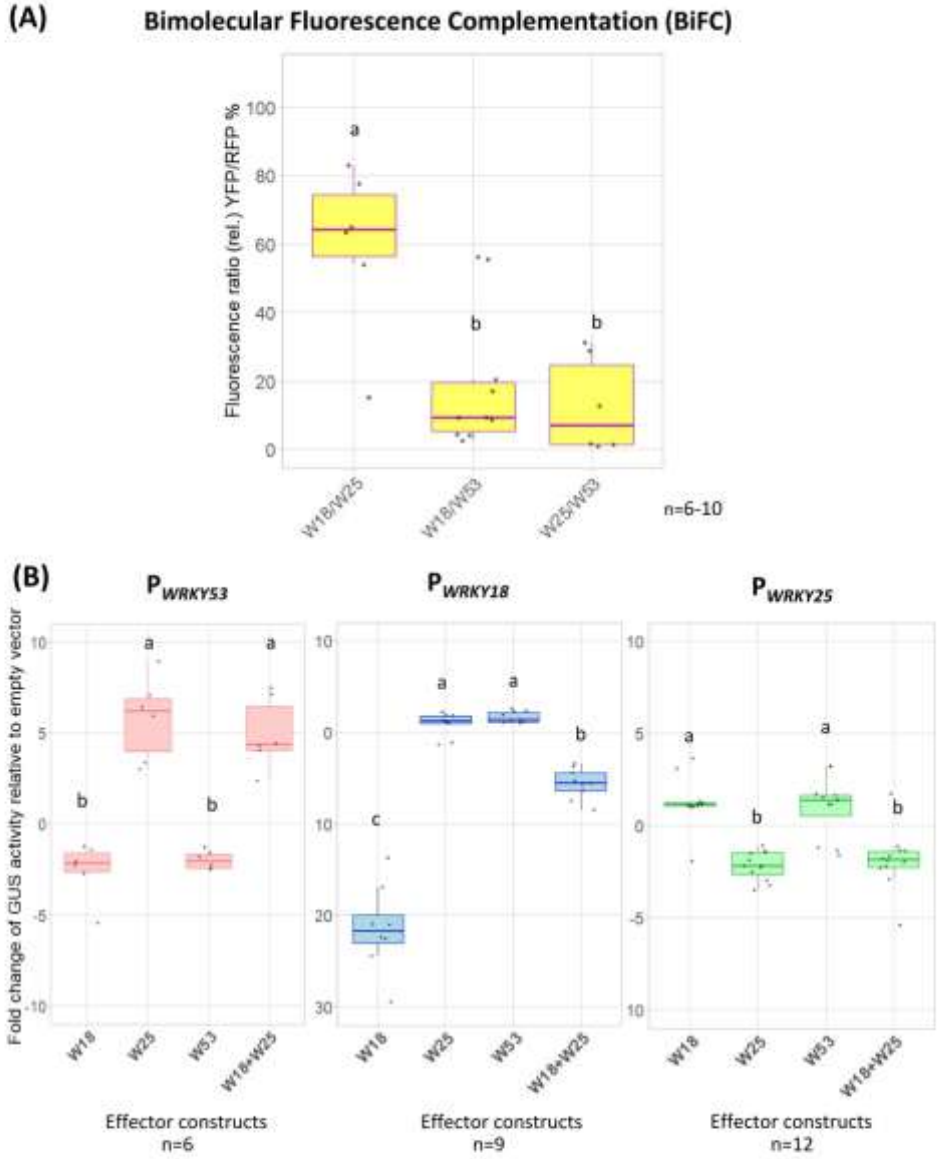

The N-terminus of WRKY25 is necessary for the activation of the WRKY53 and WRKY18 promoters while the C-terminus interferes with dimerization

Next, we wondered how the repressor and activator functions of WRKY18 and WRKY25 are achieved. WRKY25 belongs to the group I family members and contains two DNA-binding domains (DBDs) while WRKY18 belongs to group II and has only one DBD in the more C-terminal part of the protein. For the closely related group I WRKYs, in which all contain two DBDs domains, it was shown that both domains can bind to DNA[33,34]. However, it remains unclear whether these different domains have distinct activator or repressor functions in plants. Therefore, we employed a domain-swapping approach focusing on the structural domains of these WRKYs. We tested different deletion and chimeric constructs in the transactivation assay in Arabidopsis protoplasts for their impact on the *WRKY53* promoter driving the *GUS* expression. These constructs were created by deleting parts of the coding sequences of *WRKY25* or by exchanging the coding sequences for the N-terminal and C-terminal regions between *WRKY18* and *WRKY25* (Fig. 3A and S3A).

◂**Fig. 2**. *In planta* heterodimerization of WRKY18, WRKY25, and WRKY53 in *N. benthamiana*, and transactivation assays in Arabidopsis protoplasts for the effect of WRKY18/WRKY25 heterodimer effect on the P_{WRKY53}. (**A**) Leaves of *N. benthamiana* were transformed with pBiFCt2in1-NN constructs containing the possible combinations for the heterodimerization of the three WRKYs of the subnetwork. The transformed leaves were analyzed under a confocal laser scanning microscope: yellow fluorescence (YFP) indicates interaction (BiFC), and red fluorescence (RFP) serves as a transformation control. Boxplots representing the relative fluorescence ratio (%YFP/RFP) are presented. Sample size (n) is indicated in the figure and represents independent biological replicates. (**B**) Arabidopsis protoplasts were transformed with fragments of the promoters of *WRKY18* (3000 bp), *WRKY25* (3000 bp), and *WRKY53* (2759 bp), each fused to the *GUS* reporter gene, along with 35S:*WRKY18* (W18), 35S:*WRKY25* (W25), 35S:*WRKY53* (W53), or 35S:*WRKY18*/*WRKY25* (W18 + W25) as effector constructs. Values relative to values of the empty vector control are presented as boxplots, with sample sizes (n) shown for each group within the plot representing independent biological replicates. In both (**A**) and (**B**) one-way ANOVA followed by Tukey's HSD post-hoc test was performed. Lowercase letters indicate statistically significant differences between groups ($p \leq 0.05$).

The deletion construct W25N*, which lacks both DBDs and the C-terminal region of WRKY25, was unable to activate the expression of *WRKY53*. A similar lack of activation was observed with W25ΔpD1, which lacks a large part of the N-terminal DBD1, and W25ΔD2, which lacks the C-terminal DBD2 of WRKY25 (Fig. S3B). Interestingly, the chimera W18N-W25C downregulated *WRKY53* expression, whereas W25N-W18C upregulated it, mimicking the activator effect of the native WRKY25 protein. (Fig. 3B). These results suggest that, although both DBDs appear to be necessary for WRKY25 function, the N-terminal domain plays a critical role in activating *WRKY53* expression.

In addition, the effect of the two chimeras on the expression of *WRKY18* and *WRKY25* were tested in the transactivation assay. The two chimeras were used as effector constructs in a transactivation assay with a dual luciferase reporter system in Arabidopsis leaf protoplasts. For these assays, constructs harboring *WRKY18* and *WRKY25* promoters driving the expression of firefly luciferase, respectively, were co-transfected with effector constructs of WRKY18, WRKY25, WRKY53, W18N-W25C, and W25N-W18C. Consistent with our previous observations using *GUS* as reporter gene (Fig. 1A and 2B), the dual luciferase assays showed similar results with the native WRKY18, WRKY25 and WRKY53 on the promoter of *WRKY25* and *WRKY18* (Fig. S4A, B). For W18N-W25C and W25N-W18C the expression of the reporter gene driven by the *WRKY18* promoter was slightly upregulated, whereas reporter gene expression driven by the *WRKY25* promoter was downregulated in both cases (Fig. S4A, B). This demonstrates for these two promoters, that both, C-terminal or N-terminal domains of WRKY25, can mimic the effect of the wildtype WRKY25 and can override the WRKY18 effect.

To assess the influence of different protein domains on protein–protein interactions, the deleted and the chimeric proteins were analyzed using the BiFC system in *N. benthamiana* leaves, as previously described. Protein–protein interactions were observed in all cases, except for WRKY25 with W25ΔpD1 and the chimera W18N-W25C. In the case of the deletion construct, only a weak interaction was detected compared to the strong intensity observed in WRKY18 homodimers or WRKY18/WRKY25 heterodimer, based on the YFP/RFP fluorescence intensity ratio calculated from microscopy images. Interestingly, the chimera W25N-W18C interacted with both WRKY18 and WRKY25, to a similar extent as the WRKY18 homodimers or WRKY18/WRKY25 heterodimer. In contrast, W18N-W25C did not show any interaction with WRKY25 (Fig. 3C and S5). The chimera W18N-25C, which carries the C-terminal domain of WRKY25, did not interact with either WRKY18 or WRKY25 (Fig. 3C and S5). The observed interaction between W25N-W18C and WRKY25 is particularly noteworthy, given that WRKY25 does not homodimerize (Fig. 1B, 3C and S1, S5), and W18N-W25C failed to interact with WRKY25. (Fig. 3C and S5). These results suggest that the N-terminal domain of WRKY25 plays a significant role in protein–protein interactions, while the C-terminal domain of WRKY25 may abolish an interaction. All these results reinforced that the N-terminal domain of WRKY25 is more important for the modulation of the subnetwork.

The C-terminus of WRKY25 prevents an overshoot of WRKY53 expression while the N-terminus of WRKY25 modulates a fine-tuning in the senescence

In order to characterize the impact of this subnetwork on senescence in more detail, we complemented *wrky25* mutant plants with the deletion constructs (*wrky25*:W25N*, *wrky25*:W25ΔpD1, *wrky25*:W25ΔD2) and the two chimeric constructs (*wrky25*:W18N-W25C and *wrky25*:W25N-W18C), alongside the native WRKY25 (*wrky25*:W25) as control. All complementing constructs were driven by the *UBIQUITIN10* promotor. All lines were grown alongside the Col-0 wild type and the *wrky25* mutant for comparison and the senescence phenotype was assessed by evaluating leaf color, chlorophyll content and maximum photochemical quantum yield of photosystem II (PAM fluorometry) over development using 6 to 8 plants per line for these analyses.

First, we compared the complementation line carrying the native *WRKY25* construct (*wrky25*:W25) with the wild type plants Col-0 and the *wrky25* mutants. The 4-week-old plants showed similar phenotypes across all lines. However, after 6 to 8 weeks, the *wrky25*:W25 plants displayed a phenotype more similar to Col-0, than to the *wrky25*, which exhibited accelerated senescence. This trend was consistent in all measurements: i) the automated colorimetric assay (ACA), a tool developed by our group that automatically identifies and quantifies the different colors of each leaf within a rosette by measuring the number of pixels corresponding to each color category (green, green/yellow, yellow, brown/dry, and purple) ii) chlorophyll content and iii) photosystem II functionality using pulse amplitude modulation (PAM) fluorometry (Fig. S7A-C). Col-0 and *wrky25*:W25 generally did not

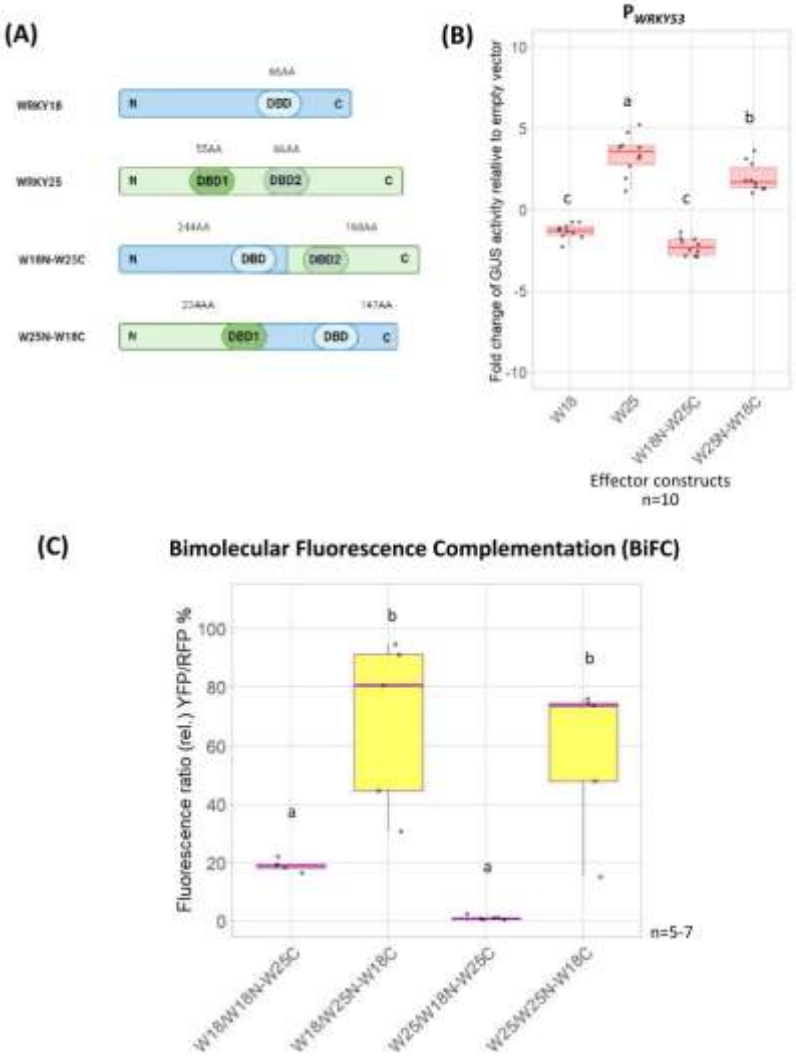

Fig. 3. Transactivation assay in Arabidopsis protoplasts for the P_{WRKY53} and the effect of the chimeras on it, and *in planta* protein–protein interactions of WRKY18 and WRKY25 with the chimeras in *N. benthamiana*. **(A)** Schematic drawing represents the native WRKY18 and WRKY25 protein as well as the chimeras between these WRKYs: W18N-W25C and W25N-W18C. **(B)** Arabidopsis root protoplasts were transiently transformed with the fragment of the *WRKY53* promoter (2759 bp), fused to the *GUS* gene as a reporter construct, along with 35S:*WRKY18* (W18), 35S:*WRKY25* (W25), 35S:*W18N-W25C*, or 35S:*W25N-W18C* as effector constructs. GUS activity values, expressed relative to the values of the empty vector, are shown as boxplots. Sample size (n = 10) corresponds to independent biological replicates. **(C)** Leaves of *N. benthamiana* were transformed with pBiFCt2in1-NN constructs containing the possible combinations for the interactions between WRKY18 or WRKY25 with the chimeras: W18N-W25C and W25N-W18C. These transformed leaves were analyzed under a confocal laser scanning microscope: yellow fluorescence (YFP) indicates interaction (BiFC), and red fluorescence (RFP) serves as a transformation control. Boxplots represent the relative fluorescence ratio (%YFP/RFP). Sample size (n) is indicated in the figure and represents independent biological replicates. In both (**B**) and (**C**), one-way ANOVA followed by Tukey's HSD post-hoc test was performed. Different lowercase letters denote statistically significant differences among groups ($p \leq 0.05$).

show significant differences (Fig. S6A, S7A), indicating that the transformed *WRKY25* construct substituted for the loss of a functional WRKY25 protein in *wrky25* mutant plants.

Based on these results, we tested the complementation lines with the chimeric constructs (*wrky25*:W18N-W25C and *wrky25*:W25N-W18C) and also the deletion constructs (*wrky25*:W25N*, *wrky25*:W25ΔpD1, *wrky25*:W25ΔD2) alongside Col-0 and *wrky25*. Here, we used the entire rosette for the ACA. Initially, in 4-week-old plants, all lines exhibited uniformly green leaves (Fig. 4A, Fig. S7A). In 6-week-old plants, differences between the lines became apparent. In the *wrky25* mutant, the complementation lines *wrky25*:W25N*, *wrky25*:W25ΔpD1, *wrky25*:W25ΔD2, *wrky25*:W18N-W25C and *wrky25*:W25N-W18C, senescence was accelerated, as indicated by a reduced percentage of green leaves and an increased percentage of brown leaves compared to Col-0 (Fig. 4A, Fig. S6B, Fig. S8A), in which *wrky25*:W25ΔpD1 and both chimere complementation lines appear to be a bit less accelerated (Fig. 4A, Fig. S6B, Fig. S8A). The differences between the lines became even more pronounced in 7-week-old plants. While the *wrky25* mutant and the *wrky25*:W25N*, *wrky25*:W25ΔpD1, *wrky25*:W25ΔD2 lines continued to exhibit accelerated senescence, the *wrky25*:W18N-W25C line showed a deceleration in senescence progression, with a higher percentage of green leaves not only compared to *wrky25* but also to Col-0 (Fig. 4A, Fig. S6B, Fig. S8A). In contrast, the *wrky25*:W25N-W18C line displayed an even more accelerated senescence phenotype than *wrky25*, with a significantly higher percentage of brown leaves and a lower percentage of greenish leaves compared not only to Col-0 but also to *wrky25* (Fig. 4A).

In addition, the loss of photosystem II functionality was monitored over time. To ensure appropriate comparisons, leaves of defined positions within the rosette were selected for analysis. Leaf No. 5 (Fig. 4B, Fig. S8B, S9A) and No. 10 (Fig. S9B) were first used for PAM fluorometry, after which chlorophyll was extracted from these same leaves (Fig. S8C, S9B). Both parameters exhibited trends like those observed with the ACA. In leaf No. 5, the *wrky25*:W25N, *wrky25*:W25ΔpD1, and *wrky25*:W25ΔD2 lines showed a slightly faster decline in photosystem functionality compared to both Col-0 and the *wrky25* mutant (Fig. S8B). Although the differences were not statistically significant, the trend was consistent with the pattern observed in the ACA analysis. Additionally, the *wrky25*:W25N-W18C line exhibited a significantly faster decline in photosystem functionality compared to Col-0, and to a lesser extent, compared to the *wrky25* mutant. In contrast, the *wrky25*:W18N-W25C line behave more comparable to Col-0 (Fig. 4B). This accelerated loss of photosystem functionality in *wrky25*:W25N-W18C was also evident in leaf No. 10 at week 7, where it contrasted with both Col-0 and *wrky25* (Fig. S9A). A similar pattern was observed for the chlorophyll content (Fig. S8C, S9B). Again, no statistically significant differences were detected among the lines for this parameter, the *wrky25*:W25N-W18C line showed a slightly more pronounced decline in chlorophyll content by week 7 in leaves No. 5 and 10 compared to Col-0 and the *wrky25* mutant, whereas the *wrky25*:W18N-W25C line remained more comparable to Col-0 (Fig. S9B).

As the phenotyping parameters gave us more insights into influences of the different domains of WRKY25, the expression of *WRKY53* was monitored using qRT-PCR in Col-0, *wrky25*, *wrky25*:W18N-W25C, and *wrky25*:W25N-W18C at weeks 6 and 7. At week 6, *wrky25*:W18N-W25C exhibited the highest expression levels of *WRKY53* (Fig. 4C). This complementation line showed significantly higher levels of *WRKY53* compared to Col-0 and *wrky25*, and to a lesser extent, compared to the other complementation line, *wrky25*:W25N-W18C (Fig. 4C). Interestingly, by week 7, there was a shift in *WRKY53* expression, in which *wrky25*:W25N-W18C along with *wrky25* displayed the highest levels of *WRKY53*, surpassing not only Col-0 but also *wrky25*:W18N-W25C (Fig. 4C). It is also noteworthy that Col-0 and *wrky25* increased *WRKY53* expression from week 6 to week 7, while the opposite trend was observed in *wrky25*:W18N-W25C, which showed a reduction in *WRKY53* levels over the same period (Fig. 4C). However, this is consistent with the senescence phenotype, meaning that *WRKY53* mRNA increased and showed its peak expression earlier in the lines with accelerated senescence.

In conclusion, the senescence phenotypes revealed that only the W18N-W25C construct was able to rescue the phenotype of *wrky25* plants. In contrast, the deletion constructs exhibited senescence patterns similar to the *wrky25* mutant, while *wrky25*:W25N-W18C displayed an even more pronounced accelerated senescence phenotype. Together with the *WRKY53* expression data, these results suggest that both domains of WRKY25 are involved in senescence regulation, but in distinct ways: the N-terminal domain appears to be essential for activating *WRKY53* expression, whereas the C-terminal domain may serve to limit or fine-tune this activation to prevent excessive *WRKY53* expression.

ROS molecules modulate the WRKY18/WRKY25/WRKY53 subnetwork

Whether a specific cue or signal is necessary for WRKY25 to exert its function within the subnetwork is still an open question. Previously, our group identified WRKY25 as a redox-sensitive protein. Moreover, it was demonstrated that *WRKY25* expression is induced by H_2O_2 treatment, whereas *WRKY25* overexpression at the same time reduces intracellular H_2O_2 contents[13] indicating that WRKY25 is part of redox feed-back loop. Given its ability to sense oxidative signals, we hypothesize that WRKY25 might act as a switch within the subnetwork. To assess this in more detail, we conducted the previously used transactivation assay in Arabidopsis protoplasts under oxidative conditions. For this purpose, 3-Amino-1,2,4-triazole (3'-AT) was added after the transformation process to induce oxidative conditions. 3'-AT inhibits catalase activity, thereby increasing intracellular H_2O_2 levels within a physiological range, while having no effect on GUS activity measurement[31]. The upregulation of the reporter gene expression driven by the *WRKY53* promoter through the effector protein WRKY25 was significantly reduced under oxidative conditions. Surprisingly, the WRKY18/WRKY25 heterodimer did not significantly change its ability to upregulate *WRKY53* expression under oxidative conditions (Fig. 5A) even though the activity of the heterodimer was more similar to WRKY25 alone.

To decipher the influence of H_2O_2 on the activator effect of WRKY25, we first tested the influence of a cysteine at position 17 in the WRKY25 protein, which is the only cysteine not involved in the formation of the DNA-binding zinc finger structure. Therefore, this cysteine was replaced by a serine (W25cysmut) by site-directed mutagenesis using PCR. This change had no influence on the redox response of the WRKY25 protein

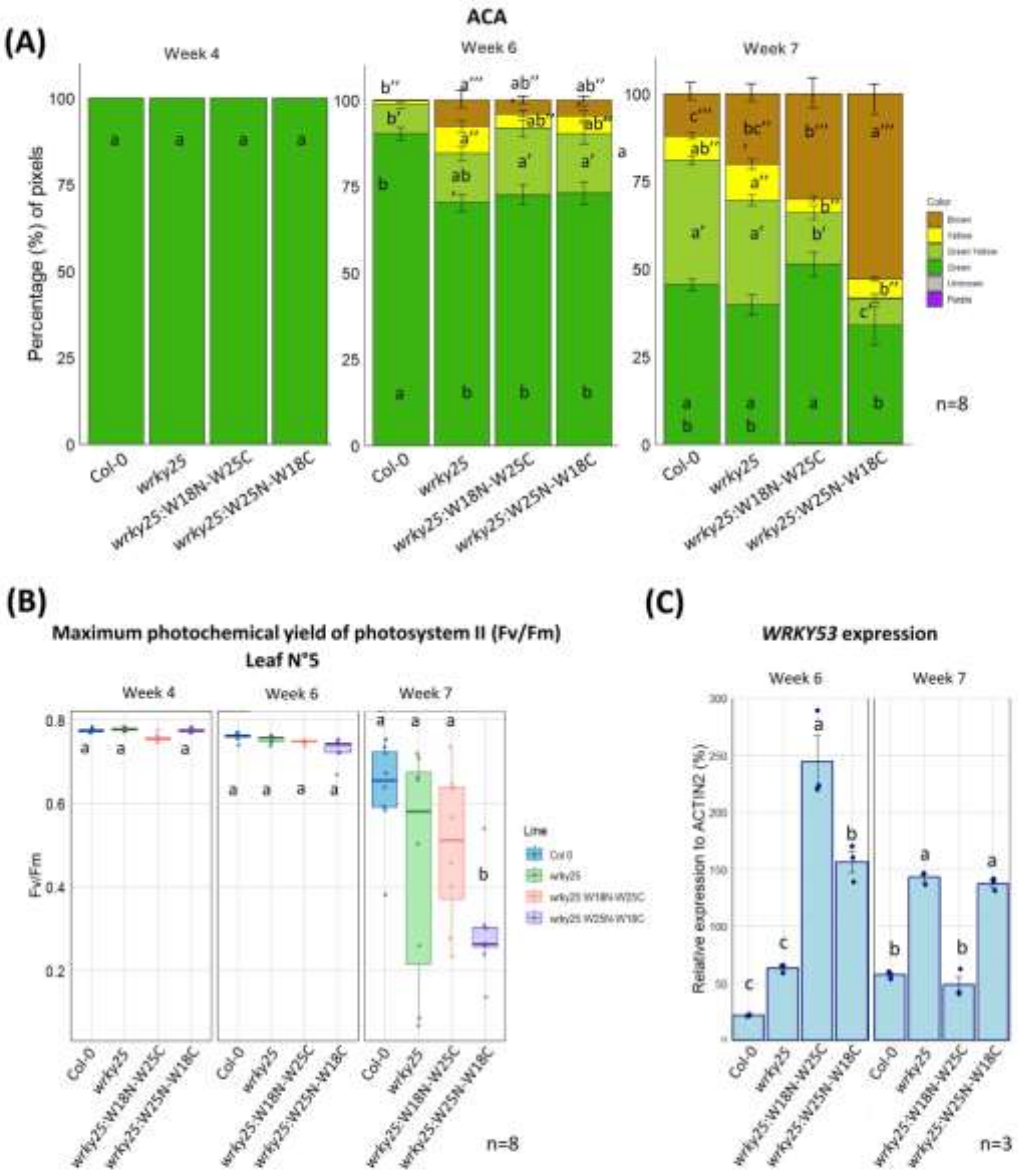

Fig. 4. Senescence phenotyping of the complementation lines: *wrky25*:W18N-W25C and *wrky25*:W25N-W18C compared with Col 0 and *wrky25*. *(A)* The Automated Colorimetric Assay (ACA) categorizes the pixels corresponding to the color of individual leaves from 8 plants into five categories: green, green-yellow, yellow, brown, and purple. Quantification is presented as the percentage of each category relative to the total pixel number across all leaves (n = 8 biological replicates). **(B)** Boxplots present Fv/Fm values measured with PAM fluorometry for leaf No. 5 from 4-, 6-, and 7-week-old plants (n = 8 biological replicates). One-way ANOVA followed by Tukey's HSD post hoc test was performed; different lowercase letters indicate statistically significant differences among groups ($p \leq 0.05$). **(C)** Gene expression of *WRKY53* was analyzed by qRT-PCR and normalized to *ACTIN2* expression. Data are shown as mean ± SD (n = 3 biological replicates). Lowercase letters indicate statistically significant differences according to one-way ANOVA followed by Tukey's HSD test ($p \leq 0.05$).

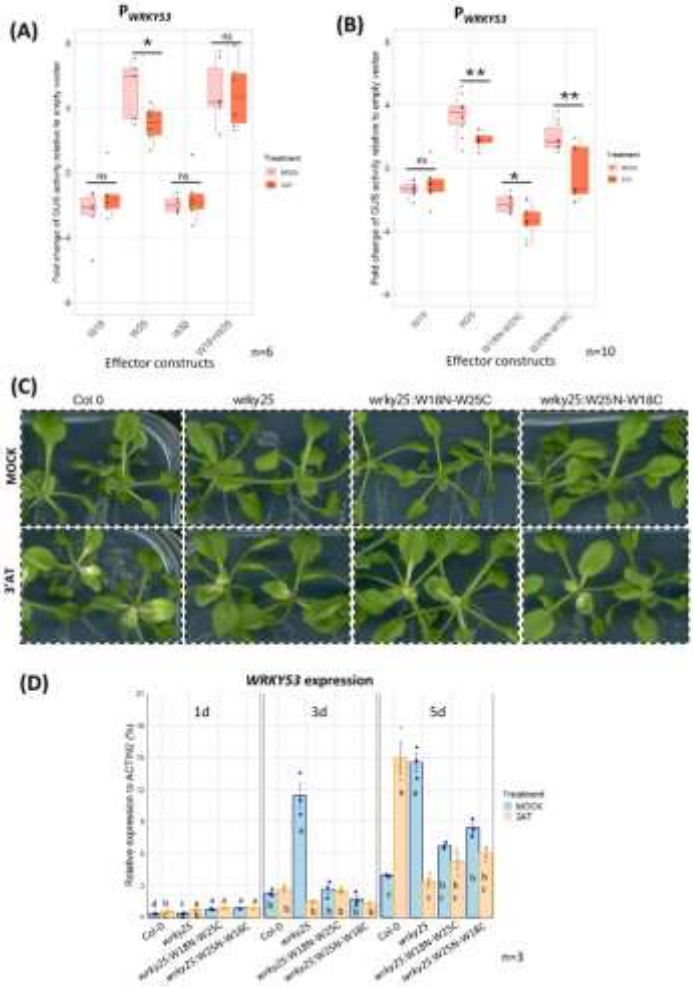

Fig. 5. Oxidative stress effect on the transactivation assays in Arabidopsis protoplast for the P_{WRKY53} and the effect of oxidative stress *in planta* on young plants of the complementation lines *wrky25*:W18N-W25C and *wrky25*:W25N-W18C. Arabidopsis root protoplasts were transiently transformed with a fragment of the *WRKY53* (2759 bp) promoter fused to the *GUS* reporter gene, along with 35S:*WRKY18* (W18), 35S:*WRKY25* (W25), 35S:*WRKY53* (W53), or 35S:*WRKY18*/*WRKY25* (W18 + W25) **(A)** or, in a second series, 35S:*WRKY18* (W18), 35S:*WRKY25* (W25), 35S:*W18N-W25C* (W18N-W25C) and 35S:*W25N-W18C* (W25N-W18C) **(B)** as effector constructs. In both series, half of the transfected protoplasts were simultaneously incubated with 10 mM 3'-AT or the same volume of water for the MOCK conditions, respectively. The boxplots present the values relative to the empty vector control. Sample size (n) is indicated in the figure and represents independent biological replicates. Statistical significance was assessed using a two-tailed Student's t-test (*$p \leq 0.05$; **$p \leq 0.01$; ns: not significant). **(C)** 2-week-old seedlings of *wrky25*:W18N-W25C and *wrky25*:W25N-W18C, Col-0 and *wrky25* were transferred onto new plates with or without 3'-AT. 5 days after transfer a bleaching of the leaves to a different extent in the different lines could be observed. **(D)** Gene expression of *WRKY53* with and without 3'-AT was analyzed by qRT-PCR in different lines and normalized to the expression of the *ACTIN2* gene (mean values ± SD, n = 3). A one-way ANOVA followed by Tukey's HSD post-hoc test was performed. Different lowercase letters denote statistically significant differences among groups ($p \leq 0.05$).

indicating that this cysteine is most likely not involved in redox sensing (Fig. S10). We also tested the deletion constructs W25N*, W25ΔpD1, W25ΔD2, and the two chimeric constructs W18N-W25C and W25N-W18C in the same transactivation assay under oxidative conditions. Neither W25N* nor W25ΔD2 showed any difference in *WRKY53* expression (Fig. S11). W25ΔpD1 exhibited a slight but still negative effect but there is no statistically significant difference (Fig. S11). Intriguingly, in the case of the chimeras, we could observe that W18N-W25C consistently downregulated *WRKY53* expression, while W25N-W18C, which retains the N-terminal region and DBD1 of WRKY25, completely shifted its activity from a positive regulator under normal conditions to a negative regulator of *WRKY53* expression under oxidative stress (Fig. 5B).

The effect of H_2O_2 on the two chimeras was further investigated *in planta* using young plants to avoid the influence of other factors which are activated in older plants already undergoing senescence. Col-0, *wrky25*:W18N-W25C and *wrky25*:W25N-W18C seeds were grown on agar plates and seedlings were transferred to new media with and without 3'-AT after two weeks. Subsequently, they were photographed 1, 3, and 5 days later and harvested to evaluate the expression of *WRKY53* by qRT-PCR. After 5 days of treatment, degreening of the leaves was observed in Col-0 plants treated with 3'-AT in some of the leaves (Fig. 5C). However, in both complementation lines with the chimeric constructs only a milder or almost no effect of the oxidative conditions was observed (Fig. 5C). Especially, *wrky25*:W25N-W18C showed little to no leaf bleaching due to the oxidative stress (Fig. 5C). The expression of *WRKY53* increased over time in all 4 lines but this increase was much stronger in *wrky25*. After 5 days of 3'-AT treatment, *WRKY53* expression was highly induced in Col-0 plants compared to non-oxidizing conditions, while expression was even repressed by 3'-AT in *wrky25* mutant plants. This effect could already be observed after 3 days of 3'-AT treatment. The repressing effect was also visible after 5 days of 3'-AT treatment in *wrky25*:W18N-W25C and *wrky25*:W25N-W18C plants but to a lesser extend (Fig. 5B). Taken together, this suggests that both the N- and C-terminus of WRKY25 may be involved in the recognition of oxidative signals, in which the N-terminus appears to have a higher impact on activation of *WRKY53* expression and heterodimer formation.

WRKY25 harbors putative redox switches in the N and C-terminal WRKY domain

Given that the WRKY25 protein can sense oxidative signals, we wondered which structural feature enables this function. It is well-documented that disulfide bonds formed by cysteine residues play a crucial role not only in the structural integrity and stability of proteins but also as redox switches that regulate protein function[35–37]. Interestingly, a novel redox switch involving a lysine-cysteine crosslink with a covalent NOS bridge has recently been identified as a potential regulatory element in proteins that modulate function in response to redox changes[35]. Furthermore, the NOS bridge was observed in proteins from diverse domains of life. In some cases, lysine residues were concurrently connected to two cysteine residues, resulting in the formation of a sulfur-oxygen–nitrogen-oxygen-sulfur (SONOS) bridge[38].

With this in mind, we modeled the WRKY25 protein using AlphaFold, along with two representative proteins (the rat Galectin-1 and the human hematopoietic cell receptor CD69) in which such redox switches had been previously identified[18]. Upon analyzing the predicted structures of Galectin-1 and CD69 and comparing them with the WRKY25 model, we identified a similar spatial arrangement of one lysine and two cysteine residues in WRKY25 (Fig. S12), suggesting analogous redox switches. Specifically, two potential lysine-cysteine redox switches were identified in WRKY25, each located within one of the WRKY domains at the N- and C-terminus of the protein (Fig. 6A).

Since WRKY18 appeared not to be redox-sensitive, we also modeled the WRKY18 protein for comparison. Notably, the predicted redox switch in the WRKY motif of WRKY25 was absent in WRKY18, which lacks the crucial lysine residue found in WRKY25 (Fig. 6B). We also modeled the two chimeras, and the putative redox switch was detected in the C-terminal of W18N-W25C (Fig. 6C) and in the N-terminal of W25N-W18C (Fig. 6D). Therefore, we speculate that this novel redox switch might be the key feature that allows WRKY25 to sense oxidative signals. In addition, we modeled the electrostatic surface potential of WRKY25 to assess whether the region or the amino acid residues involved in the potential redox switches exhibited reduced charge or a more neutral environment (Fig. S13), which could indirectly suggest the feasibility of bond formation. However, based on this analysis, we could not conclusively determine whether the formation of these redox switches is indeed possible.

Based on the evidence of these putative redox switches, targeted Liquid Chromatography-Mass Spectrometry (LC–MS) analysis was employed to verify their existence. Therefore, the N-8xHis-tagged recombinant WRKY25 protein was expressed in *E. coli* and purified. Subsequently, this recombinant protein was proteolytically cleaved under non-reducing conditions and the possible no-bridge and NOS-bridge peptides (Fig. S14A, B) were evaluated. If no bridge is formed, two separate peptides, SYFK and CTYPDCVSK, for DBD1 as well as SYYK and CTFQGCGVK for DBD2 should be detected. If a NOS bridge is formed, the two peptides would be linked resulting in a larger peptide, respectively. Mass/charge signals for all four no-bridge peptides of DBD1 and DBD2 could be detected (Fig. S14C) in the LC–MS chromatogram. In addition, peptide pairs for all possible four NOS-bridge combinations (DBD1: pos1 K-C1, pos1 K-C6, DBD2: pos2 K-C1 and pos2 K-C6) were also detected in the same LC–MS run (Fig. S14D). All represented transitions in Table S5 are unique for the four different NOS-bridge combinations except for the peptide/fragment pair m/z 524.89/588.25 (see method section for definition of uniqueness). The retention times of the K-C1 and K-C6 peptides were always similar as they are representing peptide isomers, which could not be separated on the LC–MS platform. Taken together, this is a strong indication that the NOS bridges are indeed formed.

Discussion

Senescence is a very important developmental process at the end of plant development and is regulated in a very complex crosstalk to other processes. Besides almost all plant hormones, reactive oxygen species, especially H_2O_2,

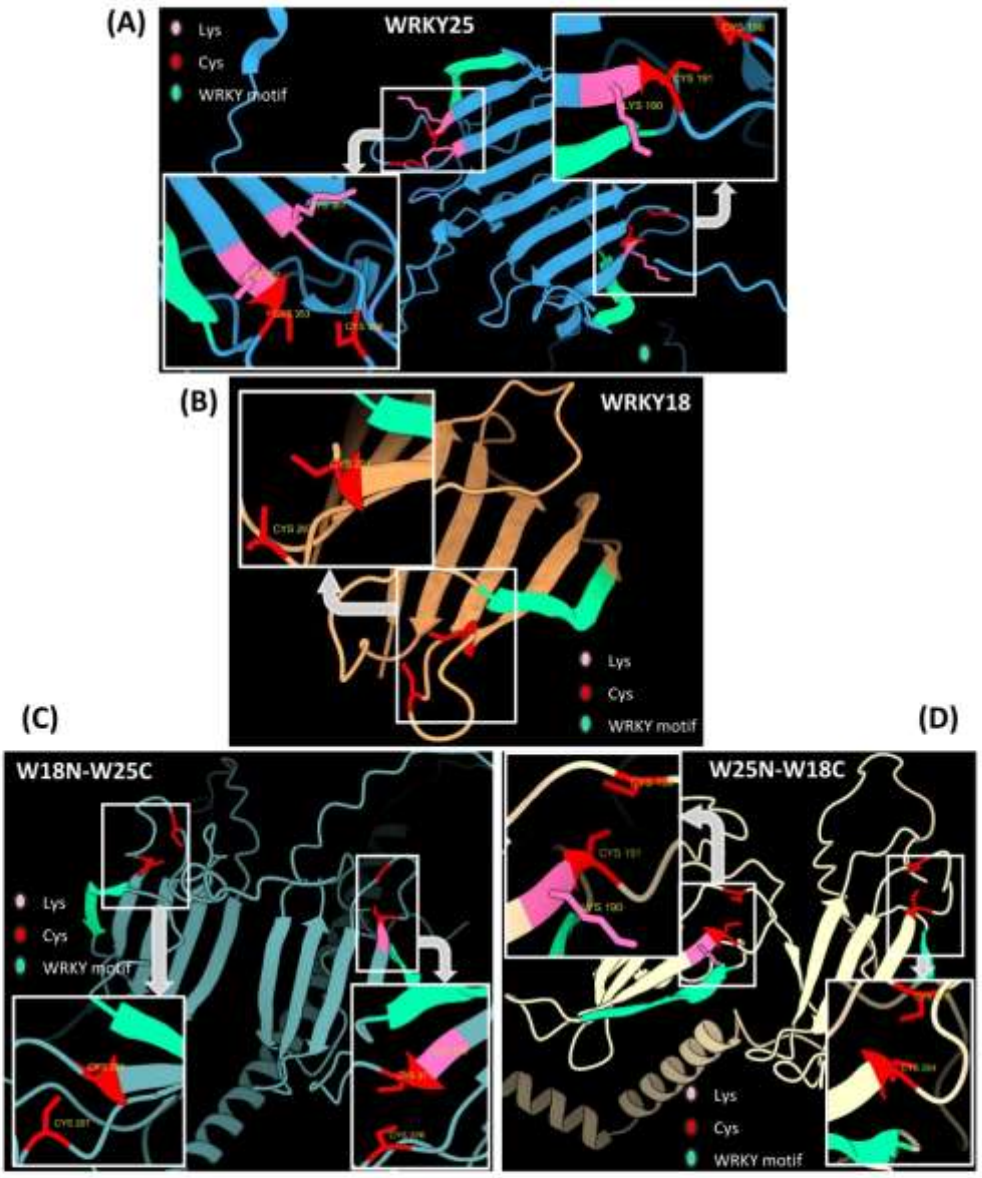

Fig. 6. Alpha fold modeling of WRKY25, WRKY18 and the two chimeric proteins. **(A)** WRKY25 protein model illustrating the putative NOS bridge formed between Lys and Cys residues at the N-terminal region and at the C-terminal region. **(B)** WRKY18 protein model showing the presence of a Cys residue but the absence of the Lys residue is necessary to form the NOS bridge. **(C)** W18N-W25C chimeric protein model, depicting the putative NOS bridge in the C-terminal region. **(D)** W25N-W18C chimeric protein model, illustrating the putative NOS bridge in the N-terminal region. In all models, Lys residues are shown in pink, and Cys residues are shown in red, and the conserved WRKY motif (WRKYGQ) is depicted in mint. Grey arrows indicate closeups of the respective regions in the DBDs with the possible NOS bridges between Lys and Cys.

have been identified as important signaling components. A long-term increase in intracellular H_2O_2 contents has been characterized in Arabidopsis and rapeseed plants at the onset of senescence[8] and genes responding to ROS are activated early in the chronology of gene expression changes[10]. However, how hydrogen peroxide signals are transmitted into transcriptional changes is a field with many open questions. Several transcription factors have already been characterized to change their DNA-binding affinity due to oxidative conditions, however, the detailed molecular mechanisms remain elusive in many cases.

A role for WRKY25 in senescence through the activation of *WRKY53* in a small subnetwork with the participation of WRKY18 has already been suggested, but the precise regulatory interactions among these WRKY transcription factors, including the role of WRKY18 as an effective repressor of *WRKY53*, had not been fully elucidated. In addition, previous studies have shown that *WRKY53* expression can be induced by H_2O_2 treatment and is upregulated in parallel to long-term increase in intracellular H_2O_2 contents at the onset of senescence[27,39]. Interestingly, WRKY25 has been characterized as a redox-sensitive transcription factor with a higher potential to activate *WRKY53* expression under more reducing conditions. Additionally, *WRKY25* expression is induced by H_2O_2, and *WRKY25* overexpression reduced intracellular H_2O_2 levels indicating complex regulatory feedback loops between H_2O_2 signals and WRKY transcription factors[13]. However, the precise mechanism by which WRKY25 senses and integrates oxidative signals within the WRKY18/WRKY25/WRKY53 subnetwork remained to be described.

Notably, WRKY25 belongs to the group I WRKY proteins, which are characterized by possessing two DBDs. We aimed to identify which domain was responsible for which regulatory function. Therefore, we created different deletion constructs and domain-swapping chimeras between WRKY18 and WRKY25. One chimera contained the N-terminal region of WRKY25 with its WRKY DBD1 (W25N-W18C), while the other chimera had the C-terminal region of WRKY25, which included its WRKY DBD2 (W18N-W25C). Our transactivation assays with the deletion constructs demonstrated that two DNA-binding domains are needed for a functional protein. The chimeric constructs revealed that the N-terminus of WRKY25 is necessary to activate *WRKY53* expression. Even though it was initially believed that only the C-terminal domains of group I WRKY proteins were responsible for DNA-binding[34,40], subsequent research revealed that both WRKY DBDs (N- and C-terminal) are capable of binding DNA, with each displaying different binding specificities[33,41,42]. In our study, the chimera containing the N-terminus of WRKY25 retained this activating effect on *WRKY53* expression, similar to the native WRKY25, whereas the chimera with only the C-terminal DBD of WRKY25 lost this ability.

Another notable finding was WRKY25's inability to homodimerize. However, WRKY25 did form heterodimers, particularly with WRKY18. Both chimeras were able to interact with native WRKY18, in which interactions involving the N-terminus of WRKY25 produced a stronger signal. In contrast, only W25N-W18C could form a dimer with WRKY25. This suggests a predominant role of the WRKY25 N-terminus in protein–protein interactions, while the C-terminus of WRKY25 appears to abolish the interactions with itself. This aligns with previous findings on the importance of N-terminal leucine zipper sequences in mediating WRKY-WRKY interactions[32,33,43].

Another intriguing aspect was the activator effect of the WRKY18/WRKY25 heterodimer on *WRKY53* expression, despite WRKY18 alone or as homodimer acts as a strong repressor of *WRKY53* and its own expression. However, WRKYs are known to form homo- or hetero-complexes which exhibit varying DNA-binding activities and regulatory capabilities depending on the context[32]. For instance, WRKY18 enhances resistance to *Pseudomonas syringae*, but coexpression with WRKY40 or WRKY60 can increase susceptibility[44]. Moreover, it has been shown that WRKY60-WRKY18 interaction increases DNA-binding ability of WRKY18 while WRKY60-WRKY40 interaction decreases DNA-binding ability of WRKY40[31]. In our case, we speculate that WRKY25, in response to a signal, shifts the equilibrium between positive and negative effects on *WRKY53* expression within the subnetwork by sequestering WRKY18 to heterodimers, thereby reducing its repressor effect and increasing *WRKY53* expression.

To provide further insights into how WRKY25 modulates the subnetwork and *WRKY53* expression *in planta*, complementation lines of *wrky25* mutant plants were created using WRKY25, the deletion constructs and the chimeras between WRKY25 and WRKY18. As described before, the senescence phenotype of *wrky25* conflicts with its role as direct *WRKY53* activator, which clearly indicates that WRKY25 is part of a more complex regulatory network, in which the loss of a functional WRKY25 most likely leads to an imbalance in this network, making such a contradictory senescence phenotype possible[13]. However, for the analysis of the potential of various construct to complement the loss of a functional WRKY25 protein, this is not relevant. While the transformation of the wild type *WRKY25* construct could fully complement for the loss of a functional WRKY25 protein in the *wrky25* mutant, the accelerated senescence phenotype was not complemented by the deletion constructs and only partially by the two chimeric constructs. In 7-week-old plants, senescence was altered by transformation of both chimeras, respectively, but with different outcomes: while the presence of the N-terminus of WRKY25 even pronounced the accelerated senescence phenotype, the presence of C-terminus of WRKY25 started to delay senescence compared with *wrky25* or even Col-0. Consistently, *WRKY53* expression levels changed compared to Col-0 in different ways. These observations suggest that the two domains appear to have contradictory functions: the N-terminus of WRKY25 activates *WRKY53* expression while the C-terminus appears to prevent excessive *WRKY53* expression and fine-tunes the senescence process.

Further evidence from transactivation assays in Arabidopsis protoplasts revealed that the chimera containing the N-terminus of WRKY25 switched from an activator to a repressor of *WRKY53* expression under oxidative conditions. This was corroborated in young plants of the complementation lines which were exposed to oxidative stress through the inhibition of the catalases. Under these oxidative conditions, the Col-0 plants showed a very clear activation of the *WRKY53* expression compared to the two chimeras. While, under normal conditions, *WRKY53* expression in both chimeras was significantly higher than in Col-0, an additional activation of WRKY53 under oxidative conditions was not observed. This is consistent with the downregulation of *WRKY53*

under oxidative conditions in the transactivation assays but also indicates that both, the C- and N-terminal domain of WRKY25 are involved in the transduction of the H_2O_2 signal and further supports that WRKY25 is most likely the driving force to balance of *WRKY53* expression and prevent overshooting reactions under oxidative stress conditions. Thereby, WRKY25 might also prevent a too early activation of premature senescence under stress conditions still contributing to the onset and progression of natural senescence.

Overall, our findings suggest that WRKY25 senses oxidative signals, specifically H_2O_2, through a structural feature, most likely a putative redox switch, which modulates the regulatory function, particularly influencing *WRKY53* expression. It is widely known that reactive oxygen species (ROS) can oxidize cysteine residues, which do not only play a role in scavenging ROS but also contribute to cellular signaling across various biological and pathological contexts[36]. Cysteine residues can form disulfide bonds, which are crucial for maintaining protein structure and stability, and can also function as redox switches that regulate protein activity[35–38]. Until recently, regulatory switches involving covalent crosslinks other than disulfide bridges had not been described. In this context, we tested a mutated version of WRKY25 in its cysteine at position 17 to evaluate the response under oxidative conditions. In the transactivation assays no change in the response to the oxidative conditions could be detected, indication that this cysteine appears to have no influence on the redox responsivity of WRKY25.

However, a novel covalent crosslink between a cysteine and one or two lysine residues, involving NOS or SONOS bridges, was recently identified as an allosteric redox switch[35,38]. The widespread occurrence of covalent lysine-cysteine redox switches has been identified in many proteins ranging from human to plant pathogenic proteins. For plants, a NOS bridge was suggested in the inositol monophosphatase from *Medicago truncatula*[38] but this NOS bridge was not confirmed experimentally. NOS bridges have also been predicted in many different DNA-binding proteins, in which the formation of the NOS bridge mostly interferes with DNA–protein interaction[38]. Therefore, we tried to explore the potential presence of these novel redox switches in the WRKY25 protein, given its characterized sensitivity to oxidative signals. Using AlphaFold modeling, we identified two putative redox switches in WRKY25, located in the N-terminal and C-terminal DBDs. WRKY18, known as a non-redox-sensitive WRKY, lacked these putative redox switches, in fact, a lysine in the same position as the one found in the putative redox switches in the WRKY domain of WRKY25 is missing. As expected, the chimera W25N-W18C contained a redox switch at the N-terminus of WRKY25, consistent with the sensitivity to oxidative signals in the transactivation assays. Also, the chimera with the C-terminus of WRKY25 presented the putative redox switch which is consistent with its role *in planta* in the complementation lines. As an initial step to validate the existence of this redox switch, we digested purified recombinant WRKY25 proteins and analyzed the resulting peptides using LC–MS. Interestingly, we could support the presence of these putative redox switches, as the NOS-linked peptides could be detected. However, without isotopically labeled synthetic standard peptides, no quantitative conclusions can be drawn regarding the relative concentrations of specific peptides in the protein digest, as they may exhibit different response factors. Nevertheless, the detection of mass/charge signals (each verified by 5 to 9 transitions representing distinct peptide/fragment ion pairs) allows us to speculate that the NOS bridges in the WRKY25 protein really exist, but the evidence that changes in redox conditions lead to a reversible establishment of these NOS bridges is still pending. Establishing oxidative or non-oxidative conditions throughout the whole LC–MS procedure remains a significant challenge for further experimental analysis. At the same time, this limitation opens new questions and opportunities for a deeper investigation in this area.

Based on the evidence presented, we propose a model (Fig. 7) for the interaction in a small subnetwork: WRKY25 senses oxidative stress and regulates *WRKY53* expression. Under oxidative conditions, WRKY25 is higher expressed but less efficient in activating *WRKY53* expression. However, as WRKY25 protein levels increase, the WRKY25/WRKY18 heterodimer forms, mitigating WRKY18's repressive effect and further activating *WRKY53* expression. Additionally, WRKY25 and WRKY18 downregulate their own expression to prevent an excessive response. In this way, WRKY25 balances the expression and activity within the WRKY53/WRKY25/WRKY18 network to ensure a slow but progressive induction of senescence. Taken together, our results contribute to our mechanistic understanding of senescence regulation and suggest that the novel NOS redox switch also exists in plant regulatory proteins.

Materials and methods

Plant material and cultivation

Plants were grown on standard soil. An amount of 70 l of the standard soil CL Topf (Art.Nr.:10–00,300, PATZER ERDEN GmbH, Sinntal, Germany) was mixed with 8 l of sand (Flammer Bauunternehmung GmbH & Co. KG, Rheinsand, Tuebingen, Germany) and sieved with a mesh width of 8 × 10 mm. For all senescence phenotyping experiments the plants were grown under long-day conditions (16 h/8 h, light/dark), and moderate light intensity (80–100 µmol s^{-1} m^{-2}) was applied in a climatic chamber at an ambient temperature of 20 °C. Individual leaf positions within the rosettes were color-coded with different threads, allowing for the analysis of individual leaves according to their age, even at very late stages of development[26,45]. The leaves were numbered starting from leaf No. 1 for the first true leaf, while the cotyledons were not considered in the enumeration. To avoid circadian effects, the plant material was always harvested at the same time of the day.

The lines used for senescence phenotyping experiments were: Col-0, *wrky25*, *wrky25*:UBI::W18N-W25C, *wrky25*:UBI::W25N-W18C, *wrky25*:UBI::W25. The Nottingham Arabidopsis Stock Centre (NASC) kindly provided seeds for Col-0 and the T-DNA insertion line of *WRKY25* (SAIL_529_B11; previously characterized in[46]) The complementation lines were produced for this manuscript as described below and seeds are available upon request.

For the experiments on the oxidative signal effect on seedlings, seeds of the different plant lines were sterilized first with 70% (v/v) ethanol, 0,05% (v/v) triton and subsequently with 100% ethanol. The sterilized seeds were grown on ½ Murashige and Skoog (MS) medium (1 l: 2.17 g MS micro and macro elements (Duchefa

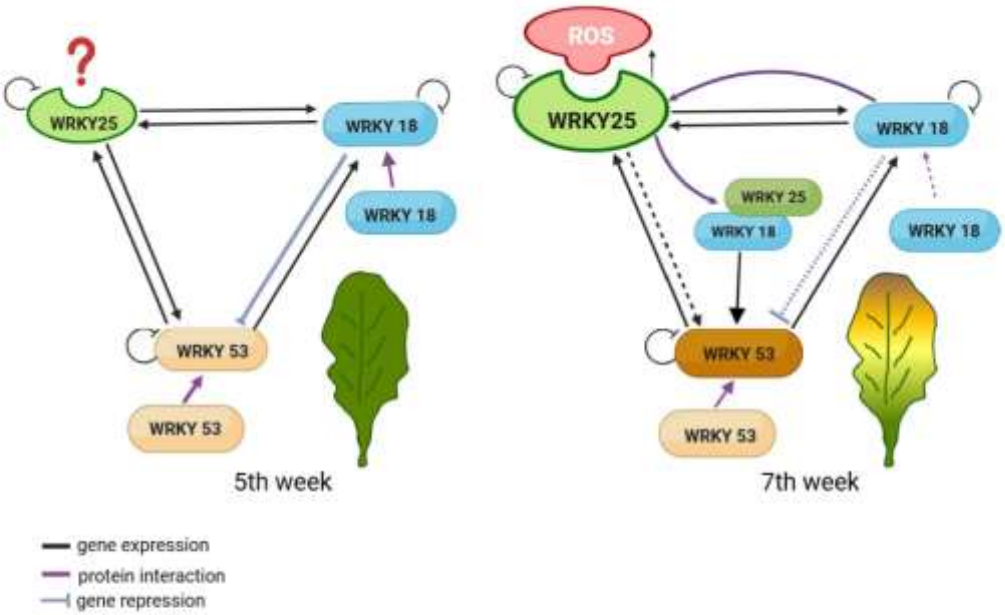

Fig. 7. Model proposed for the subnetwork WRKY18/WRKY25/WRKY53 under the influence of an oxidative signal to induce senescence through WRKY53. The equilibrium of WRKY18/WRKY25/WRKY53 network encounters modifications at the onset of senescence. WRKY25 senses increasing H_2O_2 contents, and the oxidized form is less efficient in DNA-binding and upregulation of *WRKY53* expression. However, at the same time, increasing H_2O_2 contents lead to increasing *WRKY25* expression, so that the WRKY25/WRKY18 heterodimer forms, mitigating WRKY18's repressive effect on *WRKY53* expression and increasing a positive effect on *WRKY53* expression. Additionally, WRKY25 and WRKY18 downregulate their own expression to prevent an excessive response. In this way, WRKY25 balances the expression and activity within the WRKY53/WRKY25/WRKY18 network to ensure a slow but progressive induction of senescence.

M0222.0025), pH 5.7–5.8, 8 g agar) with or without 20 µM of 3-Amino-1,2,4-triazole (3'-AT) added for oxidative conditions. For RNA extraction, two-week-old seedlings grown on MS medium without 3'AT were transferred to a new MS medium with or without 3'AT.

Cloning and plant transformation

For ß-Glucuronidase reporter assays, a 3,000 bp promoter fragment upstream of the WRKY18 or WRKY25 start codon and a 2,759 bp sequence upstream of the WRKY53 start codon were cloned into the binary vector pBGWFS7.0 and used as reporter constructs, respectively. For the effector constructs, the cDNAs of WRKY18 (1701 bp, At4g31800), WRKY25 (1751 bp, At2g30250), WRKY53 (1501 bp, At4g23810) were cloned into the vector pJAN33. In addition, deletion constructs of WRKY25: W25N* (498 bp), W25ΔpD1 (1020 bp), W25ΔD2 (987 bp) and the chimeric constructs W18N-W25C (1239 bp) and W25N-W18C (1125 bp) were used also as effectors. Naturally occurring *BsaI* restriction sites in *WRKY18* or *WRKY25* DNA sequences were mutated by site-directed mutagenesis. Deletion constructs of *WRKY25* were generated as follows. For W25N*, a fragment of 498 bp corresponding only to the N-terminal region up to (but not including) the first DNA-binding domain (DBD1) was amplified. For W25ΔpD1, two fragments were amplified: one from the N-terminal region upstream of DBD1 (429 bp), and one from the C-terminal region downstream of DBD1, containing the second DNA-binding domain (DBD2) (591 bp). For W25ΔD2, a fragment containing DBD1 from the N-terminal region just upstream of the DBD2 (939 bp), and a fragment from the C-terminal region downstream of DBD2 (48 bp), were amplified. For the chimeric constructs, the N-terminal (732 bp) and C-terminal (438 bp) sequences of *WRKY18*, and the N-terminal (681 bp) and C-terminal (489 bp) DNA sequences of *WRKY25*, were individually amplified. The respective fragments were ligated to generate the desired deletion and chimeric constructs. Additionally, a mutated version of *WRKY25* was generated in which the cysteine at position 17 was replaced with a serine via a site-directed G-to-C substitution using PCR.

All assembled fragments and the *WRKY25* version mutated at the Cys at pos. 17 (W25cysmut) were cloned into the pENTR-BsaI entry vector (described in[47]) using Golden Gate cloning. The deletion and chimeric constructs were subsequently transferred to the pJan33 destination vector via Gateway cloning. Correct insertions and ligation were verified by DNA sequencing. All primers used in these cloning steps are listed in Table S1.

For Dual Luciferase reporter assays, the same fragments upstream of the start codons of *WRKY18*, *WRKY 25* or *WRKY53* mentioned above, were cloned into the gateway destination vector pGWL7. The cDNAs of *WRKY18*, *WRKY25* and *WRKY53* were cloned into the gateway destination vector p2GW7 and used as effector constructs. In addition, the chimeric sequences generated for GUS reporter assays were used as template, amplified and cloned into the gateway vector p2GW7 to use the same vector for the effector constructs. All primers used for this cloning process are described in Table S1.

For Bimolecular Fluorescence Complementation (BiFC), the cDNAs of *WRKY18*, *WRKY25* and *WRKY53* as well as the deletion and chimeric sequences were cloned into the gateway vector pDONR221. Subsequently, they were cloned with the possible combinations of each other into the pBiFCt2in1-NN vector[48,49] carrying both genes of interest. By this cloning step, the genes of interest were fused to the sequences encoding the N- or the C-terminal part of the yellow fluorescent protein (YFP), respectively. In the same vector backbone, an internal red fluorescent protein (RFP) gene is present as transformation and expression control. The expression of the fusion proteins is driven by the cauliflower mosaic virus 35S promoter. All primers used are presented in Table S2.

For plant complementation lines, the protein coding sequence of *WRKY25* (with previously removed *BsaI* restriction site), the deletion, and chimeric sequences were cloned into the Green Gate entry vector pG00C (Table S3). The moderate constitutively active promoter of the *UBIQUITIN10* gene of Arabidopsis was used for all constructs as the 35S promoter led to gene silencing when combined with WRKY25[13]. All constructs were assembled into the final vector pZ03 with modular Green Gate technology described in[50]. The final vectors obtained were transformed into *Agrobacterium tumefaciens* strain GV3101. Finally, the transformed Agrobacterium was used to transform the *wrky25* mutant plants was transformed through floral dipping.

Protoplast preparation and transformation

For the ß-Glucuronidase (GUS) reporter assays, the protoplasts were obtained from a root cell culture of *Arabidopsis thaliana* ecotype Col-0 as described before[29]. Protoplasts were transiently transformed using 20–40% (w/v) Polyethylenglycol (PEG1500) with different concentrations of the respective plasmid DNA as is described in[51].

The protoplasts for the Dual-Luciferase reporter assay were obtained from fresh mesophyll tissue and transiently transformed with different concentrations of the respective plasmid DNA following the protocol published by[52] with some minor variations in the transformation part. The number of resuspended protoplasts used for transformation was doubled as well as the amounts of PEG and W5 solutions. Finally, the protoplasts were resuspended in 250 µl instead of 1 ml of WI solution.

ß-Glucuronidase reporter assay

Arabidopsis protoplasts from root cell culture were transformed using 5 µg of effector plasmid (pJAN33) and 5 µg of reporter plasmid (pBGWFS7) DNA. As an internal transformation control, 0.5 µg of a luciferase construct (pBT8-35SLUCm3) was co-transfected. After overnight incubation (15–17 h) in the dark at 20 °C, 10 ml of fall buffer (0.5 M mannitol, 15 m M $MgCl_2$, 5 mM MES) was added to the protoplasts, which were then collected by centrifugation (200 g, 4 °C). The collected protoplast pellet was subjected to lysis for protein extraction. 100 µl of lysis buffer (PROMEGA Luciferase Assay System E1500) was added to the pellet, followed by vigorous agitation using a vortex and incubation on ice for 5 min. The protein lysate was then concentrated by centrifugation (17,000 g, 10 min).

For luminescence measurements, 25 µl of Luciferase Assay Reagent (PROMEGA Luciferase Assay System E1500) was added to 20 µl of protein lysate. Luminescence was measured for 10 s using a TriStar2S Multimode Reader 941 plate reader (Berthold Technology). The fluorometric determination of β-Glucuronidase reporter activity followed the protocol described by[53]. The fluorometric measurements were performed using the same TriStar2S Multimode Reader 941 plate reader. To correct for transformation efficiency, β-Glucuronidase activity was normalized to luciferase luminescence. This was done by dividing the fluorometric measurements of each sample by their corresponding luminescence values. The resulting values were then normalized to those of an empty vector, which was used as a control. Additionally, GUS reporter assays with 3'-AT were performed as described above, except that 10 mM 3'-AT or an equivalent volume of water was added before the overnight incubation of the protoplasts.

Dual-luciferase reporter assay

Arabidopsis protoplasts from mesophyll tissue were transformed using 4 µg each of effector (p2GW7), promoter (pGWL7), and internal transformation control (P2GW7-35S:RNLuc) plasmid DNA. After overnight incubation (15–17 h) in the dark at 20 °C, the protoplasts were collected by centrifugation at 200 g. For lysis, 100 µl of Passive Lysis Buffer (from Dual-Luciferase Reporter Assay System E1910 of PROMEGA) were used.

The measurements of both Firefly luciferase activity and Renilla luciferase activity were performed using a BertholdTech TriStar2S plate reader. Firefly luciferase activity was determined by adding 40 µl of Luciferase Assay Reagent II (LARII from Dual-Luciferase Reporter Assay System E1910) to the protoplast lysate and measuring the luminescence. Immediately afterwards, 40 µl of Stop & Glo® Reagent (SG from Dual-Luciferase Reporter Assay System E1910 of Promega) were added to the same sample, and the Renilla luciferase activity was measured.

To correct for transformation efficiency, the ratio of Firefly to Renilla luciferase activity was divided by the corresponding values of an empty vector (P2GW7-35S) used as a control. This step was performed to normalize the values. For reporter constructs, the same promoter fragments of the *WRKY18*, *WRKY25*, and *WRKY53* were used, but this time they were cloned into the vector p2GWL7.

Transient transformation of Nicotiana benthamiana leaves

Suspension cultures of *Agrobacterium tumefaciens* containing the BiFC constructs were used to infiltrate *Nicotiana benthamiana* plants. Overnight cultures of *Agrobacterium tumefaciens* strain GV3101, which have been transformed with the BiFC constructs, were used to inoculate LB media containing the respective antibiotics. After 4–6 h of incubation, this culture was centrifuged at 18 000 g for 10 min. The bacterial pellet was diluted in infiltration media (10 mM MgCl2, 0.5 M MES, 100 mM Acetosyringone) to an OD_{600} of 0.5. Leaves of 4-week-old tobacco plants were infiltrated by manual injection using a 1-ml needleless syringe.

Bimolecular fluorescence complementation (BiFC), confocal microscopy and cytometry

Assays with BiFC 2-in-1 constructs were used to study homo- and heteromeric interactions between the three WRKYs involved in our small subnetwork as well as with deletion W25N*, W25ΔpD1, W25ΔD2 and the domain swapping chimera between WRKY18 and WRKY25, W18N-W25C and W25N-W18C. In the same vector backbone, an internal RFP gene is present as transformation and expression control. Protein interactions were monitored using confocal microscopy. The interactions were detected and localized within the cells two days after the infiltration of the *N. benthamiana* leaves, as described above. At least three leaves of different plants were analyzed under the confocal microscope (LSM880, Zeiss, Jena, Germany) by using the preset sequential scan settings for YFP (Ex: 514 nm, Em: 517–553 nm) and for RFP (Ex: 561 nm, Em: 597–625 nm). The experiments were repeated at least three times. Images were acquired and analyzed using ZEN 3.0 (Blue edition) software (Zeiss). The mean fluorescence intensity of YFP and RFP was measured for each nucleus obtained from leaves of different plants. The YFP/RFP ratio was then calculated for each nucleus from independent biological samples. For each interaction type, at least four nuclei from distinct samples were analyzed.

Additionally, ratiometric BiFC assays were performed to ascertain the homodimeric interactions of the three WRKYs of our subnetwork mentioned above. The same pBiFCt-2in1-NN vectors[48,49] carrying both genes of interest were used for transformation of Arabidopsis protoplasts. In this case, 8 µg of the plasmid DNA was used to express the fusion proteins. After overnight incubation in the dark, interactions were visualized by flow cytometry using CytoFLEX (Beckman Coulter, Brea, CA, USA). Both the internal mRFP and any reconstituted YFP were excited by the 488 nm laser. Peak emission was captured for YFP in FL1 (525/40 nm) and for RFP in FL3 (610/20 nm). All experiments were performed independently at least three times.

Senescence phenotyping

To evaluate senescence phenotypes, various parameters indicating the state of senescence were considered. Leaves from seven to eight plants per time point were analyzed. The rosette leaves were detached and aligned according to their age, using a previously established color-coding system. These leaves were photographed, and an automated colorimetric assay (ACA) was used to group the pixels into four categories: green leaves (green), leaves starting to turn yellow (green-yellow), completely yellow leaves (yellow), and brown and/or dead leaves (brown/dead)[45].

Leaves at positions 5 and 10 within the rosette were used to determine Fv/Fm values using the Imaging-Pulse-Amplitude-Modulation (PAM) method, indicating the activity of photosystem II (PSII) (PAM fluorometer Maxi version; ver. 2-461, Walz GmbH, Effeltrich, Germany). These same leaves were also collected to determine the chlorophyll content as described in[45].

Gene expression analysis under oxidative conditions using qRT-PCR

Two-week-old seedlings grown on MS medium were transferred to a new MS medium with or without 3'-AT. These seedlings were collected after 1, 3 and 5 d, and total RNA was extracted with the GeneMATRIX Universal RNA Purification Kit (EURx) following the protocol provided by the manufacturer. Afterward, RevertAid RT Kit K1691 (Thermo Fisher Scientific Inc., Waltham, MA, USA) using oligo-dT primers was used for cDNA synthesis following the manufacturer's instructions.

qRT-PCR was performed with the Master Mix KAPA SYBR® FAST following the manufacturer's protocol in a thermal cycler CFX384 Bio-Rad (Bio-Rad Laboratories Inc., Hercules, CA, USA). The calculation method was the ΔΔCT described in[54]. In addition, the expression of the analyzed genes obtained was normalized to *ACTIN2* which has been characterized as a suitable reference gene for senescence[55]. The primers listed in Table S4 were used.

Liquid chromatography-mass spectrometry (LC–MS)

The WRKY25 protein was ordered as N-terminally 8xHis-tagged proteins from Biomatik (Cambridge, Ontario, Canada). The protein was expressed in *E. coli* cells and purified by affinity purification (Biomatik, Canada). The quality and purification of the WRKY25 was controlled by SDS-PAGE, Coomassie staining and Western blotting followed by immune detection using anti-HIS antibodies[10]. This recombinant protein was used for the NOS-bridge peptide analysis. The authenticity of the protein was verified using non-targeted LC–MS profiling. All solvents used in the peptide profiling analyses were LC–MS grade.

Proteolytical protein digest: An in-solution digest of the recombinant protein (0.2 µg µl^{-1} in water) was performed by incubating 60 µl of the sample ON at 37 °C with 5 µl Trypsin (0.2 µg µl^{-1}, proteomics grade, porcine, Merck) and 12 µl digestion buffer (7 µl 400 mM ABC buffer (NH4HCO3), 5 µl acetonitrile (ACN)). Finally, the protease digest was diluted 1:3 using 13% ACN in acidic water (1% (v/v) formic acid). As no Dithiothreitol (DTT) and iodoacetamide were added to the reaction, the digest took place under non-reducing conditions.

Targeted LC–MS Profiling Analysis: The targeted LC–MS profiling analysis was performed using a Micro-LC M5 (Trap and Elute) and a QTRAP6500 + (Sciex) operated in MRM (Multiple Reaction Monitoring) mode. Chromatographic separation was achieved on a HaloFused C18 column (150 × 0.5 mm (particle size 2.7 µm; 90 Å; Sciex) and a Luna C18(2) trap column (5 µm; 100 Å; 20 × 0.5 mm; Phenomenex) with a column

temperature of 55 °C. The following binary gradient was applied for the main column at a flow rate of 16 µl min-1: 0—0.5 min, isocratic 98% A; 0.5—9 min, linear from 98% A to 60% A; 9—10 min, linear from 60% A to 5% A; 10—11 min, isocratic 5% A; 11—12 min, linear from 5% A to 98% A; 12—15 min, isocratic 98% A (A: water, 0.1% aq. formic acid; B: acetonitrile, 0.1% aq. formic acid). The samples were concentrated on the trap column using the following conditions: flow rate 25 µl min^{-1}: 0—2.7 min isocratic 95% A; at 2.5 min start main gradient. The injection volume was 50 µl. Analytes were ionized using an Optiflow Turbo V ion source equipped with a SteadySpray T micro electrode in positive ion mode (ion spray voltage: 4800 V). Following additional instrument settings were applied: nebuliser and heater gas, nitrogen, 25 and 45 psi; curtain gas, nitrogen, 30 psi; collision gas, nitrogen, medium; source temperature, 200 °C; entrance potential, + 10 V; collision cell exit potential, + 10 V. The dwell time for all MRMs was 10 ms except for the trypsin autolysis control peaks, which were recorded with 5 ms. The declustering potential was kept at 80 V.

All MRM information was calculated using the Skyline 23.1 software[56]. Quantitative data extraction was performed using the vendor software Sciex OS. In the Skyline software all peptide transitions were screened for uniqueness against the protein sequences of the *E. coli* proteome, porcine trypsin and WRKY25 itself. All represented transitions in Fig S5 are unique for the four different NOS-bridge combinations except for the peptide/fragment pair m/z 524.89/588.25 which can be found on Pos1 K-C1 as well as in Pos1 K-C6. The transitions monitored for each peptide are shown in Table S5.

Software used for modeling and statistical analysis of data

For Protein Modeling ColabFold was used following the indications of[57]. For viewing and manipulation of data obtained from ColabFold from proteins and chimeras PyMOL TM 2.5.5 (Schrödinger, LLC) was used. In addition, for modeling and determination of the electrostatic surface potential ChimeraX 1.9 was used. For the elaboration of constructs and sequence alignments CLC Main Workbench 21 (QIAGEN) was used. For analysis and image processing, ImageJ was used. In the case of ACA the leaves were individually processed in single images using a semi-automatic ImageJ macro described in[45].

The statistical analysis was performed using EXCEL and R version 4.4.1 (The R Foundation for Statistical Computing). The specific statistical method was chosen based on the characteristics of the experiment. The statistical method used is detailed in the legends.

Data availability

All data generated or analyzed during this study are included in this published article (and its Supplementary Information files). DNA and protein sequence of all Arabidopsis WRKY factors are available at TAIR (https://www.arabidopsis.org/): WRKY25 (AT2G30250), WRKY18 (AT4G31800), WRKY53 (AT4G23810). Protein data on human hematopoietic cell receptor CD69 (PDB: 4GA9) and Galectin-1 of rats (PDB: 1E8I, chain A) are available at worldwide ProteinDataBank (https://www.wwpdb.org/).

Received: 3 February 2025; Accepted: 21 July 2025
Published online: 29 July 2025

References

1. Zhou, M. & Yang, J. Delaying or promoting? manipulation of leaf senescence to improve crop yield and quality. *Planta* **258**, 48 (2023).
2. Zhang, Z. et al. Identification of transcription factors associated with leaf senescence in tobacco. *Sci. Rep.* **14**, 21556 (2024).
3. Gregersen, P. L., Culetic, A., Boschian, L. & Krupinska, K. Plant senescence and crop productivity. *Plant Mol. Biol.* **82**, 603–622 (2013).
4. Schippers, J. H. M., Schmidt, R., Wagstaff, C. & Jing, H. C. Living to die and dying to live: The survival strategy behind leaf senescence. *Plant Physiol.* **169**, 914–930 (2015).
5. Noodén, L. D., Guiamét, J. J. & John, I. Senescence mechanisms. *Physiol. Plant* **101**, 746–753 (1997).
6. Bieker, S., Riester, L., Stahl, M., Franzaring, J. & Zentgraf, U. Senescence-specific alteration of hydrogen peroxide levels in arabidopsis thaliana and oilseed rape spring variety brassica napus L. cv mozart. *J. Integr. Plant Biol.* **54**, 540–554 (2012).
7. Jiang, Y., Liang, G., Yang, S. & Yu, D. Arabidopsis WRKY57 functions as a node of convergence for jasmonic acid- and auxin-mediated signaling in jasmonic acid-induced leaf senescence. *Plant Cell* **26**, 230–245 (2014).
8. Li, Z., Peng, J., Wen, X. & Guo, H. Ethylene-Insensitive3 is a senescence-associated gene that accelerates age-dependent leaf senescence by directly repressing miR164 transcription in arabidopsis. *Plant Cell* **25**, 3311–3328 (2013).
9. He, Y., Fukushige, H., Hildebrand, D. F. & Gan, S. Evidence supporting a role of jasmonic acid in arabidopsis leaf senescence. *Plant Physiol.* **128**, 876–884 (2002).
10. Andrade Galan, A. G., Doll, J., Faiß, N., Weber, P. & Zentgraf, U. Complex formation between the transcription factor WRKY53 and antioxidative enzymes leads to reciprocal inhibition. *Antioxidants* **13**, 315 (2024).
11. Zimmermann, P., Heinlein, C., Orendi, G. & Zentgraf, U. Senescence-specific regulation of catalases in arabidopsis thaliana (L.) Heynh. *Plant Cell Environ.* **29**, 1049–1060 (2006).
12. Zhang, H. et al. AtWRKY75 positively regulates age-triggered leaf senescence through gibberellin pathway. *Plant Divers* **43**, 331–340 (2021).
13. Doll, J. et al. Arabidopsis thaliana WRKY25 transcription factor mediates oxidative stress tolerance and regulates senescence in a redox-dependent manner. *Front. Plant Sci.* **10**, 1734 (2020).
14. Huang, P., Li, Z. & Guo, H. New advances in the regulation of leaf senescence by classical and peptide hormones. *Front. Plant Sci.* **13**, 923136 (2022).
15. Balazadeh, S., Riaño-Pachón, D. M. & Mueller-Roeber, B. Transcription factors regulating leaf senescence in arabidopsis thaliana. *Plant Biol.* **10**, 63–75 (2008).
16. Guo, Y., Cai, Z. & Gan, S. Transcriptome of arabidopsis leaf senescence. *Plant Cell Environ.* **27**, 521–549 (2004).
17. Schippers, J. H. M. Transcriptional networks in leaf senescence. *Curr. Opin. Plant Biol.* **27**, 77–83 (2015).
18. Buchanan-Wollaston, V. et al. The molecular analysis of leaf senescence – a genomics approach. *Plant Biotechnol. J.* **1**, 3–22 (2003).
19. Buchanan-Wollaston, V. et al. Comparative transcriptome analysis reveals significant differences in gene expression and signalling pathways between developmental and dark/starvation-induced senescence in arabidopsis. *Plant J.* **42**, 567–585 (2005).

20. Breeze, E. et al. High-resolution temporal profiling of transcripts during arabidopsis leaf senescence reveals a distinct chronology of processes and regulation. *Plant Cell* **23**, 873–894 (2011).
21. Cao, J., Liu, H., Tan, S. & Li, Z. Transcription factors-regulated leaf senescence: Current knowledge challenges and approaches. *Int. J. Mol. Sci.* **24**, 9245 (2023).
22. Guo, Y. et al. Leaf senescence: Progression, regulation, and application. *Mol. Hortic.* **1**, 5 (2021).
23. Goyal, P. et al. WRKY transcription factors: Evolution, regulation, and functional diversity in plants. *Protoplasma* **260**, 331–348 (2023).
24. Kim, H. J., Nam, H. G. & Lim, P. O. Regulatory network of NAC transcription factors in leaf senescence. *Curr. Opin. Plant Biol.* **33**, 48–56 (2016).
25. Dong, J., Chen, C. & Chen, Z. Expression profiles of the arabidopsis WRKY gene superfamily during plant defense response. *Plant Mol. Biol.* **51**, 21–37 (2003).
26. Hinderhofer, K. & Zentgraf, U. Identification of a transcription factor specifically expressed at the onset of leaf senescence. *Planta* **213**, 469–473 (2001).
27. Miao, Y., Laun, T., Zimmermann, P. & Zentgraf, U. Targets of the WRKY53 transcription factor and its role during leaf senescence in arabidopsis. *Plant Mol. Biol.* **55**, 853–867 (2004).
28. Zentgraf, U. & Doll, J. Arabidopsis wrky53, a node of multi-layer regulation in the network of senescence. *Plants* **8**, 578 (2019).
29. Potschin, M., Schlienger, S., Bieker, S. & Zentgraf, U. Senescence networking: WRKY18 is an upstream regulator, a downstream target gene, and a protein interaction partner of WRKY53. *J. Plant Growth Regul.* **33**, 106–118 (2014).
30. Xie, Z. et al. Interactions of two abscisic-acid induced WRKY genes in repressing gibberellin signaling in aleurone cells. *Plant J.* **46**, 231–242 (2006).
31. Xu, X., Chen, C., Fan, B. & Chen, Z. Physical and functional interactions between pathogen-induced Arabidopsis WRKY18, WRKY40, and WRKY60 transcription factors. *Plant Cell* **18**, 1310–1326 (2006).
32. Chi, Y. et al. Protein-protein interactions in the regulation of WRKY transcription factors. *Mol. Plant* **6**, 287–300 (2013).
33. Xu, Y. et al. Crystal structures of N-terminal WRKY transcription factors and DNA complexes. *Protein Cell* **11**, 208–213 (2020).
34. Eulgem, T., Rushton, P. J., Schmelzer, E., Hahlbrock, K. & Somssich, I. E. Early nuclear events in plant defence signalling: Rapid gene activation by WRKY transcription factors. *Embo. J.* **18**, 4689–4699 (1999).
35. Wensien, M. et al. A lysine–cysteine redox switch with an NOS bridge regulates enzyme function. *Nature* **593**, 460–464 (2021).
36. Paulsen, C. E. & Carroll, K. S. Cysteine-mediated redox signaling: Chemistry, biology, and tools for discovery. *Chem. Rev.* **113**, 4633–4679 (2013).
37. Hogg, P. J. Disulfide bonds as switches for protein function. *Trends Biochem. Sci.* **28**, 210–214 (2003).
38. Rabe von Pappenheim, F. et al. Widespread occurrence of covalent lysine–cysteine redox switches in proteins. *Nat. Chem. Biol.* **18**, 368–375 (2022).
39. Xie, Y. et al. REVOLUTA and WRKY53 connect early and late leaf development in arabidopsis. *Dev. (Cambridge)* **141**, 4772–4783 (2014).
40. Maeo, K., Hayashi, S., Kojima-Suzuki, H., Morikami, A. & Nakamura, K. Role of conserved residues of the WRKY domain in the dna-binding of tobacco WRKY family proteins. *Biosc. Biotecnol. Biochem.* **11**, 2428–2436 (2001).
41. Ciolkowski, I., Wanke, D., Birkenbihl, R. P. & Somssich, I. E. Studies on DNA-binding selectivity of WRKY transcription factors lend structural clues into WRKY-domain function. *Plant Mol. Biol.* **68**, 81–92 (2008).
42. Brand, L. H., Fischer, N. M., Harter, K., Kohlbacher, O. & Wanke, D. Elucidating the evolutionary conserved DNA-binding specificities of WRKY transcription factors by molecular dynamics and in vitro binding assays. *Nucleic Acids Res.* **41**, 9764–9778 (2013).
43. Cheng, X. et al. Structural basis of dimerization and dual W-box DNA recognition by rice WRKY domain. *Nucleic Acids Res.* **47**, 4308–4318 (2019).
44. Chen, H. et al. Roles of arabidopsis WRKY18, WRKY40 and WRKY60 transcription factors in plant responses to abscisic acid and abiotic stress. *BMC Plant Biol.* **10**, 281 (2010).
45. Bresson, J., Bieker, S., Riester, L., Doll, J. & Zentgraf, U. A guideline for leaf senescence analyses: From quantification to physiological and molecular investigations. *J. Exp. Bot.* **69**, 769–786 (2018).
46. Jiang, Y. & Deyholos, M. K. Functional characterization of Arabidopsis NaCl-inducible WRKY25 and WRKY33 transcription factors in abiotic stresses. *Plant Mol. Biol.* **69**, 91–105 (2009).
47. Binder, A. et al. A modular plasmid assembly kit for multigene expression, gene silencing and silencing rescue in plants. *PLoS ONE* **9**, e88218 (2014).
48. Grefen, C. & Blatt, M. R. A 2in1 cloning system enables ratiometric bimolecular fluorescence complementation (rBiFC). *Biotechniques* **53**, 311–314 (2012).
49. Mehlhorn, D., Wallmeroth, N., Berendzen, K. W. & Grefen, C. 2 in 1 Vectors Improve in Planta BiFC and FRET Analysis. In *The plant endoplasmic reticulum . Methods in molecular biology* (eds. Hawes, C. & Kriechbaumer, V.) vol. 1691 149–168 (Humana Press, New York, 2018).
50. Lampropoulos, A. et al. GreenGate - A novel, versatile, and efficient cloning system for plant transgenesis. *PLoS ONE* **8**, e83043 (2013).
51. Mehlhorn, D. G., Wallmeroth, N., Berendzen, K. W. & Grefen, C. Methods in molecular biology. in (2018).
52. Yoo, S. D., Cho, Y. H. & Sheen, J. Arabidopsis mesophyll protoplasts: A versatile cell system for transient gene expression analysis. *Nat. Protoc.* **2**, 1565–1572 (2007).
53. Jefferson, R. A., Kavanagh, T. A. & Bevan, M. W. GUS fusions: beta-glucuronidase as a sensitive and versatile gene fusion marker in higher plants. *Embo. J.* **6**, 3901–3907 (1987).
54. Pfaffl, M. W. A new mathematical model for relative quantification in real-time RT-PCR. *Nucleic Acids Res.* **29**, e45 (2001).
55. Panchuk, I. I., Zentgraf, U. & Volkov, R. A. Expression of the Apx gene family during leaf senescence of arabidopsis thaliana. *Planta* **222**, 926–932 (2005).
56. MacLean, B. et al. Skyline: An open source document editor for creating and analyzing targeted proteomics experiments. *Bioinformatics* **26**, 966–968 (2010).
57. Mirdita, M. et al. ColabFold: Making protein folding accessible to all. *Nat. Methods* **19**, 679–682 (2022).

Acknowledgements

We thank Rosanna Saur and Laura Schaffer for excellent technical assistance. We also thank the NASC for supplying Arabidopsis seeds of the WRKY25 T-DNA insertion lines (SAIL_529_B11). We acknowledge support by Open Access Publishing Fund of University of Tübingen. This work was funded by the Deutsche Forschungsgemeinschaft (DFG) CRC 1101 (B06). The laser scanning microscope was also supported by the Deutsche Forschungsgemeinschaft (DFG) by a grant for scientific equipment (INST 37/965-1 FUGG). Targeted LC-MS analysis was funded by the DFG (Project number 442641014).

Author contributions

Conceptualization: U.Z. and J.D.; methodology: A.G.A.G, J.D., E.vR.-L., and N.F.; formal analysis: A.G.A.G., E.vR.-L., investigation: A.G.A.G., J.D., E.vR.-L., and N.F.; writing-original draft preparation: A.G.A.G; writing-review and editing: all authors.; visualization: A.G.A.G., and E.vR.-L.; supervision: U.Z., and J.D.; project administration: U.Z.; funding acquisition: U.Z.; All authors have read and agreed to the published version of the manuscript.

Funding

Open Access funding enabled and organized by Projekt DEAL. Deutsche Forschungsgemeinschaft,CRC1101,B06.

Declarations

Competing interests

The authors declare no competing interests.

Additional information

Supplementary Information The online version contains supplementary material available at https://doi.org/10.1038/s41598-025-13023-1.

Correspondence and requests for materials should be addressed to U.Z.

Reprints and permissions information is available at www.nature.com/reprints.

Publisher's note Springer Nature remains neutral with regard to jurisdictional claims in published maps and institutional affiliations.

The transcription factor WRKY25 can act as redox switch to drive the expression of *WRKY53* during leaf senescence in Arabidopsis

Ana Gabriela Andrade Galan, Jasmin Doll, Edda von Roepenack-Lahaye, Natalie Faiss, and Ulrike Zentgraf *

Center for Plant Molecular Biology (ZMBP), University of Tübingen, Auf der Morgenstelle 32, 72076 Tübingen, Germany

* Correspondence: ulrike.zentgraf@zmbp.uni-tuebingen.de

The following **Supporting Information** is available for this article:

Fig. S1: Homodimerization of WRK18, WRKY25, and WRKY53 using BiFC in transiently transformed Arabidopsis protoplasts and *Nicotiana benthamiana* leaves.

Fig. S2: Heterodimerization of WRK18, WRKY25, and WRKY53 using BiFC in transiently transformed *N. benthamiana* leaves.

Fig. S3. GUS transactivation assays in Arabidopsis protoplasts from root on the P_{WRKY53} and the effect of the deletions on it.

Fig. S4: Dual luciferase assays in Arabidopsis protoplasts from leaves on the P_{WRKY18} and P_{WRKY25} and the effect of the chimeras on them.

Fig. S5: Dimerization of WRK18 or WRKY25 with the deletion and chimeric versions, using BiFC in transiently transformed *N. benthamiana* leaves.

Fig. S6. Pictures of the leaves of representative plants of all lines used for senescence phenotype.

Fig. S7. Additional parameters used for senescence phenotyping of the complementation lines *wrky25*:W25 compared to Col-0 and *wrky25*.

Fig. S8. Additional parameters used for senescence phenotyping of the complementation lines *wrky25*:W25N*, *wrky25*:W25ΔpD1, *wrky25*:W25ΔD2 compared to Col-0 and *wrky25*.

Fig. S9. Additional parameters used for senescence phenotyping of the complementation lines *wrky25*:W18N-W25C and *wrky25*:W25N-W18C compared to Col-0 and *wrky25*.

Fig. S10. GUS transactivation assays in Arabidopsis protoplasts from root on the P_{WRKY33} and the effect of the Cys^{pos17} mutated version of WRKY25 under oxidative conditions.

Fig. S11. GUS transactivation assays in Arabidopsis protoplasts from root on the P_{WRKY33} and the effect on the deletions under oxidative conditions.

Fig. S12: Comparison of previously identified redox switches and the putative redox switches in WRKY25.

Fig. S13: Electrostatic surface potential map of WRKY25.

Fig. S14. Targeted LC-MS analysis of possible NOS-bridge peptides in WRKY25.

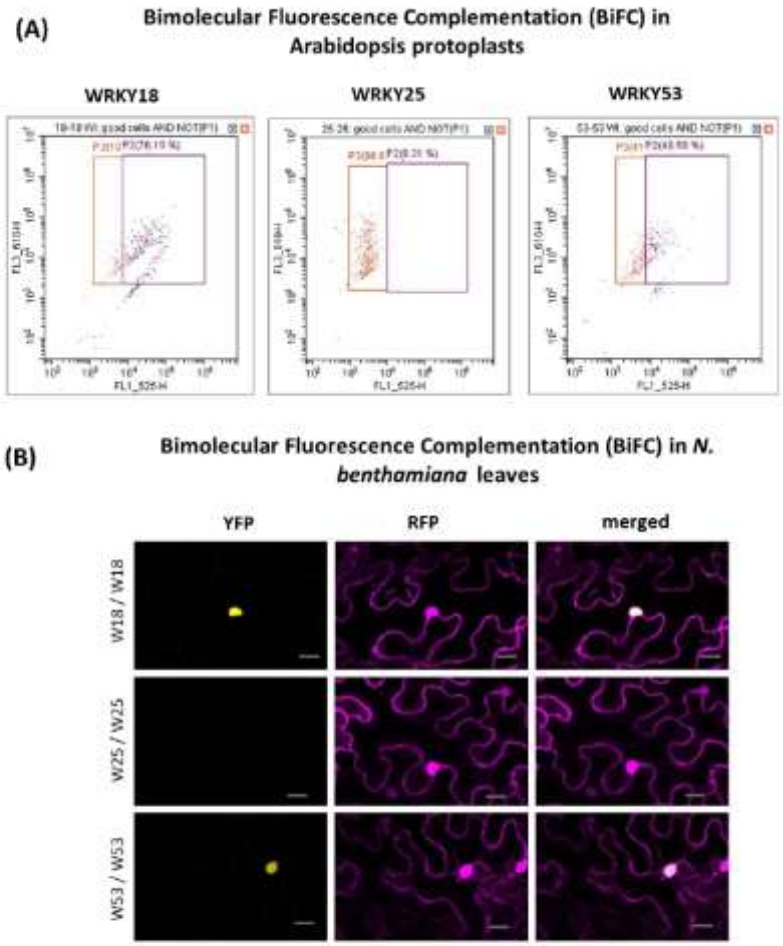

Fig. S1: Homodimerization of WRK18, WRKY25, and WRKY53 using BiFC in transiently transformed Arabidopsis protoplasts and *Nicotiana benthamiana* leaves.
(A) Arabidopsis protoplasts were transformed with pBiFCt2in1-NN constructs containing the possible combinations for the homodimerization of the three WRKYs of the subnetwork and were subsequently analyzed with the cytoflex cell sorter. The orange squares indicate transformed protoplasts (RFP), and purple squares indicate interaction via BiFC (YFP). **(B)** Leaves of *N. benthamiana* were transformed with pBiFCt2in1-NN constructs containing the possible combinations for the homodimerization of the three WRKYs of the subnetwork. These transformed leaves were analyzed under a confocal laser scanning microscope: yellow fluorescence (YFP) indicates interaction (BiFC), and red fluorescence (RFP) serves as a transformation control. Representative pictures are presented. The scale bar represents 20 µm.

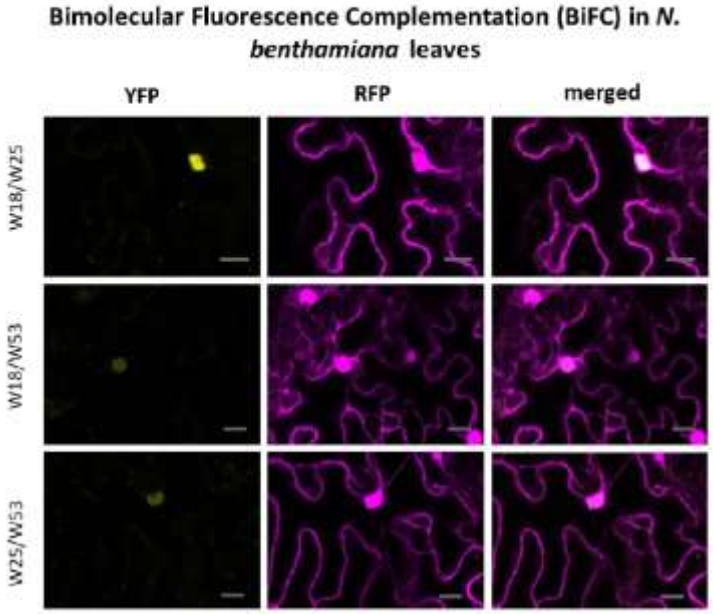

Fig. S2: Heterodimerization of WRK18, WRKY25, and WRKY53 using BiFC in transiently transformed *N. benthamiana* leaves.
Leaves of *N. benthamiana* were transformed with pBiFCt2in1-NN constructs containing the possible combinations for the heterodimerization of the three WRKYs of the subnetwork. These transformed leaves were analyzed under a confocal laser scanning microscope: yellow fluorescence (YFP) indicates interaction (BiFC), and red fluorescence (RFP) serves as a transformation control. Representative pictures are presented. The scale bar represents 20 µm.

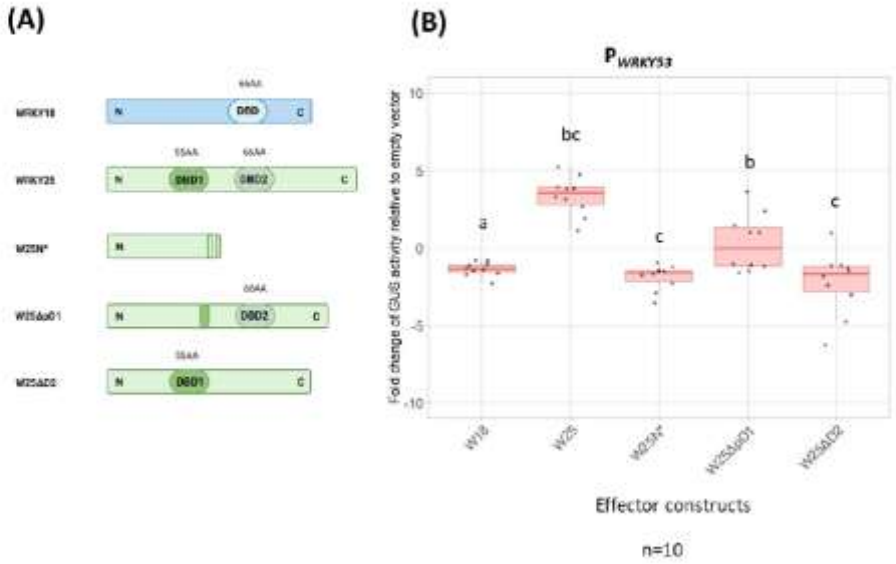

Fig. S3: GUS transactivation assays in Arabidopsis protoplasts from root on the P_{WRKY53} and the effect of the deletions on it.
(A) Schematic drawing represents the native WRKY18 and WRKY25 protein with their DNA-binding domains DBD1 and DBD2s well as deletions *W25N**, *W25ΔpD1*,and *W25ΔD2* **(B)** Arabidopsis protoplasts from root were transformed with a fragment of the promoter of *WRKY53* (2759 bp), fused to the *GUS* reporter gene, along with 35S:*WRKY18*, 35S:*WRKY25*, 35S:*W25N**, 35S:*W25ΔpD1*,or 35S:*W25ΔD2* as effector constructs. Values relative to the empty vector are presented as boxplots, with sample size (n) shown under the plot. The n represents independent biological replicates. One-way ANOVA followed by Tukey's HSD post-hoc test was performed. Lowercase letters indicate statistically significant differences between groups ($p \leq 0.05$).

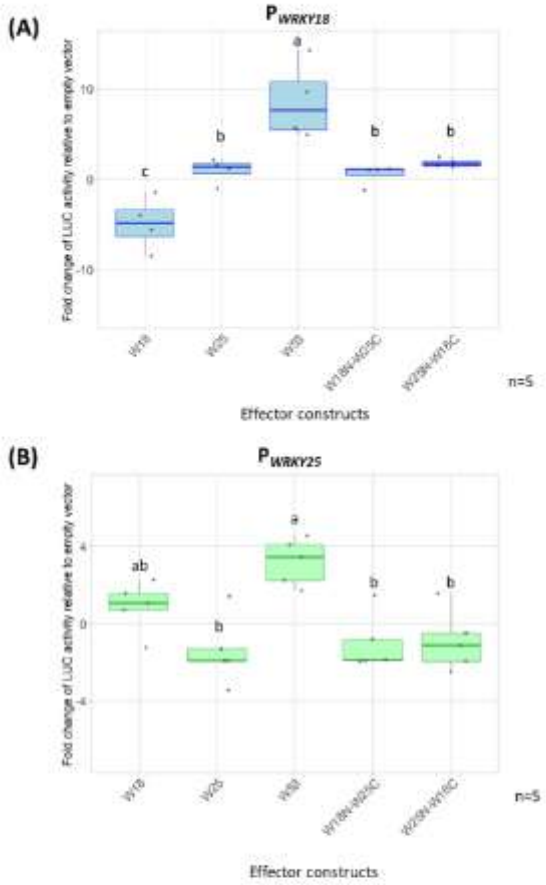

Fig. S4: Dual luciferase assays in Arabidopsis protoplasts from leaves on the P_{WRKY18} and P_{WRKY25} and the effect of the chimeras on them.
Arabidopsis leaf protoplasts were transformed with the fragment of the promoter of **(A)** *WRKY18* (3000 bp) or **(B)** *WRKY25* (3000 bp), fused to the firefly luciferase (*fLUC*) gene as a reporter construct, along with 35S:*WRKY18*, 35S:*WRKY25*, 35S:*WRKY18*, 35S:*W18N-W25C* or 35S:*W25N-W18C* as effector constructs. Values relative to the empty vector are presented as boxplots, with sample size (n) shown at the right side of the plot. The n represents independent biological replicates. One-way ANOVA followed by Tukey's HSD post-hoc test was performed. Lowercase letters indicate statistically significant differences between groups ($p \leq 0.05$).

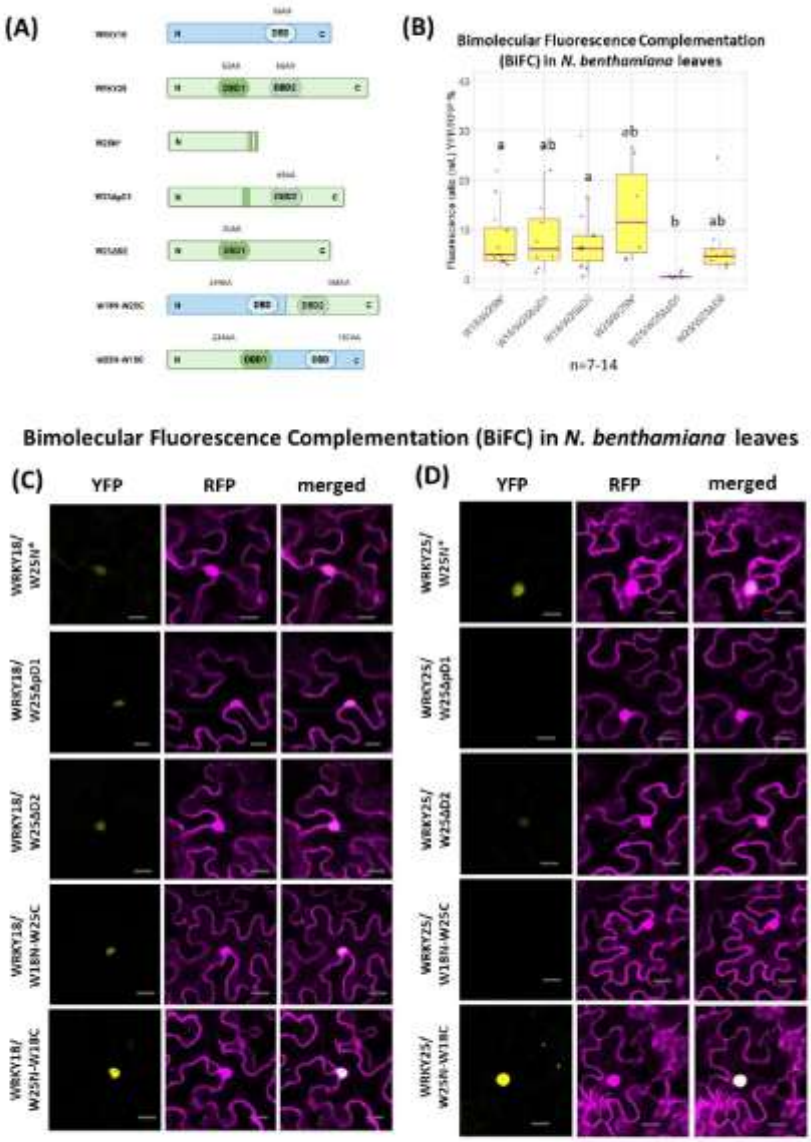

Fig. S5: Dimerization of WRK18 or WRKY25 with the deletion and chimeric versions, using BiFC in transiently transformed *N. benthamiana* leaves.
(A) Schematic drawing represents the native WRKY18 and WRKY25 protein with their DNA-binding domains DBD1 and DBD2s well as deletions *W25N**, *W25ΔpD1*, *W25ΔD2*, and the chimeras W18N-W25C and W25N-W18C. **(B)** Boxplots representing the relative fluorescence ratio (% RFP/YFP) are presented.

Sample size (n) is indicated under the plot and represents independent biological replicates. In both (B) and (C), one-way ANOVA followed by Bonferroni post hoc correction was performed. Different lowercase letters indicate statistically significant differences among groups ($p \leq 0.05$). **(C)** Leaves of *N. benthamiana* were transformed with pBiFCt2in1-NN constructs containing the possible combinations for the dimerization of WRKY18 with the deletions of WRKY25 and the chimeras of domain swapping between WRKY18 and WRKY25. These transformed leaves were analyzed under a confocal laser scanning microscope: yellow fluorescence (YFP) indicates interaction (BiFC), and red fluorescence (RFP) serves as a transformation control. Representative pictures are presented. The scale bar represents 20 µm. **(D)** Leaves of *N. benthamiana* were transformed with pBiFCt2in1-NN constructs containing the possible combinations for the dimerization of WRKY25 with the deletions of WRKY25 and the chimeras of domain swapping between WRKY18 and WRKY25. These transformed leaves were analyzed under a confocal laser scanning microscope: yellow fluorescence (YFP) indicates interaction (BiFC), and red fluorescence (RFP) serves as a transformation control. Representative pictures are presented. The scale bar represents 20 µm.

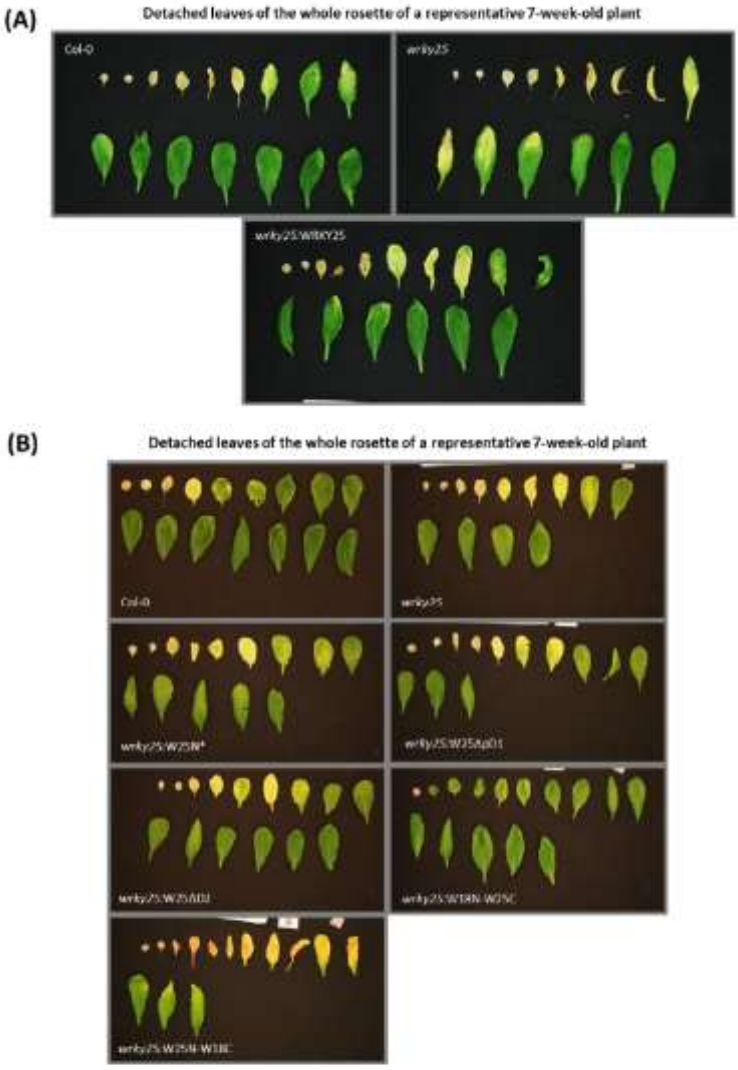

Fig. S6: Pictures of the leaves of representative plants of all lines used for senescence phenotyping.
(A) Representative pictures of all leaves of the whole rosette detached showing the differences between the complementation line: *wrky25:W25* compared with Col 0 and *wrky25*.
(B) Representative pictures of the whole rosette of the plants used for senescence phenotyping the complementation lines: *wrky25*:W25N*, *wrky25*:W25ΔpD1, *wrky25*:W25ΔD2, *wrky25*:W18N-W25C and *wrky25*:W25N-W18C compared with Col 0 and *wrky25*.

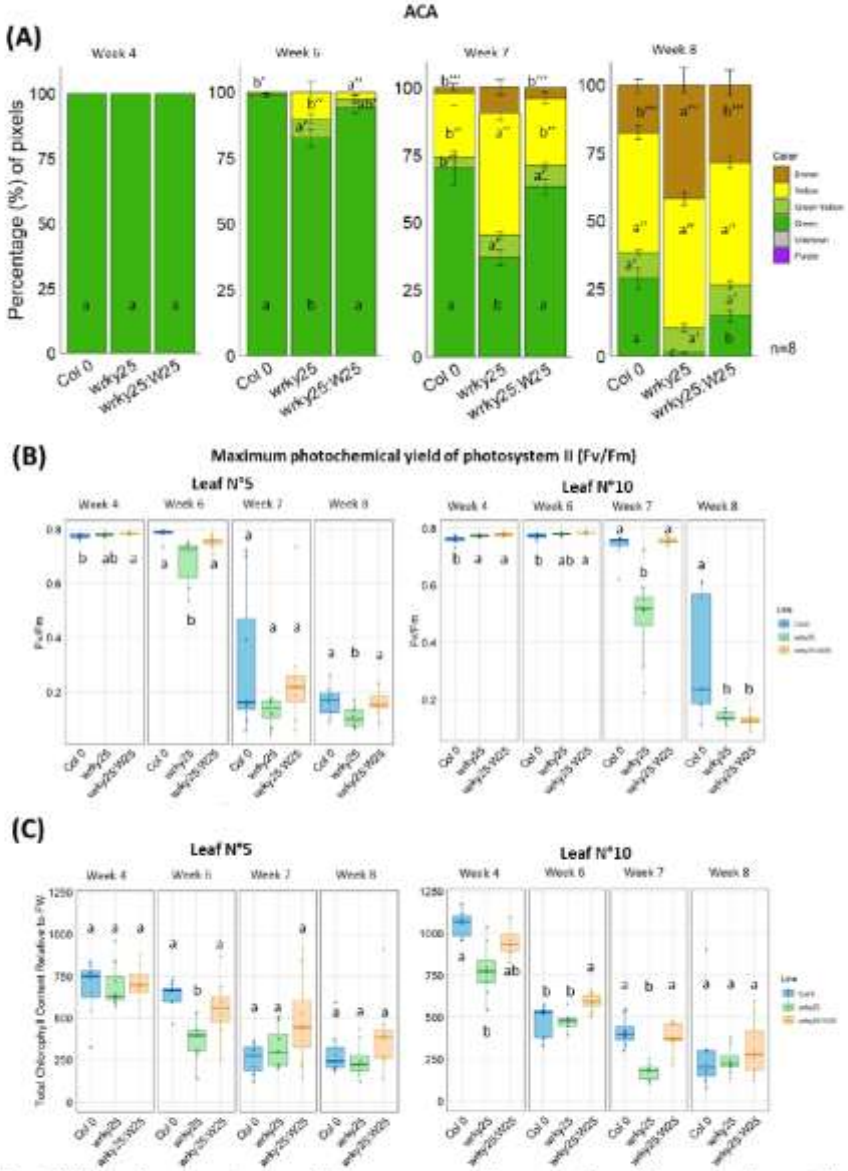

Fig. S7: Additional parameters used for senescence phenotyping of the complementation line *wrky25*:W25 compared to Col-0 and *wrky25*.

(A) The Automated Colorimetric Assay (ACA) categorizes the pixels corresponding to the color of individual leaves from 8 plants into five categories: green, green-yellow, yellow, brown, and

purple. Quantification is presented as the percentage of each category relative to the total pixel number across all leaves (n=8). **(B)** Boxplots of Fv/Fm values measured with PAM fluorometry for leaves No. 5 and No. 10 from 4-, 6-, 7-, and 8-week-old plants (n=8). **(C)** Chlorophyll content relative to fresh weight for leaves No. 5 and No. 10 from 4-, 6-, 7-, and 8-week-old plants (n=8). In all cases, n refers to independent biological replicates. Statistical analysis was performed using one-way ANOVA followed by Tukey's HSD post hoc test. Lowercase letters indicate statistically significant differences between groups ($p \leq 0.05$).

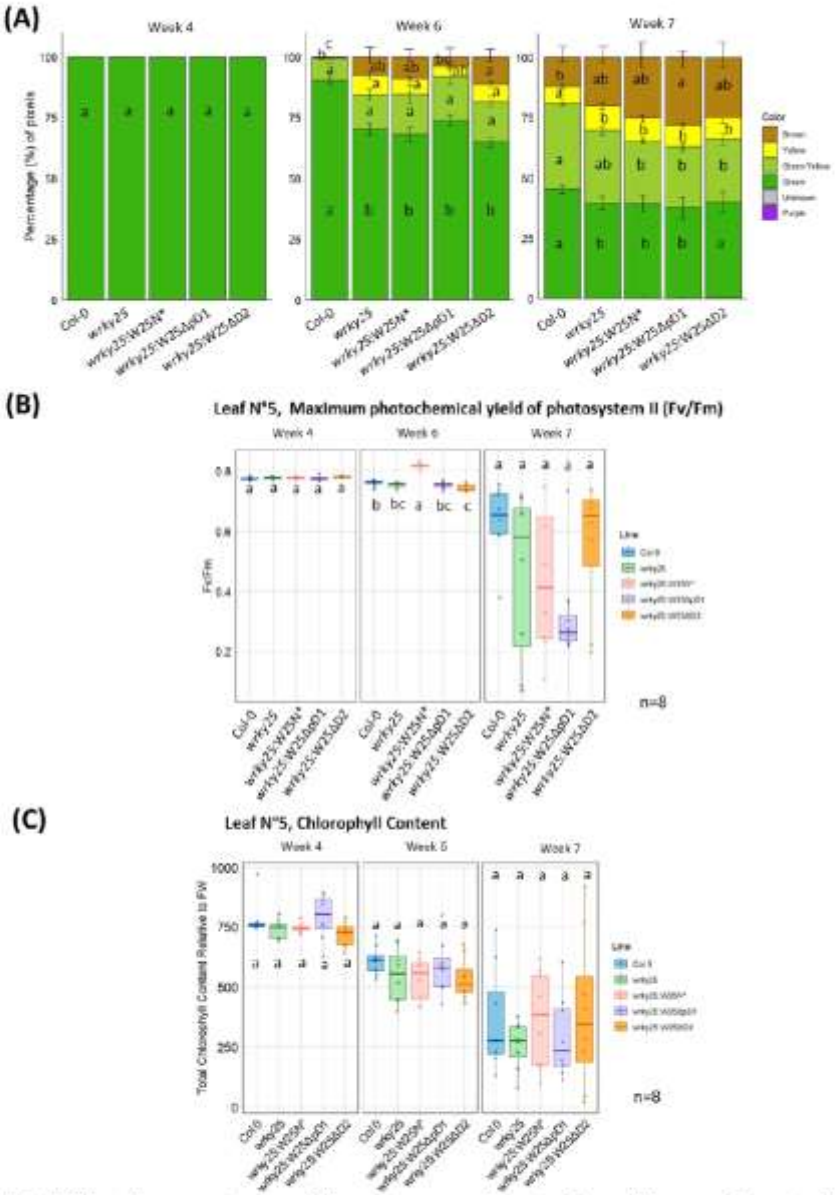

Fig. S8. Additional parameters used for senescence phenotyping of the complementation line *wrky25*:W25N*, *wrky25*:W25ΔpD1, *wrky25*:W25ΔD2 compared to Col-0 and *wrky25*.
(A) The Automated Colorimetric Assay (ACA) categorizes the pixels corresponding to the color of individual leaves from 8 plants into five categories: green, green-yellow, yellow, brown, and

purple. Quantification is presented as the percentage of each category relative to the total pixel number across all leaves (n = 8). **(B)** Boxplots of Fv/Fm values measured with PAM fluorometry for leaves No. 5 from 4-, 6-, 7-, and 8-week-old plants (n = 8). **(C)** Chlorophyll content relative to fresh weight for leaves No. 5 from 4-, 6-, 7-, and 8-week-old plants (n = 8). In all cases, n refers to independent biological replicates. Statistical analysis was performed using one-way ANOVA followed by Tukey's HSD post hoc test. Lowercase letters indicate statistically significant differences between groups ($p \leq 0.05$).

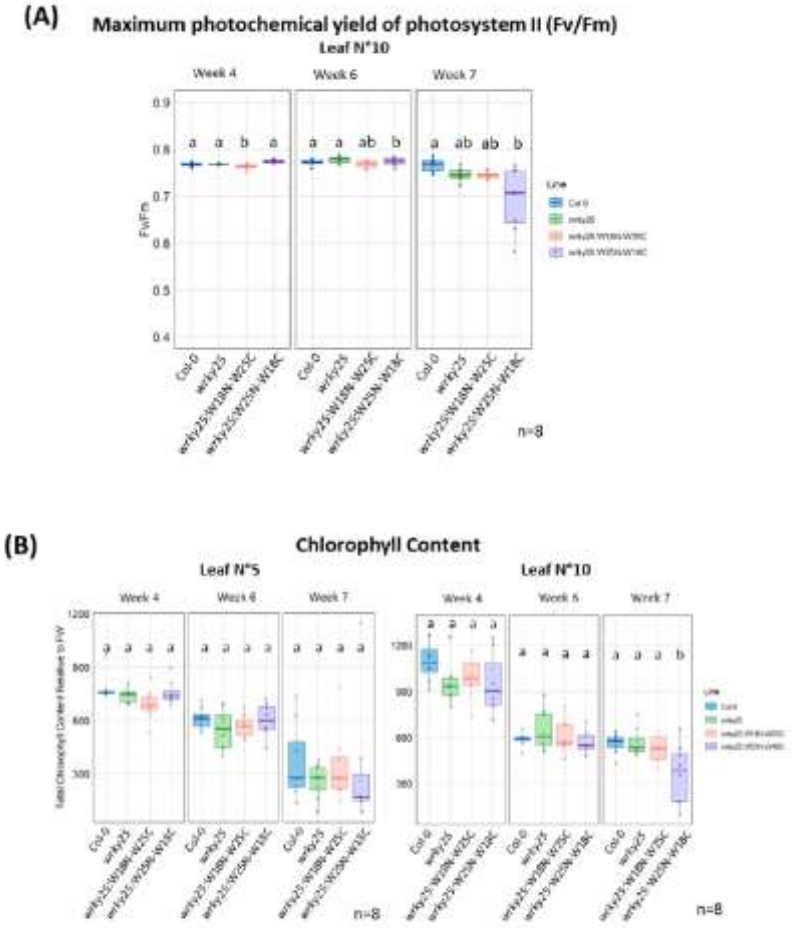

Fig. S9: Additional parameters used for senescence phenotyping of the complementation lines *wrky25*:W18N-W25C and *wrky25*:W25N-W18C compared to Col 0 and *wrky25*.
(A) Boxplots of Fv/Fm values measured with PAM fluorometry for leaf No. 10 from 4-, 6-, and 7-week-old plants (n=8). **(B)** Chlorophyll content relative to fresh weight for leaves No. 5 and No. 10 from 4-, 6-, and 7-week-old plants (n=8). In all cases, n refers to independent biological replicates. Statistical analysis was performed using one-way ANOVA followed by Tukey's HSD post hoc test. Lowercase letters indicate statistically significant differences between groups ($p \leq 0.05$).

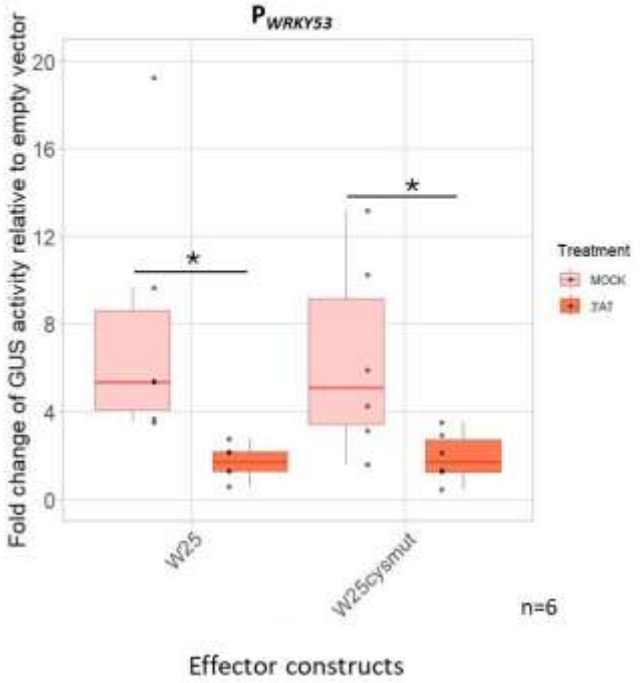

Fig. S10: GUS transactivation assays in Arabidopsis protoplasts from root on the P_{WRKY53} and the effect of the Cys^{pos17} mutated version of WRKY25 under oxidative conditions. Arabidopsis protoplasts from root were transformed with a fragment of the promoter of *WRKY53* (2759 bp), fused to the *GUS* gene as a reporter construct, along with 35S:*WRKY25*, 35S:*W25cysmut*, as effector constructs. In this case half of the transfected protoplasts were simultaneously incubated with 10 mM 3'-AT or the same volume of water for the MOCK conditions, respectively. The values relative to the empty vector control are presented as boxplots (n=6), in which n refers to the number of biological replicates. Statistical significance was assessed using a two-tailed Student's t-test (*$p \leq 0.05$; **$p \leq 0.01$; ns: not significant).

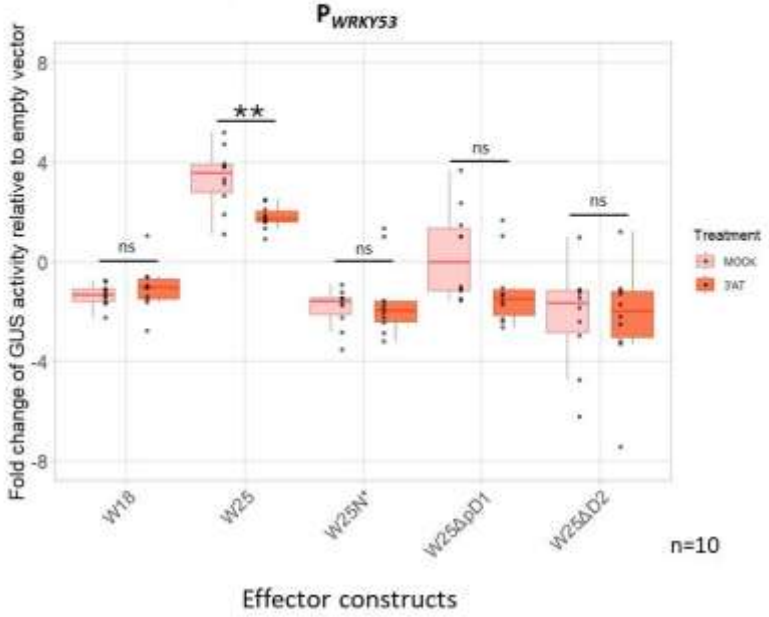

Fig. S11: GUS transactivation assays in Arabidopsis protoplasts from root on the P_{WRKY53} and the effect on the deletions under oxidative conditions.
Arabidopsis protoplasts from root were transformed with a fragment of the promoter of *WRKY53* (2759 bp), fused to the *GUS* gene as a reporter construct, along with 35S*WRKY18*, 35S:*WRKY25*, 35S:*W25N**, 35S:W25ΔpD1, 35S:*W25ΔD2, as* effector constructs. In this case half of the transfected protoplasts were simultaneously incubated with 10 mM 3'-AT or the same volume of water for the MOCK conditions, respectively. The values relative to the empty vector control are presented as boxplots (n=10), in which n refers to the number of biological replicates. Statistical significance was assessed using a two-tailed Student's t-test (*p ≤ 0.05; **p ≤ 0.01; ns: not significant).

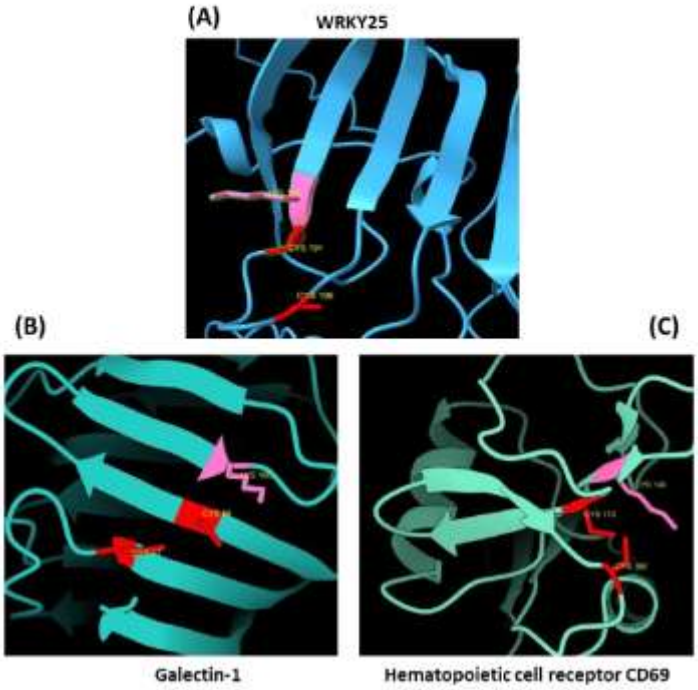

Fig. S12: Comparison of previously identified redox switches and the putative redox switches in WRKY25.
(A) Spatial arrangement of the potential redox switch located at the N-terminus of WRKY25. **(B)** Spatial arrangement of the redox switch previously identified in Galectin-1 of rats (PDB: 1E8I, chain A). **(C)** Spatial arrangement of the redox switch previously observed in the human hematopoietic cell receptor CD69 (PDB: 4GA9). In all models, LYS residues are shown in pink, and CYS residues are shown in red, and the conserved WRKY motif (WRKYGQ) is depicted in mint.

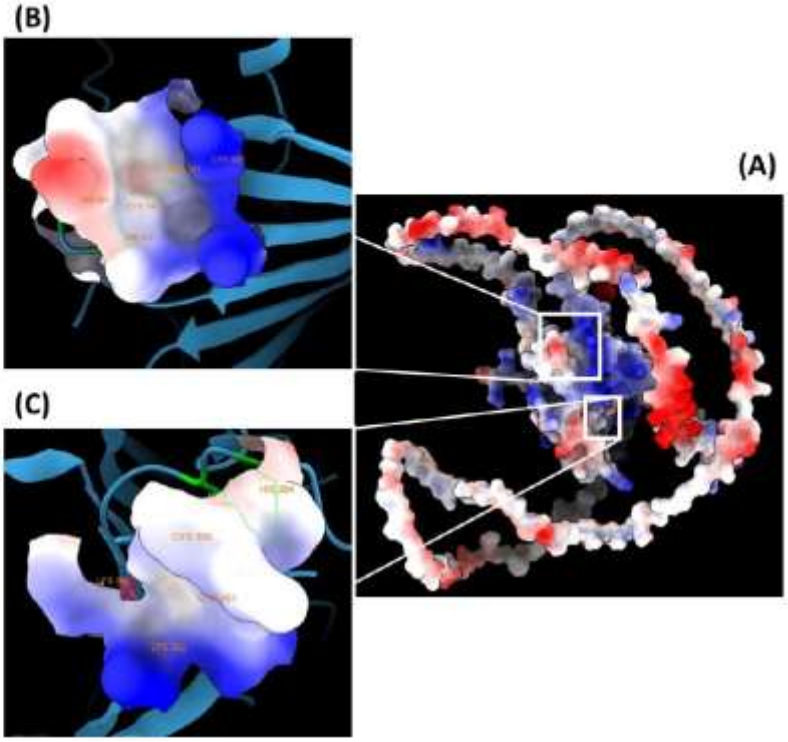

Fig. S13: Electrostatic surface potential map of WRKY25.
(A) Electrostatic surface potential of the full WRKY25 protein. **(B)** Electrostatic surface potential of the putative redox switch located at the N-terminus of WRKY25. **(C)** Electrostatic surface potential of the putative redox switch located at the C-terminus of WRKY25. Color scale: red indicates negatively charged regions, blue indicates positively charged regions, and white represents neutral or uncharged areas.

(A) **WRKY25 amino acid sequence**

MSSTSFTDLLGSSGVDCYEDDEDLRVSGSSFGGYYPERTGSGLPKFKTAQPPPLPISQSSHNFTFSDY

LDSPLLLSSSHSLISPTTGTFPLQGFNGTTNNHSDFPWQLQSQPSNASSALQETYGVQDHEKKQEMI

PNEIATQNNNQSFGTERQIKIPAYMVSRNSNDGYG**WRKY**GQKQVKKSENPRSYFK CTYPDCVSKKI

VETASDGQITEIIYKGGHNHPKPEFTKRPSQSSLPSSVNGRRLFNPASVVSEPHDQSENSSISFDYSDL

EQKSFKSEYGEIDEEEEQPEMKRMKREGEDEGMSIEVSKGVKEPRVVVQTISDIDVLIDGFR**WRKY**G

QKVVKGNTNPRSYYK CTFQGCGVK KQVERSAADERAVLTTYEGRHNHDIPTALRRS

(B) **peptides after digestion**

no-bridge pos1 peptides : SYFK (M+2H m/z 272.6); CTYPDCVSK (M+2H m/z 508.2)
no-bridge pos2 peptides : SYYK (M+2H m/z 280.6); CTFQGCGVK (M+2H m/z 471.7)
NOS-bridge pos1 K-C1 peptide: SYFK CTYPDCVSK (M+3H m/z 524.9)
NOS-bridge pos1 K-C6 peptide: SYFK CTYPDCVSK (M+3H m/z 524.9)
NOS-bridge pos2 K-C1 peptide: SYYK CTFQGCGVK (M+3H 505.9)
NOS-bridge pos2 K-C6 peptide: SYYK CTFQGCGVK (M+3H 505.9)

(C) **LC-MS chromatograms for no-bridge peptides**

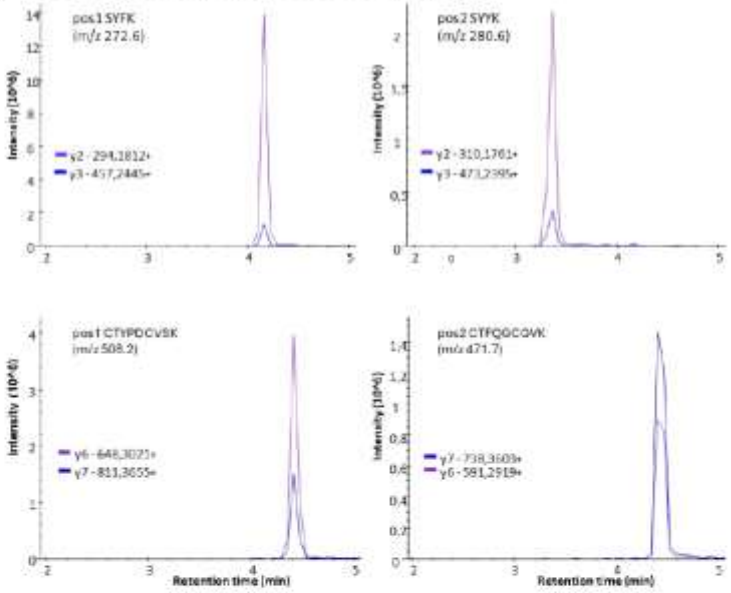

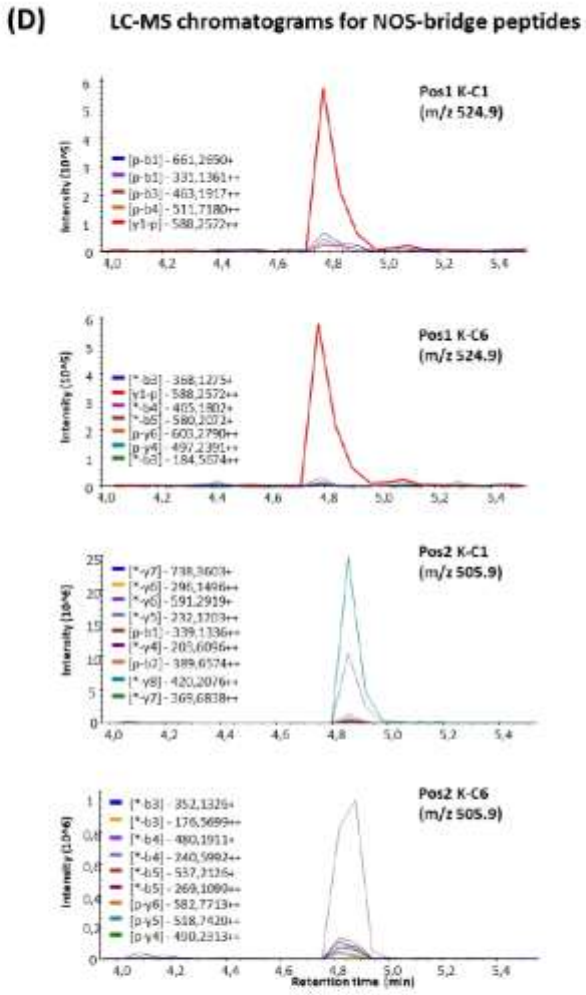

Fig. S14: Targeted LC-MS analysis of possible NOS-bridge peptides in WRKY25.
(A) In the amino acid sequence of the WRKY25 protein the DNA-binding WRKY domains are underlined and the possible positions of the NOS bridge between the (LYS (K) and the Cys (C) are shown in either solid (position 1) or dashed lines (position 2). **(B)** Proteolytic *in-silico* digest with Trypsin (cleavage sides after arginine (R) and lysine (K)) results in 8 different possible peptides. **(C)** Mass signals for transitions of the no bridge peptides SYFK, CTYPDCVSK, SYYK and CTFQGCGVK could be seen in a tryptic in-solution digest of the WRKY25 protein under non-reducing conditions. **(D)** In the same sample digest mass signals for all four of the possible NOS bridge peptide combinations (NOS bridge K-C1 and KC6 in both position 1 and 2) could also be measured.

Table S1: Primer sequences used for different experiments for transactiviation assays

Primer	Sequence	Purpose
PW18 3kb-F	CACCATCTCTTGTTAACAATATCCAA	Amplification Prom. WRKY18 3kb
PW18 3kb-R	AAAAGAAACCTTTATCTTAAGA	Amplification Prom. WRKY18 3kb
PW53 2.8 kb-F	CACCGTTTGGCATTTTCCTACTTTAC	Amplification Prom. WRKY53 2.8 kb
PW53 2.8kb-R	TTTTAGTATATGATTCCCAAAATAG	Amplification Prom. WRKY18 2.8 kb
pBGWFS7_seq_F	CGTTGCGGTTCTGTCAGTTC	Sequencing reporter
pBGWFS7_seq_R	CGTTTACGTCGCCGTCCA	Sequencing reporter
W18-F	CACCATGGACGGTTCTTCGTTTCTCGACATCTC T	Amplification WRKY18
W18-R	TCAATGGTGATGGTGATGATGTGTTCTAGATT GCTCCATTAACC	Amplification WRKY18
W25-F	CACCATGTCTTCCACTTCTTTCACCGACCTTCT TGG	Amplification WRKY25
W25-R	TCAATGGTGATGGTGATGATGCGAGCGACGTA GCGCGGTTG	Amplification WRKY25
W53-F	CACCATGGAAGGAAGAGATATGTTAAGTTGGG AG	Amplification WRKY53
W53-R	TCAATGGTGATGGTGATGATGATAATAAATCG ACTCGTGTAAAA	Amplification WRKY53
pJAN33 Sequ. F	ATCCGACTACAAAGACCA	Sequencing effector
BsaI mutagenesis primer W18 Forward	GAAGAAGGAAGTCTCAGTTTTGG	Mutagenesis of natural BsaI restriction site GAG (Glu) → GAA (Glu)
BsaI mutagenesis primer W18 Reverse	CCAAAACTGAGACTTCCTTCTTC	Mutagenesis of natural BsaI restriction site GAG (Glu) → GAA (Glu)
BsaI mutagenesis primer W25 Forward	TCACCAAGCGACCATCTCAAT	Mutagenesis of natural BsaI restriction site AGA (Arg) → CGA (Arg)
BsaI mutagenesis primer W25 Reverse	ATTGAGATGGTCGCTTGGTGA	Mutagenesis of natural BsaI restriction site AGA (Arg) → CGA (Arg)
W25_Cys17_mut_for	CGTTGACTCTTACGAAGA	Mutagenesis of Cys 17 UGC (Cys) → UCC (Ser)

W25_Cys17_mut_rev	TCGTAAGAGTCAACGCCG	Mutagenesis of Cys 17 UGC (Cys) → UCC (Ser)
W25N*_Forward	TTG GGTCTCA CACC ATGTCTTCCACTTCTTTCACCGACCTTC	Amplification of W25N*
W25N*_Reverse	TAA GGTCTC T CGCC ATTAGAGTTCCTACTCACCATGTA	Amplification of W25N*
W25_ΔpD1_55AA_Reverese_1	TAA GGTCTC T CGCC GTTTTGTGTTGCAATCTCATTAG	Amplification of the N-terminal fragment for W25ΔpD1
W25_ΔpD1_55AA_Forward_2	TTT GGTCTC T GGCG AAGAAGATTGTTGAGACGGCTTCTG	Amplification of the C-terminal fragment for W25ΔpD1
W25_ΔpD1_55AA_Reverse_2	TCA GGTCTC T CCTT TCACGAGCGACGTAGCGCGGTT	Amplification of the C-terminal fragment for W25ΔpD1
W25_ΔD2_66AA_ Forward_1	TTG GGTCTC A CACC ATGTCTTCCACTTCTTTCACCGACCTTC	Amplification of the N-terminal fragment for W25ΔD2
W25_ΔD2_66AA_ Reverse_1	GGTCTC T CGCC CTCTTTAACTCCTTTGCTTACTTC	Amplification of the N-terminal fragment for W25ΔD2
W25_ΔD2_66AA_ Forward_2	GGTCTC T GGCG GGAAGACACAATCACGATAT	Amplification of the C-terminal fragment for W25ΔD2
W25_ΔD2_66AA_ Reverse_2	TCA GGTCTC T CCTT TCACGAGCGACGTAGCGCGGTT	Amplification of the C-terminal fragment for W25ΔD2
BsaI Primer W18 N-Terminus Forward	TTG GGTCTC A CACC ATGGACGGTTCTTCGTTTCTCGACA	Amplification of W18N-fragment Creation of BsaI restriction site
BsaI Primer W18 N-Terminus Reverse	AAG GGTCTC A TGGT TGTAGCATCCCCTTCAGAAGCAT	Amplification of W18N-fragment Creation of BsaI restriction site
BsaI Primer W25 C-Terminus Forward	TC ACCA AGAGACCATCTCAATCTTCA	Amplification of W25C-fragment Creation of BsaI restriction site
BsaI Primer W25 C-Terminus Reverse	TCA GGTCTC T CCTT TCACGAGCGACGTAGCGCGGTT	Amplification of W25C-fragment Creation of BsaI restriction site
BsaI Primer W25 N-Terminus Forward	TTG GGTCTC A CACC ATGTCTTCCACTTCTTTCACCGACCTTC	Amplification of W25N-fragment and N-terminal fragment for W25ΔpD1 Creation of BsaI restriction site
BsaI Primer W25 N-Terminus Reverse	TGAAGATTGAGAT GGTCTC T TGGT GAA	Amplification of W25N-fragment Creation of BsaI restriction site
BsaI Primer W18 C-Terminus Forward	GCT GGTCTC T ACCA CTACTGAAACATCGGACACAAG	Amplification of W18C-fragment Creation of BsaI restriction site

BsaI Primer W18 C-Terminus Reverse	GAA GGTCTC G CCTT TCATGTTCTAGATTGCTCCATTAAC	Amplification of W18C-fragment Creation of BsaI restriction site
M13 Forward sequencing primer	GTAAAACGACGGCCAG	Sequencing
M13 Reverse sequencing primer	CAGGAAACAGCTATGAC	Sequencing

Table S2: Primers used for cloning BiFC constructs.

Primer	Sequence	Purpose
WRKY18_attB1_F	GGGG ACA AGT TTG TAC AAA AAA GCA GGC TTAATGGACGGTTCTTCGTTTCTCGACA	Amplification WRKY18 and W18N
WRKY18_attB4_R	GGGG ACAACTTTGTATAGAAAAGTTGGGT TCATGTTCTAGATTGCTCCATTAAC	Amplification WRKY18 and W18C
WRKY18_attB3_F	GGGGACA ACT TTG TAT AAT AAA GTT GGAATGGACGGTTCTTCGTTTCTCGAC	Amplification WRKY18 and W18N
WRKY18_attB2_R	GGGG ACCACTTTGTACAAGAAAGCTGGGT TCATGTTCTAGATTGCTCCATTA	Amplification WRKY18 and W18C
WRKY25_attB1_F	GGGG ACA AGT TTG TAC AAA AAA GCA GGC TTA ATGTCTTCCACTTCTTTCACCGAC	Amplification WRKY25 and W25N*, W25ΔpD1,W25ΔD2, W25N
WRKY25_attB4_R	GGGG ACAACTTTGTATAGAAAAGTTGGGT TCACGAGCGACGTAGCGCGGTTG	Amplification WRKY25 and W25N*, W25ΔpD1,W25ΔD2, W25C
WRKY25_attB3_F	GGGG ACA ACT TTG TAT AAT AAA GTT GGA ATGTCTTCCACTTCTTTCACCGAC	Amplification WRKY25 and W25N*, W25ΔpD1,W25ΔD2, W25N
WRKY25_attB2_R	GGGG ACCACTTTGTACAAGAAAGCTGGGT TCACGAGCGACGTAGCGCGGTTG	Amplification WRKY25 and W25ΔpD1,W25ΔD2, W25C
WRKY53_attB1_F	GGGG ACA AGT TTG TAC AAA AAA GCA GGC TTA ATGATGGAAGGAAGAGATATGTTAAGTT	Amplification WRKY53
WRKY53_attB4_R	GGGG ACAACTTTGTATAGAAAAGTTGGGT TTAATAATAAATCGACTCGTGTAAAA	Amplification WRKY53
WRKY53_attB3_F	GGGG ACA ACT TTG TAT AAT AAA GTT GGA ATGATGGAAGGAAGAGATATGTTAAGTT	Amplification WRKY53
WRKY53_attB2_R	GGGG ACCACTTTGTACAAGAAAGCTGGGT TTAATAATAAATCGACTCGTGTAAAA	Amplification WRKY53
M13-F	GTAAAACGACGGCCAG	Sequencing
M13-R	CAGGAAACAGCTATGAC	Sequencing

Table S3: Primers sequences used to clone and create the complementation lines

Primer	Sequence	Purpose
WRKY25_FW_GG	AACAGGTCTCAGGCTCAATGTCTTCC ACTTCTTTCACCGA	Amplification W25 and W25N*, W25ΔpD1, W25ΔD2,W25N
WRKY25_RV_GG	AACAGGTCTCACTGACGAGCGACGT AGCGCGGTTGGGATAT	Amplification W25 and W25ΔpD1, W25ΔD2,W25C
WRKY18_FW_GG	AACAGGTCTCAGGCTCAATGGACGG TTCTTCGTTTCTCG	Amplification W18 and W18N
WRKY18_RV_GG	AACAGGTCTCACTGATGTTCTAGATT GCTCCATTAACCT	Amplification W18 and W18C
EGFP_FW_B_1GG	AACAGGTCTCAAACAATGGTGAGCA AGGGCGAGGAGC	Amplification GFP
EGFP_RV_Cr_1GG	AACAGGTCTCATGCCCTTGTACAGCT CGTCCATGCC	Amplification GFP
GGseq F	TCATTAGGCACCCCAGGCTT	Sequencing
GGseq R	TCTTCGCTATTACGCCAGCT	Sequencing
Z03_F	TGT GGT GTA ACG TTG GAT CTG G	Sequencing
Z03_R	AACTAGGCTCGGACGAAGTAAGC	Sequencing

Table S4: Primers used for qRT-PCR analyses

Primer	Sequence	Purpose
ACTIN	AAGCTCTCCTTTGTTGCTGTT	qRT_PCR foward
ACTIN	GTTGTCTCGTGGATTCCAGCAGCTT	qRT_PCR reverse
WRKY53	CAGACGGGGATGCTACGG	qRT_PCR foward
WRKY53	GGCGAGGCTAATGGTGGT	qRT_PCR reverse

Table S5: Peptide description of LC-MS analyses

peptide	Q1 (m/z)	Q3 (m/z)	CE (Volts)
SYFK pos1 +2 F[y2] +1	272.642	294.181	15
SYFK pos1 +2 Y[y3] +1	272.642	457.245	15
SYYK pos2 +2 Y[y2] +1	280.639	310.176	15
SYYK pos2 +2 Y[y3] +1	280.639	473.239	15
CTYPDCVSK pos1 +2 P[y6] +1	508.215	648.302	23.9
CTYPDCVSK pos1 +2 Y[y7] +1	508.215	811.365	23.9
CTFQGCGVK pos2 +2 Q[y6] +1	471.712	591.292	22.1
CTFQGCGVK pos2 +2 F[y7] +1	471.712	738.36	22.1
SYFK-CTYPDCVSK-pos1K-C1 +3[p-b1]C+2	524.895	331.136	23.2
SYFK-CTYPDCVSK-pos1K-C1 +3[p-b1]C+1	524.895	661.265	23.2
SYFK-CTYPDCVSK-pos1K-C1 +3[p-b3]Y+2	524.895	463.191	23.2
SYFK-CTYPDCVSK-pos1K-C1 +3[p-b4]P+2	524.895	511.718	23.2
SYFK-CTYPDCVSK-pos1K-C1 +3 K[y1-p]+2	524.895	588.257	23.2
SYFK-CTYPDCVSK-pos1K-C6 +3[p-y4]C+2	524.895	497.239	23.2
SYFK-CTYPDCVSK-pos1K-C6 +3[*-b3]Y+1	524.895	368.127	23.2
SYFK-CTYPDCVSK-pos1K-C6 +3[*-b3]Y+2	524.895	184.567	23.2
SYFK-CTYPDCVSK-pos1K-C6 +3 K[y1-p]+2	524.895	588.257	23.2
SYFK-CTYPDCVSK-pos1K-C6 +3[*-b4]P+2	524.895	465.18	23.2
SYFK-CTYPDCVSK-pos1K-C6 +3[*-b5]D+1	524.895	580.207	23.2
SYFK-CTYPDCVSK-pos1K-C6 +3[p-y6]P+2	524.895	603.279	23.2
SYYK-CTFQGCGVK-pos2K-C1 +3[*-y8]T+2	505.892	420.208	22.3
SYYK-CTFQGCGVK-pos2K-C1 +3[*-y7]F+1	505.892	738.36	22.3

SYYK-CTFQGCGVK-pos2K-C1 +3[*-y7]F+2	505.892	369.684	22.3
SYYK-CTFQGCGVK-pos2K-C1 +3[*-y6]Q+2	505.892	296.15	22.3
SYYK-CTFQGCGVK-pos2K-C1 +3[*-y6]Q+	505.892	591.292	22.3
SYYK-CTFQGCGVK-pos2K-C1 +3[*-y5]G+2	505.892	232.12	22.3
SYYK-CTFQGCGVK-pos2K-C1 +3[*-y4]C+2	505.892	203.61	22.3
SYYK-CTFQGCGVK-pos2K-C1 +3[p-b2]T+2	505.892	389.657	22.3
SYYK-CTFQGCGVK-pos2K-C1 +3[p-b1]C+2	505.892	339.134	22.3
SYYK-CTFQGCGVK-pos2K-C6 +3[*-b3]F+1	505.892	352.133	22.3
SYYK-CTFQGCGVK-pos2K-C6 +3[*-b3]F+2	505.892	176.57	22.3
SYYK-CTFQGCGVK-pos2K-C6 +3[*-b4]Q+1	505.892	480.191	22.3
SYYK-CTFQGCGVK-pos2K-C6 +3[*-b4]Q+2	505.892	240.599	22.3
SYYK-CTFQGCGVK-pos2K-C6 +3[*-b5]G+1	505.892	537.213	22.3
SYYK-CTFQGCGVK-pos2K-C6 +3[*-b5]G+2	505.892	269.11	22.3
SYYK-CTFQGCGVK-pos2K-C6 +3[p-y6]Q+2	505.892	582.771	22.3
SYYK-CTFQGCGVK-pos2K-C6 +3[p-y5]G+2	505.892	518.742	22.3
SYYK-CTFQGCGVK-pos2K-C6 +3[p-y4]C+2	505.892	490.231	22.3
Trypsin autolysis peptide 1	421.75	472.3	20
Trypsin autolysis peptide 2	421.75	571.4	20

Publish manuscript 2: The Non-JAZ TIFY Protein TIFY8 of Arabidopsis thaliana Interacts with the HD-ZIP III Transcription Factor REVOLUTA and Regulates Leaf Senescence

Andrade Galan, A.G., Doll J, Saile, S.C., Wünsch, M., von Roepenack-Lahaye, E.V., Pauwels, L., Goossens, A., Bresson, J., Zentgraf, U. The Non-JAZ TIFY Protein TIFY8 of Arabidopsis thaliana Interacts with the HD-ZIP III Transcription Factor REVOLUTA and Regulates Leaf Senescence. Int J Mol Sci. 2023 Feb 4;24(4):3079. doi: 10.3390/ijms24043079. PMID: 36834490; PMCID: PMC9967580.

International Journal of
Molecular Sciences

MDPI

Article

The Non-JAZ TIFY Protein TIFY8 of *Arabidopsis thaliana* Interacts with the HD-ZIP III Transcription Factor REVOLUTA and Regulates Leaf Senescence

Ana Gabriela Andrade Galan [1], Jasmin Doll [1], Svenja Corina Saile [1], Marieluise Wünsch [1], Edda von Roepenack-Lahaye [1], Laurens Pauwels [2,3], Alain Goossens [2,3], Justine Bresson [1] and Ulrike Zentgraf [1,*]

[1] Center for Plant Molecular Biology (ZMBP), University of Tübingen, Auf der Morgenstelle 32, 72076 Tübingen, Germany
[2] Department of Plant Biotechnology and Bioinformatics, Ghent University, 9052 Ghent, Belgium
[3] Center for Plant Systems Biology, VIB, 9052 Ghent, Belgium
* Correspondence: ulrike.zentgraf@zmbp.uni-tuebingen.de

Abstract: The HD-ZIP III transcription factor REVOLUTA (REV) is involved in early leaf development, as well as in leaf senescence. REV directly binds to the promoters of senescence-associated genes, including the central regulator *WRKY53*. As this direct regulation appears to be restricted to senescence, we aimed to characterize protein-interaction partners of REV which could mediate this senescence-specificity. The interaction between REV and the TIFY family member TIFY8 was confirmed by yeast two-hybrid assays, as well as by bimolecular fluorescence complementation in planta. This interaction inhibited REV's function as an activator of *WRKY53* expression. Mutation or overexpression of *TIFY8* accelerated or delayed senescence, respectively, but did not significantly alter early leaf development. Jasmonic acid (JA) had only a limited effect on *TIFY8* expression or function; however, REV appears to be under the control of JA signaling. Accordingly, REV also interacted with many other members of the TIFY family, namely the PEAPODs and several JAZ proteins in the yeast system, which could potentially mediate the JA-response. Therefore, REV appears to be under the control of the TIFY family in two different ways: a JA-independent way through TIFY8, which controls REV function in senescence, and a JA-dependent way through PEAPODs and JAZ proteins.

Keywords: TIFY8; REVOLUTA; transcription factor regulation; leaf senescence; *Arabidopsis thaliana*; jasmonic acid signaling; PEAPOD; JAZ proteins

Citation: Andrade Galan, A.G.; Doll, J.; Saile, S.C.; Wünsch, M.; Roepenack-Lahaye, E.v.; Pauwels, L.; Goossens, A.; Bresson, J.; Zentgraf, U. The Non-JAZ TIFY Protein TIFY8 of *Arabidopsis thaliana* Interacts with the HD-ZIP III Transcription Factor REVOLUTA and Regulates Leaf Senescence. *Int. J. Mol. Sci.* **2023**, *24*, 3079. https://doi.org/10.3390/ijms24043079

Academic Editor: Tomotsugu Koyama

Received: 2 January 2023
Revised: 1 February 2023
Accepted: 2 February 2023
Published: 4 February 2023

1. Introduction

Leaf polarity, polarity along the shoot–root axis, and stem cell specification and proliferation are regulated by class III homeodomain leucine zipper (HD-ZIP III) transcription factors [1–3]. However, these factors, namely REVOLUTA (REV), not only control these critical steps in early plant development, but are also involved in later steps of development such as leaf senescence and reproduction [4–6]. Chromatin-IP revealed that REV binds directly to the promoter of the senescence-associated transcription factor *WRKY53*, which is one of the hubs of senescence regulation and is tightly controlled on multiple levels [4,7]. REV appears to be an important driver for senescence, as the delayed-senescence phenotype of the *rev5* mutant is stronger than that of the *wrky53* mutant. This can be easily explained by the fact that several other senescence-associated genes (SAGs) are direct targets of REV, as shown by a ChIP-Seq experiment [4,5,8]. Vice versa, there is little indication that WRKY53 plays a role in early leaf development and leaf polarity. Accordingly, the interaction of REV and *WRKY53* appears to be dependent on the developmental stage, and the influence of REV on *WRKY53* expression seems to be most efficient at the onset of monocarpic senescence. One possible explanation could be that REV needs specific modifications or specific interaction partners to act as an activator of *WRKY53* expression

and senescence. We can already show that the redox state of the REV protein can alter its binding to the *WRKY53* promoter, in which the reduced form binds more efficiently to the DNA [4]. However, on the other hand, *WRKY53* expression is induced by increasing levels of hydrogen peroxide, and the REV protein is somehow involved in this response, as the amplitude of this response is dampened in the *rev5* mutants. This is a contradiction that has not yet been solved and points to a more complex scenario. Moreover, the binding preference of REV to the different binding-sites in the *WRKY53* promoter changes during the progression of development and senescence, also indicating an adaptation of the REV properties to certain developmental stages [4].

On the molecular level, the expression of HD-ZIP III transcription factors is controlled by miRNA165/166, and the functionality of the proteins is controlled by the interaction with mircoProteins called LITTLE ZIPPER [9,10]. A leucin zipper domain mediates homo- and heterodimerization between HD-ZIP III factors as well as interaction with the LITTLE ZIPPER proteins, which then block the dimerization and the function [10]. In addition, the C-terminal MEKHLA domain of the HD-ZIP III factor REV was suggested to inhibit dimerization through a steric masking mechanism [11]. In general, PAS domains are sensor domains that respond to a variety of chemical and physical stimuli that regulate a wide range of signal transduction pathways [12]; however, the redox sensitivity of REV is not mediated by the PAS domain [4]. Already in 2013, Reinhart and colleagues characterized proteins that could interact with the full-length REV protein and a truncated version that lacks the MEKLHA domain using the yeast two-hybrid system [13]. One of these proteins was TIFY8, a non-canonical member of the TIFY family.

TIFY proteins are defined by a highly conserved TIFY motif (TIF[F/Y]XG) that resides within the larger ZIM domain (Zinc-finger protein expressed in Inflorescence Meristem). In Arabidopsis, TIFY proteins are represented by 18 family members which are subdivided into two classes due to the presence or absence of a C2C2-GATA domain. Three members that have this C2C2-GATA domain belong to class I, whereas the fifteen other members lack this domain. Twelve of the class II members are so-called JAZ proteins. JAsmonate ZIM-domain (JAZ) proteins are repressors that prevent the action of multiple transcription factors which execute the response of the plant to the hormone jasmonic acid (JA). Most JAZ proteins use the TIFY/ZIM domain to interact with an adapter protein called NINJA (NOVEL INTERACTOR OF JAZ). The NINJA protein contains an EAR (ERF-associated Amphiphilic Repression) motif to recruit the repressor TOPLESS [14–16]. JAZ-bound transcription factors are inactive due to the presence of TOPLESS in the complex, but the transcription factors can be activated rapidly in response to jasmonoyl-L-isoleucine (JA-Ile), the bioactive form of JA. JA-Ile can bind to the Jas domain of the JAZ proteins, thereby acting as a "molecular glue" between the JAZ proteins and CORONATINE-INSENSITIVE1 (COI1) [17]. COI1 represents the F-Box protein of the E3-ubiquitin ligase complex SCF^{COI1} [18], which directs the JAZ proteins to 265-mediated proteasomal degradation in the presence of JA-Ile.

In contrast to the JAZ protein, the TIFY proteins PEAPOD1 (PPD1) and PEAPOD2 (PPD2) contain a divergent C-terminal Jas domain and an additional N-terminal PPD-domain. PEAPOD proteins control lamina size and curvature in Arabidopsis [19] and are negative regulators of meristematic proliferation to control organ size [20]. It was recently described that PEAPOD repressors modulate and coordinate developmental responses to light intensity [21]. For PPD1 and PPD2, TOPLESS can be recruited by KIX8 (KINASE-INDUCIBLE DOMAIN INTERACTING8) or KIX9 instead of NINJA [22]. TIFY8, which is even more divergent, completely lacks a Jas domain for the response to JA-Ile but still contains a ZIM domain [23]. In accordance with the lack of the Jas domain, TIFY8´s stability is not affected by JA treatment. No other specific protein domains other than the ZIM domain have been described so far; moreover, no direct DNA-binding could be observed. Despite the functional ZIM domain, no interaction with the JAZ proteins was found; only the two PEAPOD proteins PPD1 and PPD2 as well as NINJA were able to interact via the ZIM domain of Arabidopsis TIFY8. KIX8 and KIX9 were also identified in Arabidopsis TIFY8 protein complexes [23]. Therefore, we hypothesized that TIFY8 could

recruit the repressor TOPLESS via NINJA or KIX8/9 to the REV complex and counteracts REV function as an activator of transcription.

Here, we analyzed the interaction interface between REV and TIFY8 in more detail. Using the yeast-two-hybrid system, we could demonstrate that REV interacts with the ZIM domain of TIFY8. However, the ZIM domain is necessary but not sufficient for REV-binding; the surrounding regions as well as the C-terminal residues are also involved. The REV and TIFY8 interactions were confirmed in planta, using Arabidopsis protoplasts and *Nicotiana benthamiana* leaves. Moreover, we analyzed the impact of TIFY8 on senescence regulation in *tify8* mutants and *TIFY8* overexpression (*TIFY8*-OE) plants. Here, a clear repressing effect of TIFY8 on senescence was observed, indicating that the interaction between TIFY8 and REV might have a biological function. However, the effect on early leaf development was less pronounced, as leaf morphology was only slightly affected in the *tify8* mutants and *TIFY8*-OE plants.

Even though JA-Ile and the PPD proteins are known to be involved in the repression of cell proliferation and cell size during leaf growth [24], and although TIFY8 appears to have a function in the PPD/KIX repressor complex in Arabidopsis, the relationship between JA-Ile and PPD and TIFY8 function is still unclear. Therefore, we analyzed whether JA has a role in TIFY8-REV regulation.

2. Results

2.1. TIFY8 and REVOLUTA Proteins Physically Interact

In order to characterize the interaction of REV with TIFY8 in more detail, we analyzed the interaction of REV with the full length TIFY8, as well as with several truncated versions of TIFY8 in yeast cells using the Matchmaker® Gold Yeast-Two-Hybrid (Y2H) System. As previously reported, TIFY8 has been identified as an interacting partner of REV in a screen using a yeast library prepared from mRNA of inflorescence meristems [13]. In this analysis, the presence of the MEKLHA domain of REV did not influence the interaction in the re-testing. Here, we tested whether REV interacts with the full length TIFY8 protein, with the C- and the N-terminal part of the protein, and with several truncated versions (Figure 1a). Mating was repeated 3–7 times, and yeast cells were grown on selective media with increasing stringency (Figure 1b). Expression of the fusion proteins in the yeast cells was confirmed by Western Blot and immune detection (Figure S1a). One example of the yeast colonies´ growth on selection media is shown in Figure 1b, and a summary of the 3–7 mating approaches is displayed as a heat map in Figure S1b. An interaction between REV and the full-length TIFY8 was observed in all matings, as well as an interaction with the C-terminal half of the protein (TIFY8-C) that included the TIFY/ZIM domain (Figures 1b and S1b). The N-terminal protein parts without the TIFY/ZIM domain (TIFY8-N, TIFY8-N1) were not able to bind to the REV protein even though we could clearly show that the truncated proteins were expressed in the yeast cells (Figure S1a). To narrow down the interaction interface, we divided the C-terminal half into several subdomains C1 to C4. Here, only the constructs containing the TIFY/ZIM domain were able to interact with REV. However, the interaction between REV and the TIFY/ZIM domain alone (TIFY8-C4) appears to be only weak (Figure 1b and Figure S1b). This clearly indicates that the TIFY/ZIM domain together with the flanking regions is the interaction interface between REV and TIFY8.

In order to confirm the interaction between REV and TIFY8 in planta, we used bi-molecular fluorescence complementation assays (BiFC). Therefore, Arabidopsis protoplasts that were prepared from cell culture cells, as well as leaves of *Nicotiana bentamiana*, were transiently transformed with BiFC constructs bearing REV fused to one half of the yellow fluorescent protein (YFP) and TIFY8 or the TIFY8-C terminus and its truncations fused to the other half of the YFP. In addition, a red fluorescence protein (RFP) was encoded by the same construct to control for transformation efficiency. The fluorescent protoplasts were analyzed with the CYTOFLEX cell sorter, indicating the portion of protoplasts with BiFC of

YFP compared to RFP-transformed cells. The infiltrated tobacco leaves were analyzed by confocal laser scanning microscopy.

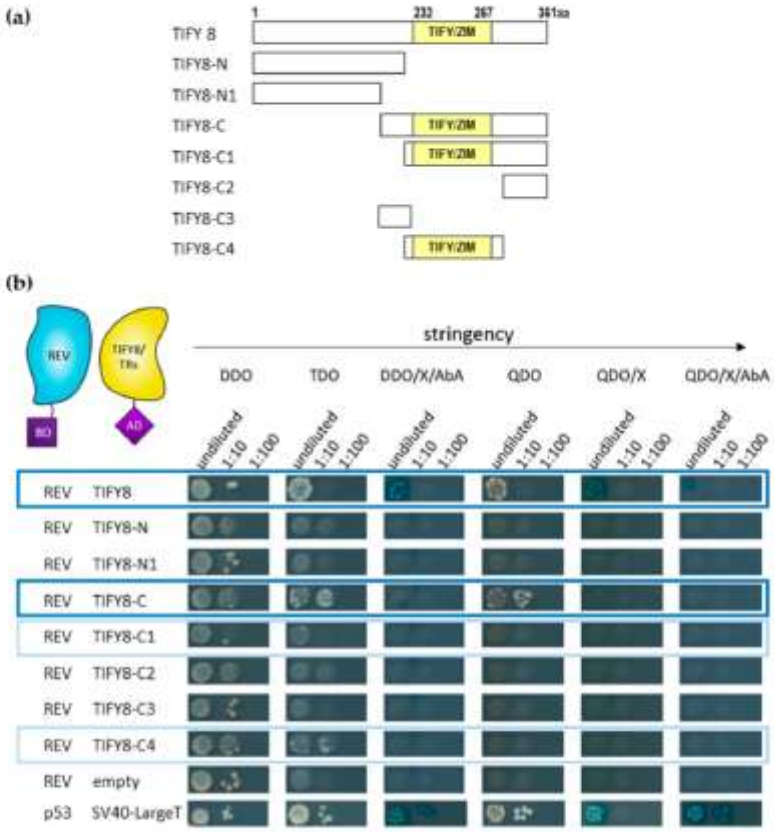

Figure 1. Yeast two-hybrid interactions between REV and TIFY8 and truncated proteins. (**a**) Scheme of TIFY8 and the truncated versions used in the yeast two-hybrid assay. The yellow box represents the TIFY/ZIM domain. TIFY8 full length (1 to 361aa), TIFY8-N (1 to 229aa), TIFY8-N1 (1 to 176aa), TIFY8-C (176 to 361aa), TIFY8-C1 (230 to 361aa), TIFY8-C2 (284 to 361aa), TIFY8-C3 (176 to 229aa), and TIFY8-C4 (239 to 283aa). (**b**) Representative yeast two-hybrid assay between GAL4-BD-REV and TIFY8, as well as a series of truncated versions of the TIFY8 protein shown in (**a**), fused with GAL4-AD. A serial 1:10 dilution of each transformed yeast was spotted onto control (DDO) and different protein–protein interaction selective media with increasing stringency. Blue boxes indicate interactions, and light blue boxes indicate weak interactions.

In both systems, we could clearly confirm that the full length TIFY8 protein could interact with REV also in planta. The interaction takes place predominantly in the nucleus, as expected for a transcription factor (Figure 2). As in the yeast cells, two TIFY8-truncated versions containing the TIFY/ZIM domain (TIFY8-C, TIFY8-C1) were able to interact with REV, even though it appears that the interactions were not as efficient as with the full-length TIFY8. However, the TIFY8-C4 construct containing only the TIFY/ZIM domain, which was sufficient to interact with REV in yeast cells, appears not to be sufficient to produce a fluorescence signal in the BiFC in planta. Moreover, although TIFY8-C2 and TIFY8-C3 were not able to interact with REV in yeast cells, we observed that the C-terminal part that is

downstream of the TIFY/ZIM domain is also able to contribute to the interaction with REV in plant cells. This could possibly indicate that in plant cells, an additional plant protein or a plant-specific modification is involved in the interaction. In conclusion, the TIFY/ZIM domain, as well as the C-terminal regions, is involved in the interaction with REV.

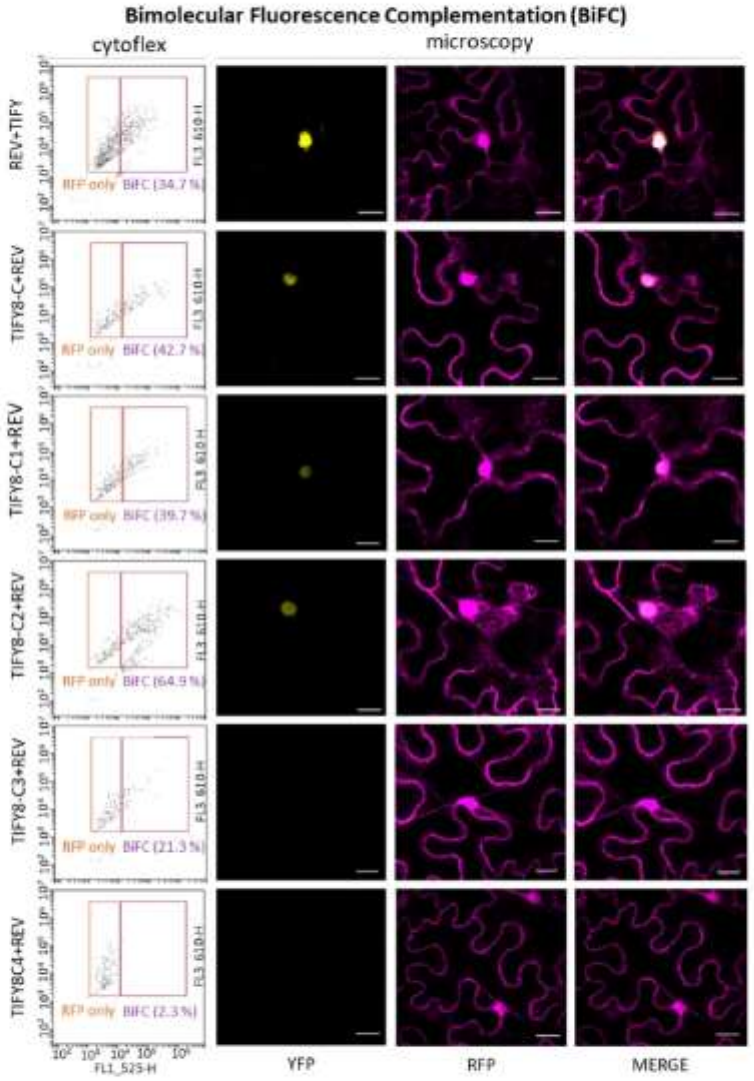

Figure 2. In planta protein–protein interaction between TIFY8 or TIFY8-truncated versions (see Figure 1a) with REV using BiFC in transiently transformed Arabidopsis protoplasts or tobacco leaves. Protoplasts were analyzed with the cytoflex cell sorter (**left**), orange squares indicate transformed protoplasts (RFP), and purple squares indicate interaction via BiFC (YFP). Transiently transformed *Nicotiana benthamiana* leaves were analyzed under the confocal laser scanning microscope (**right**). YFP indicates BiFC; RFP is used as a transformation control. Scale bar indicates 20 µm.

2.2. TIFY8 Inhibits the Transactivation Capacity of REV

To ascertain the consequences of REV/TIFY8 interaction on the regulatory function of REV, we tested the induction of the direct target gene *WRKY53* by REV in the absence or presence of TIFY8. Col-0 Arabidopsis protoplasts were transiently transformed with the reporter construct P_{WRKY53}:*GUS* together with the effector constructs 35S:*REV*, 35S:*TIFY8*, or both in combination. Moreover, we aimed to investigate whether JA influences TIFY8/REV interaction. As expected, REV induced the expression of the promoter-*WRKY53*-driven reporter gene. In contrast, TIFY8 had a clear repressive effect on the *WRKY53* promoter. If both effector proteins were co-expressed in the protoplasts, an even stronger repressing effect became obvious. This non-additive effect and the fact that the repressing effect of TIFY8 is even enhanced when both proteins are highly expressed can only be interpreted that with increased amounts of REV, the repressor function of TIFY8 is more pronounced due to the direct interaction between them and the dominant repressing effect of TIFY8. To our surprise, JA had an enhancing effect on the induction of *WRKY53* expression by REV, whereas no influence on the repressor function of TIFY8 could be observed (Figure 3).

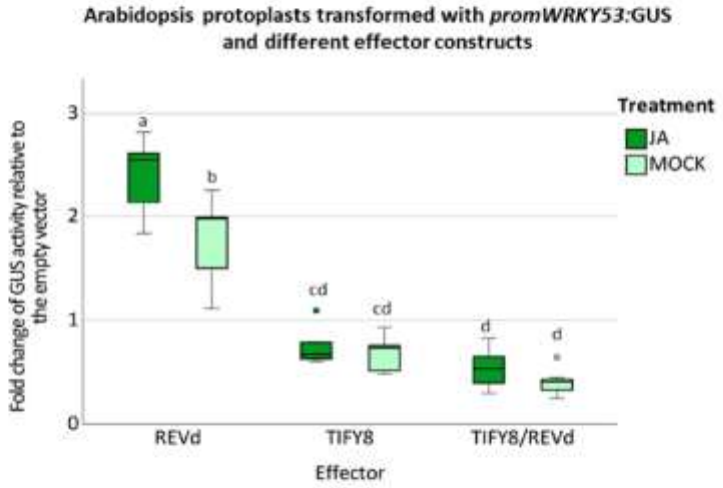

Figure 3. Arabidopsis protoplasts were transiently transformed with a 2.8-kbp-fragment of the *WRKY53* promoter fused to the *GUS* gene as a reporter construct; 35S: *REVd* and 35S: *TIFY8* constructs were used as effector plasmids. These transfected protoplasts were simultaneously incubated with 40 µM JA or the same volume of water for the MOCK condition. A boxplot of the values relative to the empty vector control is presented ($n = 7$). One-way ANOVA test was performed, lowercase letters indicate significant differences among groups ($p \leq 0.05$).

It has been previously described that in contrast to the other class II TIFY proteins, TIFY8 stability is not regulated by JA, as it also lacks a Jas domain for JA–Ile binding [23]. However, it has not been observed before that REV function can be enhanced by JA. The JA effect is most likely mediated on the protein level, as in this case, *REV* expression is driven by the 35S cauliflower mosaic virus promoter, which is not sensitive to JA. In addition, we used a REV construct which is no longer responsive to miRNA165/166 (REVd) [10] so that the JA effect is not related to miRNA expression.

2.3. Expression Pattern of REV and TIFY8

If the interaction between TIFY8 and REV is of biological relevance, a temporal and spatial overlap in their expression patterns should be observed. As it was already shown that REV has a positive regulatory effect on leaf senescence [4–6], we tested leaf tissue of different developmental stages for the expression of *TIFY8* and *REV*—as well as the direct target gene of REV, *WRKY53*—using qRT-PCR. *ACTIN2* was used as a reference gene. As expected for a regulator and its direct target gene, the *REV* and *WRKY53* expression patterns were very similar. In the youngest plants analyzed here (4-week-old plants), *REV* expression and *WRKY53* expression were low, but both genes were upregulated at the onset of monocarpic senescence in leaves of 6- and 7-week-old plants. In contrast, *TIFY8* had its lowest expression in 6- and 7-week-old plants and its highest in 4-week-old plants when *REV* and *WRKY53* expression was low. This is consistent with the function of TIFY8 as a repressor of REV function. The expression pattern of *TIFY8* appears to ensure that in younger plants, senescence is not induced, and *WRKY53* and other direct senescence-associated target genes of REV are not activated. In contrast, in older plants, when *REV* expression increased and SAGs such as *WRKY53* were activated, *TIFY8* expression and its repressing effect on REV should be low. Interestingly, not only the amount of the *TIFY8* transcripts was reduced in older plants, but also the ratio between the two described splicing variants (Figure S2) was altered, and the portion of splicing variant 2 was decreased (Figure 4). As was the case for the JAZ proteins, the C-terminus is truncated in splicing variant 2; however, in the JAZ proteins, retention of the so-called Jas intron generates truncated proteins that lack C-terminal amino acids. These truncated JAZs retain the ability to interact with transcription factors, such as MYC2, but have a reduced capacity to form complexes with COI1 in comparison to their respective full-length isoforms. Therefore, these truncated splice variants of the JAZ proteins are dominant repressors of JA signaling and provide a general mechanism to reduce the fitness costs associated with over-stimulation of the JA signaling pathway [25]. Whether the TIFY8 splice variants also expand the functional repertoire still has to be elucidated.

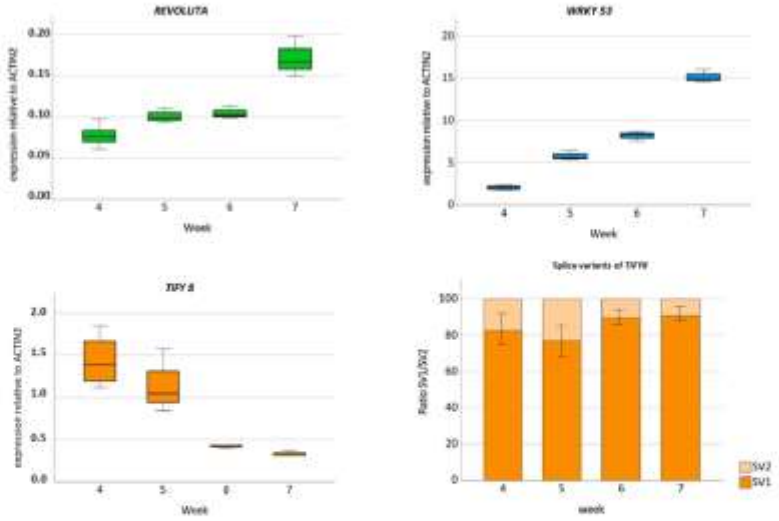

Figure 4. Boxplots presenting the expression of *REVOLUTA*, *WRKY53*, and *TIFY8* over time in leaf tissue of Arabidopsis wildtype plants Col-0. Leaves No. 6 and 7 of each rosette were harvested from 4- to 7-week-old plants. Expression levels were determined via qRT-PCR, and values were normalized to *ACTIN2* ($n = 3$). In the case of *TIFY8*, the ratio for the two existing splicing variants (SV1, SV2, see Figure S2) was determined.

2.4. Involvement of TIFY8 in Early Leaf Development and Senescence

To unravel the biological function of the REV/TIFY8 interaction, we analyzed early leaf development as well as monocarpic senescence in *tify8* mutants and a *TIFY8*-OE line. We used two previously characterized T-DNA insertion lines, *tify8-1T* and *tify8-2T*, and the highly overexpressing *TIFY8*-OE line 1 [23]. Moreover, we describe here two additional *TIFY8* alleles that we constructed using CRISPR/Cas9. As the T-DNA insertions were localized in the first exon and first intron, we hypothesized that these insertion lines might not be full KO [23]. Hence, we targeted *TIFY8* with two constructs, each with two sgRNAs [26], targeting exon 5 and either the sequence encoding the TIFY domain (exon 4) or exon 3 (Figure S3). Both lines are homozygous for indels at the targeted sites. All lines were grown side by side with the Col-0 wildtype plants and the *rev5* mutant line for comparison. The mutant lines and the overexpressor line have been analyzed in two separate experiments due to space limitations in the climate chambers and are, therefore, presented separately with their corresponding controls. The phenotyping was repeated several times with the same outcome, and one example is presented here.

First, the different colors of the leaves of one rosette were quantified using an automated colorimetric assay (ACA) tool (Figure 5a) which was developed in our lab [27]. In Figure 5, we show the results of only one of the mutant lines, *tify8-4;* the results of all four *tify8* mutant lines are presented in Figure S4a. In addition, the phenotypical appearance of the leaves is shown in Figure S5a; both pointing already to an acceleration of senescence in *TIFY8* loss-of-function lines, whereas the *TIFY8*-OE line showed delayed senescence more similar to the *rev5* mutant. (Figure 5a and Figure S6a). However, the length of the main shoot as well as the number of side shoots was not significantly different in all lines except the *rev5* mutant, which had a shorter main shoot (Figure S8a) but more side shoots (Figure S8b), which was already described before [5]. This indicates that TIFY8 might alter predominantly the senescence effects of REV.

Moreover, additional parameters were analyzed to describe different changes in the complex process of senescence. Chlorophyll loss, functionality of photosystem II using pulse amplitude modulation (PAM) fluorometry, deterioration of the plasma membrane measured by ion leakage and lipid peroxidation (the latter also giving hints on oxidative stress), and senescence-associated gene (SAG) expression were monitored over time. For more reliable comparisons, leaves of defined positions within the rosette were used to analyze the different parameters in the same plant following the guidelines given in [27]. Leaf No. 5 and 10 were first used for PAM fluorometry, and subsequently, chlorophyll was extracted from Leaf No. 5. The loss of *TIFY8* function accelerated chlorophyll loss, as well as loss of the functionality of photosystem II (Figures 5b, S4b and S5b,c), which is consistent with the phenotypical appearance. Even though the differences were not significant except for *rev5*, all mutants had lower Fv/Fm values compared to Col-0 and *rev5* plants (Figure S4b), whereas the *TIFY8*-OE displayed a delayed senescence phenotype similar to that of *rev5* (Figure 5 and Figure S6b). Ion leakage was measured in leaf No. 4, and lipid peroxidation was analyzed in Leaf No. 9. Both ion leakage and lipid peroxidation were more pronounced in the *tify8* mutants and less pronounced in the *rev5* mutant and *TIFY8-OE* (Figures 5c and S7).

In addition, expression of two senescence-associated marker genes, namely the cysteine protease *SAG12* and the short-chain alcohol dehydrogenase *SAG13*, was analyzed in Leaf No. 7 using qRT-PCR and again *ACTIN2* as a reference gene. *SAG12* and *SAG13* are expressed more highly in all *tify8* mutant lines in week 7 compared to Col-0 wildtype plants. In contrast, *TIFY8*-OE leaves had lower *SAG12* and *SAG13* expression than Col-0 leaves and behaved more similarly to the *rev5* mutants (Figures 5d, S4d and S6c).

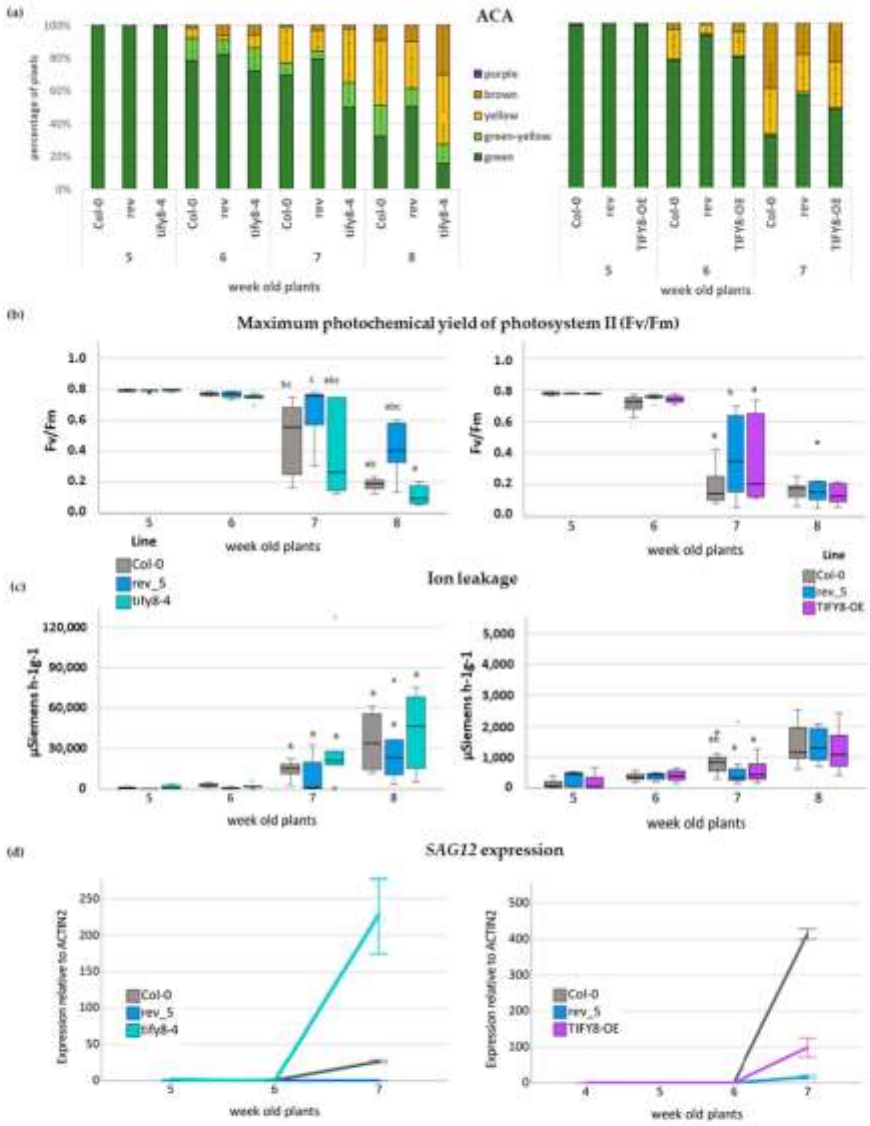

Figure 5. Photosynthetic parameters analyzed for the senescence phenotyping of *tify8-4* and *TIFY8*-OE compared to *rev5* mutants and wildtype Col-0 plants. (**a**) The Automated Colorimetric Assay (ACA) to categorize the color of individual leaves of at least six plants pixelwise into five categories: green, green-yellow, yellow, brown, and purple. The percentage of each group with respect to total pixel number of all leaves (1–10) is presented ($n = 6$). (**b**) Boxplot of Fv/Fm values measured with PAM for leaves No. 5 of 4- to 7-week-old plants ($n = 6$–8). (**c**) Boxplot of the decrease in solute retention determined through ion leakage in leaves No. 4 of 4- to 7-week-old plants ($n = 6$–8). One-way ANOVA test was performed, lowercase letters indicate significant differences among groups ($p \leq 0.05$). (**d**) Gene expression of the senescence-associated marker genes SAG12 was analyzed by qRT-PCR and normalized to the expression of the *ACTIN2* gene (mean values ± SD, $n = 3$).

In conclusion, TIFY8 acts as a repressor of leaf senescence, most likely through the interaction with REV. In contrast to the clear effects on senescence, the impact of TIFY8 appears to be less pronounced in the early stages of leaf development. The *rev5* mutant plants showed the clear downward curvature of the leaves as described before [8,10], whereas the Col-0 wildtype plants, as well as the *tify8* mutants, had flat leaves. The *TIFY8*-OE line also developed slightly downward-curled leaves, but this tendency was much less pronounced than in *rev5* mutants (Figure S9).

Taken together, TIFY8 has a regulatory impact on REV function but preferentially in late leaf developmental stages and less pronounced in early leaf development.

2.5. Impact of JA on the REV/TIFY8/WRKY53 Network

As the activation of the *WRKY53* promoter by REV was enhanced by JA in the transiently transformed protoplasts and JA was shown to be involved in senescence regulation [28,29], we aimed to investigate how JA influences the REV/TIF8/WRKY53 network. Therefore, we measured JA levels in the Col-0 wildtype plants, in two *tify8* mutants, and in the *TIFY8*-OE line, as well as in the *rev5* mutant. We could confirm that JA levels increased with the age of the plants, as already observed before [30]. However, there was no significant difference between the lines (Figure 6), indicating that there is no feedback regulation of REV or TIFY8 on JA biosynthesis.

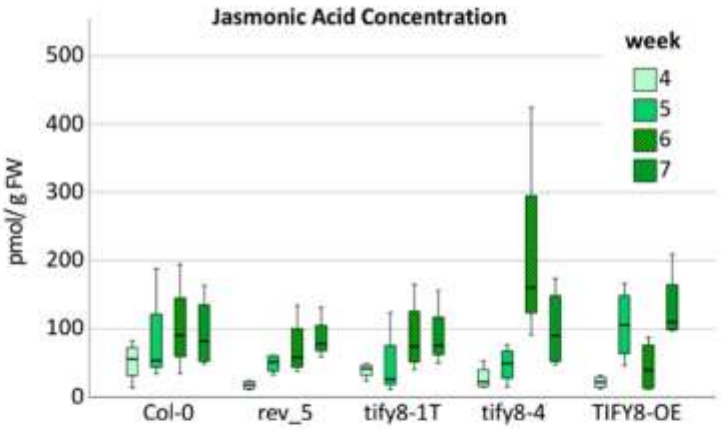

Figure 6. Boxplot of JA concentrations measured by LCMS in Col-0, *rev5*, *tify8-1T*, and *tify8-4* mutants and *TIFY8*-OE plants. The concentration was determined in pools of leaves No. 5 to 9 of 4- to 7-week-old-plants ($n = 4$).

Moreover, the expression of *REV*, *TIFY8*, and *WRKY53* was analyzed by qRT-PCR in the wildtype and the mutant lines after JA treatment. Short-term effects 6 h after treatment as well as long-term effects after 24 h and 96 h were determined. Two different developmental stages, namely 3- and 5-week-old plants, were analyzed to test whether there is an influence of the developmental stage on hormone response. The expression of the *REV*, *TIFY8*, and *WRKY53* genes are presented as heat maps relative to the expression levels of the respective genes after MOCK treatment (Figure 7).

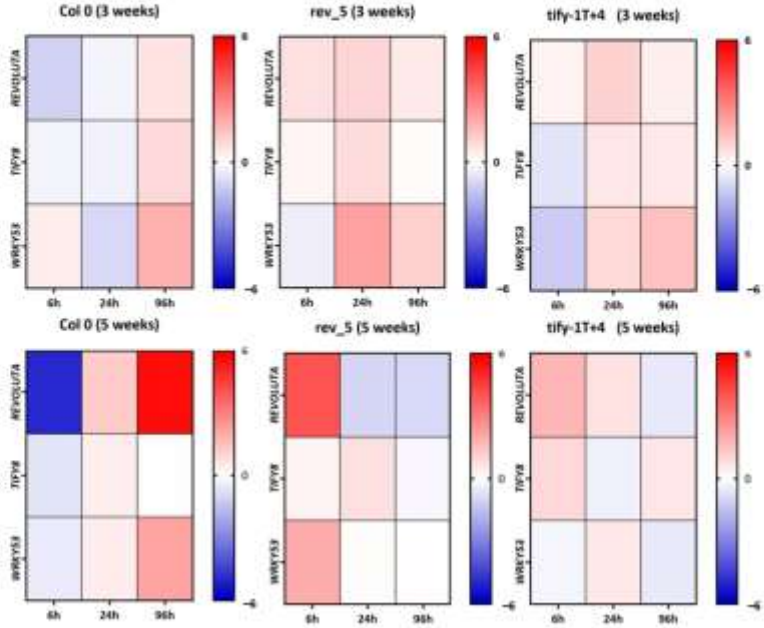

Figure 7. Heat map of the gene expression measured by qRT-PCR of *REV*, *TIFY8*, and *WRKY53* in Col-0, *rev5*, and *tify8* mutant plants for 3-week-old and 5-week-old plants 6 h, 24 h, and 96 h after JA treatment. Expression is shown as log2-fold changes relative to the respective MOCK treatments; blue color indicates repression, whereas red color indicates induction.

In Col-0, there appears to be a difference between 3- and 5-week-old plants, as *REV* and *TIFY8* are more severely downregulated 6 h after treatment in 5-week-old plants. After 24 h in 5-week-old plants, there is a switch in the response; now *REV* and *TIFY8* are more strongly expressed after JA treatment, which is even intensified for *REV* after 96 h. This effect appears to be delayed in the 3-week-old plants. Here, the switch can be observed only after 96 h and is also less severe.

In contrast, *WRKY53* expression was slightly induced by JA treatment in 3-week-old plants after 6 h, then slightly reduced after 24 h, and increased again after 96 h. Again, this pattern changed in 5-week-old plants, in which the expression was slightly reduced 6 h after treatment and then increased 24 h after treatment, which was also intensified after 96 h. *REV* expression appears to be more responsive to JA than *TIFY8* and *WRKY53* expression, at least in 5-week-old plants, and the *WRKY53* pattern resembles the *REV* pattern more in 5-week-old plants.

This is consistent with the previously observed influence of REV on *WRKY53* expression during senescence, but a less clear connection between these partners during early leaf development appears to exist. From the expression pattern of all three genes in the *rev5* and *tify8* mutant lines, in which the leaf material of the two mutants *tify8-1T* and *tify8-4* has been combined, we can conclude that REV as well as TIFY8 are somehow involved in the regulation of each other, as the expression patterns change for *REV* in the *tify8* mutant and vice versa. Moreover, both genes appear to be part of a feedback regulation on their own expression. Again, this appears to be more pronounced in 5-week-old plants than in 3-week-old plants. Taken together, JA has short- and long-term effects on the expression of all three genes. The effects are different and more pronounced in 5-week-old plants, but REV and TIFY8 proteins appear to be involved in the response of all three genes to JA in a complex and developmentally dependent manner.

2.6. Is the JA Influence on REV Function Mediated by Interaction with Other Proteins of the TIFY Family?

It has become clear that TIFY8 interacts directly with REV and has a repressing function on REV. However, TIFY8 has no Jas domain and is not able to sense JA-Ile directly. Therefore, the question as to how the enhancement of the REV function by JA is mediated is still open. Thus, we evaluated whether REV can also interact with other members of the TIFY family. We first tested the two class II TIFY PEAPOD proteins, as TIFY8 can interact with these two proteins but not with all other JAZ proteins [23]. Moreover, the PEAPOD proteins are involved in the early stages of leaf development in the formation of flat leaves in Arabidopsis [31], which would fit very well with the REV function in early leaf development. Therefore, we analyzed the two PEAPOD proteins in the yeast two-hybrid system, and both were able to interact not only with TIFY8 but also with REV (Figures 8 and S10).

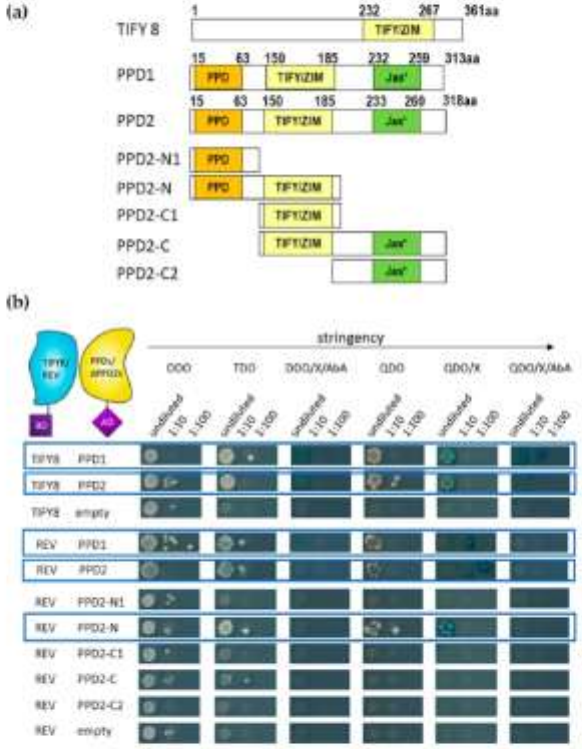

Figure 8. Yeast two-hybrid interactions between PEAPODs, PPD2-truncated proteins, TIFY8, and REV. (**a**) Scheme of the PPD1, PPD2, TIFY8, and truncated PPD2 versions used in the yeast two-hybrid assay. The orange box represents the PEAPOD domain (PPD), the yellow box represents the TIFY/ZIM domain, and the green box represents the Jas-like domain (Jas*). PPD2 full length (1 to 318aa), PPD2-N1 (1 to 117aa), PPD2-N (1 to 204aa), PPD2-C1 (117 to 204aa), PPD2-C (117-316aa), and PPD2-C2 (205 to 316aa). (**b**) Representative yeast two-hybrid assay between GAL4-BD-TIFY8 or GAL4-REV and PPDs, as well as a series of truncated versions of the PPD2 protein shown in (**a**) fused with GAL4-AD. A serial 1:10 dilution of each transformed yeast was spotted onto control (DDO) and different protein-protein interaction selective media with increasing stringency. Blue boxes indicate interactions.

For PPD2, we could also show with truncated versions that the TIFY/ZIM domain is necessary but not sufficient to mediate the association with REV. In this case, the N-terminal region with the PPD domain appears to be involved in addition to the TIFY/ZIM domain (Figures 8 and S10).

In addition to the PEAPOD proteins, the JAZ proteins were tested for interaction with REV in the yeast two-hybrid system. REV was also able to interact with many other JAZ proteins, namely JAZ1, 2, 4, 5, 9, and 10, but not or almost not with JAZ3, 6, 7, 8, and 12 (Figures 9 and S11), clearly indicating that REV appears to be controlled by JAZ proteins and JA signaling. However, how this selective interaction is mediated and whether this interaction is of biological relevance will be the subjects of further investigations.

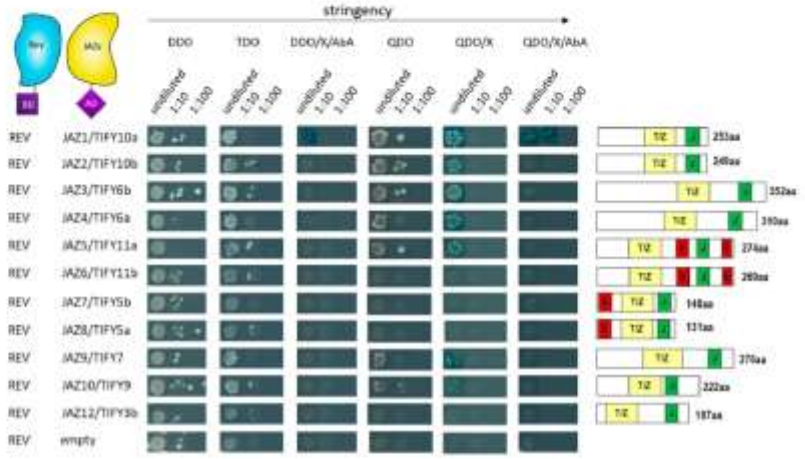

Figure 9. *Yeast two-hybrid interactions between REV and JAZ proteins.* Representative yeast two-hybrid assay between Gal4-BD-REV and GAL4-AD-JAZ fusion proteins. A serial 1:10 dilution of each transformed yeast was spotted onto control (DDO) and different protein–protein interaction-selective media with increasing stringency. Blue boxes indicate interactions. Protein domains of the different JAZ proteins are indicated on the right. The yellow box represents the TIFY/ZIM domain. The green box represents the Jas domain. The red box indicates the repressing EAR domain.

3. Discussion

Under optimal and stress-free conditions, leaf senescence is governed by the age of the leaves and the whole plant [32]. It has developed to allow efficient usage of the resources of the plant for growth, as well as for storage for the sake of the next generation via a well-organized recycling program to remobilize carbon, nitrogen, and mineral resources out of the senescing tissue into the developing parts of the plant, such as new leaves or fruits and seeds. However, long-lasting unfavorable stress conditions, such as drought, salinity, and nutrient deficiency, lead to premature senescence as an exit strategy. This ensures the production of offspring even under such a barren environment. Premature senescence is often combined with a tradeoff in seed number and quality [33]. To integrate all kinds of stress responses into this developmental process, highly complex gene regulatory networks have to be in place [7]. Approximately one fourth of all Arabidopsis genes are differentially regulated during the onset and progression of senescence [30,32]. Detailed transcript profiling over 22 time points of a defined leaf of *Arabidopsis thaliana* during onset and progression of leaf senescence enabled researchers to build a distinct chronology of events [30]. Genes related to the regulation of intracellular ROS levels as well as genes involved in abscisic acid (ABA) and JA production and signaling are among the early induced transcripts, indicating that ROS, ABA, and JA are important early signals in leaf senescence. This fact is in agreement with a relatively early increase in JA levels in Leaf

No. 7 in Arabidopsis rosettes shown by Breeze and colleagues [30], which was confirmed here in our studies (Figure 6). Likewise, an increase in intracellular hydrogen peroxide contents during the onset of monocarpic senescence has been described [34,35].

This massive reprogramming of the transcriptome implies a central function for transcription factors. Almost all transcription factor families in plants are involved in senescence regulation processes; however, the families of WRKY and NAC factors, which largely expanded in the plant kingdom, are overrepresented in the senescence transcriptome of Arabidopsis [36]. In contrast to systems biology approaches, we tried to understand these complex interactions starting from one of the regulatory hub proteins, namely WRKY53. Expression, activity, and degradation of the WRKY53 protein are tightly controlled, involving many feedback loops and double bottoms [7]. Moreover, a "leaf developmental memory" that links early developmental processes to leaf senescence appears to exist [4,7,37], and by this mechanism, if early development is somehow disturbed, senescence is delayed. The transcription factor REV appears to be part of this memory, as REV is involved in early developmental processes, such as the establishment of leaf polarity, lateral meristem initiation, or vascular development, but also directly regulates the expression of *WRKY53* during leaf senescence [4]. However, a function of WRKY53 in early development has not yet been described, indicating that the interaction of REV with the promoter of *WRKY53* appears to be dependent on the developmental stage. The preferential binding of REV to different *cis*-elements in the *WRKY53* promoter [4] points to the involvement of an additional factor driving this selectivity. Here, we could characterize the non-canonical TIFY protein TIFY8 as a possible regulator. TIFY8 can interact with REV in yeast cells and in planta (Figures 1 and 2) and can block the inducing function of REV on the promoter of *WRKY53* (Figure 3). This is consistent with the function described for TIFY8 as a repressor of transcription via the interaction with NINJA and/or KIX8/9 function as adapters for TOPLESS, which mediates transcriptional repression [14,22]. Moreover, *TIFY8* is more highly expressed in leaves during early developmental stages before the onset of senescence, when REV induction of *WRKY53* expression should still be inhibited. In contrast, *REV* and *WRKY53* expression increase during the onset of senescence, whereas *TIFY8* expression is lowered again (Figure 4). If this is the case and TIFY8 is involved in REV repression as described, a loss of TIFY8 function would lead to early activation of REV function and, thereby, to accelerated senescence. This is exactly what could be observed in the T-DNA insertion lines, as well as in the CRISPR/Cas lines of *TIFY8*. Here, we clearly observed an accelerated loss of photosynthetic activity and chlorophyll content, an early expression of *SAG*s (Figures 5, S4 and S5), and an earlier deterioration of the plasma membrane documented by higher ion leakage and higher lipid peroxidation rate (Figures 5 and S7) in the loss-of-function mutant lines compared to wildtype plants or *rev5* mutants. In contrast, the *TIFY8*-OE line phenocopied the *rev5* mutant in all these aspects (Figures 5, S6 and S7). Therefore, we concluded that TIFY8 has a role as a negative regulator of senescence, most likely through the inhibition of REV, which can activate direct senescence-associated target genes such as *WRKY53*.

We have identified the TIFY/ZIM domain of TIFY8 to be involved in the interaction with REV. However, in planta, the TIFY/ZIM domain is not sufficient for the contact, but additional regions in the C-terminal part of the protein are required (Figures 1 and 2). Moreover, REV does not interact exclusively with TIFY8 of the TIFY family. The two PEAPOD proteins, PPD1 and PPD2, can also interact with REV, but in this case, the N-terminal PPD domain is required in addition to the TIFY/ZIM domain. Moreover, several but not all JAZ proteins are also able to interact with REV in yeast, indicating a certain selectivity that might be mediated by the additional regions, as the TIFY/ZIM domain is highly conserved between the TIFY proteins (Figure S12). The interactions with the JAZ proteins could explain why in the reporter assay with the P_{WRKY53}:*GUS* construct, activation by REV was increased after JA treatment. JAZ proteins are degraded upon JA-Ile perception via SCF^{COI1} and the 26S proteasome [14]. TIFY8 and PEAPOD proteins are also able to interact with each other (Figure 8), whereas all other JAZ proteins

were not able to interact with Arabidopsis TIFY8 [23], demonstrating clear differences between the PEAPOD and the JAZ proteins. JAZ proteins have been shown to recognize MYC transcription factors; this process occurs most likely via a conserved linear motif SL●●FL●●●R. However, PEAPOD proteins which lack this motif do not recognize MYC protein unless this motif is implemented into the proteins by mutagenesis [38]. MYC2-5 redundantly regulates JA-induced leaf senescence under the control of JAZ proteins [39]. So far, there are no indications that PEAPOD proteins regulate senescence, but they are involved in early leaf development in Arabidopsis to form a flat leaf [31]. Accordingly, PEAPODs could be involved in early developmental processes directed by REV, and TIFY8 could be involved in late developmental processes directed by REV. However, we still need to analyze the impact of PEAPOD proteins on REV function and senescence in more detail in the future.

The JA effect on the *REV*, *TIFY8,* and *WRKY53* expression appears to be complex and development-dependent. Short- and long-term effects can be different at different developmental stages (Figure 7). However, JA appears to have the highest effects on *REV* expression in 5-week-old plants. Here, JA could induce high *REV* expression after 96 h so that a long-term increase in JA, as it is observed during early senescence (Figure 6), could contribute to the increased expression of *REV*, as *REV* mRNA and JA levels increase in parallel. In the *tify8* mutants, as well as in the *rev5* mutant, differences in expression of *REV* and its direct target gene *TIFY8* could be observed, indicating that complex cross- and feedback regulation occur but with milder effects. However, JA levels appear to be not significantly different in all tested lines, indicating that there is no influence of TIFY8 or REV on the JA biosynthesis. Vice versa, an influence of JA on the REV activity was observed (Figure 3) which is most likely mediated by either the PEAPOD and/or the JAZ interactions with REV. In conclusion, a JA-independent regulation of REV via TIFY8 and a JA-dependent regulation of REV via PEAPOD and JAZ proteins appear to exist, and these regulation mechanisms might act in concert and/or in different developmental stages. A simplified model of this complex interplay is presented in Figure 10. Here, we speculated that the interaction between PPDs or JAZs with REV also inhibits the function of REV as an activator; however, the impacts of PPD and JAZ proteins on early and late developmental functions of REV will be the subject of future investigations. In addition, the genetic background of the JA-insensitive mutants *jar1* and *coi1* will be used to characterize the role of JA signaling in more detail.

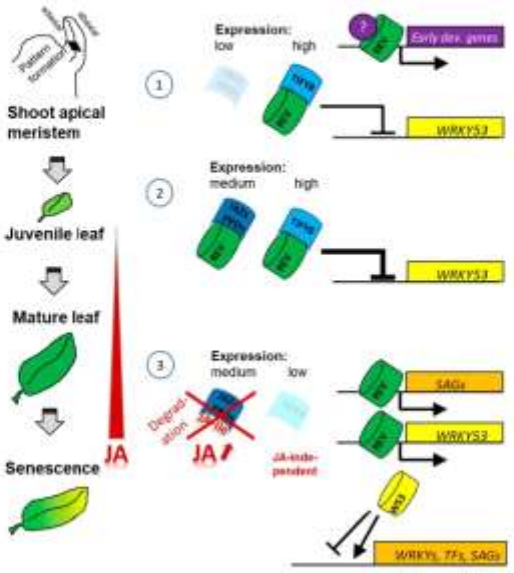

Figure 10. Model of the development-specific regulatory effects of TIFY8, PPDs, and JAZs on REV. (**1**) TIFY8, which is highly expressed during early development, blocks *WRKY53* expression by its interaction with REV. How REV activates other early developmental genes is still unclear and needs most likely additional factors or modifications. In this stage, *JAZ* as well as *PPD* expression is low. (**2**) In juvenile leaves, *JAZs* and *PPDs* are expressed, but JA levels are still low; therefore, even enhanced repression of *WRKY53* is achieved by the additional complex formation of JAZs/PPDs with REV. (**3**) At the transition from maturation to senescence, JA levels increase, and JA-Ile mark the JAZs and PPDs for degradation via the 26S proteasome through the interaction with the F-box protein COI1. However, TIFY8 has no Jas domain and cannot be marked for degradation by JA. Instead, expression of the *TIFY8* gene is strongly reduced. Both the JA-dependent and the JA-independent pathways lead to an activation of gene expression of REV target genes, including *WRKY53*, which then activates other *WRKY*s, other *TF*s, and additional *SAG*s. TF: transcription factors; SAGs: senescence-associated genes.

4. Materials and Methods

4.1. Yeast Two-Hybrid Assays

The TIFY8, PEAPOD, and JAZ yeast constructs used were described before in [22,23]. The yeast strain Y2H Gold (mating type a; Clontech; Takara Bio Europe SAS, Saint-Germain-en-Laye, France) was transformed with the bait expressed from the pGBKT7 vector containing the GAL4 DNA-binding domain and the *TRP1* marker gene. The yeast strain Y187 (mating type α; Clontech) was transformed, with the preys expressed from the pGADT7 vector containing the GAL4 activation domain and the *LEU2* marker gene. Yeast transformation was performed using a lithium acetate (LiAc)-based transformation. Empty yeast strains were grown overnight at 30 °C and 180 rpm in 1× Yeast Peptone Dextrose Adenine (YPDA) media, (2% (*w*/*v*) Bacto peptone; 1% (*w*/*v*) Bacto yeast extract; 0.003% (*w*/*v*) adenine hemisulfate; 2% (*w*/*v*) glucose pH 2.5). The overnight cultures were diluted to a concentration of OD546 0.2–0.4 with 1× YPDA and regrown at 30 °C to a final concentration of OD_{546} 0.6–0.8. Cultures were centrifuged for 5 min at 2.500 g, and pellets were resuspended in 2.5 mL sterile water, respectively. 100 µL resuspended yeast cells were added to a polyethylene glycol (PEG)/LiAc mastermix (240 µL 50% PEG, 36 µL 1M LiAc 2xH2O, 2 µL carrier DNA (Clontech)) and 250–600 ng of the appropriate plasmids. Samples were mixed and incubated at 42 °C for 45 min. After the incubation, yeast cells were collected by centrifugation (5 min at 700 g), and pellets were resuspended in 100 µL

0.9% (w/v) NaCl. Cells were then plated on the appropriate synthetic defined (SD) dropout media to select for transformants, including SD-Trp media (0.67% (w/v) yeast nitrogen base without amino acids; 0.074% (w/v)—Trp DO supplement; 2% (w/v) Bacto agar; 2% (w/v) glucose, pH 5.8) and SD-Leu media (0.67% (w/v) yeast nitrogen base without amino acids; 0.069% (w/v)—Leu DO supplement; 2% (w/v) Bacto agar; 2% (w/v) glucose, pH 5.8). After three days of growth at 30 °C, one colony from each transformation was picked, streaked on a fresh plate (SD-Trp/SD-Leu), and incubated for two more days at 30 °C. The two-hybrid assay was performed by mating the transformed yeast strains, as described in the Matchmaker® Gold Yeast Two-Hybrid System User Manual (Clontech). A serial 1:10 dilution of the yeast cells was spotted onto the control DDO media (0.67% (w/v) yeast nitrogen base without amino acids; 0.064% (w/v)—Leu-Trp DO supplement; 2% (w/v) Bacto agar; 2% (w/v) glucose, pH 5.8) and interaction-selective media, including TDO (0.67% (w/v) yeast nitrogen base without amino acids; 0.069% (w/v)—Leu-Trp-His DO supplement; 2% (w/v) Bacto agar; 2% (w/v) glucose, pH 5.8), DDO/X/AbA (0.67% (w/v) yeast nitrogen base without amino acids; 0.064% (w/v)—Leu-Trp DO supplement; 2% (w/v) Bacto agar; 2% (w/v) glucose, pH 5.8; 0.004 (w/v) X-α-Gal; 0.0002% (w/v) Aureobasidin A), QDO (0.67% (w/v) yeast nitrogen base without amino acids; 0.060% (w/v)—Leu-Trp-His-Ade DO supplement; 2% (w/v) Bacto agar; 2% (w/v) glucose, pH 5.8), QDO/X (0.67% (w/v) yeast nitrogen base without amino acids; 0.060% (w/v)—Leu-Trp-His-Ade DO supplement; 2% (w/v) Bacto agar; 2% (w/v) glucose, pH 5.8; 0.004% (w/v) X-α-Gal) and QDO/X/AbA (0.67% (w/v) yeast nitrogen base without amino acids; 0.060% (w/v)—Leu-Trp-His-Ade DO supplement; 2% (w/v) Bacto agar; 2% (w/v) glucose, pH 5.8; 0.004% (w/v) X-α-Gal; 0.0002% (w/v) Aureobasidin A). An overview of the used media is listed in Table 1. Yeast growth was monitored after four to five days at 30 °C, and plates were scanned using an Epson Perfection V700 Photo Scanner (Epson Europe B.V., Amsterdam, The Netherlands).

Table 1. Media used for the yeast two-hybrid assay.

Function	Name	Description
vector selection	Double dropout (DDO)	SD/-Trp/-Leu
interaction	Triple dropout (TDO)	SD/-Trp/-Leu/-His
	Quadruple dropout (QDO)	SD/-Trp/-Leu/-His/-Ade
	QDO/X	SD/-Trp/-Leu/-His/-Ade supplemented with X-α-Gal (X)
	QDO/X/AbA	SD/-Trp/-Leu/-His/-Ade supplemented with X-α-Gal (X) and Aureobasidin A (AbA)

4.2. Protein Extraction from Yeast Cells and Western Blot Analysis

To confirm protein expression, yeast cells grown on DDO plates were inoculated into 4.5 mL DDO medium and grown overnight at 30 °C while being shaken (180 rpm). For protein extraction, overnight cultures were centrifuged (5 min at 13,000 rpm), and pellets were resuspended in 100 µL deionized water, respectively. An amount of 100 µL 0.2 M NaOH was added, and samples were incubated for 5 min at room temperature (RT). Samples were centrifuged (5 min at 13,000 rpm), and pellets were resuspended in 30 µL sodium dodecyl sulfate (SDS) sample buffer (0.06 M Tris-HCl pH 6.8; 5% (v/v) glycerol; 2% (w/v) SDS). Protein concentration was determined using Bradford Roti-Quant (Roth) according to the manufacturer's protocol. In total, 20 µg total protein of each sample was diluted with 3× Laemmli buffer (3.4% (w/v) SDS; 62.5 mM Tris pH 6.8; 10% (v/v) glycerol; 0.075% (w/v) bromophenol blue; 5% (v/v) β-mercaptoethanol). Proteins were denatured by incubation at 95 °C for 5 min. Protein samples were separated on a 10–12% SDS-polyacrylamide gel electrophoresis (PAGE, 20V, 90 min); 1× SDS-running buffer was used (25 mM Tris, 200 mM glycine, 0.1% (w/v) SDS, pH 8.3). Proteins were transferred to a polyvinylidene difluoride (PVDF) membrane (Roth) using semi-dry transfer (Peqlab; 300 mA, 1 h). Membranes were blocked using 3% (w/v) milk powder (Sucofin) in 1× TBS-T

(25 mM Tris; 137 mM NaCl; 0.1% (*v*/*v*) Tween-20, pH 7.6) for 1 h at RT or overnight at 4 °C. After membranes were washed for 5 min with 1× TBS-T, membranes were incubated for 1 h with the primary antibodies in 1.5% (*w*/*v*) milk powder in 1× TBS-T. Antibodies against GAL4-BD and GAL4-AD, respectively, were used. After being washed three times with 1× TBS-T, membranes were incubated with the corresponding secondary antibody (goat anti-mouse horseradish peroxidase conjugates) followed by another round of washing. After applying luminol (Bio-Rad Laboratories Inc., Hercules, CA, USA) to the membranes, signals were detected using an Amersham Imager600 (GE Healthcare, Chicago, IL, USA). Images were processed with Adobe Photoshop CS5 (Adobe Inc., San José, CA, USA) for adjustment of brightness and contrast.

4.3. Protoplast Transformation

Protoplasts were prepared from a root cell culture of *Arabidopsis thaliana* ecotype Col-0 and transformed as described in [40]. Protoplasts were transiently transformed with different concentrations of the respective plasmid DNA; for details, also see https://uni-tuebingen.de/fakultaeten/mathematisch-naturwissenschaftliche-fakultaet/fachbereiche/zentren/zentrum-fuer-molekularbiologie-der-pflanzen/research/central-facilities/plant-transformation/.

4.4. MUSCLE Alignment of TIFY/ZIM Domains

Domain sequences of TIFY8 and PPD1 and 2, as well as those of the JAZ proteins, were taken from TAIR using the database HMMSMART. All sequences were aligned according to the multiple alignment tool MUSCLE using CLC Main Workbench 8.1.3 (QIAGEN, Aarhus, Denmark).

4.5. Bimolecular Fluorescence Complementation (BiFC), Cytometry, and Confocal Microscopy

Ratiometric BiFC assays were performed to study the homo- and heteromeric interaction of TIFY8 and REV as well as REV interaction with truncated versions of TIFY8 (see Figure 1). Therefore, a single vector which carries a red fluorescent protein (RFP) gene as the expression control as well as both candidate genes which were cloned simultaneously to the N- or the C-terminal part of the yellow fluorescent protein (YFP), respectively, was used. The expression of the fusion proteins is controlled by the 35S promoter in the pBiFCt-2in1-NN vector [41]. For protoplast transfection, 4 µg of the plasmid DNA was used to express the fusion proteins. If the proteins interact with each other, YFP fluorescence is restored by bringing the YFP-N and YFP-C parts together. Interactions were visualized 1 day after transfection by flow cytometry using CytoFLEX (Beckman Coulter, Brea, CA, USA). Both the internal mRFP and any reconstituted YFP were excited by the onboard 488nm laser. Peak emission was captured for YFP in FL1 (525/40 nm) and for RFP in FL3 (610/20 nm). All experiments were performed independently at least 4 times. To detect and localize the interaction in the cells, transfected tobacco leaves were analyzed using confocal microscopy (LSM880, Zeiss, Oberkochen, Germany). Therefore, *Nicotiana benthamiana* plants were cultivated and infiltrated with an *Agrobacteria tumefaciens* suspension, which contained the above-mentioned pBiFCt-2in1 constructs. In total, 500 mL of the bacteria overnight culture was inoculated into fresh LB media with the respective antibiotics and incubated for 4–6 h. This culture was centrifuged at 4000 rpm for 10 min. The pellet obtained was diluted in infiltration media (10 mM MgCl2; 0.5M MES; 100 mM Acetosyringone) to an OD600 of 0.5. Leaves of 4-week-old plants were infiltrated by manual injection with a 1-mL needleless syringe. Imaging was performed 2 days later. At least 3 leaves of different plants were analyzed under a Zeiss LSM 880 Airyscan confocal microscope by using the preset sequential scan settings for YFP (Ex: 514 nm, Em: 517–553 nm) and for RFP (Ex: 561 nm, Em: 597–625 nm). The experiment was performed independently 3 times.

4.6. β-Glucuronidase Reporter Assays

Arabidopsis protoplasts were transformed using 5 µg of effector (pJAN33) and 5 µg of the reporter (pBGWFS7) plasmid DNA. A luciferase construct (pBT8-35SLUCm3) was co-transfected as an internal transformation control. After incubation overnight at 20 °C in darkness, GUS activity assays were performed with the protoplasts, as described by [42]. The basal GUS level at 0min was subtracted from the values of the GUS activity after 2 h of incubation at 37 °C. To correct transformation efficiency, GUS activity was normalized to luciferase fluorescence. As effectors, we analyzed either REV and TIFY8 or a combination of both. Therefore, the coding sequences were cloned into pJAN33. As a reporter, a 2759-bp sequence upstream of the start codon of *WRKY53* was cloned into the binary vector pBGWFS7.0. The JA GUS assays were performed as described above, except that 40 µM JA or the same volume of water was added before overnight incubation.

4.7. Plant Cultivation and Plant Lines

Arabidopsis thaliana plants were grown on standard soil under short- or long-day conditions. Long-day conditions included 16 h of light; short-day conditions included 8 h of light with only moderate light intensity (60–100 µmol s^{-1} m^{-2}) in a climatic chamber at an ambient temperature of 20 °C. Individual leaf positions within the rosette were color-coded according to their age [27]. Plant material was harvested always at the same time of the day to avoid circadian effects. In all experiments, *A. thaliana* Ecotype Columbia-0 was used as wildtype control. The mutant lines used were as follows: *rev5* (EMS mutant; A260V), *tify8-1T* (GK_738B03), *tify8-2T* (SAIL_409_A07), *tify8-3* (CRISPR-CAS 2959-3-4-20/1), *tify8-4* (CRISPR-CAS 2960-21-7-33/3). For CRISPR/Cas9 constructs, design, cloning, genotyping, and selection of homozygous lines were as described [26]. In brief, we designed sgRNA69, sgRNA45, and sgRNA36 to target exon 3, 4, and 5, respectively. Spacers were cloned in pMR218 (sgRNA36) and pMR217 (sgRNA69 and sgRNA45) via a cut–ligation reaction of annealed oligonucleotides with BbsI (Table 2). Vectors were recombined using Gateway in pDE-Cas9 and transformed in Arabidopsis using floral dip. Plants were genotyped each generation using Sanger sequencing and TIDE (Table 2). Finally, two lines were obtained: *tify8-3* (2959-3-4-20/1, with −1;−1 at sgRNA36 and +1;+1 at sgRNA45) and *tify8-4* (2960-21-7-33/3, with −1;−1 at sgRNA36 and −1;−1 at sgRNA69) (Figure 5).

Table 2. Primers for CRISPR/Cas9.

Oligonucleotides uses for cloning spacers			
LAPAU*3124	ATTGCAAACCAGCCTCCACGCGG	Fw	sgRNA69
LAPAU3125	AAACCCGCGTGGAGGCTGGTTTG	Rv	sgRNA69
LAPAU3126	ATTGCTTGACCGCCATAGAAGA	Fw	sgRNA45
LAPAU3127	AAACTCTTCTATGGCGGTCAAG	Rv	sgRNA45
LAPAU3128	ATTGCCTTGGCAGGATCAAGCGG	Fw	sgRNA36
LAPAU3129	AAACCCGCTTGATCCTGCCAAGG	Rv	sgRNA36
Genotyping primers			
CROPGEN *68	TCACTTCACGACTCAGGAGC	Fw	Genotype sgRNA 69
CROPGEN69	CCATTATCACATCCGCCTGC	Rv	Genotype sgRNA 69
CROPGEN70	AACAGGGATGAAAGGTCCCG	Fw	Genotype sgRNA 45 or 36
CROPGEN71	AGACCTGATTACTCTACTCCACTCA	Rv	Genotype sgRNA 45 or 36

* LAPAU and CROPGEN are internal names and are not meaningful.

4.8. Phenotyping

To analyze onset and progression of senescence in different plant lines, we analyzed a variety of parameters once a week from week 4 to week 8. For this purpose, the corresponding color-coded leaves were used to analyze specific parameters as described in [27]. Before leaves were harvested, the number of leaves, the size of the stems, and the time point of bolting and flowering were determined. Leaf colors were quantified via the automated colorimetric assay (ACA). Electrolyte leakage was measured in leaf No. 4 using

a conductivity meter (CM100-2, Reid and Associates, Durban, South Africa). In leaf No. 5 and leaf No. 10, first the activity of the photosystem II (PSII) was assessed by Fv/Fm values using the Imaging-PAM chlorophyll fluorometer (Maxi version, v2-46i, Walz GmbH, Effeltrich, Germany), and subsequently, the chlorophyll was extracted. For qRT-PCR of senescence-associated marker genes, total RNA was extracted from leaves No. 6 and 7. Lipid peroxidation measurements were performed using leaf No. 9. All methods are described in detail in [27]. All phenotyping experiments were performed with a minimum of 6 biological replicates and were independently performed at least three times. All raw data of the phenotyping experiments except for ACA are provided in Table S1.

4.9. Gene Expression Analyses Using qRT-PCR

Total RNA was extracted with the GeneMATRIX Universal RNA Purification Kit (EURx). Subsequent cDNA synthesis was performed with RevertAid Reverse Transcriptase (Thermo Fisher Scientific Inc., Waltham, MA, USA) using oligo-dT primers. For the qRT-PCR, KAPA SYBR® Fast Bio Rad iCycler (Bio-Rad Laboratories Inc., Hercules, CA, USA) and Master Mix was used following the manufacturer´s protocol. For calculation, we used the ΔΔCT method according to [43], in which the expression of the analyzed genes was normalized to *ACTIN2* and set in % of *ACTIN2*. *ACTIN2* has been characterized as suitable reference gene for senescence [44] and is used in many studies that analyze gene expression during senescence, not only in Arabidopsis, but also in other plant species. A list of all primers used can be found in Table 3.

Table 3. Primers for qRT-PCR.

Gene Name	Accession Number	Primer Sequence (for/rev)
Phenotyping *ACTIN2*	At3g18780	ACCCGATGGGCAAGTCATCACG TCCCACAAACGAGGGCTGGA
SAG12	At5g45890	GCTTTGCCGGTTTCTGTTG GTTTCCCTTTCTTTATTTGTGTTG
SAG13	At2g29350	AGGGAGCATCGTGCTCATATCC CCAGCTGATTCATGGCTCCTTTG
Development and *ACTIN2*	MeJA treatment At3g18780	AAGCTCTCCTTTGTTGCTGTT GTTGTCTCGTGGATTCCAGCAGCTT
TIFY8	At4g32570	CCGACAGACAGAACAAGATAAGC AAGCAGAAGCCGTGGAAGG
REVOLUTA	At5g60690	TCAGCTTGTCTGCGAAAATG ACCCAATCAACAGCAGTTCC
WRKY53	At4g23810	CAGACGGGGATGCTACGG GGCGAGGCTAATGGTGGT
Splicing variants *TIFY8-SV1*	At4g32570	TGTATGAAGGAGGCAGCTCTAAG TCATGTGGCTTCTTTTTCAGGATC
TIFY8-SV2	At4g32570	TGTATGAAGGAGGCAGCTCTAAG TCAGTATTTGTAAGAAGCTAACCA

4.10. Jasmonic Acid Treatment

Three-week-old Col-0 plants and five-week-old Col-0 plants as well as rev5, tify8-1T, and tify8–4T mutants were sprayed with 100 µM MeJA in DMSO and 0.01% Silwet L-77 every 24 h for 96 h. The second set of plants was treated with the corresponding MOCK solution as a control. Three replicates of each line and time point (6 h, 24 h, and 96 h) were generated. For each replicate, leaves No. 4, 5, and 6 were pooled, and RNA was extracted for quantitative RT-PCR.

4.11. Jasmonic Acid Measurements

Four- to seven-week-old Col-0 plants, as well as *rev5*, *tify8-1T*, *tify8–4*, and *TIFY8-OE* plants, were used to determine the JA contents over the development of the different plant lines. For each line and time point, 4 replicates were analyzed. For each replicate,

always the same number of punches of the Leaves No. 5 to No. 9 were pooled, and 50 mg (±10%) of leaf material was then analyzed per sample. The frozen sample was retched (5 mm ceramic ball; 30 s) with intermittent cooling. The retched plant material was extracted with 200 µL 80% Methanol (MeOH), which contained 200 nm of D5 JA as a control. The obtained supernatant was transferred to a precooled fresh tube, and the obtained pellet was re-extracted with 200 µL of H_2O with 0.1% Formic Acid (FA, H_2CO_2). Then, this supernatant was combined with the previously transferred 80% MeOH fraction and thoroughly mixed. Both extraction processes included a 5 min ultra-sonic bath at RT, followed by a centrifugation step (5 min, 4 °C, 14,000 rpm). Subsequently, another centrifugation step (10 min. 4 °C, 14,000 rpm) with the combined supernatants was performed. For the analysis of the phytohormone JA, the final supernatant was used directly. An amount of 100 µL of the sample was pipetted into a vial and diluted with 100 µL of H_2O and 0.1% formic acid. The LCMS profiling analysis was performed using a Micro-LC M5 (Trap and Elute) and a QTRAP6500+ (Sciex) operated in MRM mode. For all MRMs (Ja (1) Q1/Q3 209.1/59, Ja (2) Q1/Q3 209.1/165.1, D5 Ja (1) Q1/Q3 214.1/62, D5 Ja (2) 214.1/170.1) a declustering potential of DP-40, a collision energy of CE-20, and a Dwell time of 5 ms were applied. Chromatographic separation was achieved on a Luna Omega Polar C18 column (3 µm; 100 Å; 150 × 0.5 mm; Phenomenex, Aschaffenburg, Germany) and a Luna C18(2) trap column (5 µm; 100 Å; 20 × 0.5 mm; Phenomenex) with a column temperature of 55 °C. The following binary gradient was applied for the main column at a flow rate of 28 µL min^{-1}: 0–0.2 min, isocratic 90% A; 0.2–2 min, linear from 90% A to 30% A; 2–4.5 min, linear from 30% A to 10% A; 4.5–5 min, linear from 10% A to 5% A; 5–5.3 min, isocratic 5% A; 5.3–5.5 min, linear from 5% A to 90% A; 5.5–6 min, isocratic 90% A (A: water, 0.1% aq. formic acid; B: acetonitrile, 0.1% aq. formic acid). The samples were concentrated on the trap column using the following conditions: flow rate 50 µL min^{-1}: 0–1.5 min isocratic 95% A; 1.5 min start main gradient; 1.5–1.7 min isocratic 95% A. The injection volume was 50 µL. Analytes were ionized using an Optiflow Turbo V ion source equipped with a SteadySpray T micro electrode (10–50 µL min^{-1}) in negative (ion spray voltage: −4500 V) ion mode. The following additional instrument settings were applied: nebulizer and heater gas, nitrogen, 25 and 45 psi; curtain gas, nitrogen, 30 psi; collision gas, nitrogen, medium; source temperature, 200 °C; entrance potential, ±10 V; collision cell exit potential, ±25V. The JA content in a sample was normalized against the D5 Ja values.

4.12. Statistical Analyses

All analyses were performed using IBM SPSS Statistics Software (IBM Corp. Released 2021. IBM SPSS Statistics for Windows, Version 28.0. Armonk, NY, USA: IBM Corp.). Comparisons of mean trait values between the different lines were performed using a one-way between-subjects ANOVA. The one-way ANOVA is the simplest case of ANOVA test and is used to compare the mean of multiple groups. If the average variation between groups is large enough compared to the average variation within groups, then it can be concluded that at least one group mean is not equal to the others. A p-value of $p \leq 0.05$ was used in all analyses.

Supplementary Materials: The following supporting information can be downloaded at: https://www.mdpi.com/article/10.3390/ijms24043079/s1.

Author Contributions: Conceptualization, U.Z. and J.B.; methodology, A.G.A.G., J.D., S.C.S. and J.B.; validation, A.G.A.G., J.D., S.C.S. and M.W.; formal analysis, A.G.A.G., J.D. and S.C.S.; investigation, A.G.A.G., J.D., S.C.S., M.W., E.v.R.-L. and J.B.; CRISPR-Cas9 lines and resources, L.P. and A.G.; writing—original draft preparation, U.Z.; writing—review and editing, all authors.; visualization, A.G.A.G., J.D., S.C.S. and U.Z.; supervision, U.Z., J.B. and J.D.; project administration, U.Z.; funding acquisition, U.Z. All authors have read and agreed to the published version of the manuscript.

Funding: This work was funded by the Deutsche Forschungsgemeinschaft (DFG) CRC 1101 (B06). J.B. was supported by the Alexander von Humboldt foundation. L.P. was supported by a postdoctoral fellowship by FWO (3E001810). Metabolite analytics as well as laser scanning microcopy were funded

by the Deutsche Forschungsgemeinschaft (DFG, German Research foundation) by grants for scientific equipment, Project No. 442641014 and -INST 37/965-1 FUGG.

Institutional Review Board Statement: Not applicable.

Informed Consent Statement: Not applicable.

Data Availability Statement: Not applicable.

Acknowledgments: We thank Stephan Wenkel from the University of Copenhagen for providing *REVd* constructs and *rev5* seeds and Natalie Faiss and Els Van Lerberge for excellent technical assistance. We acknowledge support by Open Access Publishing Fund of University of Tübingen.

Conflicts of Interest: The authors declare no conflict of interest.

References

1. Talbert, P.B.; Adler, H.T.; Parks, D.W.; Comai, L. The REVOLUTA gene is necessary for apical meristem development and for limiting cell divisions in the leaves and stems of *Arabidopsis thaliana*. *Development* **1995**, *121*, 2723–2735. [CrossRef] [PubMed]
2. Otsuga, D.; DeGuzman, B.; Prigge, M.J.; Drews, G.N.; Clark, S.E. REVOLUTA regulates meristem initiation at lateral positions. *Plant J. Cell Mol. Biol.* **2001**, *25*, 223–236. [CrossRef]
3. Emery, J.F.; Floyd, S.K.; Alvarez, J.; Eshed, Y.; Hawker, N.P.; Izhaki, A.; Baum, S.F.; Bowman, J.L. Radial Patterning of Arabidopsis Shoots by Class III HD-ZIP and KANADI Genes. *Curr. Biol.* **2003**, *13*, 1768–1774. [CrossRef] [PubMed]
4. Xie, Y.; Huhn, K.; Brandt, R.; Potschin, M.; Bieker, S.; Straub, D.; Doll, J.; Drechsler, T.; Zentgraf, U.; Wenkel, S. REVOLUTA and WRKY53 connect early and late leaf development in Arabidopsis. *Development* **2014**, *141*, 4772–4783. [CrossRef] [PubMed]
5. Hong, S.Y.; Botterweg-Paredes, E.; Doll, J.; Eguen, T.; Blaakmeer, A.; Matton, S.; Xie, Y.; Skjøth Lunding, B.; Zentgraf, U.; Guan, C.; et al. Multi-level analysis of the interactions between REVOLUTA and MORE AXILLARY BRANCHES 2 in controlling plant development reveals parallel, independent and antagonistic functions. *Development* **2020**, *14*, dev183681. [CrossRef]
6. Bresson, J.; Doll, J.; Vasseur, F.; Stahl, M.; von Roepenack-Lahaye, E.; Kilian, J.; Stadelhofer, B.; Kremer, J.M.; Kolb, D.; Wenkel, S.; et al. The genetic interaction of *REVOLUTA* and *WRKY53* links plant development, senescence, and immune responses. *PLoS ONE* **2022**, *17*, e0254741. [CrossRef] [PubMed]
7. Zentgraf, U.; Doll, J. *Arabidopsis* WRKY53, a Node of Multi-Layer Regulation in the Network of Senescence. *Plants* **2019**, *8*, 578. [CrossRef]
8. Brandt, R.; Salla-Martret, M.; Bou-Torrent, J.; Musielak, T.; Stahl, M.; Lanz, C.; Ott, F.; Schmid, M.; Greb, T.; Schwarz, M.; et al. Genome-wide binding-site analysis of REVOLUTA reveals a link between leaf patterning and light-mediated growth responses. *Plant J.* **2012**, *72*, 31–42. [CrossRef]
9. Juarez, M.T.; Kui, J.S.; Thomas, J.; Heller, B.A.; Timmermans, M.C.P. microRNA-mediated repression of rolled leaf1 specifies maize leaf polarity. *Nature* **2004**, *428*, 84–88. [CrossRef]
10. Wenkel, S.; Emery, J.; Hou, B.H.; Evans, M.M.; Barton, M.K. A feedback regulatory module formed by LITTLE ZIPPER and HD-ZIPIII genes. *Plant Cell* **2007**, *19*, 3379–3390. [CrossRef]
11. Magnani, E.; Barton, M.K. A per-ARNT-sim-like sensor domain uniquely regulates the activity of the homeodomain leucine zipper transcription factor REVOLUTA in Arabidopsis. *Plant Cell* **2011**, *23*, 567–582. [CrossRef]
12. Möglich, A.; Ayers, R.A.; Moffat, K. Structure and signaling mechanism of Per-ARNT-Sim domains. *Structure* **2009**, *17*, 1282–1294. [CrossRef]
13. Reinhart, B.J.; Liu, T.; Newell, N.R.; Magnani, E.; Huang, T.; Kerstetter, R.; Michaels, S.; Barton, M.K. Establishing a framework for the Ad/abaxial regulatory network of Arabidopsis: Ascertaining targets of class III homeodomain leucine zipper and KANADI regulation. *Plant Cell* **2013**, *25*, 3228–3249. [CrossRef] [PubMed]
14. Pauwels, L.; Barbero, G.F.; Geerinck, J.; Tilleman, S.; Grunewald, W.; Pérez, A.C.; Chico, J.M.; Bossche, R.V.; Sewell, J.; Gil, E.; et al. NINJA connects the co-repressor TOPLESS to jasmonate signalling. *Nature* **2010**, *464*, 788–791. [CrossRef] [PubMed]
15. Shyu, C.; Figueroa, P.; DePew, C.L.; Cooke, T.F.; Sheard, L.B.; Moreno, J.E.; Katsir, L.; Zheng, N.; Browse, J.; Howe, G.A. JAZ8 lacks a canonical degron and has an EAR motif that mediates transcriptional repression of jasmonate responses in Arabidopsis. *Plant Cell* **2012**, *24*, 536–550. [CrossRef]
16. Causier, B.; Ashworth, M.; Guo, W.; Davies, B. The TOPLESS interactome: A framework for gene repression in Arabidopsis. *Plant Physiol.* **2012**, *158*, 423–438. [CrossRef] [PubMed]
17. Thines, B.; Katsir, L.; Melotto, M.; Niu, Y.; Mandaokar, A.; Liu, G.; Nomura, K.; He, S.Y.; Howe, G.A.; Browse, J. JAZ repressor proteins are targets of the SCF(COI1) complex during jasmonate signalling. *Nature* **2007**, *448*, 661–665. [CrossRef] [PubMed]
18. Xie, D.; Feys, B.; James, S.; Nieto-Rostro, M.; Turner, J. COI1: An Arabidopsis gene required for jasmonate-regulated defense and fertility. *Science* **1998**, *280*, 1091–1094. [CrossRef]
19. White, D.W.R. PEAPOD regulates lamina size and curvature in Arabidopsis. *Proc. Nat. Acad. Sci. USA* **2006**, *103*, 13238–13243. [CrossRef]
20. Wang, Z.; Li, N.; Jiang, S.; Gonzalez, N.; Huang, X.; Wang, Y.; Inzé, D.; Li, Y. SCF(SAP) controls organ size by targeting PPD proteins for degradation in Arabidopsis thaliana. *Nat. Commun.* **2016**, *7*, 11192. [CrossRef]

21. White, D.W.R. PEAPOD repressors modulate and coordinate developmental responses to light intensity in Arabidopsis. *New Phytol.* **2022**, *235*, 1470–1485. [CrossRef] [PubMed]
22. Gonzalez, N.; Pauwels, L.; Baekelandt, A.; De Milde, L.; Van Leene, J.; Besbrugge, N.; Heyndrickx, K.S.; Cuéllar Pérez, A.; Durand, A.N.; De Clercq, R.; et al. A Repressor Protein Complex Regulates Leaf Growth in Arabidopsis. *Plant Cell* **2015**, *27*, 2273–2287. [CrossRef] [PubMed]
23. Cuéllar Pérez, A.; Nagels Durand, A.; Vanden Bossche, R.; De Clercq, R.; Persiau, G.; Van Wees, S.C.; Pieterse, C.M.; Gevaert, K.; De Jaeger, G.; Goossens, A.; et al. The non-JAZ TIFY protein TIFY8 from Arabidopsis thaliana is a transcriptional repressor. *PLoS ONE* **2014**, *9*, e84891. [CrossRef]
24. Noir, S.; Bömer, M.; Takahashi, N.; Ishida, T.; Tsui, T.L.; Balbi, V.; Shanahan, H.; Sugimoto, K.; Devoto, A. Jasmonate controls leaf growth by repressing cell proliferation and the onset of endoreduplication while maintaining a potential stand-by mode. *Plant Physiol.* **2013**, *161*, 1930–1951. [CrossRef]
25. Chung, H.S.; Cooke, T.F.; Depew, C.L.; Patel, L.C.; Ogawa, N.; Kobayashi, Y.; Howe, G.A. Alternative splicing expands the repertoire of dominant JAZ repressors of jasmonate signaling. *Plant J.* **2010**, *63*, 613–622. [CrossRef] [PubMed]
26. Pauwels, L.; De Clercq, R.; Goossens, J.; Iñigo, S.; Williams, C.; Ron, M.; Britt, A.; Goossens, A. A Dual sgRNA Approach for Functional Genomics in *Arabidopsis thaliana*. *G3 Genes Genomes Genet.* **2018**, *8*, 2603–2615. [CrossRef]
27. Bresson, J.; Bieker, S.; Riester, L.; Doll, J.; Zentgraf, U. A guideline for leaf senescence analyses: From quantification to physiological and molecular investigations. *J. Exp. Bot.* **2018**, *69*, 769–786. [CrossRef]
28. He, Y.; Fukushige, H.; Hildebrand, D.F.; Gan, S. Evidence supporting a role of jasmonic acid in Arabidopsis leaf senescence. *Plant Physiol.* **2002**, *128*, 876–884. [CrossRef]
29. Huang, H.; Liu, B.; Liu, L.; Song, S. Jasmonate action in plant growth and development. *J. Exp. Bot.* **2017**, *68*, 1349–1359. [CrossRef]
30. Breeze, E.; Harrison, E.; McHattie, S.; Hughes, L.; Hickman, R.; Hill, C.; Kiddle, S.; Kim, Y.; Penfold, C.A.; Jenkins, D.; et al. High-resolution temporal profiling of transcripts during Arabidopsis leaf senescence reveals a distinct chronology of processes and regulation. *Plant Cell* **2011**, *23*, 873–894. [CrossRef]
31. Baekelandt, A.; Pauwels, L.; Wang, Z.; Li, N.; De Milde, L.; Natran, A.; Vermeersch, M.; Li, Y.; Goossens, A.; Inzé, D.; et al. Arabidopsis Leaf Flatness Is Regulated by PPD2 and NINJA through Repression of CYCLIN D3 Genes. *Plant Physiol.* **2018**, *178*, 217–232. [CrossRef] [PubMed]
32. Zentgraf, U.; Jobst, J.; Kolb, D.; Rentsch, D. Senescence-related gene expression profiles of rosette leaves of Arabidopsis thaliana: Leaf age versus plant age. *Plant Biol.* **2004**, *6*, 178–183. [CrossRef] [PubMed]
33. Sade, N.; Rubio-Wilhelmi, M.d.M.; Umnajkitikorn, K.; Blumwald, E. Stress-induced senescence and plant tolerance to abiotic stress. *J. Exp. Bot.* **2018**, *69*, 845–853. [CrossRef] [PubMed]
34. Zimmermann, P.; Heinlein, C.; Orendi, G.; Zentgraf, U. Senescence specific regulation of catalases in *Arabidopsis thaliana* (L.) Heynh. *Plant Cell Environ.* **2006**, *29*, 1049–1060. [CrossRef] [PubMed]
35. Bieker, S.; Riester, L.; Stahl, M.; Franzaring, J.; Zentgraf, U. Senescence-specific alteration of hydrogen peroxide levels in *Arabidopsis thaliana* and oilseed rape spring variety *Brassica napus* L. cv. Mozart. *J. Integr. Plant Biol.* **2012**, *54*, 540–554. [CrossRef] [PubMed]
36. Guo, Y.; Cai, Z.; Gan, S. Transcriptome of Arabidopsis leaf senescence. *Plant Cell Environ.* **2004**, *27*, 521–549. [CrossRef]
37. Kim, J.; Kim, J.H.; Lyu, J.I.; Woo, H.R.; Lim, P.O. New insights into the regulation of leaf senescence in Arabidopsis. *J. Exp. Bot.* **2018**, *69*, 787–799. [CrossRef]
38. Oña Chuquimarca, S.; Ayala-Ruano, S.; Goossens, J.; Pauwels, L.; Goossens, A.; Leon-Reyes, A.; Ángel Méndez, M. The Molecular Basis of JAZ-MYC Coupling, a Protein-Protein Interface Essential for Plant Response to Stressors. *Front. Plant Sci.* **2020**, *11*, 1139. [CrossRef]
39. Song, S.; Huang, H.; Wang, J.; Liu, B.; Qi, T.; Xie, D. MYC5 is Involved in Jasmonate-Regulated Plant Growth, Leaf Senescence and Defense Responses. *Plant Cell Physiol.* **2017**, *58*, 1752–1763. [CrossRef]
40. Mehlhorn, D.G.; Wallmerothm, N.; Berendzen, K.W.; Grefen, C. 2in1 vectors improve in planta BiFC and FRET analysis. *Methods Mol. Biol.* **2018**, *691*, 139–158. [CrossRef]
41. Jefferson, R.A.; Kavanagh, T.A.; Bevan, M.W. GUS fusions: Beta-glucuronidase as a sensitive and versatile gene fusion marker in higher plants. *EMBO J.* **1987**, *6*, 3901–3907. [CrossRef] [PubMed]
42. Grefen, C.; Blatt, M.R. A 2in1 cloning system enables ratiometric bimolecular fluorescence complementation (rBiFC). *Biotechniques* **2012**, *53*, 311–314. [CrossRef] [PubMed]
43. Pfaffl, M.W. A new mathematical model for relative quantification in real-time RT-PCR. *Nucleic Acids Res.* **2001**, *29*, e45. [CrossRef] [PubMed]
44. Panchuk, I.I.; Zentgraf, U.; Volkov, R.A. Expression of the Apx gene family during leaf senescence of Arabidopsis thaliana. *Planta* **2005**, *222*, 926–932. [CrossRef]

International Journal of
Molecular Sciences

MDPI

"The non-JAZ TIFY protein TIFY8 of *Arabidopsis thaliana* interacts with the HD-ZIP III transcription factor REVOLUTA and regulates leaf senescence."

Ana Gabriela Andrade Galan [1], Jasmin Doll [1], Svenja Corina Saile [1], Marieluise Wünsch [1], Edda von Roepenack-Lahaye [1], Laurens Pauwels [2,3], Alain Goossens [2,3], Justine Bresson [1] and Ulrike Zentgraf [1,*]

[1] Center for Plant Molecular Biology (ZMBP), University of Tübingen, Auf der Morgenstelle 32, 72076 Tübingen, Germany;

[2] Department of Plant Biotechnology and Bioinformatics, Ghent University, B-9052 Ghent, Belgium

[3] Center for Plant Systems Biology, VIB, B-9052 Ghent, Belgium

* Correspondence: ulrike.zentgraf@zmbp.uni-tuebingen.de

Supplemental Figures S1-S12

(a)

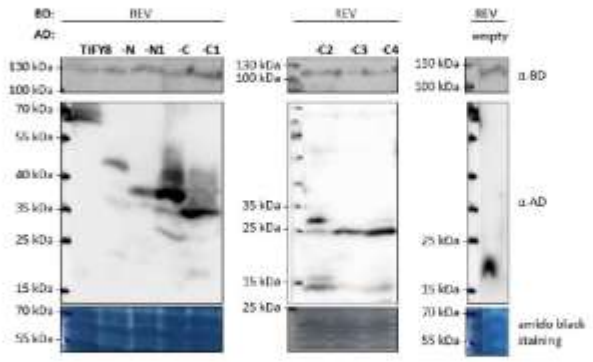

(b)

BD	AD	TDO	DDO/X/AbA	QDO	QDO/X	QDO/X/AbA	
REV	TIFY8	83%	17%	83%	0%	17%	100%
REV	TIFY8-N	20%	0%	20%	0%	0%	83%
REV	TIFY8-N1	0%	0%	0%	0%	0%	80%
REV	TIFY8-C	100%	20%	60%	100%	40%	60%
REV	TIFY8-C1	80%	20%	0%	0%	0%	40%
REV	TIFY8-C2	0%	0%	0%	0%	0%	25%
REV	TIFY8-C3	0%	0%	0%	0%	0%	20%
REV	TIFY8-C4	40%	20%	0%	0%	0%	17%
REV	empty	0%	0%	0%	0%	0%	0%

Figure S1: *Yeast two-hybrid protein expression in yeast cells and heat map of positive results in independent mating experiments.*
(a) Western blot analyzed with anti-BD and anti-AD antibodies (α) show expression of BD-REV and AD-TIFY8 fusion proteins in diploid yeast cells. Protein loading is indicated by a section of the Amido Black Staining (A.B.S) BD-REV: 114 kDa, AD TIFY8:62 kDa, AD-TIFY8-N: 48 kDa, AD-TIFY8-N1: 43 kDa, AD-TIFY8-C: 44 kDa, AD-TIFY8-C1: 38 kDa, AD-TIFY8-C2: 33 kDA, AD-TIFY8-C3: 30 kDa, AD-TIFY8-C4: 30 kDa, AD-empty: 22 kDa. **(b)** Heatmap of positive interaction results of 3 to 7 independent mating experiments in % positive results.

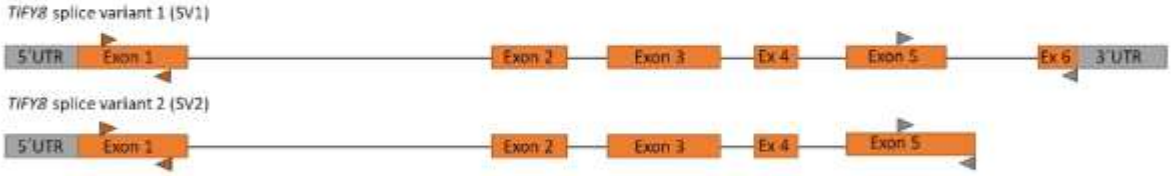

Figure S2: *Splicing variants of TIFY8.*
Two splicing variants of *TIFY8* differ in the 3'region in exon 5 and 6. Primer position used for qRT-PCR (orange) and splicing variant determination (grey) are indicated by the arrow heads).

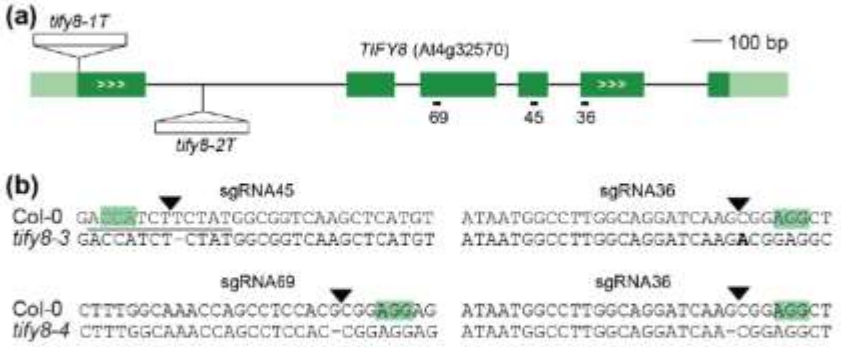

Figure S3: *Generation of tify8 CRISPR/Cas9 lines.*
(a) Genomic structure of Arabidopsis *TIFY8* and location of the T-DNA inserts and sgRNAs. Dark green boxes designate exons; light green boxes, UTRs; solid lines, introns; white arrows gene orientation. sgRNA numbers are arbitrary identifiers. Locations of the *tify8-1T* and *tify8-2T* T-DNA are indicated. **(b)** Genotypes of homozygous *tify8-3* and *tify8-4* mutants, generated by combining sgRNA45 and 3, or sgRNA69 and sgRNA36, respectively. The PAM is highlighted in green, the triangle points to the Cas9 cut site; -, deleted base, bold, inserted base. The sequence encoding the TIFY motif is underlined.

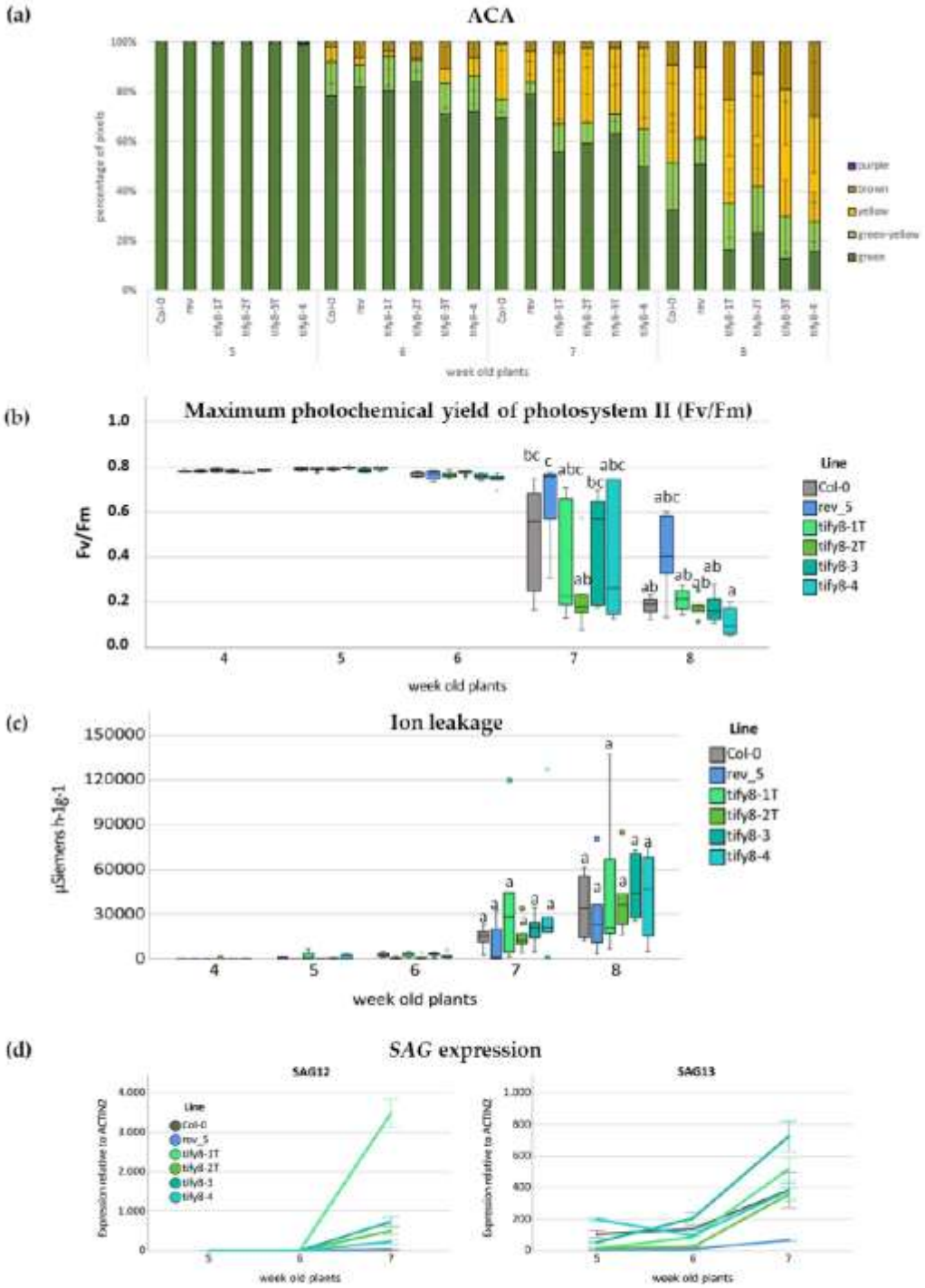

Figure S4: *Senescence parameters of all mutant lines.*
These parameters were analyzed for the senescence phenotyping of *tify8-1T*, *tify8-2T*, *tify8-3*, *tify8-4*, and *rev5* mutants compared to wildtype Col-0 plants. **(a)** Automated Colorimetric Assay (ACA) to categorize the color of individual leaves of at least six plants pixelwise into five groups: green, green-yellow, yellow, brown, and purple. The percentage of each group with respect to total pixel number of all leaves is presented (n=6). **(b)** Boxplot of Fv/Fm values measured with PAM for leaves No. 5 of 4- to 7-week-old plants (mean values ±SE, n=6-8). **(c)** Boxplot of the decrease in solute retention determined through ion leakage in Leaves No. 4 of 4- to 7-week-old plants (n=6-8). One-way ANOVA test was performed, (p≤0.05). **(d)** Gene Expression of the senescence-associated marker genes *SAG12* and *SAG13* were analyzed by qRT-PCR and normalized to the expression of the *ACTIN2* gene. The expression of both senescence-associated marker genes was analyzed in 5- to 7-week-old plants (mean values ± SD, n=3).

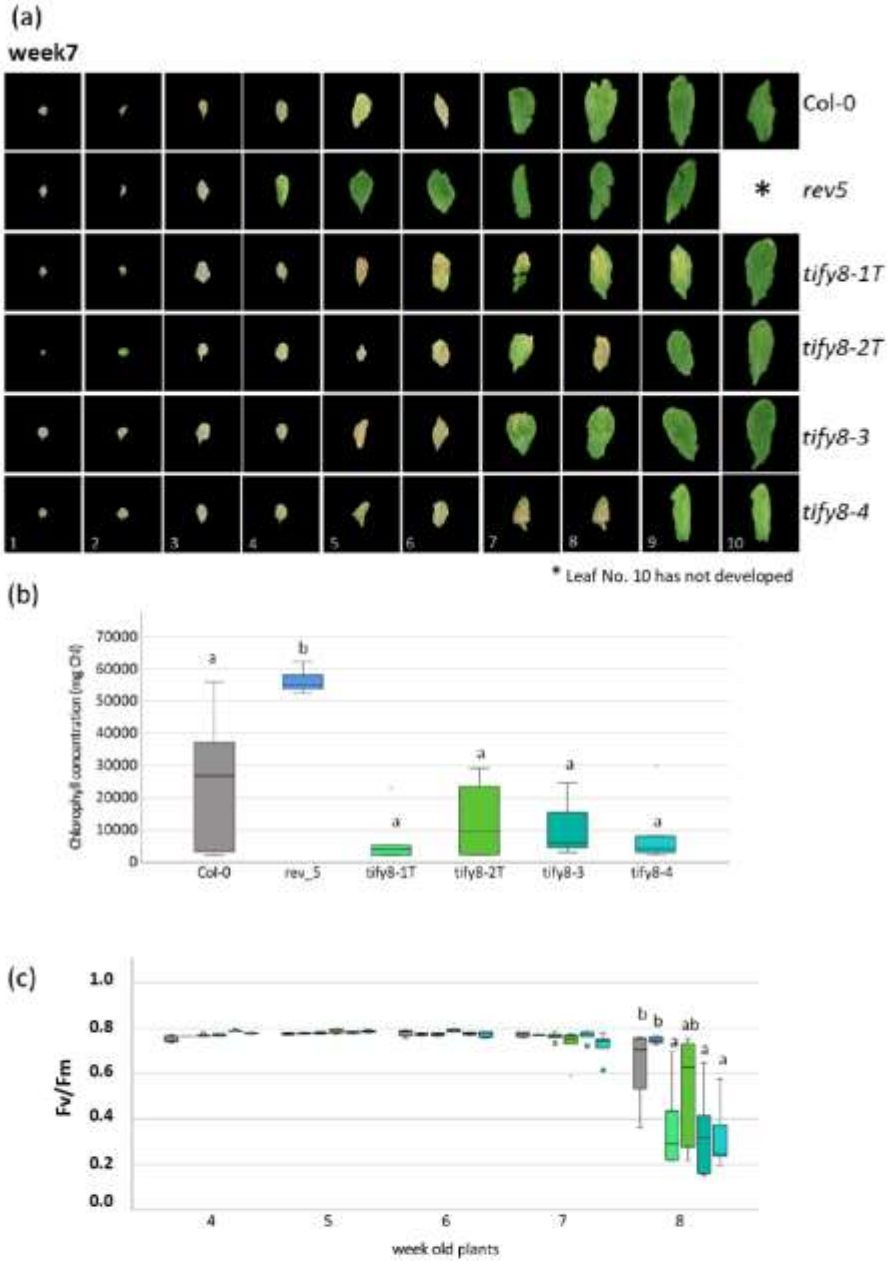

Figure S5: *Phenotypic and photosynthetic parameters.*
These parameters were analyzed for the senescence phenotyping of *tify8-1T, tify8-2T, tify8-3, tify8-4,* and *rev5* mutants compared to wildtype Col-0 plants. **(a)** Phenotypical appearance of leaves at positions 1 to 10 of 7-week-old plants. Boxplots of **(b)** the chlorophyll content per leaf determined for leaves No. 10 of 7-week-old plants (n=6) and **(c)** Fv/Fm values measured by PAM for the identical leaves (No. 10) of 4- to 7-week-old plants (n=6). One-way ANOVA test was performed, ($p \leq 0.05$).

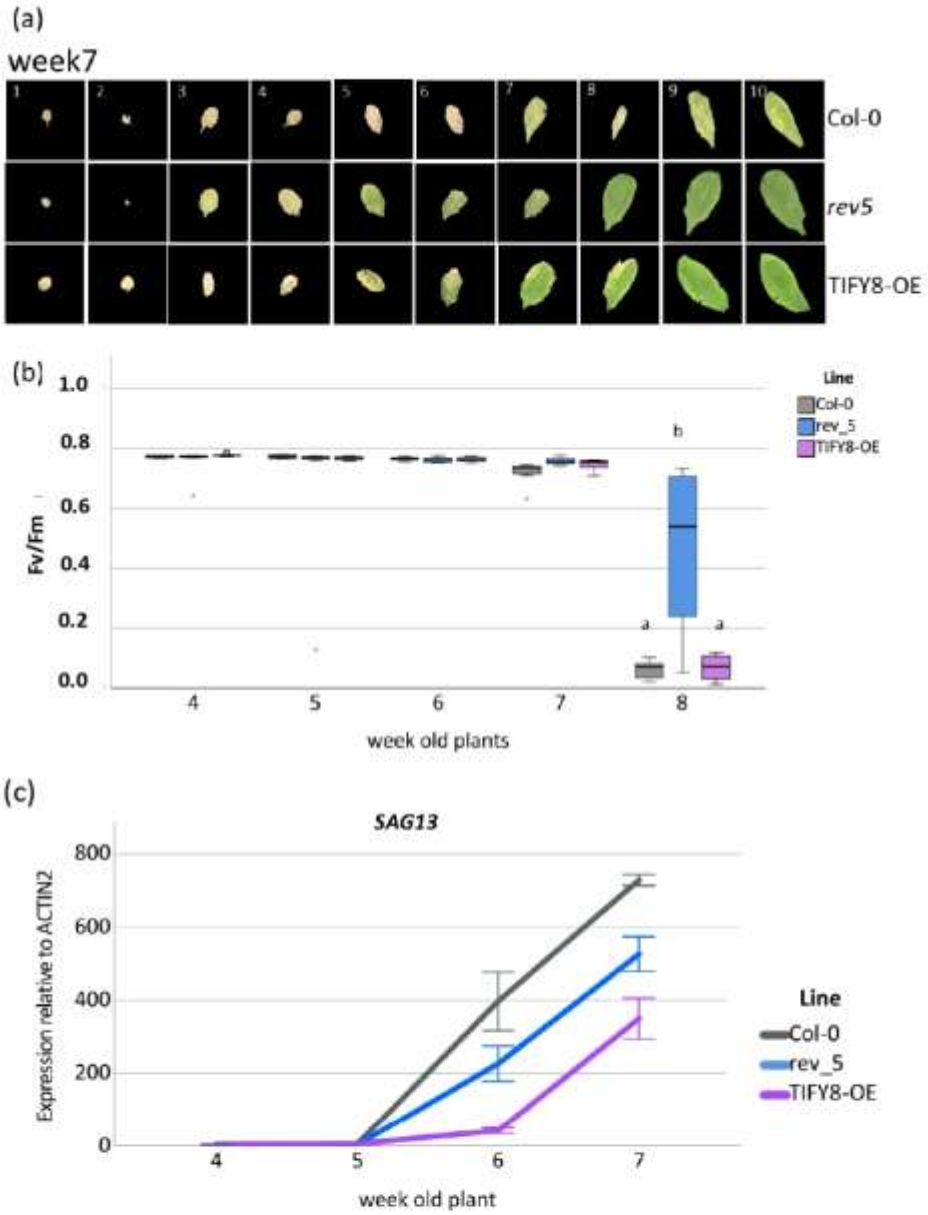

Figure S6: *Senescence parameters.*
These parameters were analyzed for the senescence phenotyping of *TIFY8*-OE and *rev5* mutants compared to wildtype Col-0 plants. **(a)** phenotypical appearance of leaves at positions 1 to 10 of 7-week-old plants, **(b)** Boxplot of Fv/Fm values measured with PAM for the leaves No. 10 of 4 to 7-week-old plants (n=8). One-way ANOVA test was performed, ($p \leq 0.05$). **(c)** Gene expression of the senescence-associated marker gene *SAG13* was analyzed by qRT-PCR and normalized to the expression of the *ACTIN2* gene. The expression was analyzed in 4- to 7-week-old plants in 2 pools of 4 leaves of 4 different plants (mean values ± SD).

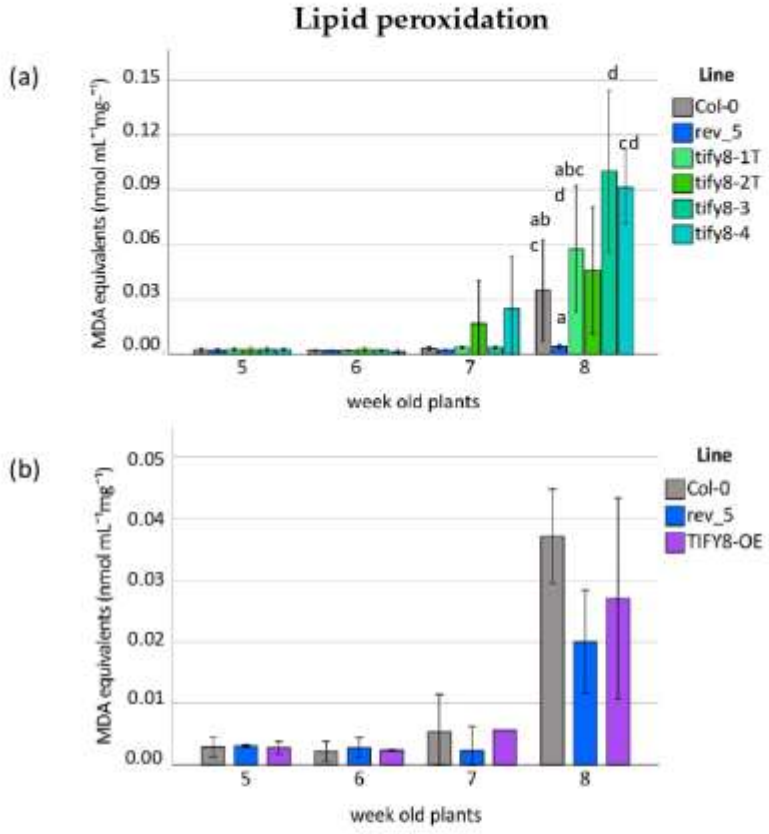

Figure S7: *Lipid peroxidation.*
Lipid peroxidation were determined by the quantification of the MDA concentration in leaves No. 9 of 5- to 7-week-old plants (a) *tify8-1T, tify8-2T, tify8-3, tify8-4*, and *rev5* mutants compared to wildtype Col-0 plants, mean ± SE, n=6 , One-way ANOVA test was performed, ($p \leq 0.05$) (b) *TIFY8*-OE and *rev5* mutants compared to wildtype Col-0 plants, mean ± SE, (2 pools of 3 leaves No. 9 of 3 different plants each)

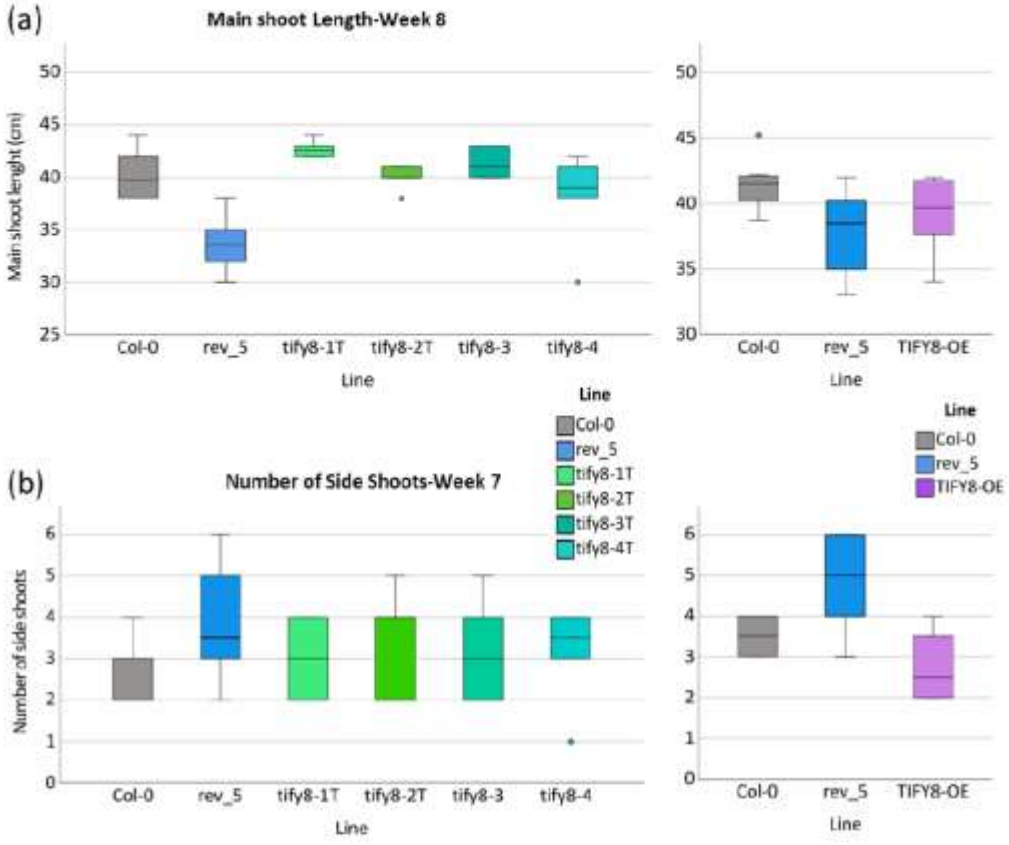

Figure S8: *Phenotypic appearance.*
Boxplots of **(a)** the length of the main shoot measured in 8-week-old plants in all *tify8* mutants as well as in the *TIFY8*-OE and the respective control Col-0 (n=6-8). **(b)** the number of side shoots determine in 7-week-old-plants in all the different lines previously mentioned (n=6-8)

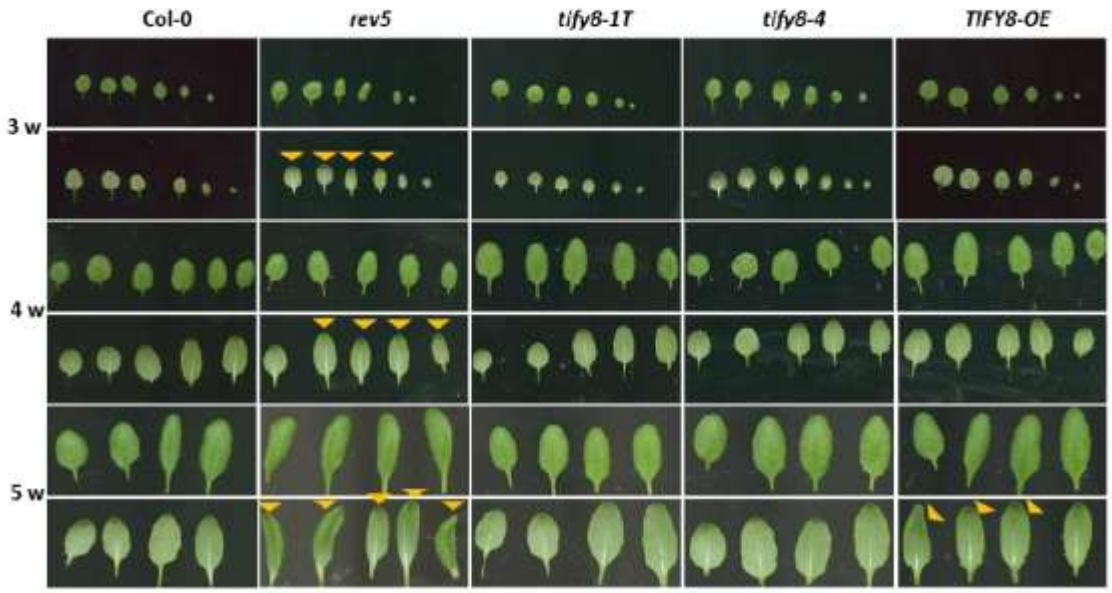

Figure S9: *Leaf phenotype in early stages.*
Leaf development of rosette leaves was documented in early stages of leaf and rosette development. Orange arrow heads point to the downward curled leaves which were typically observed in *rev5* mutant plants.

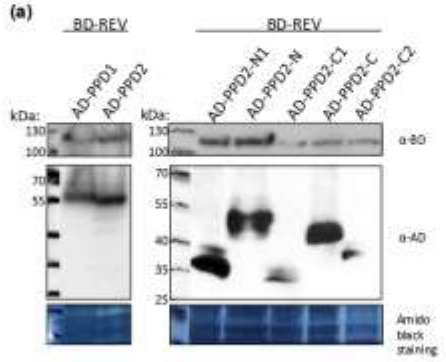

(b)

BD	AD	TDO	DDO/X/AbA	QDO	QDO/X	QDO/X/AbA	
REV	PPD1	83%	67%	67%	100%	50%	100%
REV	PPD2	100%	43%	71%	100%	29%	83%
REV	PPD2-N1	0%	0%	0%	0%	0%	71%
REV	PPD2-N	100%	0%	100%	100%	0%	67%
REV	PPD2-C1	0%	0%	0%	0%	0%	50%
REV	PPD2-C	100%	0%	0%	0%	0%	43%
REV	PPD2-C2	0%	0%	0%	0%	0%	29%
REV	empty	0%	0%	0%	0%	0%	0%

Figure S10: *Yeast two-hybrid protein expression in yeast cells and heat map of positive results in independent mating experiments.*
(a) Western blot analyzed with anti-BD and anti-AD antibodies (α) show expression of BD-REV and AD-PPD fusion proteins in diploid yeast cells. The amount of protein loaded onto the gel is indicated by a section of the Amido Black Staining. BD-REV: 114 kDa, AD-PPD1: 58 kDa, AD-PPD2: 58 kDa, AD-PPD2-N1: 37 kDa, AD-PPD2-N: 46 kDa, AD-PPD2-C1: 33 kDa, AD-PPD2-C: 46 kDa, AD-PPD2-C2: 36 kDA. **(b)** Heatmap of positive interaction results of 3 to 7 independent mating experiments in % positive results.

(a)

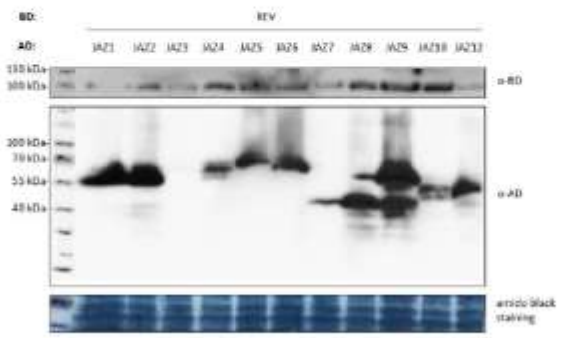

(b)

BD	AD	TDO	DDO/X/AbA	QDO	QDO/X	QDO/X/AbA	
REV	JAZ1	100%	100%	100%	100%	100%	100%
REV	JAZ2	100%	25%	100%	75%	0%	75%
REV	JAZ3	75%	50%	50%	75%	25%	50%
REV	JAZ4	100%	50%	100%	100%	25%	25%
REV	JAZ5	100%	0%	100%	100%	0%	0%
REV	JAZ6	100%	0%	50%	0%	0%	
REV	JAZ7	0%	0%	0%	0%	0%	
REV	JAZ8	100%	0%	50%	25%	0%	
REV	JAZ9	100%	0%	100%	100%	0%	
REV	JAZ10	100%	0%	75%	75%	0%	
REV	JAZ12	100%	0%	0%	0%	0%	
REV	empty	0%	0%	0%	0%	0%	

Figure S11: *Yeast two-hybrid protein expression in yeast cells and heat map of positive results in independent mating experiments.*
(a) Western blot analyzed with anti-BD and anti-AD antibodies (α) show expression of BD-REV and AD-JAZ fusion proteins in diploid yeast cells. The amount of protein loaded onto the gel is indicated by a section of the Amido Black Staining. BD-REV: 114 kDa, AD-JAZ1: 51 kDa, AD-JAZ2: 51 kDa, AD-JAZ3: 62 kDa, AD-JAZ4: 58 kDa, AD-JAZ5: 54 kDa, AD-JAZ6: 54 kDa, AD-JAZ7: 41 kDa, AD-JAZ8: 39 kDa, AD-JAZ9: 53 kDa, AD-JAZ10: 46 kDa, AD-JAZ12: 44 kDa. **(b)** Heatmap of positive interaction results of 3 to7 independent mating experiments in % positive results.

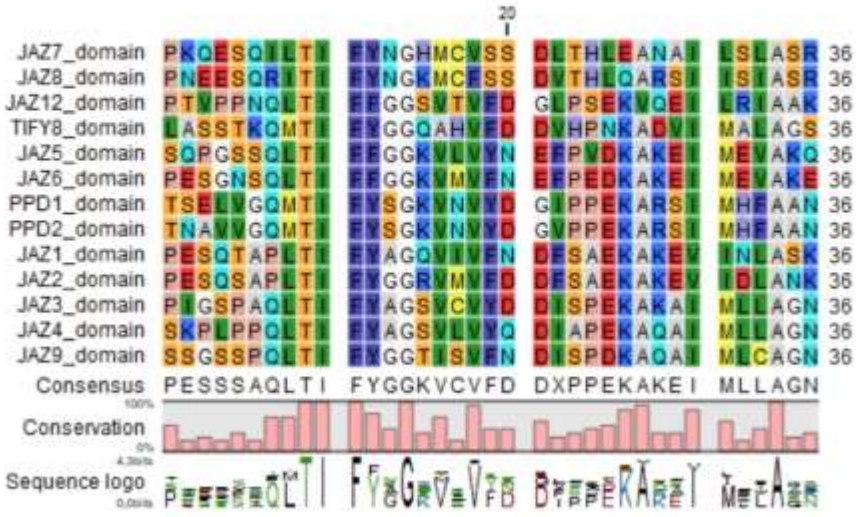

Figure S12: *Alignment of all TIFY/JAZ domains of the class two TIFY proteins.*

Publish manuscript 3: Complex Formation between the Transcription Factor WRKY53 and Antioxidative Enzymes Leads to Reciprocal Inhibition

Andrade Galan, A.G., Doll, J., Faiß, N., Weber, P., Zentgraf, U. Complex Formation between the Transcription Factor WRKY53 and Antioxidative Enzymes Leads to Reciprocal Inhibition. Antioxidants (Basel). 2024 Mar 5;13(3):315. doi: 10.3390/antiox13030315. PMID: 38539848; PMCID: PMC10967774.

antioxidants

MDPI

Article

Complex Formation between the Transcription Factor WRKY53 and Antioxidative Enzymes Leads to Reciprocal Inhibition

Ana Gabriela Andrade Galan, Jasmin Doll, Natalie Faiß, Patricia Weber and Ulrike Zentgraf *

Center for Plant Molecular Biology (ZMBP), University of Tuebingen, Auf der Morgenstelle 32, 72076 Tübingen, Germany; ana.andrade@zmbp.uni-tuebingen.de (A.G.A.G.); jasmin.doll@zmbp.uni-tuebingen.de (J.D.); natalie.faiss@zmbp.uni-tuebingen.de (N.F.); pa.weber@student.uni-tuebingen.de (P.W.)
* Correspondence: ulrike.zentgraf@zmbp.uni-tuebingen.de

Abstract: The transcription factor WRKY53 of the model plant *Arabidopsis thaliana* is an important regulator of leaf senescence. Its expression, activity and degradation are tightly controlled by various mechanisms and feedback loops. Hydrogen peroxide is one of the inducing agents for *WRKY53* expression, and a long-lasting intracellular increase in H_2O_2 content accompanies the upregulation of *WRKY53* at the onset of leaf senescence. We have identified different antioxidative enzymes, including catalases (CATs), superoxide dismutases (SODs) and ascorbate peroxidases (APXs), as protein interaction partners of WRKY53 in a WRKY53-pulldown experiment at different developmental stages. The interaction of WRKY53 with these enzymes was confirmed in vivo by bimolecular fluorescence complementation assays (BiFC) in *Arabidopsis* protoplasts and transiently transformed tobacco leaves. The interaction with WRKY53 inhibited the activity of the enzyme isoforms CAT2, CAT3, APX1, Cu/ZuSOD1 and FeSOD1 (and vice versa), while the function of WRKY53 as a transcription factor was also inhibited by these complex formations. Other WRKY factors like WRKY18 or WRKY25 had no or only mild inhibitory effects on the enzyme activities, indicating that WRKY53 has a central position in this crosstalk. Taken together, we identified a new additional and unexpected feedback regulation between H_2O_2, the antioxidative enzymes and the transcription factor WRKY53.

Keywords: catalase (CAT); ascorbate peroxidase (APX); superoxide dismutase (SOD); WRKY transcription factors; WRKY53; protein–protein interaction; zymograms; *Arabidopsis thaliana*; plant senescence

Citation: Andrade Galan, A.G.; Doll, J.; Faiß, N.; Weber, P.; Zentgraf, U. Complex Formation between the Transcription Factor WRKY53 and Antioxidative Enzymes Leads to Reciprocal Inhibition. *Antioxidants* **2024**, *13*, 315. https://doi.org/10.3390/antiox13030315

Academic Editor: Jozefus Schippers

Received: 9 January 2024
Revised: 20 February 2024
Accepted: 25 February 2024
Published: 5 March 2024

1. Introduction

Senescence is an integral part of plant development. Older or shaded leaves are not just sacrificed but exploited before shedding. Valuable nutrients are remobilized out of the senescing tissues for the sake of the whole plant during sequential senescence, and even for the next generation during monocarpic senescence. In the latter, carbon, mineral and nitrogen resources are transported to the developing fruits and seeds after the transition to the reproductive stage. Senescence in general, but especially onset and progression of monocarpic senescence, are highly complex processes which are driven by a multitude of molecular signals, including almost all plant hormones but also other small signaling molecules like small peptides, calcium or reactive oxygen species (ROS). Onset and progression of monocarpic senescence are accompanied by a drastic change in gene expression, implying a central role for transcription regulators like histone modifiers or chromatin remodeling factors, regulators of the DNA methylation and transcription activators and repressors [1–10]. Activity and function of all these components have to be tightly linked and integrated into a complex regulatory network (for review see [10–14]) to guarantee a smooth operation of senescence.

Arabidopsis, as a model system, has been extensively utilized to analyze the fundamental molecular mechanisms underlying senescence processes. This is due to the ability to progress from germination to fully senescent plants with siliques and mature seeds within approximately 10–12 weeks under long-day light conditions. Leaf material can easily be defined within the rosette using a color code considering the gradient along sequential senescence within the rosette to compare leaves which are in the same developmental stage. Moreover, a clear guideline on how senescence can be analyzed has been developed for *Arabidopsis* plants [15]. In *Arabidopsis*, two large groups of transcription factors in particular, the NAC and the WRKY transcription factor families, are overrepresented in the senescence transcriptome and play important roles in regulating developmental as well as stress-induced senescence [3–5,10–14]. Among more than a hundred transcription factors driving senescence, WRKY53 is just one cogwheel in the gear of a very complex regulatory network that drives the onset of senescence in conjunction with other. Beyond its expression, which is responsive to hydrogen peroxide, jasmonic or salicylic acid, it is regulated by at least 12 other transcription factors, and its degradation as well as its activity are also regulated. Direct phosphorylation by a MAP kinase kinase kinase 1 can increase its transactivation potential, whereas interaction with various partner proteins can inhibit its DNA-binding or change its promoter binding specificity (for review, see [14] and references therein). The HECT ubiquitin ligase (UPL5) can specifically bind to WRKY53 and send the protein to degradation via the 26S-proteasom. The opposite expression pattern compared to *WRKY53* itself ensures that WRKY53 protein is rapidly degraded when it should be expressed during stress conditions, thereby preventing premature induction of senescence [16].

It became evident during the last two decades that hydrogen peroxide, as well as other ROS, act as signaling molecules in senescence. ROS are by-products of aerobic metabolism in all organisms which cannot be avoided. They are formed by either partial reduction of or direct energy transfer to molecular oxygen (O_2). These very reactive molecules can oxidize more or less all kinds of macromolecules, influencing a plethora of physiological changes, including the activity of transcription factors [17–20]. However, when ROS are present in excess, they can be harmful to the cells; therefore, ROS production and scavenging needs to be balanced ingeniously. Furthermore, in addition to many non-enzymatic ROS scavenging molecules, antioxidative enzymes like catalases (CATs), ascorbate peroxidases (APXs), and superoxide dismutases (SODs) are present in several isoforms in different cellular compartments, counteracting ROS production. A delicate regulation of the CAT and APX activities leads to a long-lasting increase of intracellular hydrogen peroxide during the onset of monocarpic senescence for 7 to 10 days. To initiate this long-term increase, *CAT2* gene expression is inhibited by the bZIP transcription factor G-Box binding factor 1 (GBF1) [21,22]. Since CAT2 protein contributes approximately 80% of the total CAT activity in leaves and has a high turnover rate [23], this rapidly leads to a depletion of catalase activity and an increase of intracellular H_2O_2 content. Aside from that, the APX1 enzyme is rendered sensitive against H_2O_2 by a mechanism that remains unknown so far, particularly during bolting and onset of monocarpic senescence [21,24]. This further contributes to increasing levels of H_2O_2, and thereby activates a positive feedback loop. With ongoing plant development, APX1 inhibition is overridden again and, additionally, *CAT3* expression and enzyme activity start to increase, and thus antioxidative capacity is at least partially restored. This model was confirmed in *gbf1* mutant plants. If *CAT2* downregulation is abolished in *gbf1* mutant plants, no H_2O_2 increase and no positive feedback through APX1 inhibition is initiated; thus, no long-term H_2O_2 increase can be observed in *gbf1* mutants, and senescence is delayed [22,25].

Remarkably, *WRKY53* gene expression can be driven by hydrogen peroxide, and this long-term increase coincides with the increase of *WRKY53* expression at this time point. In addition, all three *CAT* genes have been identified as direct target genes of WRKY53, creating further feedback regulations [26]. Moreover, the homolog of *WRKY53* of rapeseed also feeds back on hydrogen peroxide levels, in this case by altering transcription of *RbohD* and *RbohF* [27]. However, so far there is no indication that WRKY53 regulates *Rbohs* in

Arabidopsis; this appears to be taken over by *WRKY55* [28]. Here, we characterized a new direct feedback loop involving WRKY53 and the antioxidative enzymes. While analyzing the different in vivo protein interaction partners of WRKY53 using a pulldown of WRKY53 proteins at different developmental stages, combined with LC/MS-MS, we found, beyond others, many different antioxidative enzymes including CATs, SODs and APXs. We could confirm the direct interaction between WRKY53 and these enzymes in vivo by BiFC in transiently transformed *Arabidopsis* protoplasts as well as *N. benthamiana* leaves. Interaction with WRKY53 inhibits the enzyme function of the different enzyme isoforms to different extends, and this inhibition can be realized over a wide range of plant developmental stages. Vice versa, the function of WRKY53 as transcriptional regulator is also inhibited to different extents by these interactions.

2. Materials and Methods

2.1. Plant Cultivation

Arabidopsis plants (*A. thaliana* Ecotype Columbia) were grown under long-day conditions (16h light) on standard soil. An amount of 70 L of the standard soil CL Topf (Art.Nr.: 10-00300, PATZER ERDEN GmbH, Sinntal, Germany) was mixed with 8 L of sand (Flammer Bauunternehmung GmbH & Co. KG, Rheinsand, Tuebingen, Germany) and sieved with a mesh width of 8 × 10 mm. Detailed soil composition is provided in Table S1. For all experiments, only moderate light intensity (80–100 µmol s^{-1} m^{-2}) in a climatic chamber at an ambient temperature of 20 °C was applied. As catalases show circadian regulation, plant material was harvested always at the same time of day to avoid circadian effects. The positions of the individual leaves within the rosette were color-coded according to their age using colored threats [15]. In all experiments, *A. thaliana* Ecotype Columbia-0 (Col-0), *upl5* or *wrky53* mutant plants in Col-0 background (SALK_116446; SALK_034157) were used. Tobacco plants (*N. benthamiana*) were cultivated for 4–5 weeks in the greenhouse on standard soil under long-day conditions under normal light intensity (120–150 µmol s^{-1} m^{-2}).

2.2. Zymograms for Antioxidative Enzymes

For the analysis of catalase activities, we consistently utilized leaves from the same positions within the rosette (Leaf No. 5 and No. 6). Leaves from three 4- to 8-week-old *Arabidopsis* plants were ground in a solution containing 100 mM Tris-HCl pH 8.0, 20% glycerol, and 30 mM dithiothreitol (DTT). For the analyses of ascorbate peroxidase and superoxide dismutase activities, leaves No. 5–8 from five 4- to 8-week-old *Arabidopsis* plants were ground in 50 mM potassium phosphate buffer, pH 7.8, containing 5 mM ascorbate, 2% Triton X-100, 10% glycerol, and 0.25 mM EDTA. These crude extracts were then centrifuged for 30 min at 13,000 rpm at 4 °C, and the protein concentrations of the supernatants were measured using the Bradford method [29]. The resulting protein extracts were used directly for the zymograms.

To analyze the different isoforms of catalase, 10 µg of the protein extracts were separated in 6% native polyacrylamide gels (0.375 M Tris-HCl, pH 6.8, as gel buffer) for 1 h (120 V) using 250 mM glycine and 25 mM Tris-HCl, pH 8.3, as the electrophoresis buffer. After electrophoresis, the gels were stained for CAT activity, as described in [30]. The gels were soaked in 0.01% H_2O_2 solution for 2 min, followed by washing twice in water and incubating them for 2–5 min in 1% of both $FeCl_3$ and $K_3[Fe(CN)_6]$. Rinsing the gels twice in water stopped the reaction. For immunodetection of catalases, the native polyacrylamide gels were blotted on a nitrocellulose membrane. Subsequently, the membrane was rinsed twice in Tris-buffered saline (TBS) and blocked with 3% milk powder in TBS-Tween 20 (TBS-T). Polyclonal anti-rye-CAT antibodies in 1.5% milk powder were used, followed by secondary peroxidase-conjugated antibodies for visualization.

The activity of the superoxide dismutase isoforms was analyzed using 120 µg of the protein extracts, which were separated in 13% native polyacrylamide gels (0.375 M Tris-HCl, pH 8.8, containing 10% glycerol as gel buffer). In this case, a 5% stacking gel was necessary (0.125 M Tris-HCl, pH 6.8, containing 10% glycerol as gel buffer). Electrophoresis

was performed for 1 h (120 V) using 250 mM glycine and 25 mM Tris-HCl, pH 8.3, as electrophoresis buffer. Afterwards, gels were washed in water and rinsed in staining solution (50 mM potassium phosphate buffer, pH 7.0, 1 mM EDTA, 5.2 µm Riboflavin and 0.5 mM NBT) for 30 min while shaking in the dark. Subsequently, the gels were washed twice in water and illuminated for 30 min, as described in [31].

For the analyses of the ascorbate peroxidase isoforms, 40 µg of the protein extracts were separated on the same gels as for the superoxide dismutase isoforms using 250 mM glycine and 25 mM Tris-HCl, pH 8.3, containing 2 mM ascorbate as an electrophoresis buffer. After electrophoresis, the gels were soaked 3 times in 50 mM potassium phosphate buffer, pH 7.0, containing 2 mM ascorbate for 10 min, subsequently, in 50 mM potassium phosphate buffer, pH 7.0, containing 4 mM ascorbate and 1 mM H_2O_2 for 20 min. After washing in water, 50 mM potassium phosphate buffer, pH 7.8, containing 14 mM TEMED (N,N,N′,N′-tetramethylethylenediamine) and 2.45 mM NBT (nitro blue tetrazolium) was used to stain the gels for 10–30 min [32].

2.3. Transient Transformation of Arabidopsis Protoplasts and Arabidopsis or Tobacco Leaves

A. thaliana ecotype Col-0 root cells that were grown in liquid cultures were used to prepare protoplasts and transform them transiently with plasmid DNA. For protoplast preparation and transient transformation using PEG, we followed the protocol described in [33]. *N. benthamiana* plants were infiltrated with *Agrobacterium tumefaciens* suspension cultures containing the BiFC constructs. LB media, with the respective antibiotics, was inoculated with an overnight culture of the bacteria and incubated for 4–6 h. Subsequently, this culture was centrifuged at 4000 rpm for 10 min. The bacterial pellet was diluted in infiltration media (10 mM $MgCl_2$, 0.5 M MES, 100 mM Acetosyringone) to an OD_{600} of 0.5. Leaves of 4-week-old tobacco plants were infiltrated by manual injection using a 1-mL needleless syringe. *A. thaliana* leaves of 3- to 4-week-old plants were co-infiltrated using the same procedure with *A. tumefaciens* suspension cultures containing the GUS-reporter and the effector construct, respectively.

2.4. Bimolecular Fluorescence Complementation (BiFC), Cytometry, and Confocal Microscopy

In order to study the interaction of WRKY53 with the antioxidative enzymes CAT2, CAT3, APX1, and Cu/ZnSOD1, ratiometric BiFC assays were performed. Therefore, the cDNAs of the subunits of *CAT2* (2393 bp, At4g35090) and *CAT3* (2784 bp, At1g20620), as well as the cDNAs of *APX1* (1270 bp, At1g07890) and *Cu/ZnSOD1* (873 bp, At1g08830), were cloned together with the cDNA of *WRKY53* (1514 bp, At4g23810) into the pBiFCt-2in1-NN vector carrying both genes of interest on one vector. In addition, an internal red fluorescent protein (*RFP*) gene as transformation and expression control was localized on the same vector backbone. The genes of interest were fused to the N- or the C-terminal part of the yellow fluorescent protein (*YFP*), respectively. The expression of the fusion proteins is driven by the cauliflower mosaic virus 35S promoter [34]. For the transfection of the protoplasts, 4 µg of the plasmid DNA was used to gain expression of the fusion proteins. If the fusion proteins can interact with each other, yellow fluorescence is restored by bringing the YFP-N and YFP-C parts into close proximity. These interactions were visualized by flow cytometry using CytoFLEX (Beckman Coulter, Brea, CA, USA) 1 day after transfection. The internal RFP and any reconstituted YFP were both excited by the onboard 488 nm laser. Emissions were captured for YFP in FL1 (525/40 nm) and RFP in FL3 (610/20 nm), respectively. All interaction tests were performed at least 3 times independently. In addition, confocal microscopy (LSM880, Zeiss, Jena, Germany) of transfected tobacco leaves was used to detect and localize the interaction within the cells. For this purpose, *N. benthamiana* plants were infiltrated with *A. tumefaciens* suspension cultures containing the pBiFCt-2in1 constructs described above. Microscopic analyses were performed 2 days after infiltration. At least 3 leaves of different plants were analyzed under a Zeiss LSM 880 Airyscan confocal microscope by using the preset sequential scan settings for YFP (Ex:

514 nm, Em: 517–553 nm) and for RFP (Ex: 561 nm, Em: 597–625 nm). The experiments were repeated at least 3 times.

2.5. Intracellular Hydrogen Peroxide Measurements

Whole rosette leaves were harvested from the same positions within the rosette and then incubated in 9.5 µM 5(6)-Carboxy-Di-Hydro-Di-Chloro-Fluorescein-Di-Acetate (Carboxy-H_2DCFDA) in MS-Medium (pH 5.7). Samples were incubated for 45 min in the dye solution, washed twice with distilled water, then frozen in liquid nitrogen. Samples were homogenized on ice in 500 µL 40 mM Tris-HCl pH 7.0. After centrifugation (30 min, 4 °C, 14,000 rpm), fluorescence of supernatant was measured (480 nm excitation, 525 nm emission, Berthold TriStar LB941, BERTHOLD TECHNOLOGIES, Bad Wildbad, Germany). The H_2DCFDA solution needs to be calibrated by chemical de-acetylation and oxidation following, and it has to be prepared freshly for each sample harvest [35].

2.6. Gene Expression Analyses Using qRT-PCR

The total RNA was extracted with the GeneMATRIX Universal RNA Purification Kit (*EURx*, Gdańsk, Poland). RevertAid Reverse Transcriptase (Thermo Fisher Scientific Inc., Waltham, MA, USA) and oligo-dT primers were applied for cDNA synthesis. KAPA SYBR® Fast Bio Rad iCycler (Bio-Rad Laboratories Inc., Hercules, CA, USA) and Master Mix were used for qRT-PCR analyses following the manufacturer's protocol. We used the ΔΔCT method for calculation according to [36]. *WRKY53* expression was normalized to *ACTIN2* values and given in % of *ACTIN2*. Primer design for qRT-PCR was performed via QuantPrime [37], *ACTIN2* (At3g18780): AAGCTCTCCTTTGTTGCTGTT and GTTGTCTCGTGGATTCCAGCAGCTT, WRKY53 (At4g23810): CAGACGGGGATGCTACGG and GGCGAGGCTAATGGTGGT.

2.7. Purification of 8xHis-Tagged WRKY Proteins

WRKY proteins were ordered as N-terminally 8xHis-tagged proteins from Biomatik (Cambridge, ON, Canada). Proteins were expressed in *E. coli* cells and purified by affinity purification. Concentrations of WRKYs were determined by Bradford protein measurements, while quality and purification were shown by SDS-PAGE, Coomassie staining and Western blotting, followed by immune detection using anti-HIS antibodies (Figure S2).

2.8. GUS-Reporter Gene Assays

Transiently transformed *Arabidopsis* leaves were incubated overnight in a staining solution containing a 100 mM sodium phosphate buffer pH 7.5, 10 mM EDTA pH 8.0, 0.5 mM potassium ferricyanide ($K_3[Fe(CN)_6]$), 0.5 mM potassium ferrocyanide ($K_4[Fe(CN)_6]$), 0.1% Triton X-100 and 0.5 mg/mL X-GlcA (Cyclohexylammonium salt, Duchefa, Haarlem, The Netherlands). Subsequently, the chlorophyll had to be removed for better analysis of the blue staining. This was achieved by shaking the plant material in 80% ethanol for another 24 h, during which the ethanol solution was changed several times.

2.9. Antioxidative Capacity of Leaf Discs

The decomposition of H_2O_2 can be evaluated using commercially available peroxide strips (Dosatest peroxide test strips 100, VWR Chemicals, Leuven, Belgium). Therefore, we excelled leaf discs from wild-type or transiently transformed *N. benthamiana* leaves, and these discs were incubated in a 1 mM H_2O_2 solution. To measure the H_2O_2 decomposition activity of these discs, one of the test strips was submerged for 1 s into the solution immediately after placing the leaf disc into the solution as baseline (time point 0 min). This procedure was repeated after 2 h. The given control color scale can be used to read out the amount of residual peroxide, and the weaker the blue color, the less peroxide is present in the solution.

3. Results

WRKY53 gene expression, activity and degradation are tightly controlled during plant devolvement and senescence. The WRKY53 protein can interact directly with a variety of partners in different cellular compartments ([14] and references therein). According to different yeast two-hybrid screens, WRKY53 appears to have many more different interaction partners. In order to analyze the actual in vivo protein-interaction partners of WRKY53 over plant development, we performed Co-IP experiments with 35S:*WRKY53* overexpressing plants in *upl5* background using anti-WRKY53 antibodies at different time points, then analyzed the pulled-down proteins with LC-MS/MS. To our surprise, we found many antioxidative enzymes among the direct interaction partners of WRKY53, including different isoforms of CATs, APXs and SODs (see Supplemental Figure S1 and Table S2).

3.1. Inhibition of the Activity of Different Antioxidative Enzymes by WRKY53

In order to evaluate whether this interaction with WRKY53 has any consequences for the function of the antioxidative enzymes, we analyzed the activity of the different isoforms of CATs, APXs and SODs using zymograms in the presence of WRKY53 protein. Tagged versions of WRKY53, as well as of WRKY18 and WRKY25, were expressed in *E. coli* cells and purified via the 8xhis tag. The WRKY53 highly enriched protein factions (Supplemental Figure S2) were added in increasing amounts to the crude plant protein extracts isolated from wild-type Col-0 and *wrky53* mutant plants, and myelin basic protein (MBP) was used as control protein. After incubation, the influence of WRKY53 and MBP on the activity of the different isoforms of the antioxidative enzymes was tested by enzyme-specific zymograms. Addition of WRKY53 protein had a clear inhibiting effect on the activity of the CAT2 and CAT3 homotetramers, as well as the activity of the heterotetramers (Figure 1A). The catalase isoforms can be clearly differentiated by their different reactions towards 3'amino 1,2,4 triazole, or by using catalase single and double mutants [21,30]. Inhibition appears to be concentration-dependent, and the active protein complexes appear to be slightly shifted upwards with increasing amounts of added proteins. In contrast, MBP had no effect on the activity of CAT2, CAT3 or the heterotetrameres. Moreover, the addition of WRKY18 highly enriched protein factions, as well as of WRKY25 highly enriched protein factions, had also no effect on CAT activities, indicating a WRKY53 specific inhibition (Figure 1A). As expected, CAT2 activity is higher in leaf tissue compared to CAT3; however, the protein amount appears to be more equal according to Western blotting of a native protein gel and subsequent immune detection with anti-rye catalase antibodies (Supplemental Figure S3).

Even though eight genes and several isoforms of ascorbate peroxidase exist, it is difficult to see their activities on the zymograms of crude extracts. The most prominent visible isoform is the cytosolic APX1, which can only be visualized if high amounts of ascorbate are present during the extraction and electrophoresis procedure to stabilize the enzyme. Again, the addition of WRKY53 to the crude protein extracts inhibits enzyme activity of APX1 in a concentration-dependent manner (Figure 1B). As for the CATs, the addition of MBP, as well as of WRKY18, had no effect. In this case, the addition of WRKY25 could slightly inhibit APX1 activity. Furthermore, SOD activities were inhibited by WRKY53; however, here the different isoforms were inhibited to different extents. The Cu/ZnSOD activities declined most prominently, followed by the FeSOD, while the Mn-SOD appeared to be insensitive (Figure 1C). As for APX1, the addition of MBP, as well as of WRKY18, had no effect and, again, addition of WRKY25 protein could slightly inhibit the Cu/ZnSODs.

In summary, the presence of WRKY53 selectively inhibits the activity of specific isoforms of the antioxidative enzymes, and WRKY53 is more effective than other WRKYs.

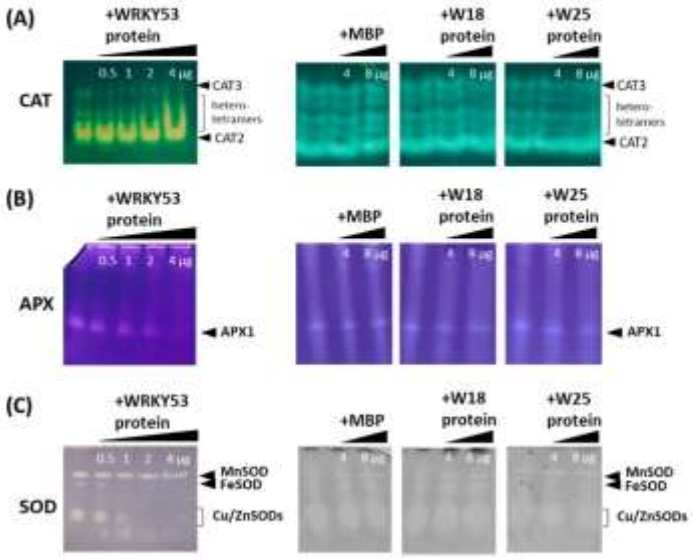

Figure 1. Zymograms of crude protein extracts isolated from leaf tissue of wild-type *Arabidopsis* plants. Staining for (**A**) CAT activity, (**B**) APX activity, (**C**) SOD activity. Visible isoforms are indicated by the arrows. Increasing amounts of highly enriched protein factions of WRKY53 (0.5–4 µg) or WRKY18 (4, 8 µg), WRKY25 (4, 8 µg), were added to the extracts before loading. MBP (4, 8 µg) was used as control protein, as indicated on each gel and lane.

3.2. Protein–Protein Interaction between WRKY53 and Different Antioxidative Enzymes

To confirm that the interaction between WRKY53 and CAT2, CAT3, APX1 and CuZnSOD1 can also be observed in living cells, we used Bimolecular Fluorescence Complementation (BiFC) assays in transiently transformed *Arabidopsis* protoplasts and *N. benthamiana* leaves. Therefore, WRKY53 was fused with the C-terminal half of YFP, while the potential interaction partners were combined with the N-terminal half of YFP, or vice versa. If interaction takes place, the two halves of the YFP come into close proximity and are able to emit a yellow fluorescence. In the case of the transiently transformed Arabidopsis protoplasts, fluorescent cells were sorted in a CytoFLEX cell sorter, in which a portion of the cells showed a YFP fluorescence, clearly indicating in vivo interaction. These experiments clearly confirmed that CAT2, CAT3, APX1 and Cu/ZnSOD1 proteins can directly interact with the transcription factor WRKY53 (Figure 2A, Supplemental Table S3). In addition, these interactions were analyzed in transiently transformed tobacco leaves using confocal microscopy. Again, yellow fluorescence can only be emitted if the two proteins interact and bring the two halves of the fluorescent protein together. Not only do the microscopy pictures confirm the interactions, the intracellular localization of the interaction could also be observed under the microscope. CAT2 and CAT3 could form a complex with WRKY53 in the peroxisomes, as well as in the nucleus; this means that either WRKY53 is taken to the peroxisomes via the interaction with the CATs, or CAT enzyme complexes or their subunits are translocated to the nucleus by the interaction with WRKY53 (Figure 2B). Interaction between WRKY53 and APX1 or Cu/ZnSOD1 has predominantly been observed in the nucleus; however, the cytoplasmic signal might have been too low and dispersed to be detected (Figure 2B). Again, so far, no nuclear localization of APX1 or Cu/ZnSOD1 was reported, so we can conclude that APX1 and Cu/ZnSOD1 are also translocated to the nucleus via the interaction with WRKY53, as was already described for another protein [14]. Yet, in contrast to catalase subunits (57 kDa), both proteins are small in size (27.5 kDa

and 16 kDa, respectively), so that, in principle, they could also diffuse freely between the nucleus and cytoplasm [38].

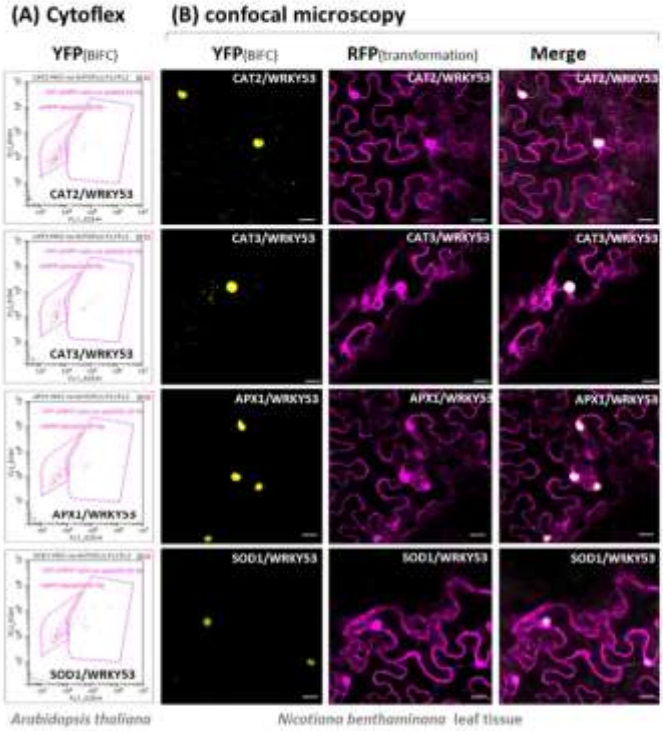

Figure 2. In planta protein–protein interaction between WRKY53 and CAT2, CAT3, APX1 or Cu/ZnSOD1 using BiFC in transiently transformed *Arabidopsis* protoplasts or tobacco leaves. (**A**) Protoplasts were analyzed with the CytoFLEX cell sorter: pink framed polygons indicate transformed protoplasts (RFP fluorescence, left polygon), purple framed polygons indicate interaction via BiFC (YFP fluorescence, right polygon). (**B**) Transiently transformed *N. benthamiana* leaves were analyzed under the confocal laser scanning microscope: yellow fluorescence (YFP) indicates BiFC, red fluorescence (RFP) is used as a transformation control. Scale bar indicates 20 µm.

In addition, the antioxidative capacity of these transiently transformed tobacco leaves was tested using leaf discs, which were then incubated in 1 mM H_2O_2 solution. We could again confirm that the presence of WRKY53 lowers the overall antioxidative capacity towards H_2O_2, even if CAT2, CAT3, APX1 or SOD1 were co-expressed (Figure 3). The leaf discs of wild-type *N. benthamiana* were able to detoxify almost all peroxides in a 1 mM solution within 2 h so that only approx. 1 mg/L peroxide was left after the incubation. However, if *WRKY53* was expressed in the leaf tissue, the antioxidative capacity of the leaf discs was lower, and still between 3–10 mg/L peroxide were left after 2 h. Moreover, if *CAT2*, *CAT3* or *APX1* were co-expressed, a higher antioxidative capacity towards H_2O_2 would have been expected, which was not the case. By overexpression of SOD1, if at all, an additional production of H_2O_2 would have been expected; however, in all cases the presence of WRKY53 appeared to block the function of the antioxidative enzymes.

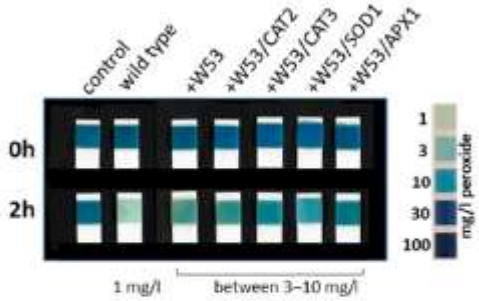

Figure 3. Leaf discs of wild-type or transiently transformed *N. benthamiana* leaves were incubated in a 1 mM H_2O_2 solution. At time points 0 h and 2 h, the concentration of H_2O_2 was determined using commercially available peroxide stripes. Color scale for peroxide content is provided on the right. Transformed effector constructs are mentioned above the stripes. As control, H_2O_2 solution without leaf discs was measured (left).

3.3. Inhibition of Antioxidative Enzymes by WRKY53 during Plant Development and Onset of Senescence

WRKY53 was shown to be one important regulatory hub in the complex network of senescence regulation. *WRKY53* gene expression, activity and degradation are tightly regulated, including even several double bottoms, e.g., *WRKY53* is highly expressed at the onset of monocarpic senescence in approx. 6- to 7-week-old plants while specific degradation of the WRKY53 protein by the HECT domain E3 ubiquitin ligase protein UPL5 is diminished at the same time by downregulation of *UPL5* expression [16,26]. Moreover, *WRKY53* gene expression can be induced by hydrogen peroxide, which increases during bolting and flowering time at the onset of monocarpic senescence [21,26]. The downregulation of *CAT2* expression, combined with an increased sensitivity of APX1 activity against hydrogen peroxide at bolting and flowering time, appear to be responsible for the production of this peak [21,22,24]. Therefore, we wanted to analyze whether inhibition of the antioxidative enzymes CAT and APX is possible throughout development and whether activity profiles change over development in a *wrky53* mutant plant. As already observed before, CAT2 activity decreased while CAT3 activity increased with age (Figure 4A). When WRKY53 protein was added to these different extracts, CAT2 and CAT3 activity could be inhibited, and an upwards-shift of the protein complexes could be observed in all developmental stages (Figure 4A). APX1 activity was down-regulated during bolting time but recovered at later stages (Figure 4B) [21,24]; this downregulation coincided with the increase in intracellular hydrogen peroxide and the expression of *WRKY53* (Figure 4C,D). Remarkably, the increase in intracellular hydrogen peroxide was more pronounced in younger than in older leaves, emphasizing the signaling character of hydrogen peroxide. Again, the addition of WRKY53 protein to the extracts could inhibit the activity of APX1 in all stages. For the SODs, we could not detect any obvious activity changes over development, and so this was not further analyzed.

In *wrky53* mutant plants, the down-regulation of CAT2 activity is diminished and/or delayed while the increase of CAT3 activity is accelerated, indicating that the WRKY53 protein contributes to the regulation of the activity of both catalases during development (Figure 5A). Still, the addition of WRKY53 protein to the extracts of *wrky53* mutants can inhibit both isoforms (Figure 5A). For APX, the decrease of APX1 activity during bolting and flowering time is prolonged in *wrky53* mutant plants (Figure 5B), which is consistent with the delayed senescence phenotype of these plants [24,26]. Again, the addition of WRKY53 protein to these extracts could inhibit APX1 activity severely (Figure 5B).

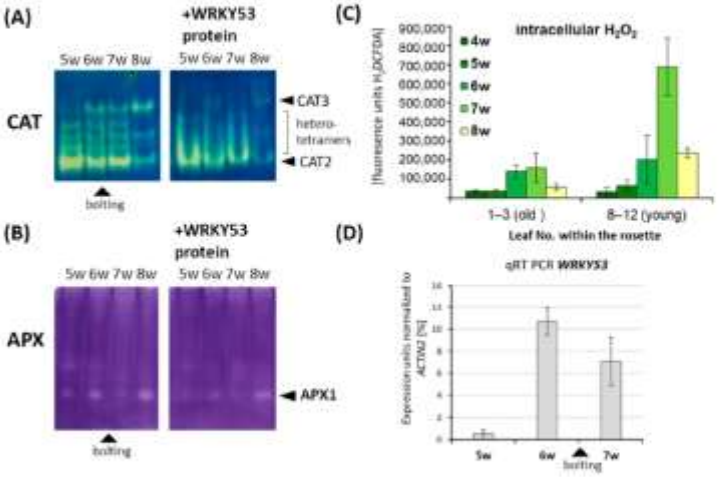

Figure 4. Zymograms of crude protein extracts isolated from leaf tissue of wild-type *Arabidopsis* plants at different developmental stages from 5 to 8 weeks (w). Staining for (**A**) CAT activity, (**B**) APX activity, 4 µg of a highly enriched protein factions of WRKY53 were added to the extracts before loading. Visible isoforms and bolting time are indicated by the black arrow heads. (**C**) H_2O_2 content was measured using H_2DCFDA fluorescence in pools of young (No. 8–12) and old leaves (No. 1–3) of the same rosette which were harvested from 4- to 8-week-old plants. H_2O_2 contents are indicated in arbitrary units of H_2DCFDA fluorescence, and error bars indicate ±SD, $n = 3$. (**D**) WRKY53 expression was analyzed by qRT-PCR in pools of rosette leaves No. 6 and 7 of three plants and were normalized to *ACTIN2* expression. Error bars indicated ±SE, $n = 3$.

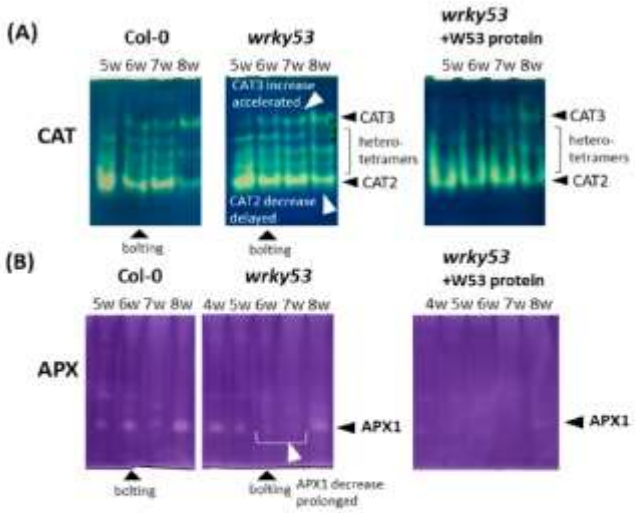

Figure 5. Zymograms of crude protein extracts isolated from leaf tissue of wild-type *Arabidopsis* (Col-0) or *wrky53* mutant plants at different developmental stages from 5 to 8 weeks (w). Staining for (**A**) CAT activity, (**B**) APX activity, 4 µg of a highly enriched protein factions of WRKY53 (W53) were added to the extracts before loading. Visible isoforms and bolting time are indicated by the black arrow heads. White arrowheads point to changes in the enzyme activities between Col-0 and *wrky53*.

3.4. Influence of the Complex Formation with the Antioxidative Enzymes on WRKY53 Function

As the protein interaction can lead to the inhibition and/or inactivation of the antioxidative enzyme, we wanted to know which influence this protein interaction has on the function of WRKY53. Therefore, we used reporter gene assays, in which a promoter sequence that can bind WRKY53 is driving the expression of the reporter gene ß-glucuronidase (*GUS*). In this reporter system, we used the promoter sequence of *WRKY53* itself (a 2,759-bp-sequence upstream of the start codon) and a 35S-driven *WRKY53* construct as effector together with 35S-driven constructs of *CAT2*, *CAT3*, *APX1* and *Cu/Zn-SOD1* as co-effectors. As observed before, WRKY53 regulates its own expression in a negative feedback loop, which is demonstrated by the lower *GUS* reporter gene expression and enzyme activity in transiently transformed *Arabidopsis* leaves (Figure 6A,B) [26]. One example of the histochemical GUS staining of these leaves is presented in Figure 6A, and a quantification of the stained regions of several transformed leaves is shown in Figure 6B,C. When we added 35S:*CAT2* or 35S:*SOD1* effector constructs as co-effector to the 35S:*WRKY53* and the P_{WRKY53}:*GUS* reporter, the negative effect of WRKY53 on the *GUS* expression was suppressed, indicating that CAT2 and Cu/Zn-SOD1 interactions with WRKY53 do not only inhibit enzyme activities of CAT and SOD but also block WRKY53 function as transcriptional repressor of its own promoter. APX1 and CAT3 interaction with WRKY53 also appear to slightly inhibit WRKY53 function, but here the observed differences were not statistically significant.

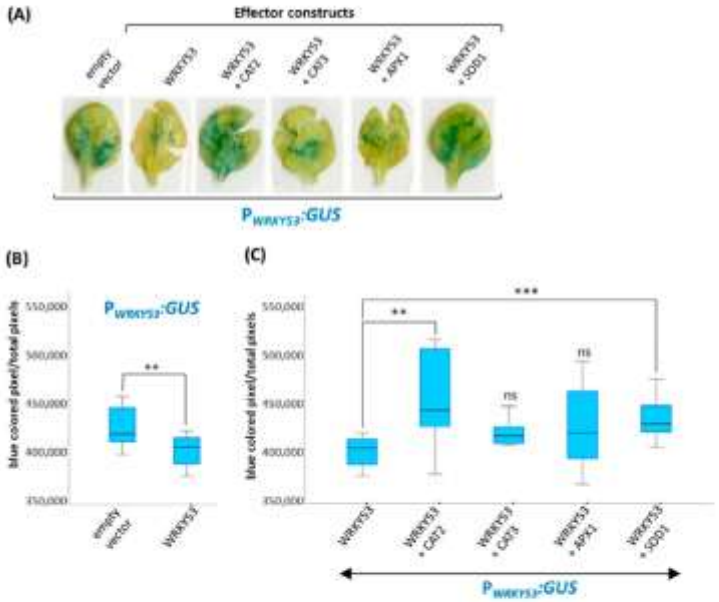

Figure 6. Histochemical GUS staining of transiently transformed *Arabidopsis* leaves. All leaves were transformed with a P_{WRKY53}:*GUS* construct. Both 35S-driven effector and co-effector constructs are indicated, while the empty vector was used as control. (**A**) One example of the GUS stained leaves is presented. (**B**) Effect of WRKY53 on the expression of its own promoter compared to the empty vector control, a boxplot of the quantification of the GUS staining is presented. (**C**) Effect of WRKY53 in the presence of different antioxidative enzymes as co-effectors, and a boxplot of the quantification of the GUS staining is presented. At least eight transformed leaves were analyzed, respectively. A *t*-test was performed for significant differences (n = 8–13), ** $p \leq 0.01$, *** $p \leq 0.001$, ns = not significant.

4. Discussion

It has become evident during the last two decades that ROS, especially hydrogen peroxide, can have a signaling function in developmental as well as stress-induced senescence. However, the mechanisms by which plants sense this parameter, and how specificity can be achieved, is still not well understood. So far it has been made clear that the ROS concentrations in the cytoplasm and different organelles have a different impact on senescence and are tightly regulated. Consistently, CAT and APX isoforms in particular are positioned strategically in different cellular compartments to control H_2O_2 levels and to ensure their function as signaling molecules [39]. Interestingly, H_2O_2 from chloroplasts and peroxisomes modulates the plant transcriptome differentially and has different impacts on senescence [40,41]. Furthermore, many senescence-associated transcription factors are upregulated in their own expression by H_2O_2 [3,17,26] or influenced in their activity by the redox conditions in the cytoplasm and nucleus [14,17,19,20] Overall, a very complex regulatory network has to be in place to regulate senescence and, more specifically, intracellular H_2O_2 concentrations.

Obviously, the complex regulatory network of senescence comprises many regulatory feedback loops, including the direct binding of *CAT1*, *CAT2*, and *CAT3* promoter elements by WRKY53, which activates the expression of the catalases, leading to the reduction of the intracellular hydrogen peroxide levels which, in turn, reduce expression of the *WRKY53* gene. Consistently, *cat2/3* double mutants with higher intracellular H_2O_2 levels showed increased expression of many WRKYs, including *WRKY53* [42]. In contrast, WRKY75 negatively regulates the expression of *CAT2* and *SID2*, leading to increasing salicylic acid and H_2O_2 levels, and thereby to a gradual but self-sustained rise of *WRKY75* expression during senescence driven by three interlinking positive feedback loops [43]. Moreover, WRKY53 can induce the expression of its family member *WRKY25* and, vice versa, WRKY25 can upregulate the expression of the *WRKY53* gene, creating a positive feedback regulation. At the same time, *WRKY25* expression diminishes intracellular H_2O_2 contents, which, in turn, leads to decreased *WRKY53* expression. As for *WRKY53*, expression of *WRKY25* can be induced by H_2O_2, and WRKY53 is involved in this induction. In addition, WRKY25 negatively regulates its own expression, which might prevent an overshooting of the reaction to H_2O_2 [17]. At first glance, these feedback regulations appear to be complex but contradictory at some points; however, these are only parts of a larger regulatory network which is likely to contain many more feedback controls. Here, we could add another feedback mechanism to the circuit between WRKYs, H_2O_2 and antioxidative enzymes. The WRKY53 protein can directly interact with different antioxidative enzymes, including CATs, APXs and even SODs (Figure 2, Supplemental Tables S2 and S3) and inhibit their function. This inhibition appears to be selective for specific isoforms, as well as for specific WRKY factors (Figure 1) in which WRKY53 is more effective than WRKY25, whereas WRKY18 had no effect. On the other hand, *WRKY53* expression is upregulated in a *cat2/3* mutant more prominent than *WRKY25* or *WRKY18* [42], also indicating that WRKY53 plays a more central role in this feedback regulation. Moreover, the inhibition of CATs and APXs by WRKY53 can take place throughout a wide range of different developmental stages, as the activity profiles differ between Col-0 and *wrky53* mutant plants (Figures 4 and 5). It was shown before that inhibition of APX activity during bolting is executed post-transcriptionally [21,44,45]. However, as this inhibition of APX activity during bolting is still visible in *wrky53* mutant plants, WRKY53 interaction appears to not be the main responsible mechanism here, even though *WRKY53* expression level rises exactly at this time point. Moreover, the inhibition of APX1 appears to be prolonged in the *wrky53* mutants, indicating that this prolonged inhibition is due to the delayed senescence in these plants [26].

Further to WRKY53, CATs can interact with many different non-peroxisomal proteins including cytoplasmic and nuclear proteins, nicely reviewed in [39]. This is possible, as CATs are not exclusively located in the peroxisomes and can also be found in the cytoplasm [46]. It has been shown before that CATs can be retained in the cytosol under

oxidative stress conditions in which the peroxisomal import receptor PEX5 functions as a stress sensor [47]. Interaction of CAT3 with a cucumber mosaic virus protein 2b can translocate CAT3 to the nucleus [48]. Here, we could show that the interaction between WRKY53 and CAT2 or CAT3 can direct the resulting complexes to the peroxisomes but also appears to foster the translocation of the CATs to the nucleus (Figure 2). The interaction inhibits catalase activity, but whether CAT is released again from the WRKY53 interaction in the nucleus is not yet clear. Moreover, whether the whole catalase complex, which consists of four subunits and four HEME groups, or only the protein subunits are imported to the nucleus has still to be analyzed. However, the interaction with the oxidoreductase NUCLOREDOXIN1 protects CATs from ROS-induced oxidation and is required for their optimal function under oxidative stress conditions [49], indicating that the interaction with the nuclear protein NUCLOREDOXIN1 involves the functional tetramer.

Furthermore, CAT activity can also be regulated by other interactions: CAT3 can interact specifically with CALCIUM-DEPENDENT PROTEIN KINASE8 and can be phosphorylated at Ser-261, which positively influences its activity [46]. In addition, CAT3 can directly interact with S-nitrosoglutathione reductase (GSNOR) and acts in this case as a transnitrosylase that specifically modifies GSNOR1 at Cys-10, which CAT2 or CAT1 cannot, indicating that CAT3 is also involved in NO redox signaling in plants [50]. This *S*-nitrosylation of GSNOR1 induces a conformational rearrangement and fosters AUTOPHAGY8 binding, which then can promote its degradation via autophagy [51]. Whether WRKY53 can also be transnitrosylated by CAT3 interaction will be the subject of further investigations.

Taken together, we provide evidence for a new feedback regulation between the transcription factor WRKY53 and the antioxidative enzymes, which is illustrated for CAT2 in a model (Supplemental Figure S4).

5. Conclusions

Senescence is an important developmental process that substantially contributes to the fitness of plants. The aim of senescence is to optimize and efficiently utilize carbon, nitrogen, and mineral resources. Reallocation of these resources from senescing tissues to maturing seeds or fruits has also a major impact on yield quantity and the quality of crop plants. However, to maximize and guarantee quality and quantity of crop harvests, the correct timing of onset and progression is essential. In contrast, premature senescence, which can be induced by abiotic and biotic stresses, is often responsible for crop losses. Therefore, understanding the regulatory networks coordinating this process will in the long-run be helpful for tightly controlling senescence and avoiding premature induction. In contrast to other research groups, which take more systemic approaches, we aim to decipher the complex regulatory network around the transcription factor WRKY53 in the model plant *Arabidopsis* in more detail. We have already uncovered different regulatory mechanisms to control expression, activity and protein amount of this transcription factor. Here, we found a new and additional regulatory cue in which a complex formation between different antioxidative enzymes and the WRKY53 protein leads to the inactivation of both partners. However, as H_2O_2 can boost the expression of the *WRKY53* gene, this creates a new positive feedback loop, as inhibition of CAT and APX activity will lead to an increase in H_2O_2 content, which further activates *WRKY53* expression. However, at least in the case of the catalases, increasing amounts of WRKY53 will activate the gene expression of all three catalases, which, in turn, then reduces H_2O_2 contents, again creating a negative feedback loop. Moreover, the responsiveness of *WRKY53* expression to H_2O_2 is dependent on the developmental stage. This indicates that a delicate balance between H_2O_2, WRKY53 protein amount, antioxidative enzyme amount and activity is installed in the leaf cells of *Arabidopsis*. As catalases in particular have a plethora of different interaction partners, the antioxidative enzyme might have a role in coordinating many different cellular functions. In the future, this knowledge will be fed into modelling approaches to achieve better insights into the functioning of such complex regulatory networks [52], which might enable us to simulate what happens if specific components of the network are manipulated. In

this sense, a detailed understanding of senescence regulation in the model plant *Arabidopsis* will provide new candidates for the further improvement of agricultural plants.

Supplementary Materials: The following supporting information can be downloaded at: https://www.mdpi.com/article/10.3390/antiox13030315/s1, Figure S1: Workflow to characterize in vivo protein interaction partners of WRKY53; Figure S2: Recombinant WRKY proteins, Figure S3: Catalase activity versus protein amount; Figure S4: Model of the feedback regulation between WRKY53 and CAT2. Table S1: soil contents; Table S2: antioxidative enzymes detected by LC/MS-MS of immunoprecipitated proteins using anti-WRKY53 antibodies; Table S3: Percentage of BiFC cells in CytoFLEX analyses.

Author Contributions: Conceptualization, U.Z. and J.D.; methodology, A.G.A.G., J.D., N.F. and P.W.; validation, A.G.A.G. and J.D.; formal analysis, A.G.A.G. and J.D., investigation, A.G.A.G., J.D., N.F. and P.W.; writing—original draft preparation, U.Z.; writing—review and editing, all authors.; visualization, A.G.A.G., J.D. and U.Z.; supervision, U.Z. and J.D.; project administration, U.Z.; funding acquisition, U.Z. All authors have read and agreed to the published version of the manuscript.

Funding: This work was funded by the Deutsche Forschungsgemeinschaft (DFG) CRC 1101 (B06). The purchase of the laser scanning microscope was also supported by the Deutsche Forschungsgemeinschaft (DFG) by a grant for scientific equipment (INST 37/965-1 FUGG).

Institutional Review Board Statement: Not applicable.

Informed Consent Statement: Not applicable.

Data Availability Statement: The original contributions presented in the study are included in the article and Supplementary Materials, further inquiries can be directed to the corresponding author.

Acknowledgments: We thank the proteome center of the University of Tuebingen for performing the LC/MS-MS analyses. We thank the Nottingham Arabidopsis Stock Centre (NASC) for providing the seeds for the T-DNA insertion lines SALK_116446 and SALK_034157. We acknowledge support by Open Access Publishing Fund of University of Tuebingen.

Conflicts of Interest: The authors declare no conflicts of interest.

References

1. Breeze, E.; Harrison, E.; McHattie, S.; Hughes, L.; Hickman, R.; Hill, C.; Kiddle, S.; Kim, Y.S.; Penfold, C.A.; Jenkins, D.; et al. High-resolution temporal profiling of transcripts during Arabidopsis leaf senescence reveals a distinct chronology of processes and regulation. *Plant Cell* **2011**, *23*, 873–894. [CrossRef] [PubMed]
2. Woo, H.R.; Koo, H.J.; Kim, J.; Jeong, H.; Yang, J.O.; Lee, I.H.; Jun, J.H.; Choi, S.H.; Park, S.J.; Kang, B.; et al. Programming of plant leaf senescence with temporal and inter-organellar coordination of transcriptome in Arabidopsis. *Plant Physiol.* **2016**, *171*, 452–467. [CrossRef] [PubMed]
3. Balazadeh, S.; Kwasniewski, M.; Caldana, C.; Mehrnia, M.; Zanor, M.I.; Xue, G.P.; Mueller-Roeber, B. ORS1, an H_2O_2-responsive NAC transcription factor, controls senescence in *Arabidopsis thaliana*. *Mol. Plant* **2011**, *4*, 346–360. [CrossRef]
4. Balazadeh, S.; Siddiqui, H.; Allu, A.D.; Matallana-Ramirez, L.P.; Caldana, C.; Mehrnia, M.; Zanor, M.I.; Köhler, B.; Mueller-Roeber, B. A gene regulatory network controlled by the NAC transcription factor ANAC092/AtNAC2/ORE1 during salt-promoted senescence. *Plant J.* **2010**, *62*, 250–264. [CrossRef]
5. Guo, Y.; Cai, Z.; Gan, S. Transcriptome of Arabidopsis leaf senescence. *Plant Cell Environ.* **2004**, *27*, 521–549. [CrossRef]
6. Zhang, Y.; Ji, T.T.; Li, T.T.; Tian, Y.Y.; Wang, L.F.; Liu, W.C. Jasmonic acid promotes leaf senescence through MYC2-mediated repression of CATALASE2 expression in Arabidopsis. *Plant Sci.* **2020**, *299*, 110604. [CrossRef]
7. Yolcu, S.; Li, X.; Li, S.; Kim, Y.J. Beyond the genetic code in leaf senescence. *J. Exp. Bot.* **2018**, *69*, 801–810. [CrossRef]
8. Ay, N.; Irmler, K.; Fischer, A.; Uhlemann, R.; Reuter, G.; Humbeck, K. Epigenetic programming via histone methylation at *WRKY53* controls leaf senescence in *Arabidopsis thaliana*. *Plant J.* **2009**, *58*, 333–346. [CrossRef]
9. Brusslan, J.A.; Rus Alvarez-Canterbury, A.M.; Nair, N.U.; Rice, J.C.; Hitchler, M.J.; Pellegrini, M. Genome-wide evaluation of histone methylation changes associated with leaf senescence in Arabidopsis. *PLoS ONE* **2012**, *7*, e33151. [CrossRef]
10. Shippers, J.H.M. Transcriptional networks in leaf senescence. *Curr. Opin. Plant Biol.* **2015**, *27*, 77–83. [CrossRef]
11. Guo, Y.; Ren, G.; Zhang, K.; Li, Z.; Miao, Y.; Guo, H. Leaf senescence: Progression, regulation, and application. *Mol. Hortic.* **2021**, *1*, 5. [CrossRef]
12. Woo, H.R.; Kim, H.J.; Lim, P.O.; Nam, H.G. Leaf senescence: Systems and dynamics aspects. *Ann. Rev. Plant Biol.* **2019**, *70*, 347–376. [CrossRef]
13. Ahmad, S.; Guo, Y. Signal transduction in leaf senescence: Progress and perspective. *Plants* **2019**, *8*, 405. [CrossRef]

14. Zentgraf, U.; Doll, J. *Arabidopsis* WRKY53, a Node of Multi-Layer Regulation in the Network of Senescence. *Plants* **2019**, *8*, 578. [CrossRef] [PubMed]
15. Bresson, J.; Bieker, S.; Riester, L.; Doll, J.; Zentgraf, U. A guideline for leaf senescence analyses: From quantification to physiological and molecular investigations. *J. Exp. Bot.* **2018**, *69*, 769–786. [CrossRef]
16. Miao, Y.; Zentgraf, U. A HECT E3 ubiquitin ligase negatively regulates Arabidopsis leaf senescence through degradation of the transcription factor WRKY53. *Plant J.* **2010**, *63*, 179–188. [CrossRef]
17. Doll, J.; Muth, M.; Riester, L.; Nebel, S.; Bresson, J.; Lee, H.C.; Zentgraf, U. *Arabidopsis thaliana* WRKY25 transcription factor mediates oxidative stress tolerance and regulates senescence in a redox-dependent manner. *Front. Plant Sci.* **2020**, *10*, 1734. [CrossRef] [PubMed]
18. Waszczak, C.; Carmody, M.; Kangasjärvi, J. Reactive oxygen species in plant signaling. *Annu. Rev. Plant Biol.* **2018**, *69*, 209–236. [CrossRef] [PubMed]
19. Li, Y.; Liu, W.; Zhong, H.; Zhang, H.L.; Xia, Y. Redox-sensitive bZIP68 plays a role in balancing stress tolerance with growth in Arabidopsis. *Plant J.* **2019**, *100*, 768–783. [CrossRef]
20. Dietz, K.J. Redox regulation of transcription factors in plant stress acclimation and development. *Antioxid. Redox Signal.* **2014**, *21*, 356–372. [CrossRef]
21. Zimmermann, P.; Heinlein, C.; Orendi, G.; Zentgraf, U. Senescence specific regulation of catalases in *Arabidopsis thaliana* (L.) Heynh. *Plant Cell Environ.* **2006**, *2*, 1049–1060. [CrossRef]
22. Giri, M.K.; Singh, N.; Banday, Z.Z.; Singh, V.; Ram, H.; Singh, D.; Chattopadhyay, S.; Nandi, A.K. GBF1 differentially regulates CAT2 and PAD4 transcription to promote pathogen defense in Arabidopsis thaliana. *Plant J.* **2017**, *91*, 802–815. [CrossRef] [PubMed]
23. Feierabend, J.; Schaan, C.; Hertwig, B. Photoinactivation of catalase occurs under both high and low temperature stress conditions and accompanies photoinhibition of photosystem II. *Plant Physiol.* **1992**, *100*, 1554–1561. [CrossRef] [PubMed]
24. Ye, Z.Z.; Rodriguez, R.; Tran, A.; Hoang, H.; de los Santos, D.; Brown, S.; Vellanoweth, R.L. The developmental transition to flowering represses ascorbate peroxidase activity and induces enzymatic lipid peroxidation in leaf tissue in *Arabidopsis thaliana*. *Plant Sci.* **2000**, *158*, 115–127. [CrossRef] [PubMed]
25. Shirzadian-Khorramabad, R.; Moazzenzadeh, T.; Sajedi, R.H.; Jing, H.C.; Hille, J.; Dijkwel, P.P. A mutation in Arabidopsis SAL1 alters its in vitro activity against IP_3 and delays developmental leaf senescence in association with lower ROS levels. *Plant Mol. Biol.* **2022**, *108*, 549–563. [CrossRef]
26. Miao, Y.; Laun, T.; Zimmermann, P.; Zentgraf, U. Targets of the WRKY53 transcription factor and its role during leaf senescence in Arabidopsis. *Plant Mol. Biol.* **2004**, *55*, 853–867. [CrossRef] [PubMed]
27. Yang, L.; Ye, C.; Zhao, Y.; Cheng, X.; Wang, Y.; Jiang, Y.Q.; Yang, B. An oilseed rape WRKY-type transcription factor regulates ROS accumulation and leaf senescence in *Nicotiana benthamiana* and Arabidopsis through modulating transcription of *RbohD* and *RbohF*. *Planta* **2018**, *247*, 1323–1338. [CrossRef] [PubMed]
28. Wang, Y.; Cui, X.; Yang, B.; Xu, S.; Wei, X.; Zhao, P.; Niu, F.; Sun, M.; Wang, C.; Cheng, H.; et al. WRKY55 transcription factor positively regulates leaf senescence and the defense response by modulating the transcription of genes implicated in the biosynthesis of reactive oxygen species and salicylic acid in Arabidopsis. *Development* **2020**, *147*, dev189647. [CrossRef]
29. Bradford, M.M. A rapid and sensitive method for the quantification of microgram quantities of protein utilizing the principle of protein-dye binding. *Anal. Biochem.* **1976**, *72*, 48–254. [CrossRef]
30. Chandlee, J.M.; Scandalios, J.C. Gene expression during early kernel development in *Zea mays*. *Dev. Genet.* **1983**, *4*, 99–115. [CrossRef]
31. Beauchamp, C.; Fridovic, I. Superoxide dismutase: Improved assays and an assay applicable to acrylamide gels. *Anal. Biochem.* **1971**, *44*, 276–287. [CrossRef]
32. Mittler, R.; Zilinskas, A.B. Detection of ascorbate peroxidase activity in native gels by inhibition of the ascorbate-dependent reduction of nitroblue tetrazolium. *Anal. Biochem.* **1993**, *212*, 540–546. [CrossRef]
33. Mehlhorn, D.G.; Wallmerothm, N.; Berendzen, K.W.; Grefen, C. 2in1 vectors improve in planta BiFC and FRET analysis. *Methods Mol. Biol.* **2018**, *691*, 139–158. [CrossRef]
34. Grefen, C.; Blatt, M.R. A 2in1 cloning system enables ratiometric bimolecular fluorescence complementation (rBiFC). *Biotechniques* **2012**, *53*, 311–314. [CrossRef]
35. Cathcart, R.; Schwiers, E.; Ames, B.N. Detection of picomole levels of hydroperoxides using a fluorescent dichlorofluorescein assay. *Anal. Biochem.* **1983**, *134*, 111–116. [CrossRef]
36. Pfaffl, M.W. A new mathematical model for relative quantification in real-time RT-PCR. *Nucleic Acids Res.* **2001**, *29*, e45. [CrossRef]
37. Arvidsson, S.; Kwasniewski, M.; Riano-Pachon, D.M.; Mueller-Roeber, B. QuantPrime-a flexible tool for reliable high-throughput primer design for quantitative PCR. *BMC Bioinf.* **2008**, *9*, 465. [CrossRef] [PubMed]
38. Knockenhauer, K.E.; Schwartz, T.U. The Nuclear Pore Complex as a Flexible and Dynamic Gate. *Cell* **2016**, *164*, 1162–1171. [CrossRef] [PubMed]
39. Sandalio, L.M.; Peláez-Vico, M.A.; Molina-Moya, E.; Romero-Puertas, M.C. Peroxisomes as redox-signaling nodes in intracellular communication and stress responses. *Plant Phys.* **2021**, *186*, 22–35. [CrossRef] [PubMed]

40. Sewelam, N.; Jaspert, N.; Van Der Kelen, K.; Tognetti, V.B.; Schmitz, J.; Frerigmann, H.; Stahl, E.; Zeier, J.; Van Breusegem, F.; Maurino, V.G. Spatial H_2O_2 signaling specificity: H_2O_2 from chloroplasts and peroxisomes modulates the plant transcriptome differentially. *Mol. Plant* **2014**, *7*, 1191–1210. [CrossRef] [PubMed]
41. Zentgraf, U.; Andrade-Galan, A.G.; Bieker, S. Specificity of H_2O_2 signaling in leaf senescence: Is the ratio of H_2O_2 contents in different cellular compartments sensed in Arabidopsis plants? *Cell. Mol. Biol. Lett.* **2022**, *27*, 4. [CrossRef] [PubMed]
42. Su, T.; Wang, P.; Li, H.; Zhao, Y.; Lu, Y.; Dai, P.; Ren, T.; Wang, X.; Li, X.; Shao, Q.; et al. The Arabidopsis catalase triple mutant reveals important roles of catalases and peroxisome-derived signaling in plant development. *J. Integr. Plant Biol.* **2018**, *60*, 591–607. [CrossRef] [PubMed]
43. Guo, P.; Li, Z.; Huang, P.; Li, B.; Fang, S.; Chu, J.; Guo, H. A tripartite amplification loop involving the transcription factor WRKY75, salicylic acid, and reactive oxygen species accelerates leaf senescence. *Plant Cell* **2017**, *29*, 2854–2870. [CrossRef] [PubMed]
44. Kandlbinder, A.; Finkemeier, I.; Wormuth, D.; Hanitzsch, M.; Dietz, K.J. The antioxidant status of photosynthesizing leaves under nutrient deficiency: Redox regulation, gene expression and antioxidant activity in Arabidopsis thaliana. *Physiol. Plant.* **2004**, *120*, 63–73. [CrossRef] [PubMed]
45. Miyake, C.; Asada, K. Inactivation mechanism of ascorbate peroxidase at low concentrations of ascorbate: Hydrogen peroxide decomposes compound I of ascorbate peroxidase. *Plant Cell Physiol.* **1986**, *37*, 423–430. [CrossRef]
46. Zou, J.J.; Li, X.D.; Ratnasekera, D.; Wang, C.; Liu, W.X.; Song, L.F.; Zhang, W.Z.; Wu, W.H. Arabidopsis CALCIUM-DEPENDENT PROTEIN KINASE8 and CATALASE3 Function in Abscisic Acid-Mediated Signaling and H_2O_2 Homeostasis in Stomatal Guard Cells under Drought Stress. *Plant Cell* **2015**, *27*, 1445–1460. [CrossRef] [PubMed]
47. Walton, P.A.; Brees, C.; Lismont, C.; Apanasets, O.; Fransen, M. The peroxisomal import receptor PEX5 functions as a stress sensor, retaining catalase in the cytosol in times of oxidative stress. *Biochim. Biophys. Acta Mol. Cell Res.* **2017**, *1864*, 1833–1843. [CrossRef]
48. Inaba, J.; Kim, B.M.; Shimura, H.; Masuta, C. Virus-induced necrosis is a consequence of direct protein-protein interaction between a viral RNA-silencing suppressor and a host catalase. *Plant Physiol.* **2011**, *156*, 2026–2036. [CrossRef]
49. Kneeshaw, S.; Keyani, R.; Delorme-Hinoux, V.; Imrie, L.; Loake, G.J.; Le Bihan, T.; Reichheld, J.P.; Spoel, S.H. Nucleoredoxin guards against oxidative stress by protecting antioxidant enzymes. *Proc. Natl. Acad. Sci. USA* **2017**, *114*, 8414–8419. [CrossRef]
50. Chen, L.; Wu, R.; Feng, J.; Feng, T.; Wang, C.; Hu, J.; Zhan, N.; Li, Y.; Ma, X.; Ren, B.; et al. Transnitrosylation Mediated by the Non-canonical Catalase ROG1 Regulates Nitric Oxide Signaling in Plants. *Dev. Cell* **2020**, *53*, 444–457.e5. [CrossRef]
51. Zhan, N.; Wang, C.; Chen, L.; Yang, H.; Feng, J.; Gong, X.; Ren, B.; Wu, R.; Mu, J.; Li, Y.; et al. S-nitrosylation targets GSNO reductase for selective autophagy during hypoxia responses in plants. *Mol. Cell* **2018**, *71*, 142–154.e6. [CrossRef] [PubMed]
52. Holzheu, P.; Kummer, U. Computational systems biology of cellular processes in *Arabidopsis thaliana*: An overview. *Cell. Mol. Life Sci.* **2020**, *77*, 433–440. [CrossRef] [PubMed]

Complex formation between the transcription factor WRKY53 and antioxidative enzymes leads to reciprocal inhibition

Ana Gabriela Andrade Galan [1], Jasmin Doll [1], Natalie Faiß [1], Patricia Weber [1], and Ulrike Zentgraf [1,*]

[1]Center for Plant Molecular Biology (ZMBP), University of Tübingen, Auf der Morgenstelle 32, 72076 Tübingen, Germany; ana.andrade@zmbp.uni-tuebingen.de, jasmin.doll@zmbp.uni-tuebingen.de, natalie.faiss@zmbp.uni-tuebingen.de, pa.weber@student.uni-tuebingen.de, ulrike.zentgraf@zmbp.uni-tuebingen.de,
*Correspondence: ulrike.zentgraf@zmbp.uni-tuebingen.de

Supplemental Figure S1-S4

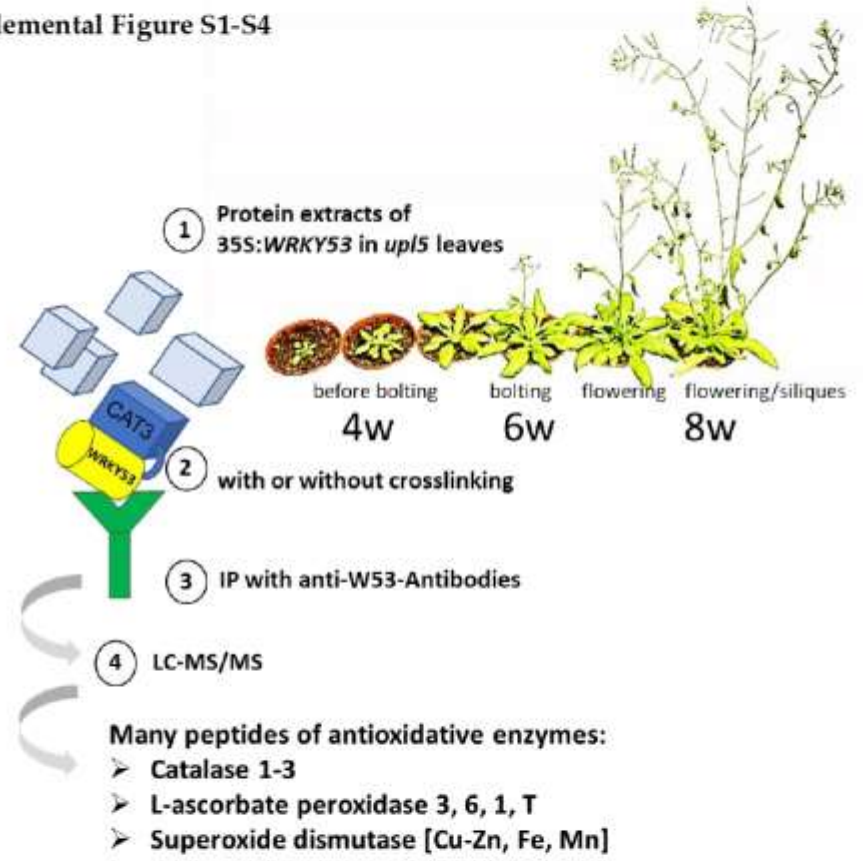

Supplemental Figure S1: Workflow to characterize *in vivo* protein interaction partners of WRKY53 using pulldown assays of WRKY53 in different developmental stages (4 week, 6 week and 8 week old plants). ① Proteins were isolated from leaves of a 35S:*WRKY53* overexpressing plants in an *upl5* mutant background. UPL5 encodes a HECT domain E3 ubiquitin ligase which is involved in the protein degradation of WRKY53, therefore higher protein levels of WRKY53 can be achieved in the *upl5* mutant background. ② Proteins were either used directly or were treated with formaldehyde or DSS for crosslinking. ③ CO-IP was performed using anti-WRKY53-Antibodies ④ Subsequently, LC-MS/MS analyses was performed with the pulled-down proteins as indicated in more detail in Supplemental Table 1, many peptides of antioxidative enzymes were identified.

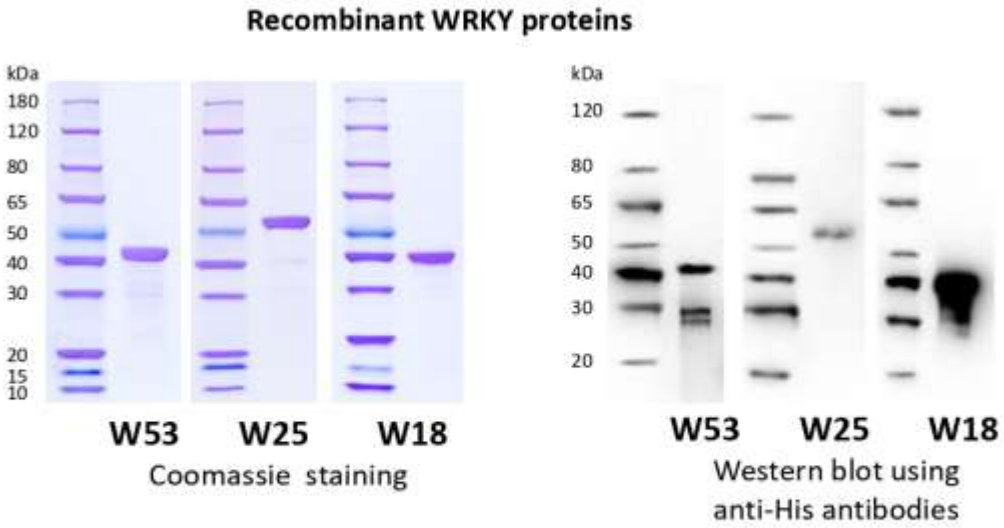

Supplemental Figure S2: SDS-PAGE of the purified proteins 8xHis tagged WRKY53, WRKY25, and WRKY18, which were used for the inhibition experiments. These proteins have been provided by Biomatik (Cambridge, Ontario, Canada).

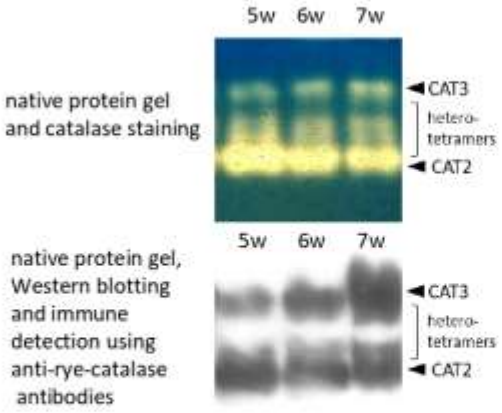

Supplemental Figure S3: Catalase activity versus protein amount.
The catalase zymogram shows catalase activities of protein extracts isolated from leaf material of 5-, 6- or 7-week-old plants (top). This native gel has been blotted and detected with anti-rye-catalase antibodies (bottom) indicating that CAT3 homotetrames are less active than CAT2 homotetrameres or heterotetrameres, if compared to the amount of proteins shown by the Wester blot.

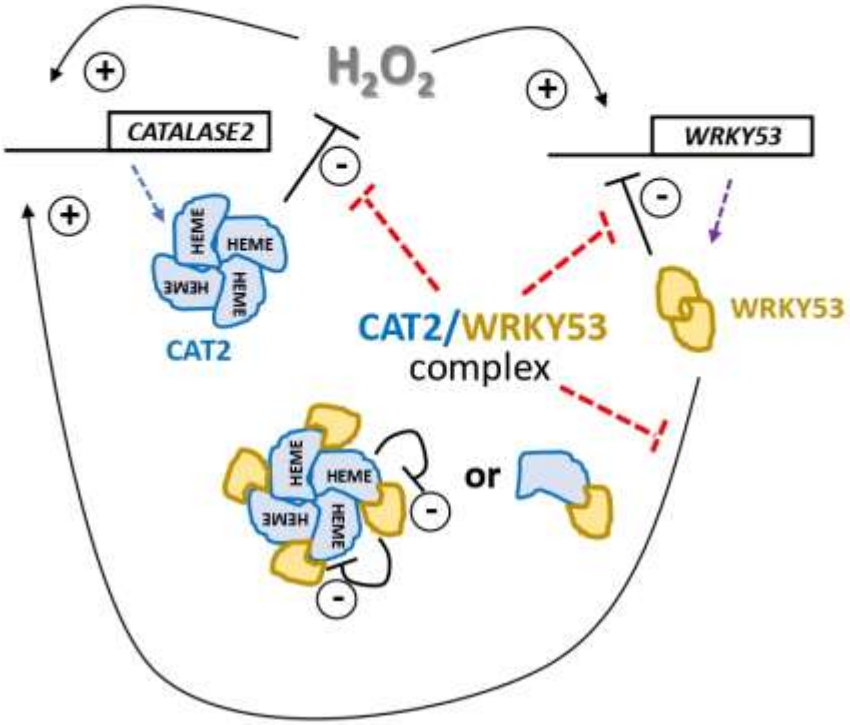

Supplemental Figure S4: Model of the feedback regulation between WRKY53 and CAT2. H_2O_2 can increase expression of the *CAT2* gene, CAT2 subunits form tetramers including a HEME group per subunit and enzyme activity can then reduce H_2O_2 content leading again to reduced gene expression (negative feed-back loop). H_2O_2 can also increase expression of the *WRKY53* gene, the WRKY53 protein can then reduce again its own expression as dimer by a direct interaction with its own promoter but also by an induction of *CAT2* gene expression which, in turn, then reduces H_2O_2 content again (negative feedback loop). However, at the same time WRKY53 protein can directly interact with either the CAT2 tetrameric complexes or only the protein subunits to inhibit CAT2 enzyme activity and WRKY53 repressor function on its own gene, both leading to increased *WRKY53* expression. This means, whenever the CAT2/WRKY53 complex is formed, WRKY53 expression is fostered, regardless whether the complex is located in the peroxisomes or in the nucleus (positive feedback loop).

Review 1: Specificity of H2O2 signaling in leaf senescence: is the ratio of H2O2 contents in different cellular compartments sensed in Arabidopsis plants?

Zentgraf, U., Andrade-Galan, A.G. & Bieker, S. Specificity of H_2O_2 signaling in leaf senescence: is the ratio of H_2O_2 contents in different cellular compartments sensed in *Arabidopsis* plants?. *Cell Mol Biol Lett* **27**, 4. 2022. https://doi.org/10.1186/s11658-021-00300-w

Zentgraf et al.
Cellular & Molecular Biology Letters (2022) 27:4
https://doi.org/10.1186/s11658-021-00300-w

Cellular & Molecular
Biology Letters

INVITED REVIEW Open Access

Specificity of H_2O_2 signaling in leaf senescence: is the ratio of H_2O_2 contents in different cellular compartments sensed in *Arabidopsis* plants?

Ulrike Zentgraf*, Ana Gabriela Andrade-Galan and Stefan Bieker

*Correspondence:
ulrike.zentgraf@zmbp.uni-tuebingen.de
ZMBP (Centre of Plant Molecular Biology), University of Tübingen, Auf der Morgenstelle 32, 72076 Tübingen, Germany

Abstract

Leaf senescence is an integral part of plant development and is driven by endogenous cues such as leaf or plant age. Developmental senescence aims to maximize the usage of carbon, nitrogen and mineral resources for growth and/or for the sake of the next generation. This requires efficient reallocation of the resources out of the senescing tissue into developing parts of the plant such as new leaves, fruits and seeds. However, premature senescence can be induced by severe and long-lasting biotic or abiotic stress conditions. It serves as an exit strategy to guarantee offspring in an unfavorable environment but is often combined with a trade-off in seed number and quality. In order to coordinate the very complex process of developmental senescence with environmental signals, highly organized networks and regulatory cues have to be in place. Reactive oxygen species, especially hydrogen peroxide (H_2O_2), are involved in senescence as well as in stress signaling. Here, we want to summarize the role of H_2O_2 as a signaling molecule in leaf senescence and shed more light on how specificity in signaling might be achieved. Altered hydrogen peroxide contents in specific compartments revealed a differential impact of H_2O_2 produced in different compartments. *Arabidopsis* lines with lower H_2O_2 levels in chloroplasts and cytoplasm point to the possibility that not the actual contents but the ratio between the two different compartments is sensed by the plant cells.

Keywords: Leaf senescence, Free oxygen radicals, ROS, Hydrogen peroxide, Stromules, Senescence regulation, Intracellular compartments

Introduction

Senescence is a phase of plant development and becomes visible by the degreening of leaves, in which the photosynthetic apparatus is dismantled and chlorophyll is broken down, leading to light green and yellowish leaves [1]. However, when the light green color becomes apparent, the senescence program has been initiated long before, and changes at the molecular and physiological level have already been executed [2]. Plant cells must integrate a myriad of different signals driving onset and progression of senescence [3].

In the extreme scenario the already started program can be stopped or even reversed [1]. Even though senescence is often designated as the last step in the plant's life history, it may occur from relatively early on throughout development. Older leaves in the lower canopy which are shaded by newly formed leaves or neighboring plants, or simply have reached a certain age, are sacrificed for the sake of newly developing organs, for example new leaves or stems. The aim of the senescence program is the remobilization of previously acquired resources such as nitrogen, carbon and mineral compounds out of the senescing tissues into developing parts of the plant. After remobilization has been executed, the senescent organs finally die and are shed. Before anthesis, this process is called sequential leaf senescence and aims at the repartitioning of nutrients from older leaves to newly developing, non-reproductive organs. In this case, the senescence program is restricted to a single organ. After anthesis, monocarpic senescence sets in and nutrients are now reallocated to the newly developing reproductive organs such as siliques and seeds. After this transition to reproductive growth during monocarpic senescence, potentially all leaves of a plant can now execute senescence, which finally leads to the death of the whole plant except for the newly formed seeds [4]. This systemic onset has to be coordinated between the different organs. However, how the local and systemic leaf senescence programs are discriminated is largely unknown. Even though a master regulator for leaf senescence was intensively searched for, it became clear that such a regulator does not exist. In contrast, multi-layered complex regulatory networks are in place to drive onset, progression and, in extreme cases, reversal of leaf senescence [3, 5]. For example, the transcription factor WRKY53 is just one of more than a hundred transcription factors driving the onset of senescence. Solely this transcription factor is tightly regulated at several levels. Not only is its expression responsive to ROS, jasmonic or salicylic acid (JA and SA) and influenced by more than 12 other transcription factors, also its activity is regulated by different molecular mechanisms, e.g. phosphorylation by MAPKKK1 or by changing interaction partners. On top of that, the degradation of the WRKY53 protein is controlled though a HECT ubiquitin ligase (UPL5) which exhibits an opposite expression pattern compared to WRKY53 itself. This ensures that even if the gene is mis-expressed for whatever reason, the protein content is still controlled by degradation and the protein will only be stable in the cells during onset of senescence [5]. To make the story even more complicated, WKRY53 also has a role in pathogen and wounding response. The overlap between senescence and pathogen response has been recognized in many instances due to similar signals which appear to be used in both processes. Recently, the cross-regulation network between leaf senescence and plant immunity, which is mediated by SA and ROS, has been nicely summarized [6].

Moreover, the senescence program adapts to diverse environmental conditions and requires very high plasticity. All kinds of stresses, abiotic as well as biotic, are sensed and constantly integrated into the regulatory networks, in which long-lasting unfavorable conditions have the potential to induce senescence prematurely [6, 7]. This serves as an exit strategy to guarantee viable offspring even under stressful conditions. As a tradeoff, seed quantity and quality are often diminished and can significantly lower productivity of plants. Consequently, in crop plants, stress-induced premature senescence can have a major negative impact on yield quantity and quality. Even though our knowledge on the physiological changes has increased enormously during the last decades

and more and more signaling molecules acting in this process have been characterized, we are still far from understanding how this complex program is coordinated and how specificity is achieved in signaling. Almost all plant hormones are involved in regulation of this process as well as smaller signaling molecules such as calcium or ROS. All these components also have roles in other processes, so the question how specificity is achieved, especially in the case of ROS signaling, is not yet answered. How does the cell differentiate between an oxidative burst elicited by pathogen infection and the oxidative burst coinciding with the induction of senescence? In this review letter, we would like to shed light on the role of the ROS hydrogen peroxide in senescence signaling with a focus on the differences in signaling of H_2O_2 produced in different organelles. Even though hydrogen peroxide appears to be used as a signaling molecule in many different plant species, we focus on the findings in the model plant *Arabidopsis thaliana*.

General alterations in different organelles during senescence

In contrast to other cell death reactions, the long lasting and complex regulatory process to adequately execute leaf senescence requires continuous control by the nucleus as well as a constant energy supply. Consequently, not only is the nucleus kept intact until late stages of senescence, but also the mitochondria need to stay active to deliver the energy driving the process. Functionality of both organelles has to be guaranteed during onset and progression of senescence until finally both are also degraded in the terminal phase. In contrast, chloroplasts are massively restructured during progression of senescence and lose their photosynthetic function while peroxisomes are converted back to glyoxysomes with changed functional properties.

Chloroplasts

Chloroplasts are converted into "gerontoplasts" during the progression of leaf senescence. These gerontoplasts are morphologically characterized by an increased number of enlarged plastoglobuli, disorientation of the grana stacks and swelling of the thylakoids [1, 8]. These structural changes are combined with loss of function of the photosynthetic apparatus, thus allowing chlorophyll loss and photochemical capacity (F_V/F_M) to be used as parameters to describe senescence. As the majority of assimilated nutrients are stored in chloroplasts in the form of photosynthetic proteins, the remobilization of chloroplastic components is a central feature of senescence. It was estimated in the 1980s that more than 10 billion tonnes of Rubisco and 1 billion tonnes of chlorophyll are produced and degraded every year [9]. Even though removal of damaged proteins from chloroplasts takes place throughout plant development as part of the quality control of chloroplasts, chloroplast dismantling and degradation of chloroplastic proteins is strongly upregulated during senescence. Besides various types of chloroplastic proteases acting inside the chloroplasts, diverse extra-plastidic pathways mediate degradation of chloroplastic proteins. Intensive formation of different vesicles can be observed during senescence ranging from RCBs (Rubisco-containing bodies) and ATG8-interacting protein1-plasmid associated (ATI-PS) bodies, which depend on the autophagy machinery for further degradation, to SAVs (senescence-associated vacuoles) and CCVs (chloroplast vesiculation-containing vesicles) acting independently of autophagy [10, 11]. Moreover, whole chloroplasts can be degraded by "chlorophagy" [12] or by the 26S proteasome mediated

by a cytosol-localized E3 ubiquitin ligase mainly targeting chloroplasts that over-accumulate singlet oxygen [13]. Degradation processes inside and outside the chloroplasts have to be coordinated and different pathways are induced at distinct time points during leaf senescence, e.g. chloroplast number is reduced at the later stages [11].

Peroxisomes

Peroxisomes consist of an amorphous matrix surrounded by a single membrane. Notably, the term "peroxisomes" originates from their high H_2O_2 content. A significant number of enzymatic systems capable of generating H_2O_2 are present in the peroxisomes, e.g. acyl CoA oxidase, glycolate oxidase, superoxide dismutase, urate oxidase and many others. The extensive production of H_2O_2 is counterbalance by the presence of large amounts of the H_2O_2 scavenging enzyme catalase. Besides being generated as a side product of various reactions, H_2O_2 itself has a critical role as a signal molecule in the crosstalk between peroxisomes and other organelles to coordinate cellular functions. Apart from the peroxisomal metabolism of ROS, reactive nitrogen species and reactive sulfur species with signaling functions are produced in peroxisomes [14]. Moreover, peroxisomes also have important roles in the biosynthesis of plant hormones, such as JA, indole-3-acetic acid (IAA) and SA, all of which influence leaf senescence in one way or another. Therefore, peroxisomes are important signal generators in the cell. Not only do peroxisomes undergo dynamic changes in metabolism and morphology, but also peroxisome abundance can be adjusted to environmental conditions. Moreover, the primary functions of plant peroxisomes vary with different developmental stages. Whereas peroxisomes in green leaves are mainly involved in photorespiration, peroxisomes in seeds harbor the glyoxylate cycle together with β-oxidation and are therefore called glyoxysomes. In senescent tissues, peroxisomes are converted into "gerontosomes" which resemble glyoxysomes in terms of their metabolic functions [14, 15].

Mitochondria

Even though mitochondria exhibit a driving force in programmed cell death (PCD) in animal systems, in which the loss of the mitochondrial membrane integrity leads to the release of PCD elicitors such as cytochrome C, plant mitochondrial membranes are maintained until very late stages of senescence. Thus, it is unlikely that plant mitochondria will trigger plant senescence in a similar way as they do during animal PCD. In *Arabidopsis*, functionality of the mitochondria is preserved until the latest stages of leaf senescence, even though their number drops by 30%. In contrast to structural changes observed in chloroplasts, the ultrastructure of the remaining mitochondria appears to be unchanged, retaining clearly demarcated cristae and membrane boundaries throughout the process of senescence. Integrity of mitochondria as well as their ability to provide energy are maintained during leaf senescence to drive the energetically demanding reallocation of nutrients. Transcriptome analysis combined with metabolomic approaches revealed that mitochondrial metabolism is partially reorganized to support the selective catabolism of both amino acids and fatty acids. Thereby, mitochondria provide the carbon backbone essential for nitrogen remobilization, which is of utmost importance during senescence [16]. In parallel, the alternative respiration pathway is activated during senescence [17]. An important function of the alternative oxidase (AOX) is to prevent

the formation of excess ROS. Hence, a low reduction status of the ubiquinone pool by oxidizing ubiquinol is ensured, and thus the electron flow is guaranteed [18].

The nucleus

The nucleus appears to be the command center for senescence coordination. Therefore, its overall structure and integrity are maintained to guarantee its function. However, onset and progression of this developmental process is driven by massive changes in gene expression; e.g. in *Arabidopsis thaliana* almost one quarter of all genes are differentially regulated during senescence [2]. While genes involved in degradation and mobilization of macromolecules are switched on, genes related to photosynthesis are turned off. A chronology of events has been determined by high-resolution temporal transcript profiling covering 22 time points of single leaves of a defined position within *Arabidopsis* rosettes [2]. In this chronology, activation of autophagy and transport as well as the response to ROS are prominent early events of leaf senescence. These massive changes in the transcriptome imply a central and important role for transcriptional regulators [19, 20]. Two transcription factor (TF) families, the WRKY and the NAC factors, which greatly expanded in the plant kingdom, appear to play outstanding roles in senescence regulation in *Arabidopsis* but also in other plant species [21, 22]. NAC proteins form one of the largest plant-specific TF super families, and its members control transcriptional reprogramming associated with many developmental processes including senescence [22, 23]. Recently, genome-wide dynamic modelling of transcriptional gene regulatory networks uncovered new and distinct pathways during the onset of *Arabidopsis* leaf senescence including miRNA action [24]. Besides the expansion in number, the WRKY family adopted a specific functional strategy of networking. Almost all *Arabidopsis* WRKY transcription factor genes are characterized by one or several binding motifs for WRKY factors, so called W-boxes, in their promoters, implying a complex WRKY-driven transcriptional network [25]. Moreover, complexity is increased even more by the fact that WRKY factors are also able to form homo- and heterodimers with different functional properties [26–28].

A long-lasting H_2O_2 increase acts as a signal in leaf senescence of *Arabidopsis*

In the absence of stress, developmental senescence is mainly driven by the actual age of the individual leaves and the age and developmental stage of the whole plant [29]; however, the mechanisms by which plants sense these parameters is still not well understood. The senescence program is synergistically as well as antagonistically influenced by almost all plant hormones [3, 20]. Moreover, during the last two decades, it became evident that ROS, and especially hydrogen peroxide, can function as signaling molecules in developmental as well as stress-induced senescence. On the one hand, ROS can have a direct impact on gene expression by altering the expression as well as the activity of transcription factors [2, 30–33], thereby modulating regulatory processes. On the other hand, ROS can oxidize more or less all kinds of macromolecules, influencing a variety of physiological changes. Less well-known signaling compounds such as melatonin are involved in postharvest senescence regulation by modulating the ROS homeostasis [34].

ROS are inevitable by-products of aerobic metabolism in all organisms. They are formed by energy transfer to or partial reduction of molecular oxygen (O_2) producing

either free radicals such as superoxide ($O^{\cdot-}_2$) and hydroxyl radicals ($OH^{\cdot}$) or non-radical but highly reactive molecules such as hydrogen peroxide (H_2O_2) and singlet oxygen ($^1O_2$), of which the latter is generated exclusively in the chloroplasts. Here, excess light energy results in an electron spin shift in the molecular orbitals, which renders $^1O_2$ very unstable and highly reactive. Except H_2O_2, which has a half-life of milliseconds to seconds [35] and can traverse longer distances, including across plant cell membranes via aquaporins [36], all ROS have very short half-lives and relatively high oxidation potentials, and thus act close to their site of production. All ROS can act as signaling molecules but, when present in excess, are toxic for the cell. Therefore, a delicate balance between ROS production and scavenging needs to be established in all cellular compartments. $OH^{\cdot}$ is the most reactive and thus most toxic ROS. Despite the apparent lack of an established system for the tight control of hydroxyl radicals, its function in multiple processes has been documented as e.g. ion flux in roots, germination, stomatal closure, or post-harvest senescence of fruits [37–40]. Most recently, Hancock and Russel [41] suggested a H_2-dependent scavenging mechanism for $OH^{\cdot}$. However, the reactive and short-lived nature of $OH^{\cdot}$ renders its study challenging. In any case, the cell should avoid the Fenton reaction between H_2O_2 and $O^{\cdot-}_2$ which produces $OH^{\cdot}$ in the presence of metal, especially iron, ions [42]. The inherent reactivity of different ROS determines their reactivity towards specific sites in all kinds of proteins. Whereas due to its high oxidative potential $OH^{\cdot}$ does not pick and choose, the superoxide anion ($O^{\cdot-}_2$) predominately attacks iron-sulfur ([Fe-S]) clusters while H_2O_2 targets Cys residues. Therefore, the subcellular colocalization of short-lived ROS and their respective targets might contribute to the ROS signaling specificity [43].

Similar to plant hormones, ROS participate in a wide range of developmental and stress-related signaling processes, leaving the question largely open, how specificity can be achieved, how the plant cells can differentiate signaling cues and elicit an appropriate response. So far, no clear signature, e.g. the amplitude, frequency or duration of Ca^{2+} spikes [44], can be linked to ROS or more specifically to H_2O_2 signaling. In contrast to calcium signaling, which is executed by storage and release of Ca^{2+} [45], ROS signaling is controlled by production and scavenging. In *Arabidopsis*, a network of at least 152 genes is involved in managing the ROS levels [46]. However, in contrast to e.g. the oxidative burst after pathogen infection or wounding lasting for minutes to hours [42], we observed a clear difference in the duration of the senescence-related H_2O_2 signal, lasting for more than a week during induction of monocarpic senescence, at least in *Arabidopsis* or oil-seed rape [47, 48]. Measurement of intracellular H_2O_2 contents in different leaves of a single *Arabidopsis* rosette indicated that the increase during onset of monocarpic senescence can be observed more prominently in the younger leaves (Fig. 1) [48], suggesting that sequential senescence might use different signals.

This long-term intracellular H_2O_2 increase at the onset of monocarpic senescence in *Arabidopsis* and oilseed rape is predominately due to sophisticated regulation of the activities of the H_2O_2 scavenging enzymes catalase (CAT) and ascorbate peroxidase (APX) [48, 49]. All subcellular compartments are equipped with their own enzymatic and non-enzymatic scavenging systems. While catalases are predominantly located in the peroxisomes, different APX isoforms are found in chloroplasts, mitochondria, the cytosol and the outer membrane of the peroxisomes. Catalases have a very low

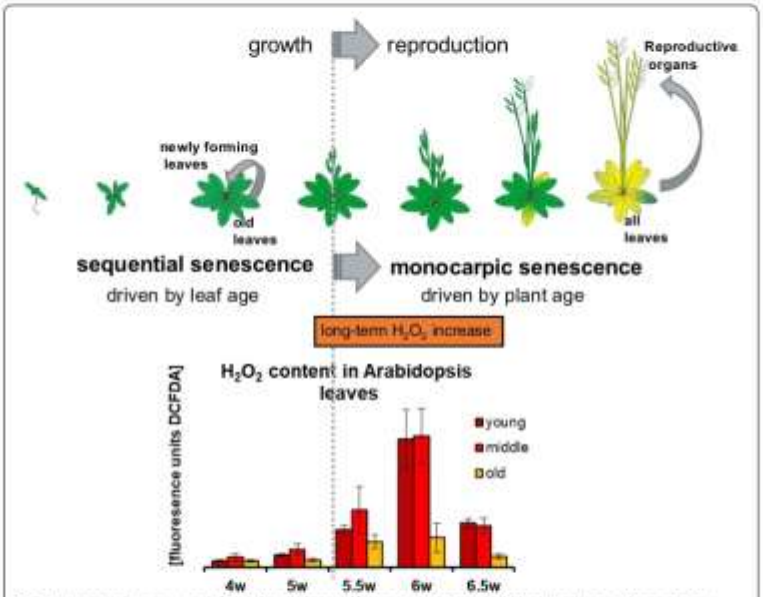

Fig. 1 A schematic drawing of the development of the model plant *Arabidopsis thaliana* is shown at the top. At the transition from growth to reproduction (dotted grey line), senescence switches from sequential senescence which remobilizes nutrients from old to young leaves to monocarpic senescence in plants which started to bolt and flower. Now nutrients are remobilized from all rosette leaves to the now developing reproductive organs. During the time interval of bolting and flowering, intracellular hydrogen peroxide contents were measured and are indicated in arbitrary units of DCFDA fluorescence. H_2O_2 levels increased during transition to reproductive growth and the long-term increase at the transition point is indicated by the orange bar. H_2O_2 concentration showed more pronounced elevations in young (dark red; pos. 8–12 within the rosette) and middle-aged leaves (red, pos.4–7 within the rosette) than in old leaves (orange, pos. 1–3 within the rosette). The age of the plants is indicated in weeks after sowing (w)

affinity for H_2O_2, with a K_m of approx. 43 mM, but have a high reaction rate and are highly abundant, which compensates for this low affinity [50]. Under oxidative stress conditions, CAT can be retained in the cytosol to protect this compartment against H_2O_2-mediated redox changes and intensify defenses against oxidative damage [51]. In *Arabidopsis*, APX3 and 5 isoforms are associated with the outer peroxisomal membrane. This localization and the much higher affinity of APXs to H_2O_2 as compared to CAT (100 µM), could be responsible for the tight control of H_2O_2 leakage from peroxisomes to the cytosol [52–55]. Furthermore, APX1, 2 and 6 are present in the cytoplasm and two additional APX isoforms are associated with the stroma (sAPX) and the thylakoid membranes (tAPX) of the chloroplasts. Therefore, CAT and APX are positioned strategically to tightly control H_2O_2 concentrations and to ensure that H_2O_2 can act as a signaling molecule [56].

To allow for a long-term intracellular H_2O_2 increase at the onset of monocarpic senescence, in the first place *CAT2* gene expression starts to decline at bolting time through inhibition of transcription by the bZIP transcription factor G-Box binding factor 1 (GBF1). This factor is most likely activated by phosphorylation through casein kinase II

and translocation to the nucleus [48, 57–59]. As CAT2 protein has a high turn-over rate and accounts for approximately 80% of the total CAT activity in leaves [60], this rapidly leads to a decline in CAT2 enzyme activity and an increase in H_2O_2 concentration. In addition, APX1 activity also declines at the same time during bolting and flowering, but its activity is restored at later time points. In this case, gene expression is not downregulated but inhibition of activity appears to be carried out post-transcriptionally [61]. All in all, this leads to low protection against H_2O_2 in the cytosol as well as in the peroxisomes. Miyake and Asada [62] found that under low concentrations of ascorbate, hydrogen peroxide damages compound I of ascorbate peroxidase and inactivates enzyme activity. Furthermore, an experiment with suspension culture cells also showed that, paradoxically, APX activity can be inhibited by its own substrate H_2O_2. H_2O_2 treatment of whole plants revealed that this inhibition can only be induced during the time window of bolting and flowering, and exogenous application of H_2O_2 is only effective during this period [48]. Moreover, removal of the stem leads to restoration of APX activity, and subsequent rebolting induces a second period of APX inactivation [63], clearly indicating a connection of the inhibitory mechanism to the bolting and flowering state. This means that APX is rendered sensitive towards hydrogen peroxide by a so far unknown mechanism during this specific period. Thus, at this time point, H_2O_2 concentrations further increase and create a positive feedback loop. After a certain time interval, inhibition of APX is released again and, in addition, *CAT3* expression and enzyme activity start to increase. This regulatory cue results in a long-term hydrogen peroxide elevation as illustrated in Fig. 1. If downregulation of *CAT2* expression and activity is abolished in *gbf1* knock-out plants, APX activity is not inhibited by increasing H_2O_2 amounts, no long-term H_2O_2 increase is created and the onset of senescence is delayed [57]. This clearly indicates that this long-lasting H_2O_2 elevation acts as a signal to induce monocarpic senescence.

Furthermore, so far only scant attention has been dedicated to the fact that the circadian clock also triggers transcriptional regulation of ROS-responsive genes, ROS homeostasis, tolerance to oxidative stress [64–66] as well as senescence [67]. Not only do hydrogen peroxide production and scavenging display time-of-day phases but also mutations in the core-clock regulator, CIRCADIAN CLOCK ASSOCIATED 1, as well as mis-expression of components of the evening complex, EARLY FLOWERING 3, LUX ARRHYTHMO, and TIMING OF CAB EXPRESSION, affect ROS production [67]. This clearly indicates a global effect of the clock on the ROS network, and hence Sanchez and Kay [68] have suggested calling the circadian clock the "mastermind" of plant life. Interestingly, the period of the diurnal rhythm also changes during senescence, decreasing from 24 h in young plants to 22–23 h in old plants [69]. Therefore, time of the day should always be considered in future research.

Impact of H_2O_2 generated in different subcellular compartments in *Arabidopsis* leaves

In the last two decades it has become clear that the ROS concentrations in the cytoplasm and in different organelles have a different impact on senescence. Changing the H_2O_2 levels in different subcellular compartments has different effects on the senescence program ([49, 70], unpublished observations). Increasing H_2O_2 production in peroxisomes or in chloroplasts induced two different types of responses, one of which is

independent and the other is dependent on the site of H_2O_2 production. While the independent response comprised the activation of more general oxidative stress response genes, an H_2O_2 increase in chloroplasts specifically induced early senescence signaling components, including transcription factors and biosynthetic genes involved in production of secondary signaling molecules [70]. In 2013, Rosenwasser et al. established a bioinformatic tool called "ROSMETER" for the identification of transcriptomic signatures related to ROS type and production site [71]. Interestingly, an unexpected but highly significant ROS transcriptome signature of mitochondrial stress was detected during the early stages of leaf senescence by the ROSMETER when the high-resolution transcriptome dataset of leaf senescence in *Arabidopsis* of Breeze et al. [2] was analyzed. This signature was defined by different reference plants: (i) rotenone treated plants and (ii) *AOX1*-T-DNA insertion lines under mild drought and light stress and (iii) antisense *AOX1a* plants. Rotenone treatment inhibits complex I of the respiratory electron transport chain and leads to induction of the AOX pathway and thereby to the reduction of ROS production [72, 73], while *AOX1*-T-DNA insertion as well as antisense *AOX1a* expression abolishes the alternative respiration pathway and would therefore increase mitochondrial ROS production, at least under stress conditions. However, there was a strong positive correlation of the early senescence expression profiles with rotenone treatment starting at 23 days after sowing and almost at the same time, from day 25 on, a negative correlation with *AOX1*-T-DNA insertion. This would mean that the transcriptome signature at early stages of leaf senescence would point to low mitochondrial ROS production. However, long-term antimycin A treatment which inhibits complex III of the respiratory chain and induces the AOX pathway or overexpression of *AOX1a* diminished ROS production but did not significantly alter senescence [74]. Therefore, the role of mitochondrial ROS in leaf senescence is still debatable. However, antimycin A also has effects on the cyclic electron flow in the chloroplasts [75].

Peroxisomes appear to be the most oxidized cellular organelles, with a redox potential of approximately − 360 mV [76]. Peroxisomes are one of the main sources of intracellular ROS generation. In photosynthetic tissue, photorespiration is the main source of H_2O_2 production in peroxisomes, contributing up to 70% to the total H_2O_2 production in plant cells [42]. In addition, photorespiration needs coordination of the chloroplasts, peroxisomes, and mitochondria in the cytosol, and often close contacts of these organelles can be observed, most likely to directly exchange substrates. Interestingly, at these contact sites H_2O_2 accumulation was observed inside the peroxisomes, also pointing to a role of H_2O_2 in organelle communication [77]. Using in vivo imaging with fluorescent proteins targeted to peroxisomes, rapid formation of tubular extensions called peroxules was observed in response to changes in ROS levels. Not only could these peroxules participate in the transfer of metabolites to mitochondria and chloroplasts, they could also be involved in ROS flux between these compartments, even though so far there is no direct evidence for this assumption [56]. In contrast, similar dynamic structures in chloroplasts called stromules can transfer H_2O_2 from chloroplasts to nuclei [78, 79]; however, to date no contact of peroxules to nuclei has been described. To counterbalance the large amounts of H_2O_2 generated in peroxisomes, 10–25% of the total peroxisomal proteins are catalases [80], in which CAT2 accounts for approximately 80% of the total catalase activity. As already mentioned above, *CAT2* regulation is a central element of

creating the long-lasting increase of intracellular H_2O_2 at bolting and flowering time, which is used as a senescence signal [48, 57]. Altering peroxisomal H_2O_2 by different means induces changes in gene expression [65, 66, 81, 82] that differ from those induced by chloroplast-derived H_2O_2 [70]. Thus, peroxisomal H_2O_2 clearly participates in retrograde signaling to the nucleus. However, the underlying molecular mechanisms and crosstalk with ROS from other compartments still have to be elucidated [56, 83]. How this specificity is produced downstream of the production is unclear. Thiol-based antioxidants such as peroxiredoxins, thioredoxins, and glutaredoxins are likely to be involved in ROS signaling cascades [84]. However, H_2O_2 can leak out of all compartments to the cytosol, so the cytosol most likely acts as a key site of redox signal integration. Thus, MAPK pathways in the cytoplasm are proposed to integrate ROS signals from different organelles to regulate the gene expression in the nucleus [85].

Like peroxisomes, plastids form stroma-filled tubular extensions surrounded by the envelope membrane called stromules. Stromules are dynamic structures that extend along actin microfilaments and the ER. In chloroplasts, stromule frequency increases during the day or in response to light-sensitive redox signals [86]. Interestingly, stromules can still form on isolated chloroplasts after extraction from the cytoplasm, pointing to the fact that stromule formation is plastid autonomous. In addition, plastid-derived vesicles are suggested to bud from stromules through tip shedding or simple breakage, either to recycle plastid content during nutrient stress, to remove toxic molecules, or for intracellular communication [87]. These stromules allow the plastid compartment to make direct contacts to other subcellular compartments such as other plastids, mitochondria or nuclei. Metabolites as well as proteins can flow through these connective tunnels. Moreover, using a nuclear-targeted H_2O_2 sensor protein (HyPER) [88], the translocation of ROS generated in chloroplasts into adjacent nuclei could be observed [89]. This suggests that stromules have a function in retrograde signaling in channeling and speeding up signal transduction directly to the nucleus, avoiding the scavenging systems of the cytoplasm [89]. Additionally, organellar H_2O_2 can oxidize thiol groups of specific proteins, thereby converting the ROS signal into thiol redox signals [90, 91].

In addition, changes in the apoplastic space appear to be involved in signaling and molecular trafficking during senescence [92]. Along with variations in the volume and pH of the apoplastic fluid, leaf senescence-related changes in the secretome included many proteins involved in stress responses and ROS metabolism, indicating that leaves of different ages control stress responses differentially to balance growth or survival at the whole plant level [93]. Moreover, production of apoplastic ROS can influence ROS generation in the chloroplast and both together can have an impact on gene expression in the nucleus [94].

On top of that, all these forms of retrograde signaling between the different organelles and the nucleus have to be integrated to finetune the final outcome of gene expression. We are far from understanding which molecular mechanisms underly this crosstalk. Recently, the protein RADICAL-INDUCED CELL DEATH1 (RCD1) has been characterized as a molecular component that allows a dialog between the retrograde signals of both mitochondria and chloroplasts. On one hand, RCD1 directly interacts and inhibits ANAC013 and ANAC017, two regulatory proteins that usually activate a set of genes involved in repair of mitochondria. On the other hand, the nuclear-localized RCD1

changes abundance, redox state and oligomerization in response to ROS generated in the chloroplasts. Interestingly, the interaction domain with the NAC factors was also necessary for the sensitivity to chloroplastic ROS [95].

The search for ROS receptors is far from complete and still has to be continued. It can be speculated that a plethora of ROS sensors is likely to exist in numerous compartments including the apoplast, cytosol, and organelles. In addition, the respective downstream signaling components are yet to be identified. Plant cells may be able to decode specific ROS-dependent signatures by monitoring the relative intensity of redox stimuli at different locations. Such signatures could be part of the activation of appropriate responses [85].

In vivo imaging using fluorescent dyes and sensor proteins

Colorimetric methods using nitro blue tetrazolium (NBT) and/or diaminobenzidine (DAB) were initially used to detect ROS in cells, tissues, and organs. However, these methods were not suitable to analyze dynamic ROS levels in vivo. To solve this problem, a collection of different fluorescent dyes was established, in which different dyes exhibit different properties with regard to specificity and cell permeability, allowing in vivo imaging in real time. From among different fluorescent probes which were tested for in vivo imaging (DHE, H2DCFDA, H2HFF-OxyBURST, Amplex red, SOSG, and PO1), H2DCFDA displayed the highest signal-to-noise ratio [96]. One of the drawbacks of these dyes is that often the reactions between ROS and dye are not reversible and the dyes have to be reapplied. In parallel, transgenic approaches were developed using ROS-responsive promoters coupled to reporter genes [97, 98], which also allow one to measure ROS contents at the whole plant level and to follow up systemic ROS signaling. Moreover, protein-based fluorescent sensors have been developed and by now a variety of genetically encoded fluorescent redox probes are available [99]. For example, the redox-sensitive roGFP [100] or the H_2O_2 sensitive HyPER [88] can image more precisely the in vivo redox conditions and/or ROS concentrations in cells utilizing ratiometric measurements with two different wavelengths of the excitation laser light. These protein-based approaches also opened up the possibility to direct the proteinaceous sensors to different subcellular compartments via signal peptides or other localization signals. In vivo imaging using these sensor proteins can now be employed to resolve the spatiotemporal dynamics inside the cells and even in different subcellular compartments. Very recently the application of this technique could demonstrate that ROS locally generated in chloroplasts of intact *Arabidopsis* seedlings by methyl viologen treatment cause changes in H_2O_2 and glutathione redox potential in other subcellular compartments such as the cytosol and mitochondria [101]. However, given the nature of these sensors, one has to keep in mind that the expression of such sensor proteins cannot only be used to measure in vivo ROS concentrations but at the same time scavenge ROS and thereby also influence intracellular ROS concentrations. When using these sensor lines for long-term studies of ROS levels during senescence, we observed differences in production in different compartments but encountered the problem that all these lines showed altered senescence phenotypes compared to non-transgenic lines ([49], unpublished observations). Therefore, the use of these sensor proteins for in vivo imaging during senescence has its limitations.

However, these lines were still useful to characterize the role of ROS, especially H_2O_2 during senescence. For sensing especially H_2O_2 the fluorescent protein HyPER was constructed, which combines the regulatory domain of the *Escherichia coli* OxyR transcription factor for sensing H_2O_2 in bacteria with a circular permutated YFP [88]. The *E. coli* OxyR transcription factor contains an H_2O_2-sensitive regulatory domain (amino acids 80–310, OxyR-RD), and a DNA-binding domain (amino acids 1–79). The reduced form of OxyR-RD is oxidized preferentially by H_2O_2. [102]. Aslund et al. suggested that OxyR acts as a peroxidase as OxyR returned to its reduced form in a time course experiment and a significant amount of NADPH was consumed in in vitro experiments [103]. Moreover, canonical H_2O_2 measurements using H2DCFDA [49] as well as H_2O_2 treatments of HyPER expressing leaf material in a perfusion chamber directly under the confocal LSM revealed that these sensor proteins scavenge H_2O_2 (unpublished observations). This means that even though the reaction is reversible, so these proteins can function as sensors, HyPER expression in plants will change the amplitude of intracellular H_2O_2 signals by consuming H_2O_2. This is exactly what has been observed during onset of monocarpic senescence; the H_2O_2 signal in the HyPER expressing lines was dampened and senescence was affected [49]. Having shown this, we now used these lines no longer as sensor lines but as lines with altered intracellular ROS levels as described in the next paragraph.

Lowering H_2O_2 contents specifically in different subcellular compartments

Costa and coworkers created transgenic lines which express this sensor protein in defined cellular compartments [104]. Yet, by directing HyPER to different compartments and thereby scavenging H_2O_2 specifically in these compartments, we could observe that the senescence process is differentially affected in these transgenic lines: While a reduction in peroxisomal and cytosolic H_2O_2 levels led to a delay in the onset of leaf senescence, low chloroplastic H_2O_2 retarded progression of leaf senescence (Fig. 2) ([49], unpublished observations). Moreover, genome wide gene expression analyses of these plants uncovered severe differences in gene expression, which were also dependent on

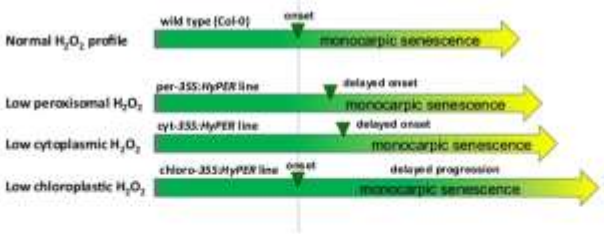

Fig. 2 Changes of intracellular H_2O_2 contents in different compartments have different impacts on onset and progression of monocarpic senescence compared to wildtype *Arabidopsis* plants Columbia-0 (Col-0). The expression of the H_2O_2 sensor HyPER under the control of the 35S-CaMV promoter leads to constant and high expression of the HyPER protein and thereby scavenges H_2O_2. By directing HyPER to specific compartments, the H_2O_2 levels were specifically reduced there. While cytoplasmic and peroxisomal HyPER protein expression caused a delay in the onset of monocarpic senescence, chloroplastic HyPER expression retarded the progression of senescence

the developmental stage. Here, plants with low chloroplastic H_2O_2 show more severe and often even opposite changes in gene expression compared to plants with lower cytoplasmic H_2O_2, which appear to be more similar in gene expression to wild type plants. Strikingly, higher expression of *CAT* and *APX* genes in plants with low chloroplastic H_2O_2 was observed. Moreover, expression of defensin genes is increased under low chloroplastic H_2O_2 but decreased under low cytoplasmic H_2O_2 (unpublished observation). In wild type plants, the expression of the pathogen-related defensin genes and genes encoding H_2O_2 scavenging proteins CAT and APX is triggered by oxidative stress but not by low H_2O_2. In the same chain of evidence, formation of stromules clearly increased under low chloroplastic H_2O_2 (Fig. 3; unpublished observation), which, again, should be opposite and rise after SA or H_2O_2 treatment [80]. These opposing expression patterns together with the unexpected increase in stromule formation prompted us to speculate that not the actual H_2O_2 concentration is sensed by the plants but more likely the ratio between the cytoplasmic and the chloroplastic H_2O_2. This would mean that low chloroplastic H_2O_2 resembles "cytoplasmic" oxidative stress (Fig. 4). If our hypothesis of sensing the H_2O_2 ratio is correct, crossings between the two HyPer transgenic lines should be similar to wild type plants as now H_2O_2 would be low in both compartments. Presumably, defensin and *CAT/APX* gene expression, stromule formation, and senescence

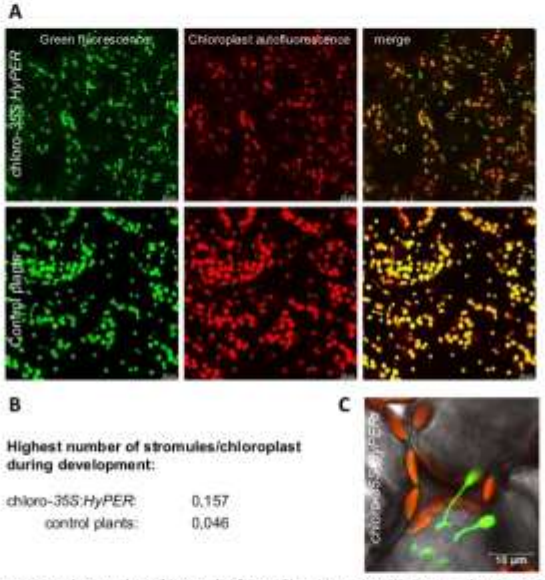

Fig. 3 **A** An increase in the number of stromules formed by chloroplasts harboring the HyPER protein which scavenges H_2O_2 or a GFP which does not scavenge H_2O_2 (control plants) was observed. HyPER fluorescence (green) and autofluorescence of the chloroplasts (red) and a merge of these are presented. **B** The highest average number of stromules per chloroplasts in leaves of the chloro-35S:HyPER line and the control plants, which was counted over different developmental stages, is indicated. **C** Stromules are able to contact the nucleus shown in a merged microscopic image of transmitted light, HyPER fluorescence (green) and autofluorescence of the chloroplasts (red)

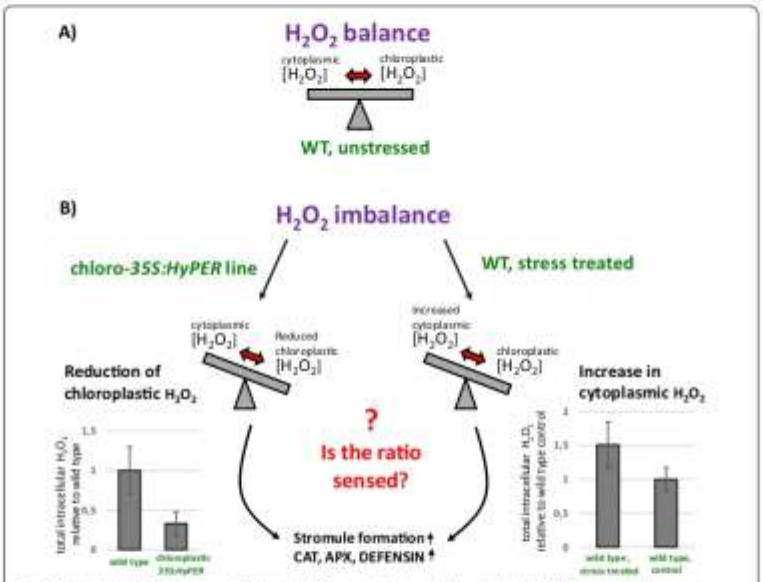

Fig. 4 Model for H_2O_2 sensing. **A** Balanced H_2O_2 contents in wild type plants (WT) in normal situations without exogenous stress. **B** Imbalanced H_2O_2 contents between chloroplast and cytoplasm in two different situations: (1) wild type versus HyPER expression in chloroplasts (left) or (2) wild type under control conditions versus wild type under stress conditions (right). Total intracellular H_2O_2 contents were measured by H2DCFDA and expressed relative to wild type or wild type control conditions. In both cases, H_2O_2 content is imbalanced in the same way and high stromule numbers as well as expression of genes induced by oxidative stress are observed, indicating that the ratio between the contents of the cytoplasm and the chloroplasts might be the parameter which is sensed by the cells. This is still a hypothesis and has to be further analyzed, e.g. in crossings between plants expressing HyPER in the cytoplasm and in the chloroplasts

onset and progression will then be more reminiscent of wild type plants. However, how this ratio is sensed by the plants still has to be elucidated.

Future perspectives

Reactive oxygen species (ROS) are inevitable by-products of many reactions of aerobic organisms, are produced in all subcellular compartments and play pivotal roles in the communication between all plant organelles [35, 105–107]. However, how specificity is achieved in H_2O_2 or ROS signaling in general is still an open question. Direct connections between different compartments such as stromules or peroxules enable small signaling molecules as well proteins or metabolites to be directly exchanged without passing through the cytoplasm. ROS, especially H_2O_2, can also pass through these tunnels to avoid the scavenging system of the cytoplasm imposing directionality in signaling. However, how the cells differentiate between stress-induced ROS signals and developmental ROS signals, e.g. the senescence-inducing H_2O_2 increase, is still not well understood. Localization of ROS production, especially for short-lived ROS, as well as duration of the production, might be part of this differentiation. However, as no "master receptors" for ROS are known so far, and a plethora of possible targets

for each ROS is available, the complex sensing process still has to be elucidated. Improvement of the sensor proteins [108] as well as of the microscopic technologies, e.g. single molecule or super resolution microscopy, will increase resolution and will help to understand the signaling processes in more detail. Single cell transcriptomics and metabolomics will also contribute to a more holistic view of the outcome of ROS signaling. In addition, artificial intelligence highly improved our understanding of protein structures [109] and could help in the future to predict structural changes under different redox conditions. So far, an enormous experimental effort has been necessary to unravel the structures of approximately 100,000 unique proteins, which still is only a tiny fraction of the billions of existing proteins. In contrast to the explosion in available genomic sequences and gene expression data produced by the technical advances in sequencing methods, a similar expansion in knowledge on available protein structures has so far been prevented by the intrinsic challenge of experimental structure determination. AlphaFold2 is a novel machine learning approach that incorporates physical and biological knowledge about protein structure which is now capable of predicting protein structures to near experimental accuracy in a majority of cases and greatly outperforms other methods [109]. Changes of protein structures by different redox environments await integration in the next step. Therefore, it can be expected that these technological advances will foster our understanding of intracellular redox signaling during development and stress and will help to determine how specificity in signaling is achieved.

Abbreviations

ROS: Reactive oxygen species; F_v/F_m: Photochemical capacity; RCBs: Rubisco-containing bodies; ATI-PS bodies: ATG8-interacting-protein1-plastid-associated bodies; SAVs: Senescence-associated vacuoles; CCVs: Chloroplast vesiculation-containing vesicles; TF: Transcription factor; APX: Ascorbate peroxidase; CAT: Catalase; GBF1: G-Box binding factor 1; AOX: Alternative oxidase; HyPER: Hydrogen peroxide sensor protein; roGFP: Redox-sensitive green fluorescent protein; RCD1: RADICAL-INDUCED CELL DEATH1 protein; NBT: Nitroblue tetrazolium; DAB: Diaminobenzidine; H2DCFDA: 2',7'-Dichlorofluorescin diacetate; OxyR-RD: OxyR transcription factor regulatory domain of *Escherichia coli*.

Acknowledgements

We apologize for not being able to cite all relevant work. We thank Prof. Dr. Christopher Grefen, University of Bochum, Germany for providing the plant line expressing GFP in chloroplasts to measure stromule formation in the wild type background. This article was specially invited by the editors and represents work by leading researchers.

Authors' contributions

UZ wrote the first draft, SB provided the confocal pictures, SB and AA-G have corrected and edited the text and the figures; all authors contributed to the final manuscript. All authors read and approved the final manuscript.

Funding

Open Access funding enabled and organized by Projekt DEAL. We acknowledge sponsorship by Open Access Publishing Fund of University of Tübingen. This work was supported by the Deutsche Forschungsgemeinschaft (DFG), CRC1101, B06.

Availability of data and materials

Not applicable.

Declarations

Ethics approval and consent to participate

Not applicable.

Consent for publication

Not applicable.

Competing interests

The authors declare that they have no competing interests.

Received: 4 October 2021 Accepted: 17 December 2021
Published online: 06 January 2022

References

1. Noodén LD, Leopold AC. Senescence and aging in plants. San Diego: Academic Press; 1988.
2. Breeze E, Harrison E, McHattie S, Hughes L, Hickman R, Hill C, et al. High-resolution temporal profiling of transcripts during Arabidopsis leaf senescence reveals a distinct chronology of processes and regulation. Plant Cell. 2011;23:873–94.
3. Ahmad S, Guo Y. Signal transduction in leaf senescence: progress and perspective. Plants. 2019;8:405.
4. Thomas H. Senescence, ageing and death of the whole plant. New Phytol. 2013;197(3):696–711.
5. Zentgraf U, Doll J. *Arabidopsis* WRKY53, a node of multi-layer regulation in the network of senescence. Plants. 2019;8(12):578.
6. Zhang Y, Wang HL, Li Z, Guo H. Genetic network between leaf senescence and plant immunity: crucial regulatory nodes and new insights. Plants. 2020;9(4):495.
7. Sade N, Del Mar R-W, Umnajkitikorn K, Blumwald E. Stress-induced senescence and plant tolerance to abiotic stress. J Exp Bot. 2018;69(4):845–53.
8. Biswal UC, Biswal B, Raval MK. Transformation of chloroplast to gerontoplast. In: Chloroplast biogenesis. Springer, Dordrecht; 2003. p. 155–242.
9. Hendry GAF, Houghton JD, Brown SB. The degradation of chlorophyll-a biological enigma. New Phytol. 1987;107:255–302.
10. Domínguez F, Cejudo FJ. Chloroplast dismantling in leaf senescence. J Exp Bot. 2021;72(16):5905–18.
11. Izumi M, Nakamura S. Chloroplast protein turnover: the influence of extraplastidic processes, including autophagy. Int J Mol Sci. 2018;19(3):828.
12. Zhuang X, Jiang L. Chloroplast degradation: multiple routes into the vacuole. Front Plant Sci. 2019;10:359.
13. Woodson JD, Joens MS, Sinson AB, Gilkerson J, Salom PA, Weigel D, et al. Ubiquitin facilitates a quality-control pathway that removes damaged chloroplasts. Science. 2015;350:450–4.
14. Corpas FJ, González-Gordo S, Palma JM. Plant peroxisomes: a factory of reactive species. Front Plant Sci. 2020;11:853.
15. Pan R, Reumann S, Lisik P, Tietz S, Olsen LJ, Hu J. Proteome analysis of peroxisomes from dark-treated senescent Arabidopsis leaves. J Integr Plant Biol. 2018;60:1028–50.
16. Chrobok D, Law SR, Brouwer B, Lindén P, Ziolkowska A, Liebsch D, et al. Dissecting the metabolic role of mitochondria during developmental leaf senescence. Plant Physiol. 2012;172(4):2132–53.
17. Maxwell DP, Nickels R, McIntosh L. Evidence of mitochondrial involvement in the transduction of signals required for the induction of genes associated with pathogen attack and senescence. Plant J. 2002;29:269–79.
18. Millenaar FF, Lambers H. The alternative oxidase: in vivo regulation and function. Plant Biol. 2003;5:2–15.
19. Bengoa Luoni S, Astigueta FH, Nicosia S, Moschen S, Fernandez P, Heinz R. Transcription factors associated with leaf senescence in crops. Plants. 2019;8:411.
20. Guo Y, Ren G, Zhang K, Li Z, Miao Y, Guo H. Leaf senescence: progression, regulation, and application. Mol Hortic. 2021;1:5.
21. Guo Y, Cai Z, Gan S. Transcriptome of Arabidopsis leaf senescence. Plant Cell Environ. 2004;27:521–49.
22. Balazadeh S, Kwasniewski M, Caldana C, Mehrnia M, Zanor MI, Xue GP, Mueller-Roeber B. ORS1, an H_2O_2-responsive NAC transcription factor, controls senescence in *Arabidopsis thaliana*. Mol Plant. 2011;4:346–60.
23. Kim HJ, Nam HG, Lim PO. Regulatory network of NAC transcription factors in leaf senescence. Curr Opin Plant Biol. 2016;33:48–56.
24. Mishra B, Sun Y, Howton T, Kumar NM, Mukhtar S. Dynamic modeling of transcriptional gene regulatory network uncovers distinct pathways during the onset of Arabidopsis leaf senescence. npj Syst Biol Appl. 2018;4:35.
25. Dong J, Chen C, Chen Z. Expression profiles of the Arabidopsis WRKY gene superfamily during plant defense response. Plant Mol Biol. 2003;51:21–37.
26. Xu X, Chen C, Fan B, Chen Z. Physical and functional interactions between pathogen-induced Arabidopsis WRKY18, WRKY40, and WRKY60 transcription factors. Plant Cell. 2006;18(5):1310–26.
27. Potschin M, Schlienger S, Bieker S, Zentgraf U. Senescence networking: WRKY18 is an upstream regulator, a downstream target gene, and a protein interaction partner of WRKY53. J Plant Growth Regul. 2014;33:106–18.
28. Llorca CM, Potschin M, Zentgraf U. bZIPs and WRKYs: two large transcription factor families executing two different functional strategies. Front Plant Sci. 2014;5:169.
29. Zentgraf U, Jobst J, Kolb D, Rentsch D. Senescence-related gene expression profiles of rosette leaves of *Arabidopsis thaliana*: leaf age versus plant age. Plant Biol. 2004;6(2):178–83.
30. Xie Y, Huhn K, Brandt R, Potschin M, Bieker S, Straub D, Doll J, Drechsler T, Zentgraf U, Wenkel S. REVOLUTA and WRKY53 connect early and late leaf development in Arabidopsis. Development. 2014;141:4772–83.
31. Doll J, Muth M, Riester L, Nebel S, Bresson J, Lee HC, Zentgraf U. *Arabidopsis thaliana* WRKY25 transcription factor mediates oxidative stress tolerance and regulates senescence in a redox-dependent manner. Front Plant Sci. 2020;10:1734.
32. Dietz KJ. Redox regulation of transcription factors in plant stress acclimation and development. Antioxid Redox Signal. 2014;21:1356–72.
33. Li Y, Liu W, Zhong H, Zhang HL, Xia Y. Redox-sensitive bZIP68 plays a role in balancing stress tolerance with growth in Arabidopsis. Plant J. 2019;100:768–83.
34. Tan XL, Zhao YT, Shan W, Kuang JF, Lu WJ, Su XG, Tao NG, Lakshmanan P, Chen JY. Melatonin delays leaf senescence of postharvest Chinese flowering cabbage through ROS homeostasis. Food Res Int. 2020;138:109790.

35. Waszczak C, Carmody M, Kangasjärvi J. Reactive oxygen species in plant signaling. Annu Rev Plant Biol. 2018;69:209–36.
36. Bienert GP, Schjoerring JK, Jahn TP. Membrane transport of hydrogen peroxide. BBA. 2006;1758(8):994–1003.
37. Duan X, Zhang H, Zhang D, Sheng J, Lin H, Jiang Y. Role of hydroxyl radical in modification of cell wall polysaccharides and aril breakdown during senescence of harvested longan fruit. Food Chem. 2011;128(1):203–7.
38. Pottosin I, Zepeda-Jazo I, Bose J, Shabala S. An anion conductance, the essential component of the hydroxyl-radical-induced ion current in plant roots. Int J Mol Sci. 2018;19(3):897.
39. Richards SL, Wilkins KA, Swarbreck SM, Anderson AA, Habib N, Smith AG, McAinsh M, Davies JM. The hydroxyl radical in plants: from seed to seed. J Exp Bot. 2015;66(1):37–46.
40. Demidchik V, Cuin TA, Svistunenko D, Smith SJ, Miller AJ, Shabala S, Sokolik A, Yurin V. Arabidopsis root K+-efflux conductance activated by hydroxyl radicals: single-channel properties, genetic basis and involvement in stress-induced cell death. J Cell Sci. 2010;123(Pt 9):1468–79.
41. Hancock JT, Russell G. Downstream signalling from molecular hydrogen. Plants. 2021;10(2):367.
42. Foyer CH, Bloom AJ, Queval G, Noctor G. Photorespiratory metabolism: genes, mutants, energetics and redox signaling. Ann Rev Plant Biol. 2009;60:455–84.
43. D'Autréaux B, Toledano M. ROS as signalling molecules: mechanisms that generate specificity in ROS homeostasis. Nat Rev Mol Cell Biol. 2007;8:813–24.
44. Sathyanarayanan PV, Poovaiah BW. Decoding Ca2+ signals in plants. CRC Crit Rev Plant Sci. 2004;23(1):1–11.
45. Schönknecht G. Calcium signals from the vacuole. Plants. 2013;2(4):589–614.
46. Mittler R, Vanderauwera S, Gollery M, Van Breusegem F. Reactive oxygen gene network of plants. Trends Plant Sci. 2004;9:490–8.
47. Zandalinas SI, Mittler R. Vascular and nonvascular transmission of systemic reactive oxygen signals during wounding and heat stress. Plant Physiol. 2021;186(3):1721–33.
48. Zimmermann P, Heinlein C, Orendi G, Zentgraf U. Senescence specific regulation of catalases in *Arabidopsis thaliana* (L.) Heynh. Plant Cell Environ. 2006;29:1049–60.
49. Bieker S, Riester L, Stahl M, Franzaring J, Zentgraf U. Senescence-specific alteration of hydrogen peroxide levels in *Arabidopsis thaliana* and oilseed rape spring variety *Brassica napus* L. cv. Mozart. J Integr Plant Biol. 2012;54(8):540–54.
50. Foyer CH, Noctor G. Stress-triggered redox signalling: what's in pROSpect? Front Plant Sci. 2016;39:951–64.
51. Walton PA, Brees C, Lismont C, Apanasets O, Fransen M. The peroxisomal import receptor PEX5 functions as a stress sensor, retaining catalase in the cytosol in times of oxidative stress. Biochim Biophys Acta. 2017;1864:1833–43.
52. Del Río LA, Corpas FJ, Sandalio LM, Palma JM, Barroso JB. Plant peroxisomes, reactive oxygen metabolism and nitric oxide. IUBMB Life. 2003;55:71–81.
53. Kaur N, Reumann S, Hu J. Peroxisome biogenesis and function. Arabidopsis Book. 2009;7:e0123.
54. Eastmond PJ. MONODEHYROASCORBATE REDUCTASE4 is required for seed storage oil hydrolysis and postgerminative growth in Arabidopsis. Plant Cell. 2007;19:1376–87.
55. Fransen M, Lismont C. Redox signaling from and to peroxisomes: progress, challenges, and prospects. Antioxid Redox Signal. 2019;30:95–112.
56. Sandalio LM, Peláez-Vico MA, Molina-Moya E, Romero-Puertas MC. Peroxisomes as redox-signaling nodes in intracellular communication and stress responses. Plant Physiol. 2021;186(1):22–35.
57. Smykowski A, Zimmermann P, Zentgraf U. G-Box binding factor1 reduces CATALASE2 expression and regulates the onset of leaf senescence in Arabidopsis. Plant Physiol. 2010;153:1321–31.
58. Smykowski A, Fischer SM, Zentgraf U. Phosphorylation affects DNA-binding of the senescence-regulating bZIP transcription factor GBF1. Plants. 2015;4(3):691–709.
59. Sibéril Y, Doireau P, Gantet P. Plant bZIP G-box binding factors. Modular structure and activation mechanisms. Eur J Biochem. 2001;268(22):5655–66.
60. Feierabend J, Schaan C, Hertwig B. Photoinactivation of catalase occurs under both high and low temperature stress conditions and accompanies photoinhibition of photosystem II. Plant Physiol. 1992;100:1554–61.
61. Panchuk II, Zentgraf U, Volkov RA. Expression of the APX gene family during leaf senescence of *Arabidopsis thaliana*. Planta. 2005;222:926–32.
62. Miyake C, Asada K. Inactivation mechanism of ascorbate peroxidase at low concentrations of ascorbate: hydrogen peroxide decomposes compound I of ascorbate peroxidase. Plant Cell Physiol. 1996;37:423–30.
63. Ye ZZ, Rodriguez R, Tran A, Hoang H, de los Santos D, Brown S, Vellanoweth RL. The developmental transition to flowering represses ascorbate peroxidase activity and induces enzymatic lipid peroxidation in leaf tissue in *Arabidopsis thaliana*. Plant Sci. 2000;158:115–27.
64. Lai AG, Doherty CJ, Mueller-Roeber B, Kay SA, Schippers JH, Dijkwel PP. CIRCADIAN CLOCK-ASSOCIATED 1 regulates ROS homeostasis and oxidative stress responses. Proc Natl Acad Sci USA. 2012;109(42):17129–34.
65. Chaouch S, Queval G, Vanderauwera S, Mhamdi A, Vandorpe M, Langlois-Meurinne M, et al. Peroxisomal hydrogen peroxide is coupled to biotic defense responses by ISOCHORISMATE SYNTHASE1 in a daylength-related manner. Plant Physiol. 2010;153:1692–705.
66. Queval G, Neukermans J, Vanderauwera S, Van Breusegem F, Noctor G. Day length is a key regulator of transcriptomic responses to both CO_2 and H_2O_2 in Arabidopsis. Plant Cell Environ. 2012;35:374–87.
67. Zhang Y, Wang Y, Wei H, Li N, Tian W, Chong K, Wang L. Circadian evening complex represses jasmonate-induced leaf senescence in Arabidopsis. Mol Plant. 2018;11(2):326–37.
68. Sanchez SE, Kay SA. The plant circadian clock: from a simple timekeeper to a complex developmental manager. Cold Spring Harb Perspect Biol. 2016;8:a027748.
69. Kim H, Kim Y, Yeom M, Lim J, Nam HG. Age-associated circadian period changes in Arabidopsis leaves. J Exp Bot. 2016;67(9):2665–73.

70. Sewelam N, Jaspert N, Van Der Kelen K, Tognetti NB, Schmitz J, Frerigmann H, et al. Spatial H_2O_2 signaling specificity: H_2O_2 from chloroplasts and peroxisomes modulates the plant transcriptome differentially. Mol Plant. 2014;7:1191–210.
71. Rosenwasser S, Fluhr R, Joshi JR, Leviatan N, Sela N, Hetzroni A, Friedman H. ROSMETER: a bioinformatic tool for the identification of transcriptomic imprints related to reactive oxygen species type and origin provides new insights into stress responses. Plant Physiol. 2013;163:1071–83.
72. Maxwell DP, Wang Y, McIntosh L. The alternative oxidase lowers mitochondrial reactive oxygen production in plant cells. Proc Natl Acad Sci USA. 1999;96(14):8271–6.
73. Saito K, Futamura Y, Shimizu T, Matsui A, Hirano H, Kondoh Y, et al. Inhibition of mitochondrial complex I by the novel compound FSL0260 enhances high salinity-stress tolerance in *Arabidopsis thaliana*. Sci Rep. 2020;10(1):8691.
74. Zentgraf U, Zimmermann P, Smykowski A. Role of intracellular hydrogen peroxide as signaling molecule for plant senescence. In: Nagata T, editor. Senescence. In-Tech Open Access Publishing; 2012. ISBN: 978-953-51-0144-4. https://doi.org/10.5772/34576.
75. Labs M, Rühle T, Leister D. The antimycin A-sensitive pathway of cyclic electron flow: from 1963 to 2015. Photosynth Res. 2016;2016(129):231–8.
76. Smirnoff N, Arnaud D. Hydrogen peroxide metabolism and functions in plants. New Phytol. 2019;221:1197–214.
77. Romero-Puertas MC, Rodríguez-Serrano M, Corpas FJ, Gómez M, del Río LA, Sandalio LM. Cadmium-induced subcellular accumulation of $O^{\cdot-}_2$ and H_2O_2 in pea leaves. Plant Cell Environ. 2004;27:1122–34.
78. Caplan JL, Kumar AS, Park E, Padmanabhan MS, Hoban K, Modla S, et al. Chloroplast stromules function during innate immunity. Dev Cell. 2015;34:45–57.
79. Kumar AS, Park E, Nedo A, Alqarni A, Ren L, Hoban K, et al. Stromule extension along microtubules coordinated with actin-mediated anchoring guides perinuclear chloroplast movement during innate immunity. eLife. 2018;7:1–33.
80. Reumann S, Ma C, Lemke S, Babujee L. AraPerox. A database of putative Arabidopsis proteins. Plan Physiol. 2004;136:2587–608.
81. Vandenabeele S, Van Der Kelen K, Dat J, Gadjev I, Boonefaes T, Morsa S, et al. A comprehensive analysis of hydrogen peroxide-induced gene expression in tobacco. Proc Natl Acad Sci USA. 2003;100:16113–8.
82. Vandenabeele S, Vanderauwera S, Vuylsteke M, Rombauts S, Langebartels C, Seidlitz HK, et al. Catalase deficiency drastically affects gene expression induced by high light in *Arabidopsis thaliana*. Plant J. 2004;39:45–58.
83. Su T, Li W, Wang P, Ma C. Dynamics of peroxisome homeostasis and its role in stress response and signaling in plants. Front Plant Sci. 2019;10:705.
84. Dietz KJ, Hell R. Thiol switches in redox regulation of chloroplasts: balancing redox state, metabolism and oxidative stress. Biol Chem. 2015;396:483–94.
85. Noctor G, Foyer CH. Intracellular redox compartmentation and ROS-related communication in regulation and signaling. Plant Physiol. 2016;171:1581–92.
86. Brunkard JO, Runkel AM, Zambryski PC. Chloroplasts extend stromules independently and in response to internal redox signals. Proc Natl Acad Sci USA. 2015;112(32):10044–9.
87. Hanson MR, Hines KM. Stromules: probing formation and function. Plant Physiol. 2018;176(1):128–37.
88. Belousov VV, Fradkov AF, Lukyanov KA, Staroverov DB, Shakhbazov KS, Terskikh AV, Lukyanov S. Genetically encoded fluorescent indicator for intracellular hydrogen peroxide. Nat Methods. 2006;3:281–6.
89. Exposito-Rodriguez M, Laissue PP, Yvon-Durocher G, Smirnoff N, Mullineaux PM. Photosynthesis-dependent H_2O_2 transfer from chloroplasts to nuclei provides a high-light signalling mechanism. Nat Commun. 2017;8(1):49.
90. Møller IM, Kristensen BK. Protein oxidation in plant mitochondria as a stress indicator. Photochem Photobiol Sci. 2004;3:730–5.
91. Nietzel T, Mostertz J, Hochgräfe F, Schwarzländer M. Redox regulation of mitochondrial proteins and proteomes by cysteine thiol switches. Mitochondrion. 2017;33:72–83.
92. Borniego ML, Molina MC, Guiamét JJ, Martínez DE. Physiological and proteomic changes in the apoplast accompany leaf senescence in Arabidopsis. Front Plant Sci. 2020;10:1635.
93. Berens ML, Wolinska KW, Spaepen S, Ziegler J, Nobori T, Nair A, et al. Balancing trade-offs between biotic and abiotic stress responses through leaf age-dependent variation in stress hormone cross-talk. Proc Natl Acad Sci USA. 2019;116(6):2364–73.
94. Shapiguzov A, Vainonen JP, Wrzaczek M, Kangasjärvi J. ROS-talk—how the apoplast, the chloroplast, and the nucleus get the message through. Front Plant Sci. 2012;212(3):292.
95. Shapiguzov A, Vainonen JP, Hunter K, Tossavainen H, Tiwari A, Järvi S, et al. Arabidopsis RCD1 coordinates chloroplast and mitochondrial functions through interaction with ANAC transcription factors. eLife. 2019;8:e43284.
96. Fichman Y, Miller G, Mittler R. Whole-plant live imaging of reactive oxygen species. Mol Plant. 2019;12:1203–10.
97. Davletova S, Schlauch K, Coutu J, Mittler R. The zinc-finger protein Zat12 plays a central role in reactive oxygen and abiotic stress signaling in Arabidopsis. Plant Physiol. 2005;139(2):847–56.
98. Miller G, Schlauch K, Tam R, Cortes D, Torres MA, Shulaev V, et al. The plant NADPH oxidase RBOHD mediates rapid systemic signaling in response to diverse stimuli. Sci Signal. 2009;2(84):ra45.
99. Ren W, Ai HW. Genetically encoded fluorescent redox probes. Sensors. 2013;13(11):15422–33.
100. Meyer AJ, Brach T, Marty L, Kreye S, Rouhier N, Jacquot JP, Hell R. Redox-sensitive GFP in *Arabidopsis thaliana* is a quantitative biosensor for the redox potential of the cellular glutathione redox buffer. Plant J. 2007;52:973–86.
101. Ugalde JM, Fuchs P, Nietzel T, Cutolo EA, Homagk M, Vothknecht UC, et al. Chloroplast-derived photo-oxidative stress causes changes in H_2O_2 and EGSH in other subcellular compartments. Plant Physiol. 2021;186(1):125–41.
102. Zheng M, Aslund F, Storz G. Activation of the OxyR transcription factor by reversible disulfide bond formation. Science. 1998;279:1718–21.
103. Aslund F, Zheng M, Beckwith J, Storz G. Regulation of the OxyR transcription factor by hydrogen peroxide and the cellular thiol-disulfide status. Proc Natl Acad Sci USA. 1999;96:6161–5.
104. Costa A, Drago I, Behera S, Zottini M, Pizzo P, Schroeder JI, et al. H2O2 in plant peroxisomes: an in vivo analysis uncovers a Ca(2+)-dependent scavenging system. Plant J. 2010;62:760–72.

105. Zimmermann P, Zentgraf U. The correlation between oxidative stress and leaf senescence during plant development. Cell Mol Biol Lett. 2005;10:515–34.
106. Dietz KJ, Turkan I, Krieger-Liszkay A. Redox- and reactive oxygen species-dependent signaling into and out of the photosynthesizing chloroplast. Plant Physiol. 2016;171(3):1541–50.
107. Noctor G, Reichheld JP, Foyer CH. ROS-related redox regulation and signaling in plants. Semin Cell Dev Biol. 2018;80:3–12.
108. Schwarzländer M, Dick TP, Meyer AJ, Morgan B. Dissecting redox biology using fluorescent protein sensors. Antioxid Redox Signal. 2016;24(13):680–712.
109. Jumper J, Evans R, Pritzel A, Green T, Figurnov M, Ronneberger O, et al. Highly accurate protein structure prediction with AlphaFold. Nature. 2021;596(7873):583–9.

Publisher's Note

Review 2: Editorial for Special Issue "Leaf Senescence" in Plants

Zentgraf, U., Andrade, A. G., & Doll, J. Editorial for Special Issue "Leaf Senescence" in *Plants*. *Plants*, *10*(8), 1490. 2021. https://doi.org/10.3390/plants10081490

plants

MDPI

Editorial

Editorial for Special Issue "Leaf Senescence" in *Plants*

Ulrike Zentgraf *, Ana G. Andrade and Jasmin Doll

Centre for Molecular Biology of Plants, University of Tuebingen, Auf der Morgenstelle 32, 72076 Tuebingen, Germany; ana.andrade@zmbp.uni-tuebingen.de (A.G.A.); jasmin.doll@zmbp.uni-tuebingen.de (J.D.)
* Correspondence: ulrike.zentgraf@zmbp.uni-tuebingen.de

Senescence in plants is often described as the last step in the life history of a plant. However, senescence takes place from early on throughout development and a plant can sacrifice older leaves for the sake of the whole plant. Leaf senescence aims at remobilizing previously acquired nitrogen, carbon and mineral resources out of the senescing tissue into developing parts of the plant, before the leaf eventually dies and is shed. Before anthesis, sequential leaf senescence leads to the repartitioning of nutrients from older leaves to newly developing non-reproductive organs. After anthesis, monocarpic leaf senescence governs nutrient reallocation to the now developing reproductive organs and, therefore, has a very critical impact on yield. During monocarpic senescence, potentially all the leaves of a plant can undergo senescence, leading to the death of the whole plant (Figure 1).

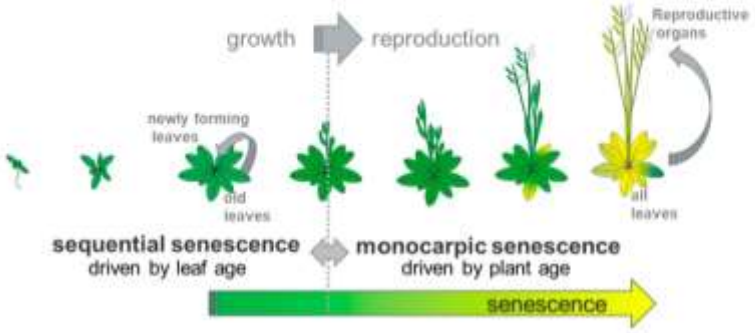

Figure 1. Leaf senescence in the model plant *Arabidopsis thaliana*. Leaf senescence takes place all over development. At the transition from the growth to reproduction phase, senescence is switched from sequential to monocarpic senescence.

In the last two decades, it became obvious that no "master regulator" for senescence exists but an extremely complex regulatory network controls all aspects of senescence. Leaf and plant age are the predominant parameters controlling the onset and the progression of developmental senescence; however, we still do not understand exactly how these parameters are sensed by the plants. Moreover, incoming environmental signals are constantly integrated and long-lasting unfavorable conditions have the potential to induce senescence prematurely. Premature senescence serves as an exit-strategy to produce offspring when biotic or abiotic stresses are encountered over longer periods and produce severe damages. As a tradeoff, seed quantity and quality are often diminished and can significantly lower the productivity of plants. In crop plants, stress-induced premature senescence can have a major impact on yield, referring to quantity and quality. Moreover, post-harvest senescence can change nutrient contents and the profile of volatile organic compounds, which relate, for example, to the aroma of vegetables or salads. As well in this case, stress conditions

Citation: Zentgraf, U.; Andrade, A.G.; Doll, J. Editorial for Special Issue "Leaf Senescence" in *Plants*. *Plants* **2021**, *10*, 1490. https://doi.org/10.3390/plants10081490

Received: 12 July 2021
Accepted: 20 July 2021
Published: 21 July 2021

during harvest, storage and transportation can influence the onset and progression of post-harvest senescence with a high impact on shelf life performance [1].

Transcriptional regulation was discovered to be one of the main drivers of senescence processes, implying a central role for transcription factors of many different transcription factor families in model plants as well as in crop plants [2–4]. However, in most cases, no simple signal transduction pathways are realized, but complex multi-layer regulatory cues including many feedback loops are in place to control senescence. Even for a single transcription factor gene, transcriptional, post-transcriptional, as well as post-translational regulatory mechanisms can act in concert [4]. In addition, the turn-over of specific regulators can also be tightly controlled with the degradation of damaged proteins by the 20S proteasome playing an important role [5]. Moreover, we are just beginning to understand the dynamic changes in chromatin structure and nuclear architecture during senescence. Alternative splicing and polyadenylation events have rarely been analyzed.

As signaling components, almost all plant hormones are involved in senescence regulation, which also pinpoints the high cross regulation to many other processes [6]. There is a large overlap and crosstalk between senescence-related processes and pathogen responses [7]. Reactive oxygen species have also been characterized as participating, especially in the early signaling events of leaf senescence and acting in concert with salicylic acid. In addition, less well-known signaling molecules such as melatonin are engaged in the control of the scavenging systems for reactive oxygen species in grape leaves and, by that, influence the expression of senescence-associated genes [8]. On this note, the role of chloroplasts was revisited in the recent years and it became clear that the redox balance in chloroplasts significantly contributes to senescence timing and progression [9].

Essential for the efficient remobilization of carbon- and nitrogen-containing compounds is not only the systematic degradation of macromolecules but also the conversion of their degradation products into transport forms and the activation of transport processes per se. Specific amino acids such as aspartate are enriched during the onset of leaf senescence and are part of the leaf curing process in tobacco leaves. For this purpose, specific enzymes have to be activated to increase the levels of specific amino acids [10]. Moreover, the expression of specific members of transporter families are activated during senescence to guarantee the increasing demand and correct the directionality of the transport of sugars and amino acids out of the senescing tissue to pods and seeds [11].

This Special Issue combines a wide range of senescence topics in five articles and six reviews on plant senescence processes. Work from all over the world including Europe (UK, Germany, Switzerland), Asia (China, Pakistan), South America (Argentina) and New Zealand was brought together, indicating that this is an important and "hot" topic in all parts of the world. Changing climate conditions will most likely produce long lasting unfavorable conditions and will lead to premature senescence induction and yield losses in many crop plants. Therefore, understanding senescence processes, their regulation and the impact of stress conditions in model and crop plants will be one of our future challenges. Increasing knowledge in this field will hopefully contribute to new transgenic lines and breeding strategies for plants with improved stress tolerance and optimized senescence programs.

Funding: Our work is financially supported by The Deutsche Forschungsgemeinschaft (DFG), CRC 1101 (B06).

Conflicts of Interest: The authors declare no conflict of interest.

References

1. Spadafora, N.D.; Cocetta, G.; Ferrante, A.; Herbert, R.J.; Dimitrova, S.; Davoli, D.; Fernández, M.; Patterson, V.; Vozel, T.; Amarysti, C.; et al. Short-Term Post-Harvest Stress that Affects Profiles of Volatile Organic Compounds and Gene Expression in Rocket Salad during Early Post-Harvest Senescence. *Plants* **2020**, *9*, 4. [CrossRef] [PubMed]
2. Bengoa Luoni, S.; Astigueta, F.H.; Nicosia, S.; Moschen, S.; Fernandez, P.; Heinz, R. Transcription Factors Associated with Leaf Senescence in Crops. *Plants* **2019**, *8*, 411. [CrossRef] [PubMed]

3. Fan, J.; Lou, Y.; Shi, H.; Chen, L.; Cao, L. Transcriptomic Analysis of Dark-Induced Senescence in Bermudagrass (*Cynodon dactylon*). *Plants* **2019**, *8*, 614. [CrossRef] [PubMed]
4. Zentgraf, U.; Doll, J. *Arabidopsis* WRKY53, a Node of Multi-Layer Regulation in the Network of Senescence. *Plants* **2019**, *8*, 578. [CrossRef] [PubMed]
5. Lan, W.; Miao, Y. New Aspects of HECT-E3 Ligases in Cell Senescence and Cell Death of Plants. *Plants* **2019**, *8*, 483. [CrossRef] [PubMed]
6. Ahmad, S.; Guo, Y. Signal Transduction in Leaf Senescence: Progress and Perspective. *Plants* **2019**, *8*, 405. [CrossRef] [PubMed]
7. Zhang, Y.; Wang, H.-L.; Li, Z.; Guo, H. Genetic Network between Leaf Senescence and Plant Immunity: Crucial Regulatory Nodes and New Insights. *Plants* **2020**, *9*, 495. [CrossRef]
8. Shi, X.; Xu, S.; Mu, D.; Sadeghnezhad, E.; Li, Q.; Ma, Z.; Zhao, L.; Zhang, Q.; Wang, L. Exogenous Melatonin Delays Dark-Induced Grape Leaf Senescence by Regulation of Antioxidant System and Senescence Associated Genes (SAGs). *Plants* **2019**, *8*, 366. [CrossRef]
9. Mayta, M.L.; Hajirezaei, M.-R.; Carrillo, N.; Lodeyro, A.F. Leaf Senescence: The Chloroplast Connection Comes of Age. *Plants* **2019**, *8*, 495. [CrossRef]
10. Bovet, L.; Cheval, C.; Hilfiker, A.; Battey, J.; Langlet, D.; Broye, H.; Schwaar, J.; Ozelley, P.; Lang, G.; Bakaher, N.; et al. Asparagine Synthesis during Tobacco Leaf Curing. *Plants* **2019**, *8*, 492. [CrossRef]
11. Ninan, A.S.; Grant, J.; Song, J.; Jameson, P.E. Expression of Genes Related to Sugar and Amino Acid Transport and Cytokinin Metabolism during Leaf Development and Senescence in *Pisum sativum* L. *Plants* **2019**, *8*, 76. [CrossRef]

Acknowledgements

I would like to express my deepest gratitude to all those who, in various ways, have supported and helped me throughout the completion of this project.

Prof. Dr. Ulrike Zentgraf deserves my sincerest thanks for her invaluable support and guidance, and for the great opportunity to be part of this academic adventure. Her unwavering patience, understanding, and human warmth throughout the entire process were truly exceptional, and I am deeply grateful for her trust and encouragement.

Special thanks to Dr. Jasmin Doll for her insightful discussions, valuable advice, and, of course, the comforting conversations that brought warmth along the way.

My heartfelt appreciation also goes to the wonderful and supportive group collaborators Natali Faiss, Marieluise Wünsch, Rosanna Saur, Laura Schaffer, and Valeriya, for their dedication and contributions to this project.

I would also like to extend my sincere thanks to the members of my TAQ committee, Prof. Dr. Klaus Harter and Prof. Dr. Suayib Üstün, for their time and feedback. I am also grateful to all the members of the ZMBP for fostering such a welcoming environment and for their constant willingness to help.

This journey would not have been possible without the unwavering love and support of my family. I thank my parents Carlos and Noralma for their love, hard work and sacrifices, and my siblings Paula and Carlos for the unique bond we share that continues to sustain us.

Finally, words cannot fully express my gratitude to my loving husband. He is not only my soul mate but also my unwavering supporter—not just throughout this process, but in every aspect of my life. His constant efforts to bring happiness into my world, along with his understanding, care, help, and love, mean more to me than words can convey.